CELLULAR GENOMICS APPROACHES TO DEFINING SUSCEPTIBILITY AND RESISTANCE TO CHEMOTHERAPEUTIC TOXICITY IN IMMUNE CELLS

Amber Frick

A dissertation submitted to the faculty at the University of North Carolina at Chapel Hill in partial fulfillment of the requirements for the degree of Doctor of Philosophy in Pharmaceutical Sciences in the Eshelman School of Pharmacy (Division of Pharmacotherapy and Experimental Therapeutics).

Chapel Hill
2014

Approved by:

Jian Liu

Kristy Richards

Yuri Fedoriw

Heyward Hull

Russell Thomas

Timothy Wiltshire

ABSTRACT

AMBER FRICK: Cellular Genomics Approaches to Defining Susceptibility and Resistance to Chemotherapeutic Toxicity in Immune Cells
(Under the direction of Timothy Wiltshire)

While the role of the immune system in cancer development is known, its role in response to chemotherapeutic agents remains elusive. Interpatient variability in immune and chemotherapeutic cytotoxic responses is likely due to complex genetic differences. Through the use of a panel of genetically diverse mouse inbred strains, we developed a drug screening platform aimed at examining novel mechanisms underlying these chemotherapeutic cytotoxic responses on immune cells. Drug effects were investigated by comparing more selective chemotherapeutic agents such as BEZ235 and selumetinib against conventional cytotoxic agents, including doxorubicin and idarubicin.

Phenotypes were quantified using flow cytometry, yielding interstrain variation for measured endpoints in different immune cells. Our flow cytometry assay produced nearly 16,000 data points that were used to generate dose response curves. The more targeted agents, BEZ-235 and selumetinib, were less toxic to immune cells than the anthracycline agents. Also, heritability for the viability of immune cells was higher for anthracyclines than the novel agents, making them ideal for genetic analysis.

Using genome-wide association studies, we identified loci that contributed to the sensitivity of doxorubicin and idarubicin in immune cells. We identified 8 QTL containing 25 potential candidate genes. Of particular interest, *App*, encoding for amyloid beta precursor

protein, was identified under a peak on chromosome 16 ($p = 5.01x10^{-8}$) in T-cells exposed to idarubicin. Dose response curves verified that T-cells in *App* knockout mice were more sensitive to idarubicin than those of C57BL/6J control mice ($p = 0.01$).

Using a cellular screening approach, we identified and subsequently validated a gene candidate encoding for amyloid beta precursor protein in T-cells exposed to idarubicin. The literature has suggested a role for *App* in in vitro and in vivo cytotoxicity to anticancer agents; the overexpression of *App* enhances resistance, while the knockdown of this gene is deleterious to cell viability. In the future, we aim to perform mechanistic studies in primary and immortalized immune cells, validate additional candidate genes, and, ultimately, to translate our findings to in vivo and human studies.

To my family, friends, and mentors. Because of you, I am not lost.

ACKNOWLEDGEMENTS

Tim Wiltshire, you are a remarkable advisor. I am thankful for your guidance, flexibility, and recognition of what is truly important in and outside of the lab setting. Oscar Suzuki, you are one of the most intelligent individuals I have ever known and am thankful to have your help and friendship. Cristina Santos, I am grateful that you graciously welcomed me into your life and the lab. You have such a big heart. Olivia Dong, I am so glad that you chose to be in our lab. Please, never lose your enthusiasm and courtesy. Emmanuel Chan, I am very glad to have had the opportunity to meet and interact with you. You have expanded my worldview, and your thoughtfulness and drive to help others is astounding. Natasha Butz, thank you for your direction during my earlier years in the lab. Also, thanks are warranted for the students in our lab, including Niraj Gowda, Nan Wang, Sarah Troutman, Krista Haywood, and others.

Jian Liu, you are my favorite mentor, and I have appreciated your wisdom over the past nine years. You have had a profound effect on me as a person, and I have wanted to be just like you in your pursuit of knowledge and the kindness you extend to those around you.

Rusty Thomas, it has been a great pleasure interacting with you and your lab at the Hamner Institutes. Bethany Parks, I have been privileged in getting to know you. You are a wonderful friend, and your energy, attention to detail, and passion amaze me. I wish I could be half the scientist you are. Joe Trask, I am grateful for the assay and flow cytometry knowledge you have imparted and for your invaluable guidance in improving our projects.

Heyward Hull, I am thankful for your help and guidance with the statistics portion of this project. Your idealism and full immersion in learning make working with you a pleasure and are personal goals to strive for.

Kristy Richards and Yuri Fedoriw, thank you so much for your clinical expertise over the years. I have taken your advice, scientific and otherwise, to heart. Blossom Damania, thank you so much for the supplies and helping make our project possible. We also thank Novartis for supplying us with the BEZ235 compound.

Lisa Tarantino, I have enjoyed cooperating with you and your lab. The lab would definitely not be the same without such friendly and fun neighbors. Amy Dorman and Robin Ervin, I have appreciated your help and insights over the past years and getting to interact with you outside of the lab. Joe Farrington, you are my favorite and are one of the people who definitely makes the world a better place just by being in it. Trey Thompson and Sara Shoenrock, you have been excellent additions to the lab, and I know you will go on to do great things.

Feng Liu, I wish you could have attended my defense. Your enthusiasm and wonderful, animated personal nature made stopping by your office the best part of my day when sharing good news or when I needed cheering up. You were one of the most creative and humble scientists I know of, but, perhaps most importantly, you were a really good person, who recognized the importance of balancing career and family life. I miss you and hope we meet again.

I am greatly indebted to the NC TraCS Institute and PhRMA Foundation for funding. The NC TraCS Research Pilot Program made my project possible. The project described was supported by the North Carolina Translational and Clinical Sciences Institute and the National Center for Research Resources and the National Center for Advancing Translational Sciences,

National Institutes of Health, through Grant Award Number UL1TR000083. The content is solely the responsibility of the authors and does not necessarily represent the official views of the NIH. This project was also supported by the Pharmaceutical Research and Manufacturers of America Foundation Pre Doctoral Fellowship in Pharmacology/Toxicology. The PhRMA Foundation's gracious Pre Doctoral Fellowship in Pharmacology/Toxicology has changed my life and will open doors. Words cannot articulate how grateful I am for these two organizations.

I acknowledge the UNC Eshelman School of Pharmacy, the Department of Pharmaceutical Sciences, the Division of Pharmacotherapy and Experimental Therapeutics and all affiliated individuals for accepting me into the graduate program and allowing me unprecedented opportunities to grow as a person and scientist over the past five years. WinNonlin software was provided to faculty and trainees in the Division of Pharmacotherapy and Experimental Therapeutics, UNC Eshelman School of Pharmacy, by Certara as a member of the Pharsight Academic Center of Excellence Program.

I am very appreciative of our incredible administration including Kathy Maboll, Arlo Brown, Jessie Bishop, Anna Crollman, and Aaron Todd. Casey Emerson, your awesome personality has made interacting with you very enjoyable. I have also enjoyed seeing how you have used your technological know-how and magic to improve the school. All of you are irreplaceable; we would not be able to function without you.

I have immeasurable gratitude for UNC Campus Health Services for helping keep me healthy. I believe that I have taken advantage of nearly every service your facility has to offer and cannot express how glad I am that you are here.

The Duke University LEAP Program and opportunities to teach at UNC have changed me for the better. Thank you, Shelly Schwartz-Bloom, Liz Godin, additional faculty, and students.

I am grateful for my supportive friends and colleagues: Gina Song, Dan and Lana Crona, Dylan Glubb, Amy Etheridge, Whitney and Justin Kirschbrown, Melanie Nicol, Christina Won, Kimlee Smith, Jing Fu, Trish Stroupe, Mandi Hart, Allison Schorzman, Sara O'Neal, Nancy Gillis, Nicole Zane, and Brian Ferslew. Rachel Selinger, not a day goes by where I am not incredibly thankful for your friendship. Thank you so much for everything over the past nine years. All of you are amazing.

Also, without Amy Schmitz-Sciborski and Jessica Spaeth McCormick, I would not be here.

Special thanks are extended to the Fleet Feet crew: Natalie, Judith, Cindy, Lynell, Kathy, Christie, Teresa, Hazel, Joan, Denise, Gini, Patty, Becca, Cheryl, and Jerry. I am a seasoned half marathoner because of you. You have also shown me that life can be approached like a marathon; persistence, self-care, and good company make the journey better.

Most importantly, I would like to thank my family: Janet, Steve, Melissa, and Kelly Frick, Linda Kimrey, our four legged family members (Chance, Squiggles, Boschkin, Gracie, Claudia, Maggie, Gretchen, and Rosie), and my most beloved cat, Gabriel. I love you all more than the world and am so proud to have you in my life.

"The Universe is rarely so lazy" in regards to coincidence. It has been my pleasure getting to know everyone over the past few years. I sincerely extend my gratitude, warmth, and best wishes to all of you.

TABLE OF CONTENTS

LIST OF TABLES

LIST OF FIGURES

LIST OF ABBREVIATIONS

7-AAD	7-aminoactinomycin D
A1bg	Alpha-1-B glycoprotein
ACK	Ammonium-chloride-potassium
Ano1	Anoctamin 1
ANOVA	Analysis of variance
Aplp	Amyloid precursor-like protein
App or *APP*	Amyloid precursor protein
Arntl2	Aryl hydrocarbon receptor nuclear translocator-like 2
ATP	Adenosine triphosphate
Atp5J	ATP synthase, H+ transporting, mitochondrial F0 complex, subunit F6
AUC	Area under the curve
β-APP	Beta amyloid fragment of amyloid precursor protein
BD	Becton Dickinson
BMI	Body mass index
C_{max}	Maximum or peak concentration
Cas-9	CRISPR-associated nuclease protein 9
Ccdc91	Coiled-coil domain containing 91
Ccdc99	Coiled-coil domain containing 99
CD	Cluster of differentiation
Cdh11	Cadherin 11
CGDSNPdb	The Center for Genome Dynamics SNP Database
CHO	Chinese hamster ovary

CI	Confidence interval
CNS	Central nervous system
CRISPR	Clustered regularly interspaced short palindromic repeats
crRNA	CRISPR RNA
CTLA	Cytotoxic T-lymphocyte-associated antigen
Cttn	Cortactin
Cybb	Cytochrome b beta
CYP	Cytochrome P450
Cyyr	Cysteine and tyrosine-rich protein 1
dbSNP	SNP Database
Ddx1	DEAD (Asp-Glu-Ala-Asp) box helicase 1
Dhrc7	7-dehydrocholesterol reductase
DMEM	Dulbecco's modified Eagle's medium
DMSO	Dimethyl sulfoxide
DNA	Deoxyribonucleic acid
Dock2	Dedicator of cytokinesis 2
EMMA	Efficient mixed model association
Fadd or *FADD*	Fas-associated protein with death domain
Fam84b	Family with sequence similarity 84, member B
FBS	Fetal bovine serum
FSC	Forward scatter
Gabpa	GA repeat binding protein, alpha
Gm5887	MANSC domain containing 5

GWA	Genome wide association
GWAS	Genome wide association study/studies
HCS	High-content cell-based screening
HEK	Human embryonic kidney
HIV	Human immunodeficiency virus
HL60	Human promyelocytic leukemia cells
HLA	Human leukocyte antigen
HMGB1	High-mobility group protein B1
IC_{50}	Half maximal inhibitory concentration
IFN	Interferon
IKMC	International Knockout Mouse Consortium
IL	Interleukin
IMDM	Iscove's modified Dulbecco's medium
JAM2	Junction adhesion molecule 2
KIT	v-kit Hardy-Zuckerman 4 feline sarcoma viral oncogene homolog
Klhdc42	Kelch-like family member 42
KLRC4	Natural killer cell lectin-like receptor subfamily C member 4
KU	Kunitz
LAR	Leukocyte common antigen–related
LILRA4	Leukocyte immunoglobulin-like receptor subfamily A member 4
MAPK	Mitogen-activated protein kinases
MDP	Mouse Diversity Panel
MDR	Multidrug resistance

MDSC	Myeloid-derived suppressor cells
MEFs	Mouse embryonic fibroblasts
MEK	Mitogen-activated protein kinase kinase
MMP	Mitochondrial membrane potential
MPD	Mouse Phenome Database
Mrgprg	Mas-related G-protein coupled receptor member G
Mrpl39	Mitochondrial ribosomal protein L39
Mrps35	Mitochondrial ribosomal protein S35
MS	Mean square
MSA	Multiple sequence alignments
mTOR	Mechanistic target of rapamycin
Mycn	v-myc myelocytomatosis viral related oncogene, neuroblastoma derived (avian)
Nadsyn1	Nicotinamide adenine dinucleotide synthetase 1
Nbas	Neuroblastoma amplified sequence
NIC	Number of independent counts
NIH	National Institutes of Health
NK	Natural killer
NKp30	Activating natural killer receptor p30
p53	Tumor protein p53
$P_{substituted}$	Probability of substituted
P_{wt}	Probability of wild type
PANTHER	Protein Analysis Through Evolutionary Relationships
PBS	Phosphate-buffered saline

PC3M	Prostate cancer cell line derived from metastatic site
PD	Pharmacodynamic
PD	Programmed death protein
PD-L	Programmed death ligand
PI3K	Phosphoinositide 3-kinase
PIN1	Peptidyl-prolyl cis-trans isomerase NIMA-interacting 1
PK	Pharmacokinetic
Ppfia1 or *PPFIA1*	Protein tyrosine phosphatase, receptor type, f polypeptide (PTPRF), interacting protein (liprin), alpha 1
Ppfibp1 or *PPFIBP1*	PTPRF interacting protein, binding protein 1 (liprin beta 1)
PROVEAN	Protein Variation Effect Analyzer
Pthlh	Parathyroid hormone-like peptide
QTG	Quantitative trait gene
QTL	Quantitative trait loci
Ras	Rat sarcoma
Rep15	RAB15 effector protein
RNA	Ribonucleic acid
RPMI	Roswell Park Memorial Institute
sAPP	Soluble amyloid precursor protein (N-terminal ectodomain)
SEM	Standard error of the mean
Shank2	SH3/ankyrin domain gene 2
siRNA	Small interfering RNA
Slit3	Slit homolog 3 (Drosophila)

SNP	Single nucleotide polymorphism
SSC	Side scatter
Stk38l	Serine/threonine kinase 38 like
subSPEC	Substitution position-specific evolutionary conservation
tacrRNA	Trans-activating crRNA
TMEM16A	Transmembrane proteins with unknown function 16
TNF	Tumor necrosis factor
T_{reg}	Regulatory T-cell
UCSC	University of California, Santa Cruz
UNC	University of North Carolina
WHO	World Health Organization
Wnt	Wingless-type mouse mammary tumor virus integration site family

CHAPTER 1[1]: THE IMMUNE SYSTEM AND ANTICANCER THERAPY: REMARKABLE ALLIES

1.1. Summary

The immune system has a crucial role in modulating tumor progression and response to therapy. For instance, the composition of intratumor immune infiltrates and polymorphisms in immunomodulating genes have been correlated with therapeutic outcomes. Furthermore, many cytotoxic and targeted anticancer agents indirectly modulate the immune system to result in therapeutic response. Given the pertinent role of the immune system in cancer pathophysiology, progression, and therapy management, we developed a novel approach that would allow for identification of genetic pathways that are involved in immune cytotoxic response. The evidence for the role of genetics in immune system and anticancer response are supported by studies that demonstrated heritability of cell-mediated immune response and function, interpatient variability in response to chemotherapeutic agents, identification of genetic variants that influence anticancer response and outcome, and heritable variants associated with cancer disease and progression. While current immunochemotherapeutic research has focused on boosting the antitumor immune response, we have approached the preservation of the immune system from an additional angle. Due to limitations in human studies, an in vitro toxicogenomic screen was developed to examine murine interstrain variability to anticancer agents in normal immune cells. Following additional analyses of this interstrain variation, genetic factors responsible for toxic

[1] Part 1.5 of this chapter is adapted from publications in *Pharmacogenomics: Methods and Protocols* (2013) and *Frontiers in Genetics* (2014).

responses to chemotherapeutics in the normal immune system were identified. These genetic biomarkers could potentially identify patients who are likely to progress in their disease or have a favorable outcome with chemotherapy and immunomodulators.

1.2. The Role of the Immune System in Cancer

In 2000, Hanahan and Weinberg revolutionized the field of cancer biology and anticancer drug therapeutics with their report on the six hallmarks of cancer.[1] All of these hallmarks result from underlying genome instability: sustained proliferative signaling, evasion of growth suppressors, resistance to cell death, activation of replicative immortality, induction of angiogenesis, and cell invasion and metastasis. Since their initial report, two more emerging hallmarks related to the tumor microenvironment have been added: deregulation of cellular energetics and avoidance of immune-driven cancer cell destruction. The latter hallmark, evasion of immune driven attack and elimination by immune cells, along with previous knowledge regarding the role of the immune system in chemotherapeutic response, highlight the important role of the immune system in antagonizing tumor development and progression as well as modulating drug response to anticancer agents.[2] In immunocompromised individuals (eg, patients with HIV or post-solid organ transplant), there is an increase in certain cancers, particularly those that are virally induced.[3] Developing tumors commonly avoid immune surveillance by inducing an immunosuppressive tumor microenvironment with regulatory T-cells, myeloid-derived suppressor cells (MDSCs), alternatively activated macrophages, and tolerant dendritic cells. Also, cancer cells paralyze infiltrating cytotoxic CD8+ T-cells and natural killer cells by secreting TNF-β and other immunosuppressive factors.[4] Thus, the induction, potency, and persistence of the patient's functional immune system is critical to combating tumor advancement.[5] This observation extends to mice genetically engineered to be

immunodeficient. Tumors are more frequent or more invasive in immunodeficient mice compared to controls, especially those lacking functional CD8+ T-cells, CD4+ Th1 cells, or natural killer cells. Thus, both the innate and adaptive immune systems affect tumor growth and surveillance in both human and animal mouse models of disease.[2,6,7]

Cancer is no longer viewed as a cell-intrinsic genetic disease, but is now well recognized as a disease with multiple etiologies resulting from a number of aberrant processes. As one of the hallmarks of cancer cells includes evasion of immunosurveillance, development of anticancer drugs that not only elicit cytotoxic response but also modulate immune cytotoxicity pathways provides a promising mechanism for combating cancer. The drug's dual action against cancer cells could lead to reduction in the dose needed to produce an anticancer effect and thus minimize unwarranted exposure to chemotherapy agents.[2,8,9]

1.3. The Role of the Immune System in Chemotherapeutic Response

In the 1890's, Coley, the father of immunotherapy and a bone surgeon at Memorial Hospital in New York, noticed that cancer patients who developed bacterial infections following surgery had better outcomes. He attributed these outcomes to stimulation of the immune system due to foreign pathogens. At first, he injected live bacteria into patients, but due to potential serious or fatal consequences, he eventually used attenuated bacteria. Coley's toxins were developed by pharmaceutical companies in the United States and used in patients up to the early 1950's, after which cytotoxic chemotherapeutics became common.[10] In the early years of cytotoxic anticancer chemotherapy, conventional anticancer agents (eg, DNA-damaging chemicals, anthracyclines, antimetabolites, and mitotic spindle poisons) were selected based on their ability to kill highly proliferating cells.[1] Because of this characteristic, these agents caused severe side effects, including myelosuppression, mucositis, and alopecia.[8]

Even with the introduction of imatinib and subsequent targeted agents, cytotoxic chemotherapy acts as a mainstay in several anticancer regimens. Beyond cytotoxicity, many agents stimulate the innate and adaptive immune systems, some of which even cause long-term memory T-cell responses leading to tumor eradication. The interaction between tumor cells and the microenvironment, including immune cells, is crucial during the genesis and progression of cancer and exposure to anticancer chemotherapeutics.[8,11]

The generation of an efficacious clinical antitumor response depends upon the successful initiation of several immune processes. In this regard, the adaptive immune system has been described as an ideal anticancer agent with features including diversity, specificity, and memory. Additionally, monitoring immune parameters may prove useful in correlating specific immune responses to patient outcomes and specific treatments.[5] These parameters may include a range of biomarkers including gene and protein expression, circulating factors, and immune cell response.[12] For instance, patients with denser T-cell, B-cell, and macrophage infiltrates in a variety of tumors have better clinical responses to traditional, cytotoxic chemotherapy compared to patients with smaller infiltrates.[8] The therapeutic effect of anthracyclines relies heavily on immune mechanisms. Doxorubicin promotes immunogenic cell death by releasing molecules such as calreticulin, which subsequently primes T-cells to modulate an antitumor Th1 phenotype, enhances the proliferation of tumor antigen specific CD8+ T-cells in tumor draining lymph nodes, and promotes tumor infiltration by stimulating IL-17-secreting γζ T-cells and IFNγ-secreting CD8+T-cells.[13,14] Another anthracycline, daunorubicin, exacerbates antigen expression by cancer cells to promote IL-2 and IFNγ synthesis by local T-cells.[15] Carboplatin and cisplatin inhibit PD-L2 expression, and cisplatin also increases the permeability of tumor cells to granzyme B.[16,17] Cyclophosphamide, though immunosuppressive at high doses, induces

immunogenic death of cancer cells, increases HLA class I expression on cancer cells, inhibits T_{reg} cells and MDSCs, restores T-cell and NK cell functions, stimulates the expansion of dendritic cells, and inhibits IL-4, IL-10, and IL-13 production at lower doses.[18-23] Similarly, mitoxantrone and oxaliplatin induce immunogenic cancer cell death. Gemcitabine increases HLA class I expression, enhances tumor antigen cross-presentation, and selectively kills MDSCs.[18,24-27] In patients who are unable to elicit an immune response following traditional cytotoxic chemotherapy, the use of immunomodulatory drugs has been suggested, which indicates optimal tumor therapies may be those that achieve synergy with cytotoxicity and immunomodulation.[28,29] Therefore, assessing the functionality of the immune system is crucial for clinical responses to cytotoxic chemotherapy.[30]

Targeted agents are more specific than conventional cytotoxic drugs, but are not fully devoid of adverse effects. In addition, the therapeutic efficacy of several targeted agents appears to partially rely on off-target mechanisms, including some that are mediated by the immune system. For instance, bevacizumab depletes circulating T_{reg} cells, repletes B- and T-cell compartments, favors the differentiation of dendritic cells, and facilitates tumor infiltration by lymphocytes.[31-33] Recent advances in immune-based therapeutic approaches have focused on boosting the adaptive antitumor immune response via various targeted approaches, including vaccination, adoptive T-cell therapy, anti-tumor antibodies, and the advent of immune checkpoint blockade agents.[34,35] Immune checkpoint blockades have been successfully targeted with anti-CTLA-4 (cytotoxic T-lymphocyte-associated antigen 4), anti-PD-1 (programmed cell death protein 1), and anti-PD-L1 (programmed cell death receptor ligand 1) inhibitors to result in durable antitumor immune responses.[36-38]

Oncologists have become increasingly interested in personalized medicine, and this has led to the identification and clinical exploitation of several biomarkers. Biomarkers for immune cell activity against cancer can be grouped into local or systemic indicators, reflecting the effect of immune cells against cancer or the generation of an antitumor humoral or cellular response by the host immune system. Local biomarkers can only be assessed at tumor sites, while systemic indicators have the potential advantage of easier assessment (ie, laboratory tests using a peripheral blood draw).[8] In addition, high levels of circulating antibodies against various antigens (eg, antibodies targeting carcinoembryonic antigen, anaplastic lymphoma kinase, zinc-binding α2-glycoprotein1, and mucin 1 in patients with colorectal cancer, anaplastic large cell lymphoma, lung adenocarcinoma, and pancreatic cancer, respectively) often correlate with improved survival.[39-42]

Systemic biomarkers, such as single nucleotide polymorphisms (SNPs) in genes coding for modulators of innate or adaptive immunity, can reveal if the host immune system has the ability to respond to malignancies or chemotherapeutics. For instance, SNPs in genes encoding interleukin 2 (IL-2), IL-8, IL-12B, and IL-1 predicted survival in a 278 patients with follicular lymphoma.[43] In patients with renal cell carcinoma, a heterozygous *IL4* genotype – 589T/C-33T/C was considered an independent prognostic risk factor.[44] SNPs influencing IL-16, IL-19, LILRA4 (leukocyte immunoglobulin-like receptor subfamily A member 4) on dendritic cells, KLRC4 (NK cell lectin-like receptor subfamily C member 4), and CD5 (a marker of T- and B-cells) have prognostic value in patients with chronic lymphocytic leukemia.[45] A SNP at position 3,790 in the 3' untranslated region of the gene *NKp30* (activating NK receptor p30) predisposes patients to an immunosuppressive isoform of the receptor, which reduces survival in patients with gastrointestinal stromal tumors independent of *KIT* mutation status that are treated with

imatinib.[46] Polymorphisms in Fcγ receptors on immune cells affect the response of several neoplasms to monoclonal antibodies. Fcγ receptors on tumor-associated lymphocytes promote cancer cell death in response to the activation of death receptors by monoclonal antibodies.[47-49] Thus, pharmacogenomics has a sizeable role in the immune response to anticancer agents.

Previous studies have noted intersubject variability in chemotherapy-induced cytotoxic responses involving the immune system.[50-52] The role of pharmacogenomics in cytotoxicity of the innate immune system has perhaps been more rigorously studied because complications such as neutropenia may result, which could lead to potentially serious consequences such as infection or dose reduction. For instance, fluorouracil and mercaptopurine may cause more severe neutropenia in individuals with genetic polymorphisms in dihydropyrimidine dehydrogenase or inosine triphosphate pyrophosphatase, respectively.[53,54] However, not much is known regarding the genetic pathways influencing the pharmacogenomics of cytotoxicity of anticancer agents within the adaptive immune system.

1.4. Clinical Trials with Immunochemotherapy

Galluzzi et al.[8] noted that three aspects were crucial for the design and clinical implementation of efficient immunochemotherapy regimens: stimulation of long-term protective T-cell responses, patient selection, and therapeutic regimens. The effects of chemotherapy on the immunosuppression of T_{reg} cells and MDSCs are transient, while immunogenic cell death inducers and vaccination protocols generate long-lasting effector memory CD8+ T cells, which persist for years and have the potential to prevent cancer relapse.[55]

In terms of patient selection, the interaction of dying cancer cells with the host immune system determines the success of immunochemotherapy. There are at least three conditions necessary for immunogenic cell death:[56] the exposure of the endoplasmic reticulum chaperone

protein calreticulin at the surface of dying cells to enhance the uptake of tumor antigens by dendritic cells,[57] the release of the non-histone chromatin-binding nuclear protein high-mobility group protein B1 (HMGB1) to stimulate antigen processing and presentation to T cells,[58] and the secretion of ATP for the activation of the inflammasome and the production of pro-inflammatory cytokines.[29] Therefore, the use of genetic biomarkers is a useful tool in identifying patients who could mount a favorable immune response following the administration of anticancer agents.[8]

Finally, the dosage, order, and interaction potential of chemotherapeutic regimens must be considered in the clinical setting.[17,59,60-62] For instance, glucocorticoids are potent immunosuppressors,[63] while histamine blockers enhance anticancer immune functions.[64] Thus, the order of administration may have a profound effect on the response to anticancer regimens. Additionally, the type of anticancer therapy given will affect the type and extent of immune system stimulation.

The development of anticancer drugs has been based upon preclinical investigations that focus on eliciting specific and nonspecific cytotoxic responses. This approach is not without complications as it results in the development of anticancer agents that have deleterious effects on healthy normal cells. Thus, a preclinical approach for assessment of anticancer agents that could both elicit cytotoxicity and modulate the immune system is warranted. This strategic approach focuses on enhancing drug efficacy by providing a dual, synergistic mechanism for killing cancer cells without exposing patients to unnecessary risks from increased drug exposure.

1.5. In Vitro Toxicogenomic Screen to Identify Genetic Mechanisms Underlying Immune Cytotoxicity Pathways

1.5.1. Genetic Mapping Analysis

The resilience of normal immune cells following exposure to toxic drugs is difficult to assess in humans, necessitating the use of an in vitro model system. Drug response and toxicity are complex, highly variable traits that are partly attributed to heredity and genetic diversity.[65] Experiments using model organisms can complement human genomic studies with unique advantages, including circumventing issues in clinical trials due to administration of toxic or narrow therapeutic index drugs, allowing for risky or invasive procedures, controlling environmental factors that influence drug response such as diet, and reducing experimental cost.[66] As we do not often have prior knowledge regarding which genes may influence drug response, hypothesis-free, genome wide association (GWA) analysis is a useful tool for identification of genetic loci significantly linked with drug response known as quantitative trait loci (QTL).

Many inbred mouse strains have been well characterized in terms of genotype and phenotype, providing effective tools for GWA studies (GWAS). The mouse genome can also be easily manipulated, making mice robust models to identify and validate genes underlying toxic and variable drug response.[67] The improved precision in QTL mapping analysis makes the identification of QTG possible. Using this approach, Guo and colleagues were able to detect the *Cyp2c29* gene, a murine homolog of human *CYP2C9*, as partially responsible for mediating warfarin metabolism in mice.[68] In another study, Harrill et al. found a strong association between a genomic region that includes *Cd44* genotype and acetaminophen-induced liver injury in the mouse. The authors subsequently performed a candidate gene study in humans and found an

association between *CD44* genetic variants and susceptibility to acetaminophen toxicity.[69] Genotype–phenotype association mapping algorithms like Efficient Mixed Model Association (EMMA) (http://mouse. cs.ucla.edu/emma)[70] and SNPster (http://snpster.gnf.org)[71,72] have been used successfully to identify QTLs. In our study, both EMMA and SNPster were used to identify QTLs associated with immune-mediated anticancer response. A graphical representation of GWA analysis resulting in QTL identification is presented in Figure 1.1.

Figure 1.1. Quantitative trait loci (QTL) analysis to identify putative genetic regions.

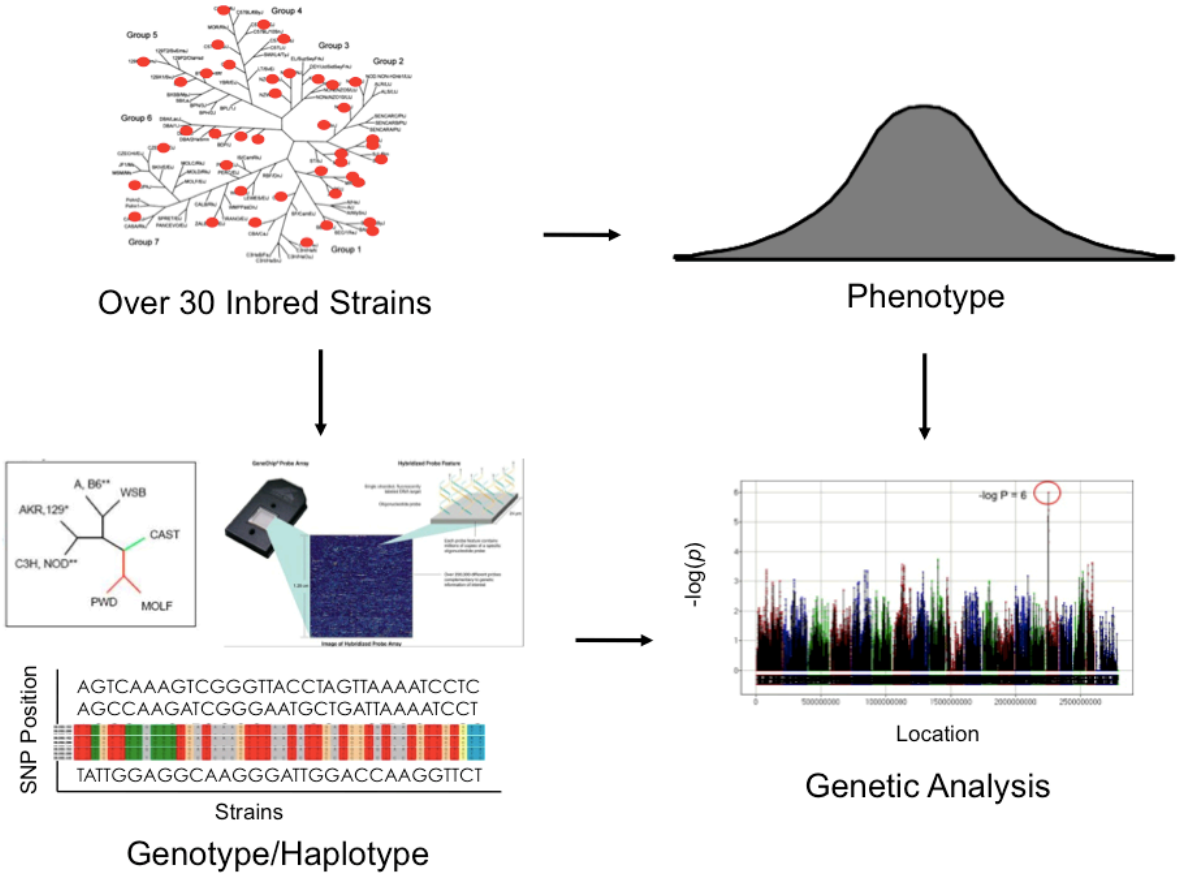

1.5.2. Assessment of Cytotoxic Response in Immune Cells

The use of in vitro cell-based assays for pharmacogenomics studies provides unprecedented opportunities for researchers to assess molecular response to drugs. In comparison to in vivo models, cell-based assays have higher assay versatility and scalability. In vitro cell-based assays can be conducted in a high-throughput fashion, allowing for multiple endpoints to be measured simultaneously. Importantly, large cell-based in vitro screens can be performed for comparison of intraindividual cellular responses to drugs and toxins, thereby making identification of drug response QTG feasible.[73] Ideally, we can measure multiple drug response phenotypes in vitro or in vivo across a panel of inbred mouse strains to identify genes underlying variable responses to drugs. Findings from mouse studies and high-throughput mouse cell-based screens can help identify which genetic variants determine positive, negative, or nonresponse to pharmacologic agents, which can then be used to develop and design subsequent clinical trials.

Conventional cytotoxicity assays typically have lower assay sensitivity and limited ability to model complex toxicity pathways because traditional cytotoxicity assays only measure a single endpoint and evaluate cytotoxic responses that occur in later stages of cell death.[74,75] Alternatively, high-throughput, high-content cell-based screening (HCS) can simultaneously measure large numbers of phenotypic endpoints in the same cell, thus facilitating detection of mechanisms underlying toxic drug response.[76] One methodology that can be used for measuring dynamic cellular processes, particularly with nonadherent cells, is flow cytometry, which combines light scatter, excitation, and fluorochrome emission to generate multiparameter data from particles and cells.[77]

Cytotoxicity studies using cells derived from inbred mouse strains have been performed,[78] but they are not typically performed in a high-content manner. Therefore, new

approaches to toxicity testing have incorporated high-throughput screening across a broad-range of *in vitro* assays to identify potential key events in response to chemical or drug treatment. Our lab previously demonstrated that genetically characterized primary cell lines from multiple inbred mouse strains can be utilized within in vitro toxicogenomic assays. As a demonstration of this approach, one candidate gene involved in rotenone sensitivity, *Cybb*, was experimentally validated in vitro and in vivo. Pathway analysis on the combined list of candidate loci across all chemicals identified a number of over-connected nodes that may serve as core regulatory points in toxicity pathways. Because this study used mouse embryonic fibroblasts (MEFs), this in vitro toxicogenomic screen was further developed in this study to test for particular drug response by cell types (eg, splenocytes), which would provide an innovative means for assessing specific drug responses on a particular system (eg, immune system) and for evaluating toxicities of particular classes of compounds (eg, cytotoxic and targeted anticancer agents).[79] A detailed description of the in vitro toxicogenomic screen is provided in Chapter 2.

1.6. Purpose of Study

The role of the immune system in cancer development and progression as well as in anticancer drug response have been well recognized, further providing a new avenue for developing drugs that both mediate cytotoxicity and stimulate immune response. Studies aimed at identifying biomarkers that are involved in immune-cytotoxicity pathways are needed to advance the development and use of drugs with dual action or bidirectional effects on these pathways. GWA analysis provides a hypothesis-free approach for investigating this anticancer-immune interaction, resulting in the identification of genetic biomarkers that could be useful for drug development or clinical application. Animal mouse studies offer several advantages over human studies in identifying genes associated with anticancer drug responses, and these

advantages include the ability to control for dietary and environmental effects as well as the use of mouse populations with well-characterized and well-maintained genetic and genomic structure. Notably, inbred mouse strains have been previously used to model the wide genetic and phenotypic variability found in human populations,[80,81] enabling high-throughput screens that capture a broad range of response variance.

In vitro toxicogenomic screens allow investigation of immune-cytotoxicity pathways on a cellular level. Unlike human cancer cell lines, murine immune cells provide a suitable approach for studying the interaction between anticancer drugs and the immune system under normal conditions. In addition, the capacity to identify genes that modify the response to chemicals at a cellular level can provide insights into human toxicity mechanisms. Lastly, in vitro toxicogenomic studies can provide useful information during the drug development and clinical trial phases, and this information can be used to identify compounds that are likely to be effective in producing immune cytotoxic effects as well as target patient populations who are likely to respond or less likely to display toxicity with the novel agent. This approach minimizes drug exposure to patients who are less likely to benefit from the new drug. Additionally, conducting clinical trials in a targeted patient population can make research efforts more cost-effective. Fewer patients may be required to observe an effect, which will reduce cost and shorten the time required to complete the study.[73]

1.7. Specific Aims

It has been predicted that the future of cancer treatment will involve precision medicine approaches combining targeted therapy or chemotherapies with immunomodulation.[82] This study was conducted to develop an in vitro toxicogenomic screen that would facilitate identification of genetic biomarkers that are involved in immune cytotoxicity pathways.

Our overall hypothesis is that we will identify genes and genetic pathways underlying the variable toxicity responses of normal immune function cells (i.e., B-cells, T-cells, monocytes, and granulocytes) to anticancer agents. Our hypothesis will be addressed by the following specific aims:

Aim 1. Develop a multiplexed assay set for measuring toxicity responses to anti-lymphoma agents in immune function cells (ie, B-cells, T-cells, monocytes, and granulocytes).

Hypothesis: We will develop a robust, replicable, multiplexed assay that can accurately describe toxicity response using flow cytometry.

Objective: To develop a standardized flow cytometry assay for the detection of immune function cells (ie, B-cells, T-cells, monocytes, and granulocytes) derived from isogenic mice strains with the quantification of various cellular health parameters (eg, caspase activity, mitochondrial health, and cellular viability).

Rationale: Recent evidence indicates the host immune system contributes to therapeutic outcomes of anticancer agents.[8] Evaluating toxic effects on normal immune cells will innovatively elucidate the role of immune cells in mediating anticancer response. Therefore, we aim to investigate the toxic effects of chemotherapeutics on immune cells using a high-throughput flow cytometry screen with genetically well-defined cells from inbred mouse strains. Flow cytometry combines light scattering, excitation, and fluorochrome emission to generate multiparameter data from heterogeneous cell populations. The effects of chemotherapeutics on specific immune cell populations will be quantified by interrogating multiple cellular parameters (*e.g.*, caspase activity, mitochondrial health, and cellular viability).

Aim 2. Measure the toxic cellular assay endpoints on immune function cells from a set of thirty-five divergent inbred mouse strains.

Hypothesis: Using this diverse genetic background, we will observe a differential response to cytotoxic drugs. From this data, we can identify variable interstrain sensitivity along a spectrum of cytotoxicity to these compounds. Significant, differential interstrain differences will occur in cell viability, mitochondrial membrane potential (MMP), and caspase activity among different immune cell types following administration of anti-lymphoma medications. These data will be used as quantitative traits for genome wide association analyses.

Objective: To collect phenotypes for genetic analysis and to identify variable interstrain sensitivity along a spectrum of cytotoxicity to anti-lymphoma compounds.

Rationale: The use of animal models to investigate pharmacologic responses has been widespread. However, there are few examples of genome wide association studies for pharmacogenetic studies.[68,69] This deficiency is largely due to the lack of an appropriate model system and suitable tools to analyze the model. We have championed the use of inbred mouse strains and developed methodological approaches to make this process a viable approach. The inbred mouse strains (thirty-five strains) provide adequate power for genome wide analysis, which is why the preliminary data from this aim will be used to identify genetic loci that underlie toxicity phenotypes.

Aim 3. Using genome wide association studies, we will identify loci that contribute to the sensitivity of the described anti-lymphoma agents.

Hypothesis: Using the data from specific aim 2, we can identify genetic loci that contribute to differences in cytotoxicity response. From these genomic regions, we will prioritize candidate genes for further study.

Objective: To identify and validate genetic determinants of toxicological insult on immune cells.

Rationale: Splenocytes are derived from mice in the Jackson Laboratory Mouse Diversity Panel (MDP). Association mapping in this fixed and inbred population utilizes existing dense maps of SNP genotype information, providing precision (greater than 1 to 2 Mb) in localizing QTL.

REFERENCES

1. Hanahan D, Weinberg RA. The hallmarks of cancer. *Cell*. 2000;100:57–70.

2. Hanahan D, Weinberg RA. Hallmarks of cancer: the next generation. *Cell*. 2011;144(5):646–674. doi:10.1016/j.cell.2011.02.013.

3. Vajdic CM, van Leeuwen MT. Cancer incidence and risk factors after solid organ transplantation. *Int J Cancer*. 2009;125(8):1747–1754. doi:10.1002/ijc.24439.

4. Alizadeh D, Larmonier N. Chemotherapeutic targeting of cancer-induced immunosuppressive cells. *Cancer Res*. 2014;74(10):2663–2668. doi:10.1158/0008-5472.CAN-14-0301.

5. Raval RR, Sharabi, AB, Walker AJ, CG D, Padmanee S. Tumor immunology and cancer immunotherapy: summary of the 2013 SITC primer. *J Immunother Cancer*. 2014;2:2014.

6. Teng MWL, Swann JB, Koebel CM, Schreiber RD, Smyth MJ. Immune-mediated dormancy: an equilibrium with cancer. *J Leukoc Biol*. 2008;84(4):988–993. doi:10.1189/jlb.1107774.

7. Kim M-Y, Oskarsson T, Acharyya S, et al. Tumor self-seeding by circulating cancer cells. *Cell*. 2009;139(7):1315–1326. doi:10.1016/j.cell.2009.11.025.

8. Galluzzi L, Senovilla L, Zitvogel L, Kroemer G. The secret ally: immunostimulation by anticancer drugs. *Nat Rev Drug Discov.* 2012:1–19. doi:10.1038/nrd3626.

9. Vesely MD, Kershaw MH, Schreiber RD, Smyth MJ. Natural innate and adaptive immunity to cancer. *Annu Rev Immunol*. 2011;29(1):235–271. doi:10.1146/annurev-immunol-031210-101324.

10. Galon J, Angell HK, Bedognetti D, Marincola FM. The continuum of cancer immunosurveillance: prognostic, predictive, and mechanistic signatures. *Immunity*. 2013;39(1):11–26. doi:10.1016/j.immuni.2013.07.008.

11. Blankenstein T. The role of tumor stroma in the interaction between tumor and immune system. *Curr Opin Immunol*. 2005;17(2):180–186. doi:10.1016/j.coi.2005.01.008.

12. Schilsky RL. Personalized medicine in oncology: the future is now. *Nat Rev Drug Discov*. 2010;9:363–366.

13. Ma Y, Aymeric L, Locher C, et al. Contribution of IL-17-producing gamma delta T cells to the efficacy of anticancer chemotherapy. *J Exp Med*. 2011;208(3):491–503. doi:10.1084/jem.20100269.

14. Mattarollo SR, Loi S, Duret H, Ma Y, Zitvogel L, Smyth MJ. Pivotal role of innate and adaptive immunity in anthracycline chemotherapy of established tumors. *Cancer Res*. 2011;71(14):4809–4820. doi:10.1158/0008-5472.CAN-11-0753.

15. Haggerty TJ, Dunn IS, Rose LB, et al. Topoisomerase inhibitors modulate expression of melanocytic antigens and enhance T cell recognition of tumor cells. *Cancer Immunol Immunother*. 2010;60(1):133–144. doi:10.1007/s00262-010-0926-x.

16. Lesterhuis WJ, Punt CJA, Hato SV, et al. Platinum-based drugs disrupt STAT6-mediated suppression of immune responses against cancer in humans and mice. *J Clin Invest*. 2011;121(8):3100–3108. doi:10.1172/JCI43656.

17. Ramakrishnan R, Assudani D, Nagaraj S, et al. Chemotherapy enhances tumor cell susceptibility to CTL-mediated killing during cancer immunotherapy in mice. *J Clin Invest*. 2010;120(4):1111–1124. doi:10.1172/JCI40269.

18. Liu WM, Fowler DW, Smith P, Dalgleish AG. Pre-treatment with chemotherapy can enhance the antigenicity and immunogenicity of tumours by promoting adaptive immune responses. *Br J Cancer*. 2009;102(1):115–123. doi:10.1038/sj.bjc.6605465.

19. Weiner HL, Cohen JA. Treatment of multiple sclerosis with cyclophosphamide: critical review of clinical and immunologic effects. *Multiple Sclerosis*. 2002;8(2):142–154. doi:10.1191/1352458502ms790oa.

20. Medina-Echeverz J, Fioravanti J, Zabala M, Ardaiz N, Prieto J, Berraondo P. Successful colon cancer eradication after chemoimmunotherapy is associated with profound phenotypic change of intratumoral myeloid cells. *J Immunol*. 2011;186(2):807–815. doi:10.4049/jimmunol.1001483.

21. Ghiringhelli F, Ménard C, Puig PE, et al. Metronomic cyclophosphamide regimen selectively depletes CD4+CD25+ regulatory T cells and restores T and NK effector functions in end stage cancer patients. *Cancer Immunol Immunother*. 2006;56(5):641–648. doi:10.1007/s00262-006-0225-8.

22. Taieb J, Chaput N, Schartz N, et al. Chemoimmunotherapy of tumors: cyclophosphamide synergizes with exosome based vaccines. *J Immunol*. 2006;176(5):2722–2729. doi:10.4049/jimmunol.176.5.2722.

23. Viaud S, Flament C, Zoubir M, et al. Cyclophosphamide induces differentiation of Th17 cells in cancer patients. *Cancer Res*. 2011;71(3):661–665. doi:10.1158/0008-5472.CAN-10-1259.

24. Nowak AK, Lake RA, Marzo AL, et al. Induction of tumor cell apoptosis in vivo increases tumor antigen cross-presentation, cross-priming rather than cross-tolerizing host tumor-specific CD8 T cells. *J Immunol*. 2003;170(10):4905–4913. doi:10.4049/jimmunol.170.10.4905.

25. Nowak AK, Robinson BWS, Lake RA. Synergy between chemotherapy and immunotherapy in the treatment of established murine solid tumors. *Cancer Res*. 2003;63:4490–4496.

26. Mundy-Bosse BL, Lesinski GB, Jaime-Ramirez AC, et al. Myeloid-derived suppressor cell inhibition of the IFN response in tumor-bearing mice. *Cancer Res*. 2011;71:5101–5110. doi:10.1158/0008-5472.CAN-10-2670.

27. Vincent J, Mignot G, Chalmin F, et al. 5-fluorouracil selectively kills tumor-associated myeloid-derived suppressor cells resulting in enhanced T cell-dependent antitumor immunity. *Cancer Res*. 2010;70(8):3052–3061. doi:10.1158/0008-5472.CAN-09-3690.

28. Hodge JW, Garnett CT, Farsaci B, et al. Chemotherapy-induced immunogenic modulation of tumor cells enhances killing by cytotoxic T lymphocytes and is distinct from immunogenic cell death. *Int J Cancer*. 2013;133(3):624–636. doi:10.1002/ijc.28070.

29. Ghiringhelli F, Apetoh L, Tesniere A, et al. Activation of the NLRP3 inflammasome in dendritic cells induces IL-1β–dependent adaptive immunity against tumors. *Nat Med*. 2009;15(10):1170–1178. doi:10.1038/nm.2028.

30. Vanneman M, Dranoff G. Combining immunotherapy and targeted therapies in cancer treatment. *Nat Rev Cancer*. 2012;12(4):237–251. doi:10.1038/nrc3237.

31. Wada J, Suzuki H, Fuchino R, et al. The contribution of vascular endothelial growth factor to the induction of regulatory T-cells in malignant effusions. *Anticancer Res*. 2009:1–8.

32. Shrimali RK, Yu Z, Theoret MR, Chinnasamy D, Restifo NP, Rosenberg SA. Antiangiogenic agents can increase lymphocyte infiltration into tumor and enhance the effectiveness of adoptive immunotherapy of cancer. *Cancer Res*. 2010;70(15):6171–6180. doi:10.1158/0008-5472.CAN-10-0153.

33. Osada T, Chong G, Tansik R, et al. The effect of anti-VEGF therapy on immature myeloid cell and dendritic cells in cancer patients. *Cancer Immunol Immunother*. 2008;57(8):1115–1124. doi:10.1007/s00262-007-0441-x.

34. Kalos M, June CH. Adoptive T cell transfer for cancer immunotherapy in the era of synthetic biology. *Immunity*. 2013;39(1):49–60. doi:10.1016/j.immuni.2013.07.002.

35. Kantoff PW, Higano CS, Shore ND, et al. Sipuleucel-T immunotherapy for castration-resistant prostate cancer. *N Engl J Med*. 2012;363(5):411–422. doi:10.1056/NEJMoa1001294).

36. Hodi FS, O'Day SJ, McDermott DF, et al. Improved survival with ipilimumab in patients with metastatic melanoma. *N Engl J Med*. 2010;363(8):711–723. doi:10.1056/NEJMoa1003466.

37. Topalian SL, Hodi FS, Brahmer JR, et al. Safety, activity, and immune correlates of anti–PD-1 antibody in cancer. *N Engl J Med*. 2012;366(26):2443–2454. doi:10.1056/NEJMoa1200690.

38. Brahmer JR, Tykodi SS, Chow LQM, et al. Safety and activity of anti–PD-L1 antibody in patients with advanced cancer. *N Engl J Med*. 2012;366(26):2455–2465. doi:10.1056/NEJMoa1200694.

39. Wu XJ, Fang YJ, Lin JZ, et al. Circulating antibodies to carcinoembryonic antigen related to improved recurrence-free survival of patients with colorectal carcinoma. *J Int Med Res*. 2011;39(3):838–845. doi:10.1177/147323001103900317.

40. Ait-Tahar K, Damm-Welk C, Burkhardt B, et al. Correlation of the autoantibody response to the ALK oncoantigen in pediatric anaplastic lymphoma kinase-positive anaplastic large cell lymphoma with tumor dissemination and relapse risk. *Blood*. 2010;115(16):3314–3319. doi:10.1182/blood-2009-11-251892.

41. Albertus DL, Seder CW, Chen G, et al. AZGP1 autoantibody predicts survival and histone deacetylase inhibitors increase expression in lung adenocarcinoma. *J Thorac Oncol*. 2008;3(11):1236–1244.

42. Hamanaka Y, Suehiro Y, Fukui M, Shikichi K, Imai K, Hinoda Y. Circulating anti-MUC1 IgG antibodies as a favorable prognostic factor for pancreatic cancer. *Int J Cancer*. 2002;103(1):97–100. doi:10.1002/ijc.10801.

43. Cerhan JR, Wang S, Maurer MJ, et al. Prognostic significance of host immune gene polymorphisms in follicular lymphoma survival. *Blood*. 2007;109(12):5439–5446. doi:10.1182/blood-2006-11-058040.

44. Kleinrath T, Gassner C, Lackner P, Thurnher M, Ramoner R. Interleukin-4 promoter polymorphisms: a genetic prognostic factor for survival in metastatic renal cell carcinoma. *J Clin Oncol*. 2007;25(7):845–851. doi:10.1200/JCO.2006.07.8154.

45. Sellick GS, Wade R, Richards S, Oscier DG, Catovsky D, Houlston RS. Scan of 977 nonsynonymous SNPs in CLL4 trial patients for the identification of genetic variants influencing prognosis. *Blood*. 2007;111(3):1625–1633. doi:10.1182/blood-2007-08-110130.

46. Delahaye NF, Rusakiewicz S, Martins I, et al. Alternatively spliced NKp30 isoforms affect the prognosis of gastrointestinal stromal tumors. *Nat Med*. 2011;17(6):700–707. doi:10.1038/nm.2366.

47. Bibeau F, Lopez-Crapez E, Di Fiore F, et al. Impact of Fc RIIa-Fc RIIIa polymorphisms and KRAS mutations on the clinical outcome of patients with metastatic colorectal cancer treated with cetuximab plus irinotecan. *J Clin Oncol*. 2009;27(7):1122–1129. doi:10.1200/JCO.2008.18.0463.

48. Ferris RL, Jaffee EM, Ferrone S. Tumor antigen-targeted, monoclonal antibody-based immunotherapy: clinical response, cellular immunity, and immunoescape. *J Clin Oncol*. 2010;28(28):4390–4399. doi:10.1200/JCO.2009.27.6360.

49. Mellstedt. FcγR polymorphisms and clinical outcome in colorectal cancer patients receiving passive or active antibody treatment. *Int J Oncol*. 2010;37(6). doi:10.3892/ijo_00000814.

50. Kreisel D, Gelman AE, Higashikubo R, et al. Strain-specific variation in murine natural killer gene complex contributes to differences in immunosurveillance for urethane-induced lung cancer. *Cancer Res*. 2012;72(17):4311–4317. doi:10.1158/0008-5472.CAN-12-0908.

51. Liu S, Kurzrock R. Toxicity of targeted therapy: implications for response and impact of genetic polymorphisms. *Cancer Treat Rev*. 2014;40(7):883–891. doi:10.1016/j.ctrv.2014.05.003.

52. Ross C, Visscher H, Rassekh SR, et al. Pharmacogenomics of serious adverse drug reactions in pediatric oncology. *J Popul Ther Clin Pharmacol*. 2011;18(1):e134–e151.

53. van Kuilenburg A, Haasjes J, Richel DJ, et al. Clinical implications of dihydropyrimidine dehydrogenase (DPD) deficiency in patients with severe 5-fluorouracil-associated toxicity: identification of new mutations in the *DPD* gene. *Clin Cancer Res*. 2000;6:4705–4712.

54. Stocco G, Cheok MH, Crews KR, et al. Genetic polymorphism of inosine triphosphate pyrophosphatase is a determinant of mercaptopurine metabolism and toxicity during treatment for acute lymphoblastic leukemia. *Clin Pharmacol Ther*. 2008;85(2):164–172. doi:10.1038/clpt.2008.154.

55. Zitvogel L, Kepp O, Senovilla L, Menger L, Chaput N, Kroemer G. Immunogenic tumor cell death for optimal anticancer therapy: the calreticulin exposure pathway. *Clin Cancer Res*. 2010;16(12):3100–3104. doi:10.1158/1078-0432.CCR-09-2891.

56. Kepp O, Galluzzi L, Martins I, et al. Molecular determinants of immunogenic cell death elicited by anticancer chemotherapy. *Cancer Metastasis Rev*. 2011;30(1):61–69. doi:10.1007/s10555-011-9273-4.

57. Obeid M, Tesniere A, Ghiringhelli F, et al. Calreticulin exposure dictates the immunogenicity of cancer cell death. *Nat Med*. 2006;13(1):54–61. doi:10.1038/nm1523.

58. Apetoh L, Ghiringhelli F, Tesniere A, et al. Toll-like receptor 4–dependent contribution of the immune system to anticancer chemotherapy and radiotherapy. *Nat Med*. 2007;13(9):1050–1059. doi:10.1038/nm1622.

59. Emens LA, Asquith JM, Leatherman JM, et al. Timed sequential treatment with cyclophosphamide, doxorubicin, and an allogeneic granulocyte-macrophage colony-stimulating factor-secreting breast tumor vaccine: a chemotherapy dose-ranging factorial study of safety and immune activation. *J Clin Oncol*. 2009;27(35):5911–5918. doi:10.1200/JCO.2009.23.3494.

60. Chakraborty M, Wansley EK, Carrasquillo JA, et al. The use of chelated radionuclide (samarium-153-ethylenediaminetetramethylenephosphonate) to modulate phenotype of tumor cells and enhance T cell-mediated killing. *Clin Cancer Res*. 2008;14(13):4241–4249. doi:10.1158/1078-0432.CCR-08-0335.

61. Lynch TJ, Bondarenko I, Luft A, et al. Ipilimumab in combination with paclitaxel and carboplatin as first-line treatment in stage IIIB/IV non-small-cell lung cancer: results from a randomized, double-blind, multicenter phase II study. *J Clin Oncol*. 2012;30(17):2046–2054. doi:10.1200/JCO.2011.38.4032.

62. Gabrilovich DI. Combination of chemotherapy and immunotherapy for cancer: a paradigm revisited. *Lancet Oncol*. 2007;8(1):2–3. doi:10.1016/S1470-2045(06)70985-8.

63. Marx J. How the glucocorticoids suppress immunity. *Science*. 1995;270(5234):232–233.

64. Kubecova M, Kolostova K, Pinterova D, Kacprzak G, Bobek V. Cimetidine: an anticancer drug? *Eur J Pharm Sci*. 2011;42(5):439–444. doi:10.1016/j.ejps.2011.02.004.

65. Zhang W, Dolan ME. Use of cell lines in the investigation of pharmacogenetic loci. *Curr Pharm Des*. 2009;15(32):3782–3795.

66. Bogaards J, Bertrand M, Jackson P, et al. Determining the best animal model for human cytochrome P450 activities: a comparison of mouse, rat, rabbit, dog, micropig, monkey and man. *Xenobiotica*. 2000.

67. Silver L. *Mouse Genetics: Concepts and Applications*. New York: Oxford University Press; 1995.

68. Guo Y, Weller P, Farrell E, et al. In silico pharmacogenetics: warfarin metabolism. *Nat Biotechnol*. 2006;24(5):531–536.

69. Harrill AH, Watkins PB, Su S, et al. Mouse population-guided resequencing reveals that variants in CD44 contribute to acetaminophen-induced liver injury in humans. *Genome Res*. 2009;19(9):1507–1515. doi:10.1101/gr.090241.108.

70. Kang HM, Zaitlen NA, Wade CM, et al. Efficient control of population structure in model organism association mapping. *Genetics*. 2008;178(3):1709–1723. doi:10.1534/genetics.107.080101.

71. McClurg P, Pletcher MT, Wiltshire T, Su AI. Comparative analysis of haplotype association mapping algorithms. *BMC Bioinformatics*. 2006;7(1):61. doi:10.1186/1471-2105-7-61.

72. Pletcher MT, McClurg P, Batalov S, et al. Use of a dense single nucleotide polymorphism map for in silico mapping in the mouse. *Plos Biol*. 2004;2(12):e393. doi:10.1371/journal.pbio.0020393.

73. Frick A, Suzuki O, Butz N, Chan E, Wiltshire T. In vitro and in vivo mouse models for pharmacogenetic studies. In: Innocenti F, Schaik RHN, eds. *Pharmacogenomics*.Vol 1015. Methods in Molecular Biology. Totowa: Humana Press; 2013:263–278. doi:10.1007/978-1-62703-435-7_17.

74. Olson H. Concordance of the toxicity of pharmaceuticals in humans and animals. *Regul Toxicol Pharmacol*. 2000;32(1):65–67.

75. Jaeschke H, Gores GJ, Cederbaum AI, Hinson JA, Pessayre D, Lemasters JJ. Mechanisms of hepatotoxicity. *Toxicol Sci*. 2002;65:166–176.

76. Abraham VC, Towne DL, Waring JF, Warrior U, Burns DJ. Application of a high-content multiparameter cytotoxicity assay to prioritize compounds based on toxicity potential in humans. *J Biomol Screen*. 2008;13(6).

77. Shapiro H. *Practical Flow Cytometry*. Hoboken: Wiley; 2003.

78. Watters JW, Kloss EF, Link DC, Graubert TA, McLeod H. A mouse-based strategy for cyclophosphamide pharmacogenomic discovery. *J Appl Physiol*. 2003;95:1352–1360. doi:10.1152/japplphysiol.00214.2003.

79. Wiltshire T. A cellular genetics approach identifies gene-drug interactions and pinpoints drug toxicity pathway nodes. *Front Genet*. 2014:1–13. doi:10.3389/fgene.2014.00272/abstract.

80. Shanks N, Greek R, Greek J. Are animal models predictive for humans? *Philos Ethics Humanit Med*. 2009;4(1):2. doi:10.1186/1747-5341-4-2.

81. Paigen K, Eppig JT. A mouse phenome project. *Mamm Genome*. 2014;11(9):715–717. doi:10.1007/s003350010152.

82. Heuvers ME, Aerts JG, Cornelissen R, Groen H, Hoogsteden HC, Hegmans JP. Patient-tailored modulation of the immune system may revolutionize future lung cancer treatment. *BMC Cancer*. 2012;12(1):580–591. doi:10.1186/1471-2407-12-580.

CHAPTER 2[2]: IMMUNE CELL-BASED SCREENING ASSAY FOR RESPONSE TO ANTI-CANCER AGENTS: APPLICATIONS IN PHARMACOGENOMICS

2.1. Overview

Background: Interpatient variability in immune and chemotherapeutic cytotoxic responses is likely due to complex genetic differences and is difficult to ascertain in humans. Through the use of a panel of genetically diverse mouse inbred strains, we developed a drug screening platform aimed at examining interstrain differences in viability on normal, noncancerous immune cells following chemotherapeutic cytotoxic insult. Drug effects were investigated by comparing selective chemotherapeutic agents, such as BEZ-235 and selumetinib, against conventional cytotoxic agents targeting multiple pathways, including doxorubicin and idarubicin.

Methods: Splenocytes were isolated from 36 isogenic strains of mice using standard procedures. Of note, the splenocytes were not stimulated to avoid attributing responses to pathways involved with cellular stimulation rather than toxicity. Cells were incubated with compounds on a 9-point logarithmic dosing scale ranging from 15 nM to 100 μM (37°C, 5% CO_2). At 4 h post-treatment, cells were labeled with antibodies and physiological indicator dyes and fixed with 4% paraformaldehyde. Cellular phenotypes (eg, viability) were collected and analyzed using flow cytometry. Dose-response curves with response normalized to the zero dose as a function of log concentration were generated using GraphPad Prism 6.

---

[2] This chapter is published in *The Journal of Pharmacogenomics and Personalized Medicine* (2014).

Results: Phenotypes were quantified using flow cytometry, yielding interstrain variation for measured endpoints in different immune cells. The flow cytometry assays produced over 16,000 data points that were used to generate dose-response curves. The more targeted agents, BEZ-235 and selumetinib, were less toxic to immune cells than the anthracycline agents. The calculated heritability for the viability of immune cells was higher with anthracyclines than the novel agents, making them better suited for downstream genetic analysis.

Conclusions: Using this approach, we identified cell lines of variable sensitivity to chemotherapeutic agents and aimed to identify robust, replicable endpoints of cellular response to drugs that provide the starting point for identifying candidate genes and cellular toxicity pathways for future validation in human studies.

Keywords: immunomodulation, cytotoxicity, chemotherapy, precision medicine

2.2. Introduction

While the role of the immune system in cancer development is well established, its role in response to chemotherapeutic agents remains more elusive. Recent studies have demonstrated that several cytotoxic chemotherapeutics work in concert with the immune system.[1] These immunomodulatory effects may occur through direct action on tumor cells or on cells of the immune system.[2,3] For example, anthracyclines and oxaliplatin generate immunogenic responses via induction of calreticulin on tumor cells, an action necessary for the therapeutic efficacy of these agents.[4,5] Additionally, docetaxel has been reported to modulate $CD4^+$, $CD8^+$, $CD19^+$, natural killer T-cells, and T-regulatory populations in nontumor-bearing mice.[6,7] This immunomodulation acts synergistically with chemotherapeutic cytotoxic effects and has been shown to improve outcomes following treatment.[8-10] For instance, increased amounts of pre-treatment tumor infiltrating lymphocytes and post-treatment immune activation have been linked

to better outcomes in patients with breast and colorectal cancer.[11] In patients who are unable to elicit an immune response following traditional cytotoxic chemotherapy, the use of immunomodulatory drugs has been suggested. Thus, optimal tumor therapies may be those that achieve synergy with cytotoxicity and immunomodulation.[6,12]

Previous studies have noted intersubject variability in immune and chemotherapy-induced cytotoxic responses, partly due to genetic differences.[13-15] The role of pharmacogenomics in cytotoxicity of the innate immune system has perhaps been more rigorously studied because complications such as neutropenia may result, leading to potentially deadly consequences such as infection or dose reduction. For instance, fluorouracil and mercaptopurine may cause more severe neutropenia in individuals with genetic polymorphisms in dihydropyrimidine dehydrogenase or inosine triphosphate pyrophosphatase, respectively.[16,17] However, the role of pharmacogenomics in cytotoxicity of the adaptive immune system requires further investigation, as both synergy and drug-induced toxicities have been observed with regards to the effects of chemotherapy agents on the immune system.

The effects of chemotherapy agents in the normal immune system are hard to quantify in humans. We therefore developed a drug-screening platform using genetically diverse inbred mouse strains to examine novel mechanisms underlying interstrain, chemotherapy-induced cytotoxic responses on functional immune cells. Murine splenocytes were isolated from a panel of genetically diverse mouse inbred strains, in which genotypes have been well characterized. This in vitro mouse model has the additional benefits of maintaining tight experimental control while circumventing the use of cytotoxic agents in humans and enabling an interrogation of the genetic components of cytotoxicity in the context of a normal functioning immune system.[18,19] In the present study, cellular health phenotypes (ie, viability, caspase-3/7 activation, and

mitochondrial health) were quantified from these primary mouse splenocytes using flow cytometry, yielding interstrain variation for measured endpoints in different immune cells (ie, T-cells, B-cells, monocytes, and granulocytes). Effects were investigated by comparing more selective chemotherapeutic agents, including a dual PI3K/mTOR inhibitor and a MEK inhibitor, against conventional cytotoxic, immunomodulatory anthracycline agents, including doxorubicin and idarubicin. BEZ-235 and selumetinib are currently in clinical trials,[20] and dual PI3K/mTOR and MEK inhibition provides broad antitumor activity in mouse models.[21] These drugs have the potential to be used in regimens including doxorubicin and idarubicin for the treatment of solid and hematological tumors,[20] and these targeted agents have been reported to have potential immunomodulatory effects. For instance, selumetinib has been shown to inhibit the release of cytokines, including IL-1, IL-6 and TNF,[22] and BEZ-235 is under investigation for enhancing the immune response to vaccination per the WHO International Clinical Trials Registry Platform[23]. In clinical trials, these drugs have greatly reduced side effects (eg, rash, fatigue, diarrhea, and peripheral edema) in comparison to traditional cytotoxic agents.[24,25] By using these phenotypes, genes and genetic pathways that underlie or modulate the variable toxicity responses of functional immune cells to chemotherapeutics can potentially be identified.

2.3. Material and Methods

2.3.1. Animals

Thirty-six male inbred mouse strains (129S1/SvImJ, 129X1/SvJ, A/J, AKR/J, BALB/cByJ, BTBR T^{+} *Itpr3*^{tf}*/J*, BUB/BnJ, C3H/HeJ, C57BLKS/J, C57BL/6J, C57BR/cdJ, C58/J, CBA/J, CZECHII/EiJ, DBA/2J, FVB/NJ, I/LnJ, KK/HiJ, LG/J, LP/J, MA/MyJ, NOD/LtJ, NON/LtJ, NZB/BINJ, NZO/HiLtJ, NZW/LacJ, PERA/EiJ, PL/J, PWD/PhJ, PWK/PhJ, RIIIS/J, SEA/GnJ, SJL/J, SM/J, SWR/J, and WSB/EiJ), aged 10-12 weeks, were obtained from The

Jackson Laboratory (Bar Harbor, ME). This panel of isogenic mice was chosen based on priority strains from the Mouse Diversity Panel (MDP) panel.[26] Four mice were used per strain. Male mice were housed four per cage in polycarbonate cages on a 12 h light/dark cycle (lights on at 0700 hours) with access to food and water ad libitum. All procedures were approved by the Institutional Animal Care and Use Committee and followed the guidelines set forth by the National Institutes of Health Guide for the Care and Use of Laboratory Animals.

2.3.2. Tissue Preparation

Following cervical dislocation, spleens were excised from the mice, and cells obtained from tissues were dissociated into a single-cell suspension by mechanical means (ie, homogenized in phosphate-buffered saline (PBS, Cellgro, Manassas, VA) with 1% v/v fetal bovine serum (FBS, Gibco, Grand Island, NY) using frosted glass slides (Thermo Fisher Scientific, Pittsburgh, PA) in a tissue culture dish (TPP, Trasadingen, Switzerland)). Cells were transferred from the tissue culture dish to a 5 mL polystyrene round-bottom tube (BD Biosciences, San Jose, CA), centrifuged at 400xg for 5 min, resuspended in ACK lysing solution (Gibco, Grand Island, NY) to avoid red blood cell interference during flow cytometry, and incubated for 10 min at room temperature in the dark. Cells were centrifuged at 400xg for 5 min and resuspended in RPMI-1640 buffer (Cellgro, Manassas, VA) supplemented with 10% v/v FBS, 0.1% v/v 2-mercaptoethanol (MP Biomedicals, Santa Ana, CA), 1% v/v sodium pyruvate (Cellgro, Manassas, VA), 1% v/v non-essential amino acids (Cellgro, Manassas, VA), and 1% penicillin G/streptomycin solution (Cellgro, Manassas, VA). Cells were aliquoted into 96-well, round-bottom plates (Globe Scientific Inc., Paramus, NJ.) at a density of 100,000 cells per mL.

2.3.3. Drug Treatment

Cells in 100 μL supplemented media per well were incubated at 37°C and 5% CO_2 with doxorubicin (Sigma-Aldrich, Milwaukee, WI), idarubicin (Sigma-Aldrich, Milwaukee, WI), BEZ-235 (provided by Novartis, Inc.), or selumetinib (ChemieTek, Indianapolis, IN). Each compound was plated using a 9-point logarithmic concentration scale ranging from 15 nM to 100 μM. Stock solutions of doxorubicin and idarubicin (10 mM) were prepared in water, while stock solutions of BEZ-235 and selumetinib (25 mM and 75 mM respectively) were prepared in 100% DMSO (Sigma-Aldrich, Milwaukee, WI). Subsequent dilutions and controls were prepared to account for the inclusion of water or DMSO in the stock solution.

2.3.4. Cell Labeling

At 4 hours post-treatment, cells were washed in wash buffer (PBS with 1% v/v FBS) and incubated for 30 min at 37°C and 5% CO_2 with the following physiological indicator dyes: 125 nM Mitotracker® Deep Red (Invitrogen, Carlsbad, CA) for mitochondrial heath, 3.75 μM CellEvent™ Caspase-3/7 Green Detection Reagent (Invitrogen, Carlsbad, CA) for caspase-3/7 activation, and 3.75 μL (0.19 μg) 7-AAD (BD Biosciences, San Jose, CA) per 100 μL well for viability. The Mitotracker® Deep Red is a mitochondrion-selective stain that is concentrated by active mitochondria and well retained during cell fixation and permeabilization due to a mildly thiol-reactive chloromethyl moiety. The CellEvent™ Caspase-3/7 Green Detection Reagent consists of a four amino acid peptide (DEVD) conjugated to a nucleic acid binding dye that is nonfluorescent until the peptide is cleaved by caspase-3/7. 7-AAD is a fluorescent intercalator that undergoes a spectral shift when associated with DNA.[27] Cells were centrifuged at 400xg for 5 min, washed, and incubated at 4°C with cell indicator antibodies, including 0.05 μg V500 Syrian hamster anti-mouse CD-3e (BD Biosciences, San Jose, CA) per 100 μL well for T-cells,

0.1 μg APC-H7 rat anti-mouse CD-19 (BD Biosciences, San Jose, CA) per 100 μL well for B-cells, 0.1 μg V450 rat anti-mouse CD-11b (BD Biosciences, San Jose, CA) per 100 μL well for monocytes, and 0.1 μg PE-Cy7 rat anti-mouse Ly-6G (BD Biosciences, San Jose, CA) per 100 μL well for granulocytes. These antibodies detect immune function cells in the spleen, and they can also be used to detect cells of interest in additional tissues such as bone marrow or peripheral blood. Cells were centrifuged at 400xg for 5 min, washed, and fixed with 4% paraformaldehyde (Thermo Fisher Scientific, Pittsburgh, PA) for 15 min at room temperature.

2.3.5. Flow Cytometry

Samples were analyzed on a BD FACSCanto II flow cytometer (BD Biosciences, San Jose, CA) equipped with three lasers (405 nm, 488 nm, and 640 nm). For each sample, 10,000 events were collected with the flow cytometer. Data were analyzed with FlowJo version X (TreeStar, Ashland, OR). The cellular populations of interest were well discriminated by forward scatter (FSC) and side scatter (SSC) properties. An unstained control was used to determine the threshold for samples positive for particular markers, facilitating gating as appropriate. After detection of the immune cell populations of interest (ie, B-cells, T-cells, monocytes, and granulocytes), the cells positive for Mitotracker® Deep Red, activated caspase-3/7, or 7-AAD in each subpopulation were determined.

2.3.6. Statistical Analysis

Dose-response curves with response normalized to the zero dose as a function of log concentration were generated using GraphPad Prism 6 (La Jolla, CA). All graphed results were expressed as mean ± standard error of the mean (SEM). IC_{50} values, slope coefficients, and area under the curve values were obtained using a four-parameter logistical model (ie, Hill equation) per NIH guidance[28] and Pharsight® WinNonlin™ 5.2 (Mountain View, CA). The Hill equation

is f(x)=Max-((Max-Min)/(1+(x/IC_{50})$^{\gamma}$)), where Max is the maximum asymptote, Min is the minimum asymptote, γ is the Hill slope, and x is the drug concentration.[29] Additional statistical analyses, including Pearson correlations, were performed with SAS (Cary, NC) with $p < 0.05$ considered to be statistically significant. Pearson correlations were performed to determine the relatedness between phenotypes rather than individual strains[30,31] and the relatedness between

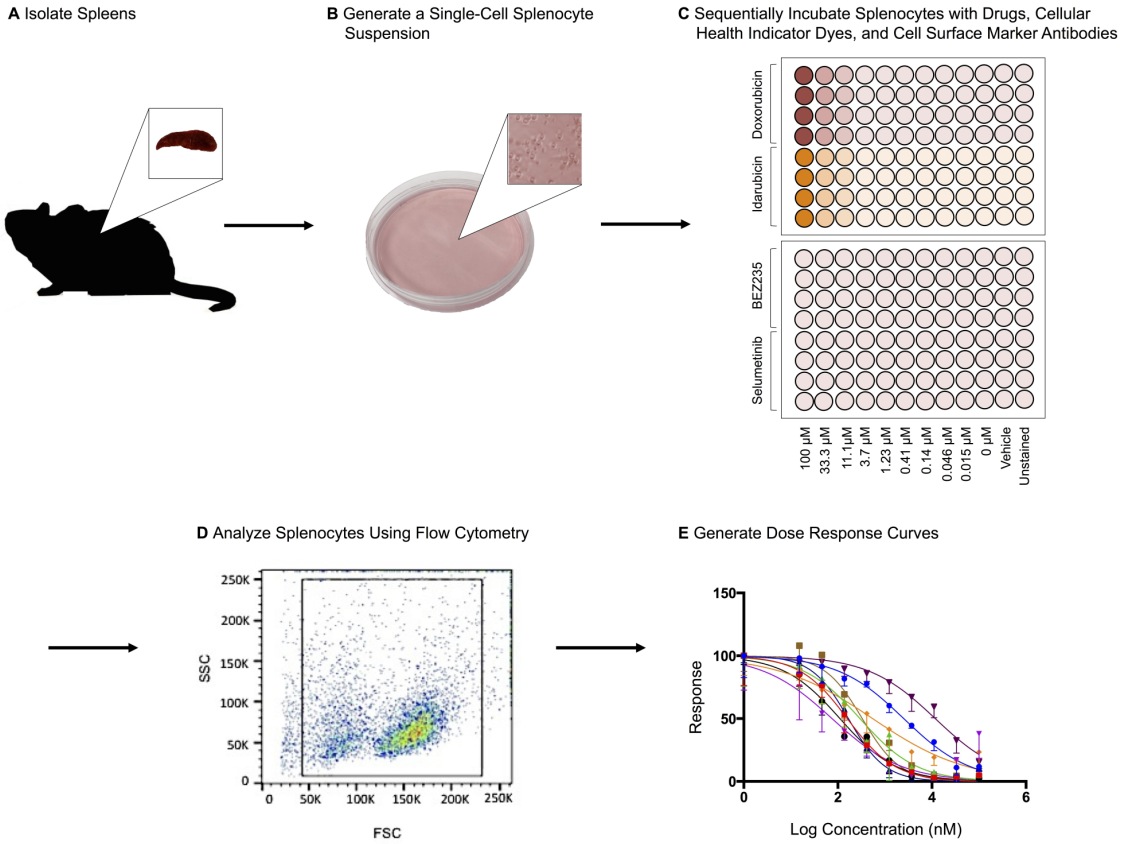

Figure 2.1. Assay methodology overview.

Notes: Spleens were isolated from inbred mice (**A**), and a single-cell splenocyte suspension was generated (**B**). Splenocytes were sequentially incubated with drugs, cellular health indicator dyes, and cell surface marker antibodies (**C**, listed in Table 2.1). The cells were fixed and analyzed using flow cytometry (**D**), and dose response curves were generated from flow cytometry data. (**E**).

metrics.[32] Heritability or the percent of variability likely due to genetics was calculated comparing intra- and interstrain variation in percent viability. The proportion of phenotype variation attributable to genetics was estimated with broad-sense heritability. Intrastrain correlations were estimated by $r_I=(MS_B-MS_W)/[MS_B+(n-1)MS_W]$, where r_I is the intrastrain correlation estimate, MS_B is the mean square of the between-strain comparison, MS_W is the mean square of the within-strain correlation, and n is the number of animals per strain.[33]

2.4. Results

An overview of the assay methodology is presented in Figure 2.1, including spleen isolation (Figure 2.1A), spleen homogenization (Figure 2.1B), incubation with drugs and multiplexed assay conditions (Figure 2.1C), flow cytometry (Figure 2.1D), and generation of dose response curves (Figure 2.1E). Splenocytes were isolated and cultured using standard methods. However, the assay was optimized in terms of culture conditions and media to best maintain cellular health under normal conditions. For instance, splenocyte and immune subpopulation viability was compared following incubation in supplemented DMEM, IMDM, and RPMI media. In particular, B-cell sensitivity limited the drug incubation time to 4 hours within the assay (data not shown). Splenocytes were not stimulated to avoid confounding cellular differentiation responses with toxicity responses, as phenotypic and genetic responses associated with chemotherapy-induced toxicity could otherwise be attributed to cellular stimulation. The cell-type composition of cultured cell populations potentially differs from cells freshly isolated and immediately analyzed via flow cytometry. However, analysis shows that our cultured assays are consistent in composition with freshly isolated splenocytes and cellular subpopulations (ie, B-cells, monocytes, and granulocytes) when compared to murine spleen cell composition in the

Mouse Phenome Database (MPD:Jaxpheno6, Supplementary Figure 2.1) using *t*-tests with $p < 0.05$ considered statistically significant.[34] Our data are also deposited in the Mouse Phenome Database at the Jackson Laboratory (MPD:Wiltshire4).[35]

Table 2.1. Multiparameter flow cytometry assay.

Excitation Wavelength (nm)	Emission Wavelength (nm)	Fluorochrome Channel	Cell Surface Marker or Dye	Parameter Investigated
405	450	PacBlue	V450 rat anti-mouse CD11b	Monocytes
405	500	AmCyan	V500 Syrian hamster anti-mouse CD3e	T-cells
488	530	FITC	CellEvent™ Caspase-3/7 green detection reagent	Caspase-3/7 activation
488	570	PE	Anthracycline autofluorescence	Anthracycline uptake
488	695	PerCPCy5.5	7-AAD	Viability
488	785	PE-Cy7	PE-Cy7 rat anti-mouse Ly-6G	Granulocytes
635	660	APC	Mitotracker® Deep Red	Mitochondrial health
635	785	APC-Cy7	APC-H7 rat anti-mouse CD19	B-cells

We developed a multiplexed flow cytometry assay (Table 2.1) to measure the health of multiple immune cell populations following exposure to anticancer agents. Further refined cell subpopulations can be examined in additional screens. The commercial availability of cellular health indicator dyes limited the fluorescent channels accessible for antibody-conjugated fluorochromes. Thus, the brightest fluorochromes were reserved for antibodies targeting less prevalent cell surface markers. Dyes were selected based on the ability to be fixed and their representation of various cellular health parameters important in early and late apoptosis and necrosis.[27] Dyes and antibody-conjugated fluorochromes were titrated and compensated during flow cytometry analysis to reduce spectral overlap.[36,37] Generous gates were applied to the plots

to capture phenotypes from less viable cells following exposure to various concentrations of anti-lymphoma compounds. The gating strategy is presented in Figure 2.2 with the following populations represented: splenocytes (Figure 2.2A), CD19+ B-cells (Figure 2.2B), CD3e+ T-cells (Figure 2.2C), CD11b+ monocytes (Figure 2.2D), Ly-6G+ granulocytes (Figure 2.2E), viable cells (Figure 2.2F), caspase-3/7 positive cells (Figure 2.2G), Mitotracker® Deep Red positive cells (Figure 2.2H), and, when applicable, anthracycline positive cells (Figure 2.2I).

Dose-response curves of the percent viability of splenocyte cell subpopulations exposed to chemotherapeutic drugs from nine of thirty-six total strains are represented in Figure 2.3. These nine strains were chosen to enhance clarity of visualization and to display diversity across the various phenotypes. Dose response curves were generated for these strains across all phenotypes. T-cells, B-cells, monocytes, and granulocytes respectively exposed to doxorubicin (Figure 2.3A-D), idarubicin (Figure 2.3E-H), BEZ-235 (Figure 2.3I-L), and selumetinib (Figure 2.3M-P) are represented. Corresponding phenotypes for all thirty-six strains are represented in Supplementary Figure 2.2A-P. Over 16,000 viability measurements were collected for T-cells, B-cells, and monocytes exposed to different concentrations of these targeted and cytotoxic anti-cancer agents. Heritability results were also calculated for viability at individual drug concentrations (Supplementary Table 2.1). As shown in Figure 2.3, all splenocyte immune cell subpopulations were less sensitive to the more selective mTOR/PI3K and MEK inhibitors than the anthracyclines. Interestingly, B-cells appear to be most sensitive to the effects of all anticancer agents, while T-cells appear to be the least sensitive. For example, a paired *t*-test indicated that T-cells were less sensitive than B-cells to idarubicin ($p < 0.0001$). T-cells appeared least sensitive to doxorubicin compared to other cell populations, with few strains reaching the

Figure 2.2. Flow cytometry gating strategy.

Notes: The population of splenocytes (**A**) was derived from SSC and FSC. Subpopulations of interest derived from **A** included CD19+ B-cells (**B**), CD3e+ T-cells (**C**), CD11b+ monocytes (**D**), and Ly-6G+ granulocytes (**E**). Viability (**F**), caspase-3/7 activation (**G**), mitochondrial health (**H**), and, when applicable, anthracycline uptake (**I**) were subsequently gated from **B-E** subpopulations.

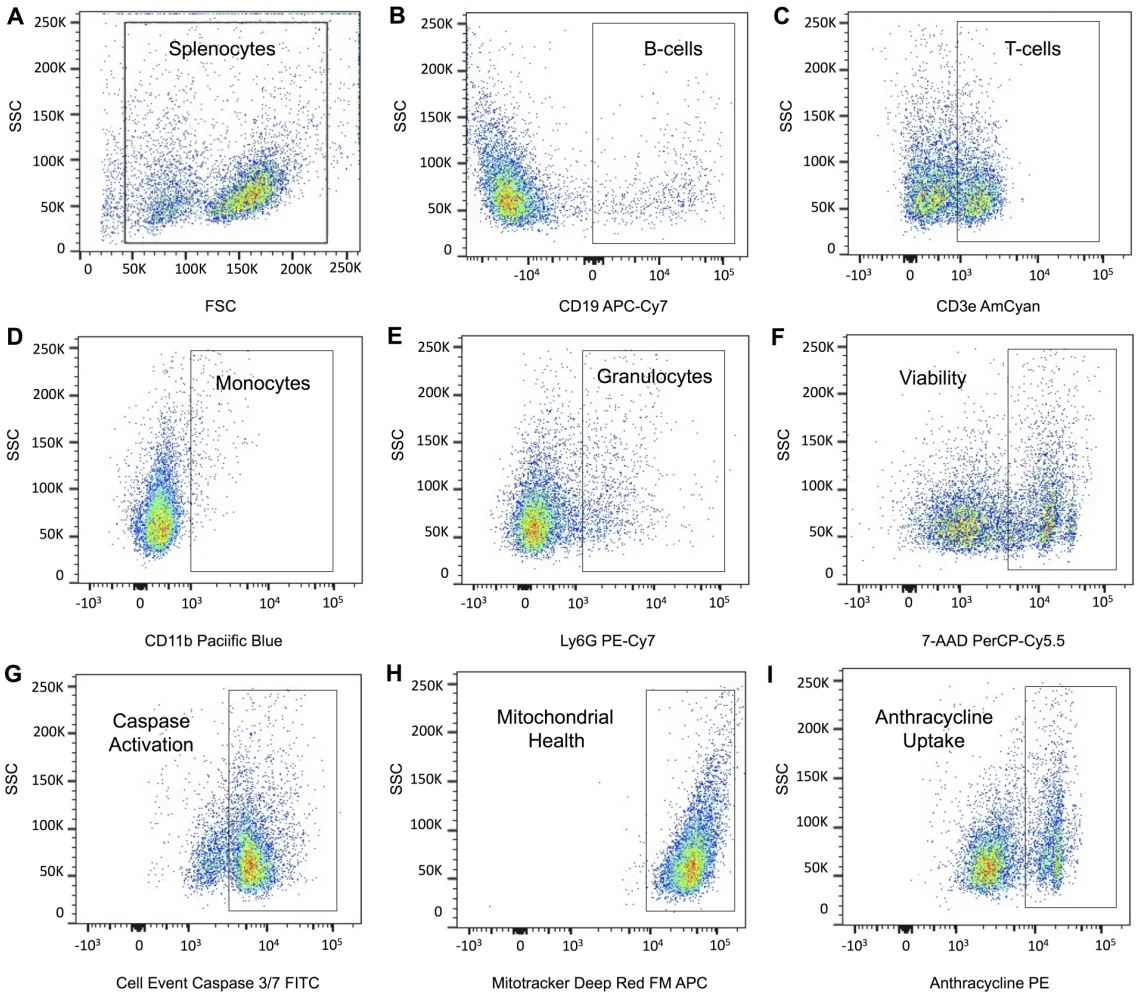

Figure 2.3. Interstrain variation of viability across immune cell types and anti-cancer drugs.

Notes: Dose response curves depict cell populations (columns, ie, T-cells, B-cells, monocytes, and granulocytes) exposed to anti-cancer drugs (rows, ie, doxorubicin, idarubicin, BEZ-235, and selumetinib). Nine strains are included: A/J —●—, C57BLKS/J —■—, CBA/J —▲—, DBA/2J —▼—, FVB/NJ —◆—, LP/J —●—, NOD/LtJ —■—, NZB/BINJ —▲—, and PWK/PhJ —▼—.

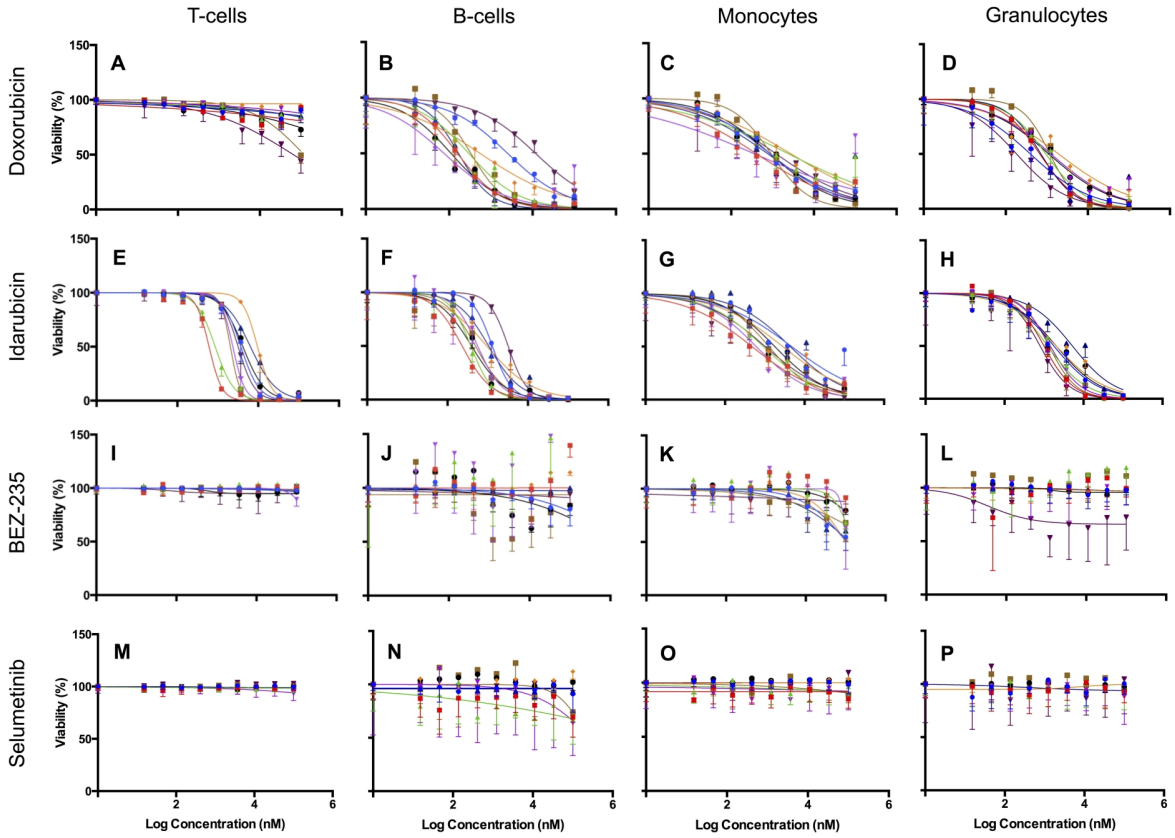

IC_{50} at the highest concentration of 100 µM, a concentration that is higher than physiological C_{max} values in humans. Furthermore, T-cells appear less sensitive and less variable to BEZ-235 and selumetinib than other cell populations with larger error bars for individual viability points for B-cells, monocytes, and granulocytes than T-cells in Figure 2.3 and Supplemental Figure 2.2 (of note, the scale of the axes is the same across all phenotypes). Also, viability does not

Figure 2.4. Replicability of dose response curves.

Notes: Four sensitive and four less sensitive strains were chosen for replication in a repeat experiment. The results for the most heritable viability phenotypes are presented: T-cells exposed to idarubicin (**A**) and B-cells exposed to doxorubicin (**B**). Eight strains are included: 129S1SvlmJ , BALB/cByJ , C57BLKS/J , CBA/J , KK/HiJ , LG/J , NZO/HiLtJ , and SEA/GnJ .

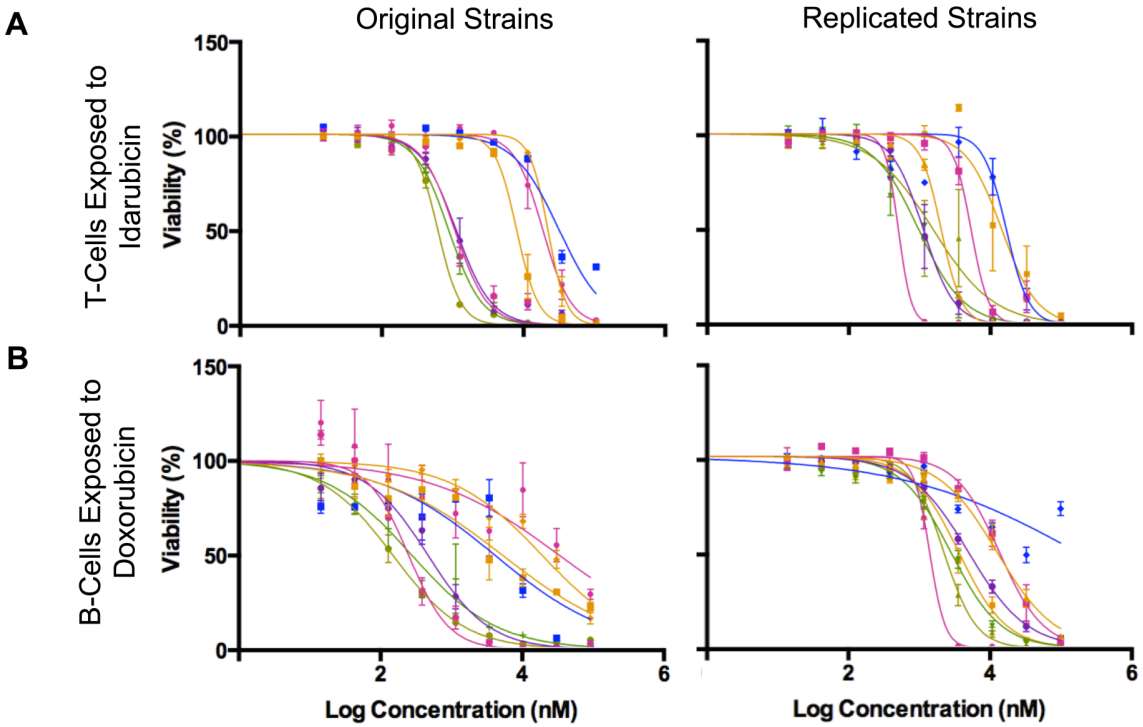

decrease with increasing drug concentration. To demonstrate the replicability of the results we selected a set of eight strains for confirmation experiments. The repeatability of this experiment is shown in Figure 2.4 using the most heritable phenotypes: T-cells exposed to idarubicin (Figure 2.4A) and B-cells exposed to doxorubicin (Figure 2.4B). In the second replicated experiment, interstrain variability to the anti-cancer agents was maintained, and the strain order for sensitivity

Figure 2.5. Interstrain phenotype comparisons for $\log_{10}(IC_{50}(nM))$.

Notes: $\text{Log}_{10}(IC_{50}(nM))$ values across strains and heritability are displayed for T-cells exposed to idarubicin (**A**), B-cells exposed to doxorubicin (**B**), B-cells exposed to idarubicin (**C**), monocytes exposed to doxorubicin (**D**), and monocytes exposed to idarubicin (**E**). Strains are arranged from least sensitive to most sensitive along the x-axis.

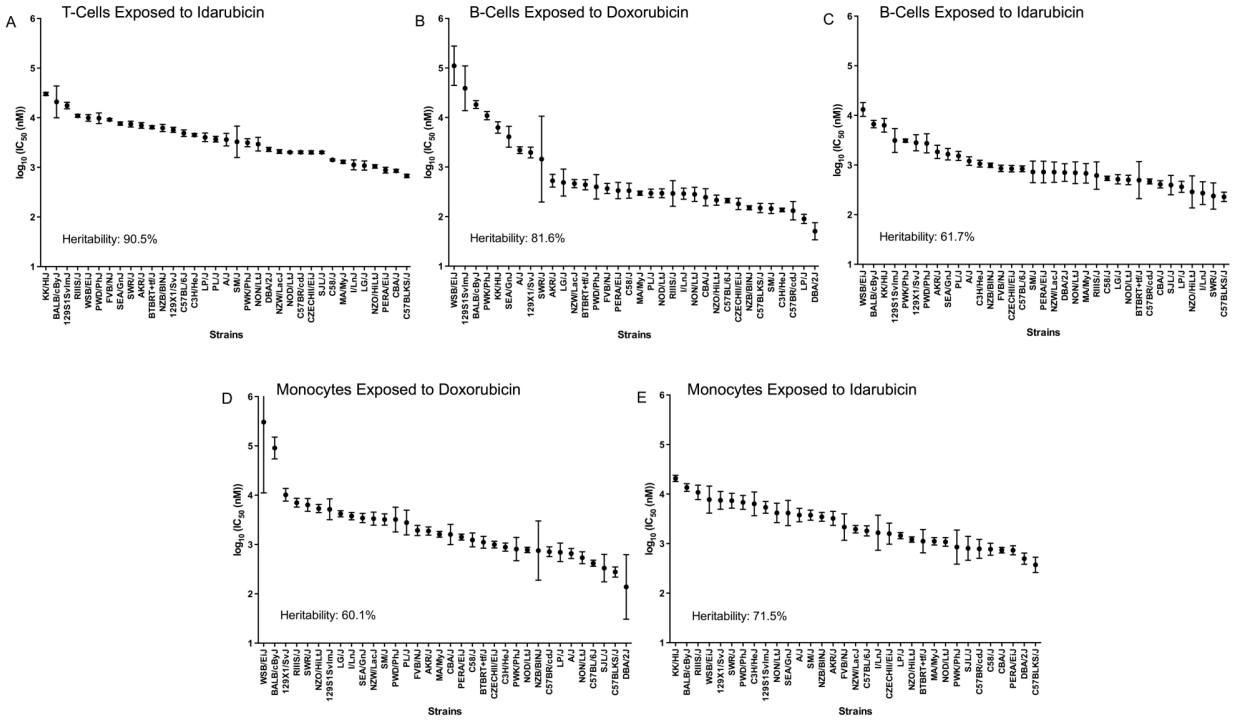

was similar though not identical to the first experiment. For instance, the *p* values for the Wilcoxon rank sum tests were > 0.05 for these most heritable phenotypes, providing no compelling evidence that the replicate IC_{50} values from these eight strains differ from those of the original assay, although the small sample size provides reduced power to detect a difference.[38] Also, the Spearman correlation of IC_{50} values for T-cells exposed to idarubicin was 0.75 ($p = 0.03$) between the original and replicated mouse strains when the most variable strain 129S1/SvlmJ was removed. Although the strain order for drug sensitivity is unique between the

anti-cancer agents and cell type, several strains repeatedly appear to be more sensitive (eg, C57BLKS/J and DBA/2J) or less sensitive (eg, BALB/cByJ, KK/HiJ, and WSB/EiJ) to the cytotoxic effects of the different anthracycline agents across cell type (Figure 2.5: T-cells exposed to idarubicin (Figure 2.5A), B-cells exposed to doxorubicin (Figure 2.5B), B-cells exposed to idarubicin (Figure 2.5C), monocytes exposed to doxorubicin (Figure 2.5D), and monocytes exposed to idarubicin (Figure 2.5E)).

Table 2.2. Phenotype correlations for $\log_{10}(IC_{50}(nM))$ values across strains.

	T-cells exposed to idarubicin	B-cells exposed to doxorubicin	B-cells exposed to idarubicin	Monocytes exposed to doxorubicin	Monocytes exposed to idarubicin
T-cells exposed to idarubicin	-	0.573 $p = 0.0004$	0.698 $p = 3.2\text{x}10^{-6}$	0.468 $p = 0.0053$	0.835 $p = 1.5\text{x}10^{-9}$
B-cells exposed to doxorubicin	-	-	0.771 $p = 9.6\text{x}10^{-8}$	0.703 $p = 5.2\text{x}10^{-5}$	0.534 $p = 0.0016$
B-cells exposed to idarubicin	-	-	-	0.585 $p = 0.00028$	0.630 $p = 8.4\text{x}10^{-5}$
Monocytes exposed to doxorubicin	-	-	-	-	0.672 $p = 2.5\text{x}10^{-5}$
Monocytes exposed to idarubicin	-	-	-	-	-

The interstrain variability within dose-response curves exposed to anthracyclines is more ideal for genetic analysis, and this is echoed in heritability calculations and differential $\log_{10}$ (IC_{50}) values as shown in Figure 2.5. The relatively high heritability of the viability of T-cells exposed to idarubicin (90.5%) and B-cells exposed to doxorubicin (81.6%) makes these phenotypes most suitable to carry forward in future genetic studies. Pearson correlations in IC_{50} values between T-cells exposed to idarubicin, B-cells exposed to doxorubicin, B-cells exposed to

idarubicin, monocytes exposed to doxorubicin, and monocytes exposed to idarubicin were statistically significant, indicating correlative effects of the different anthracycline agents on the immune cells (Table 2.2).

Because IC_{50} values were not always achieved in this screen, area under the curve (AUC) values (Supplementary Figure 2.3: T-cells exposed to selumetinib (Supplementary Figure 2.3A), T-cells exposed to BEZ-235 (Supplementary Figure 2.3B), T-cells exposed to doxorubicin (Supplementary Figure 2.3C), T-cells exposed to idarubicin (Supplementary Figure 2.3D), B-cells exposed to selumetinib (Supplementary Figure 2.3E), B-cells exposed to BEZ-235 (Supplementary Figure 2.3F), B-cells exposed to doxorubicin (Supplementary Figure 2.3G), B-cells exposed to idarubicin (Supplementary Figure 2.3H), monocytes exposed to selumetinib (Supplementary Figure 2.3I), monocytes exposed to BEZ-235 (Supplementary Figure 2.3J), monocytes exposed to doxorubicin (Supplementary Figure 2.3K), and monocytes exposed to idarubicin (Supplementary Figure 2.3L)) and slope coefficients (Supplementary Figure 2.4: T-cells exposed to idarubicin (Supplementary Figure 2.4A), B-cells exposed to doxorubicin (Supplementary Figure 2.4B), B-cells exposed to idarubicin (Supplementary Figure 2.4C), monocytes exposed to doxorubicin (Supplementary Figure 2.4D), and monocytes exposed to idarubicin (Supplementary Figure 2.4E)) were calculated for comparison when appropriate. The Pearson correlations of AUC to IC_{50} values when available were significant: T-cells exposed to idarubicin, 0.89 ($p < 0.0001$); B-cells exposed to doxorubicin, 0.98 ($p < 0.0001$); B-cells exposed to idarubicin, 0.89 ($p < 0.0001$); monocytes exposed to doxorubicin, 0.96 ($p < 0.0001$); and monocytes exposed to idarubicin, 0.99 ($p < 0.0001$). However, heritability was comparatively

reduced for AUC. In contrast, slope coefficients varied greatly from IC_{50} values. Also, the results of the Pearson's correlation test for AUC (Supplementary Table 2.2) and slope coefficients (Supplementary Table 2.3) suggest reduced correlative anthracycline effects in these parameters.

2.5. Discussion

It has been predicted that the future of cancer treatment will involve precision medicine approaches combining targeted therapy or chemotherapies with immunomodulation.[39] There is particular interest in the adaptive immune system as an additional "drug" in chemotherapeutic regimens due to its essential role in recognizing and eliminating tumor cells. However, tumor cells can adapt to evade immune surveillance, a characteristic acknowledged as an emerging hallmark of cancer.[40] The importance of the adaptive immune system in cancer and treatment is reflected in recent therapeutic advances targeting cytotoxic T-lymphocyte antigen 4 (CTLA-4) and the programmed death 1 (PD-1) receptor and its ligands (PD-L1/2). These antibody therapeutics essentially reverse tumor inhibition of the adaptive immune system, leading to more favorable clinical outcomes.[41]

Although eliciting the adaptive immune response may be an effective means to recognize and eliminate tumor cells, this strategy may also present a risk as the immune-adjuvant effects of many cytotoxic compounds rely on antigen-presenting cells processing tumor antigens for T-cell recognition.[2] For example, the anthracyclines are involved in immunomodulation by inducing calreticulin on tumor cells.[42] Thus, the success of cytotoxic chemotherapy may depend on a delicate balance between preservation of the immune system and tumor cell death. Here, we used a wide concentration range for our compounds, a typical approach within toxicological studies and multiplexed drug screens in order to generate dose response curves. For instance, a simulation of doxorubicin concentrations in women with breast cancer at the end of a 60 mg/m^2

intravenous infusion (0.66 h) calculated a plasma C_{max} of approximately 1.3 μM in women with a BMI < 25.[43] Following a 48 h infusion of 70 mg/m^2 idarubicin for consolidation therapy for metastatic breast cancer, the plasma C_{max} was approximately 0.3 μM.[44] Clinical trials to determine the pharmacokinetics of BEZ-235 and selumetinib are underway. However, at a dose of 50 mg/kg in PC3M tumor-bearing nude mice, the plasma Cmax of BEZ-235 was approximately 1.68 μM at 0.5 h and 0.03 μM at 24 h.[45] Cell-based studies, including our assay, allow for greater resolution of drug response across a spectrum of concentrations rather than limited concentrations traditionally used in toxicology studies.[28] In this assay, we are able to differentiate the variable cytotoxic response of different immune cells to anti-cancer agents, which will likely have applications in drug development and clinical settings. We identified strains with cell types universally more (eg, C57BLKS/J and DBA/2J) or less (eg, BALB/cByJ, KK/HiJ, and WSB/EiJ) sensitive to the cytotoxic effects of the anthracyclines. These strains may be useful for testing additional drugs in the future to gauge their toxicity on the immune system. T-cells were generally less sensitive to the effects of the anthracyclines, perhaps indicating that they are a favorable target for immunomodulating drugs and adaptive immune system stimulation in anti-cancer drug regimens. B-cells, on the other hand, appear to be more sensitive at lower concentrations of the drugs than T-cells. Similar differences in adaptive immune cell sensitivities to chemotherapeutic agents have been previously reported in patients.[46] Because our data corresponds to these findings, our screen across multiple strains of mice provides an interesting starting point as a model system for examining immune cell toxicity following exposure to anticancer agents.

A broad examination of chemotherapy-induced cytotoxic responses was elicited because the success of several chemotherapeutics requires interplay from a normal, functional immune system. Here, we focus on viability results obtained from broad splenic subpopulations of the adaptive immune system (ie, T- and B-cells) and monocytes exposed to various anti-cancer agents. In the spleen, B-cells promote both T-cell independent and dependent immune responses. The spleen redistributes T-cells to nonlymphoid tissue following antigen recognition. Splenic monocytes differentiate into macrophages and dendritic cells, which are antigen presenting cells and cellular components that act as liaisons between the innate and adaptive immune systems. [47] Primary cells were also used in this study to innovatively examine the effects of anti-cancer agents on normal immune cells rather than cancerous or immortalized cells. The markers of caspase-3/7 activity and mitochondrial stress were not as mechanistically useful as viability. We could not detect interstrain differences in these parameters and large error indicated that our results were not very robustly replicable (data not shown). The viability parameter was most heritable, particularly among immune cells exposed to the anthracyclines, making viability the focus of our paper and future genetic analyses. Unfortunately, the lack of unique findings among our drugs and additional parameters at the doses used for our assay is a limitation of this screening process, where we focused on more generalized viability and mechanized endpoints. Ideally, this screening process should include biomarkers specific for drugs (eg, protein targets or gene expression changes) where we can identify change in response in a more concise approach.

A general, replicable screening approach was used in mice to examine the effects of cytotoxic and targeted agents on the viability of normal immune cells. To be able to maximize the use of this data and identify genetic components of phenotype differences, genomewide

association analysis requires sufficient diversity of both genotype and phenotype among individuals in a mapping population, and both of these traits are reflected in this experiment. A panel of thirty-six strains from the Jackson Laboratory's Mouse Phenome Database MDP was selected to model genetic diversity, while phenotypic diversity was measured using IC_{50} values for viability in immune cells exposed to anthracycline agents. Importantly, this assay also identified heritable drug response phenotypes (60.1% to 90.5% for IC_{50} phenotypes), making it suitable for pharmacogenomic screening of anticancer effects on immune cells. Remarkably, the heritability for the anthracyclines was unexpectedly high, as multifactorial pathways of action may dilute phenotypic association to genetic components. Phenotypes generated from this approach will be used in genome-wide association studies (GWAS) to generate candidate genes, which may identify individuals more susceptible to immune system toxicity.[48] We have identified loci of significance from our approach, but the extension and validation of this work will be presented in a separate manuscript. Harrill et al. used a similar translational approach in a panel of inbred mouse strains to determine that acetaminophen-induced liver injury may be mediated by variation in immunogenic surface antigens affecting leukocyte signaling, particularly *CD44*.[49]

However, a general screening approach using IC_{50} values for viability as a phenotypic endpoint is not always appropriate. In a large screen, defining the best parameter for measurement is often difficult due to dose-response curve fitting. Within this experiment, dose-response curves for the PI3K/mTOR and MEK inhibitors did not achieve IC_{50} levels. Fallai-Sichani et al. found that drugs targeting the Akt/PI3K/mTOR pathway also had shallow dose-response curves in breast cancer cell lines due to significant cell-to-cell variability.[50] Going forward, more specific assays may be incorporated into high-throughput screens to examine

pathways affected by these targeted agents, as more sensitive markers are needed to produce a larger phenotypic gradient between more and less sensitive strains. Additionally, the appropriateness of IC_{50} values as a summary variable of dose-response curves for genetic analysis has been contested.[29,32,50-52] IC_{50} values, corresponding to the potency of a compound, are physiologically relevant. Nonetheless, biological and statistical assumptions are not always met, namely that differential response can be defined by one parameter from a complex non-linear model. In this study, supplementary AUC values, regarded as a global measure of compound activity,[32] and slope coefficients of curves were generated for comparison to IC_{50} values. The correlations of AUC to IC_{50} values when available were significant, while slope coefficients varied greatly from IC_{50} values. When IC_{50} values are not achieved or non-linear curve fitting is not appropriate, AUC could perhaps be a surrogate for differential interstrain response. Furthermore, a combination of biological and pharmacokinetic and -dynamic endpoints may be used to better understand the cytotoxic response to anticancer agents. In the future, these and additional approaches can be tested for use in detecting genetic associations in in vitro genetic association studies.

2.6. Conclusions

A cellular genetics screening approach with robust, replicable, multiplexed assays was developed to accurately describe toxicity response in normal immune cells. In this study, phenotypes were quantified using flow cytometry, yielding interstrain variation for measured endpoints in different immune cells. The more targeted agents, BEZ-235 and selumetinib, were less toxic to normal immune cells than the anthracycline agents. Also, heritability for the viability of immune cells was higher for anthracyclines than the novel agents, making them ideal for genetic analysis. This assay provides a novel way of identifying mouse strains that will model

sensitivity or resistance to anthracyclines in normal immune cells. High heritability indicates a very strong genetic component of response to treatment, and the genetic determinants of response including candidate genes and cellular toxicity pathways can then be identified and provide hypotheses to test and validate in human studies. Ultimately, the hope is that we can identify biomarkers in patients with immune systems less impaired by chemotherapeutic agents.

Supplementary Table 2.1. Heritability (%) of viability (%) at specific drug doses (μM) among different phenotypes.

Phenotype	0.02 μM	0.05 μM	0.1 μM	0.4 μM	1.2 μM	3.7 μM	11.1 μM	33.3 μM	100 μM
B-cells exposed to selumetinib	27.5	30.6	35.2	41.6	51.7	47.9	43.5	47.6	58.3
B-cells exposed to BEZ-235	58.6	36.1	44	41.5	46.9	45	52	46.3	56.9
B-cells exposed to doxorubicin	38.9	38.1	58.2	70.6	78.8	83.4	87.8	79.2	73.5
B-cells exposed to idarubicin	51.5	36.2	49.5	51.1	69.3	85	60.7	45.4	35.2
T-cells exposed to selumetinib	50.9	44.5	50.7	54.4	51.5	43.5	46.7	47	53.2
T-cells exposed to BEZ-235	20.4	31.7	32	42.5	40.9	55.6	52	61.8	69.1
T-cells exposed to doxorubicin	63	75.8	81.6	79.2	77.9	81.6	85.8	86.8	89.3
T-cells exposed to idarubicin	22.8	37.8	45.3	72.5	87.5	90.6	83.6	42.7	44.5
Monocytes exposed to selumetinib	26.2	27.5	27.9	43.2	50.1	47	37.5	53.2	64.4
Monocytes exposed to BEZ-235	41.9	45	52.3	49.9	74.1	79.4	83.4	87.5	83.9
Monocytes exposed to doxorubicin	40.6	44.8	66.2	75.6	71.7	77.6	81.3	59.5	76.8
Monocytes exposed to idarubicin	32	46.8	55	74.9	73.6	75.1	80.5	47.9	58.6

Supplementary Table 2.2. Phenotype correlations for area under the curve values across strains.

	T-cells exposed to selumetinib	T-cells exposed to BEZ-235	T-cells exposed to doxorubicin	T-cells exposed to idarubicin	B-cells exposed to selumetinib	B-cells exposed to BEZ-235	B-cells exposed to doxorubicin	B-cells exposed to idarubicin	Monocytes exposed to selumetinib	Monocytes exposed to BEZ-235	Monocytes exposed to doxorubicin	Monocytes exposed to idarubicin
T-cells exposed to selumetinib	-	0.49 $p = 0.003$	0.058 $p = 0.75$	0.14 $p = 0.43$	0.23 $p = 0.19$	0.053 $p = 0.76$	0.2 $p = 0.26$	0.24 $p = 0.18$	0.51 $p = 0.002$	0.26 $p = 0.12$	0.19 $p = 0.28$	0.15 $p = 0.41$
T-cells exposed to BEZ-235	-	-	0.41 $p = 0.017$	0.12 $p = 0.51$	-0.0069 $p = 0.97$	0.22 $p = 0.2$	0.48 $p = 0.004$	0.4 $p = 0.018$	0.097 $p = 0.58$	0.74 $p = 3.5 \times 10^{-7}$	0.27 $p = 0.12$	0.08 $p = 0.65$
T-cells exposed to doxorubicin	-	-	-	0.49 $p = 0.002$	0.28 $p = 0.1$	0.44 $p = 0.009$	0.38 $p = 0.021$	0.28 $p = 0.1$	0.11 $p = 0.54$	0.48 $p = 0.004$	0.21 $p = 0.21$	0.32 $p = 0.054$
T-cells exposed to idarubicin	-	-	-	-	0.49 $p = 0.003$	0.18 $p = 0.31$	0.61 $p = 9.1 \times 10^{-5}$	0.75 $p = 1.5 \times 10^{-7}$	0.3 $p = 0.087$	0.35 $p = 0.04$	0.53 $p = 0.001$	0.91 $p = 3 \times 10^{-14}$
B-cells exposed to selumetinib	-	-	-	-	-	0.47 $p = 0.004$	0.17 $p = 0.33$	0.54 $p = 0.001$	0.52 $p = 0.001$	0.19 $p = 0.28$	0.06 $p = 0.74$	0.41 $p = 0.016$
B-cells exposed to BEZ-235	-	-	-	-	-	-	0.11 $p = 0.51$	0.42 $p = 0.014$	0.41 $p = 0.02$	0.38 $p = 0.023$	-0.14 $p = 0.44$	0.037 $p = 0.84$
B-cells exposed to doxorubicin	-	-	-	-	-	-	-	0.75 $p = 1.4 \times 10^{-7}$	0.067 $p = 0.7$	0.63 $p = 6 \times 10^{-5}$	0.6 $p = 1 \times 10^{-4}$	0.55 $p = 4.6 \times 10^{-4}$
B-cells exposed to idarubicin	-	-	-	-	-	-	-	-	0.32 $p = 0.61$	0.65 $p = 2.9 \times 10^{-5}$	0.42 $p = 0.011$	0.68 $p = 5.3 \times 10^{-6}$
Monocytes exposed to selumetinib	-	-	-	-	-	-	-	-	-	0.12 $p = 0.48$	0.2 $p = 0.27$	0.31 $p = 0.075$
Monocytes exposed to BEZ-235	-	-	-	-	-	-	-	-	-	-	0.39 $p = 0.023$	0.28 $p = 0.11$
Monocytes exposed to doxorubicin	-	-	-	-	-	-	-	-	-	-	-	0.69 $p = 4 \times 10^{-6}$
Monocytes exposed to idarubicin	-	-	-	-	-	-	-	-	-	-	-	-

Supplementary Table 2.3. Phenotype correlations for slope coefficient values across strains.

	T-cells exposed to idarubicin	B-cells exposed to doxorubicin	B-cells exposed to idarubicin	Monocytes exposed to doxorubicin	Monocytes exposed to idarubicin
T-cells exposed to idarubicin	-	0.16 $p = 0.37$	0.11 $p = 0.53$	0.093 $p = 0.6$	0.11 $p = 0.55$
B-cells exposed to doxorubicin	-	-	0.3 $p = 0.085$	0.16 $p = 0.37$	0.48 $p = 0.006$
B-cells exposed to idarubicin	-	-	-	-0.066 $p = 0.7$	0.33 $p = 0.055$
Monocytes exposed to doxorubicin	-	-	-	-	0.57 $p = 0.001$
Monocytes exposed to idarubicin	-	-	-	-	-

Supplementary Figure 2.1. Cellular subpopulations of freshly isolated splenocytes.

Notes: Splenocytes were isolated from male C57BL/6J (n=4) mice. Our populations were comparable to murine spleen cell composition when available in the Mouse Phenome Database (B-cells, granulocytes, and monocytes $p < 0.05$ using *t*-tests).

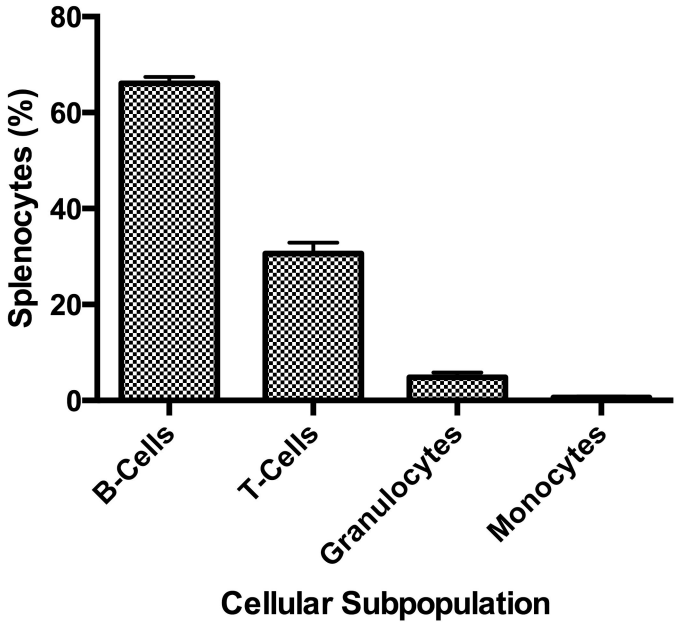

Supplementary Figure 2.2. Interstrain variation of viability across immune cell types and anti-cancer drugs.

Notes: Dose response curves depict cell populations (columns, ie, T-cells, B-cells, monocytes, and granulocytes) exposed to anti-cancer drugs (rows, ie, doxorubicin, idarubicin, BEZ-235, and selumetinib). Thirty-six strains are included: 129S1/SvImJ, 129X1/SvJ, A/J, AKR/J, BALB/cByJ, BTBR T^{+} *Itpr3*^{tf}*/J*, BUB/BnJ, C3H/HeJ, C57BLKS/J, C57BL/6J, C57BR/cdJ, C58/J, CBA/J, CZECHII/EiJ, DBA/2J, FVB/NJ, I/LnJ, KK/HiJ, LG/J, LP/J, MA/MyJ, NOD/LtJ, NON/LtJ, NZB/BINJ, NZO/HiLtJ, NZW/LacJ, PERA/EiJ, PL/J, PWD/PhJ, PWK/PhJ, RIIIS/J, SEA/GnJ, SJL/J, SM/J, SWR/J, and WSB/EiJ.

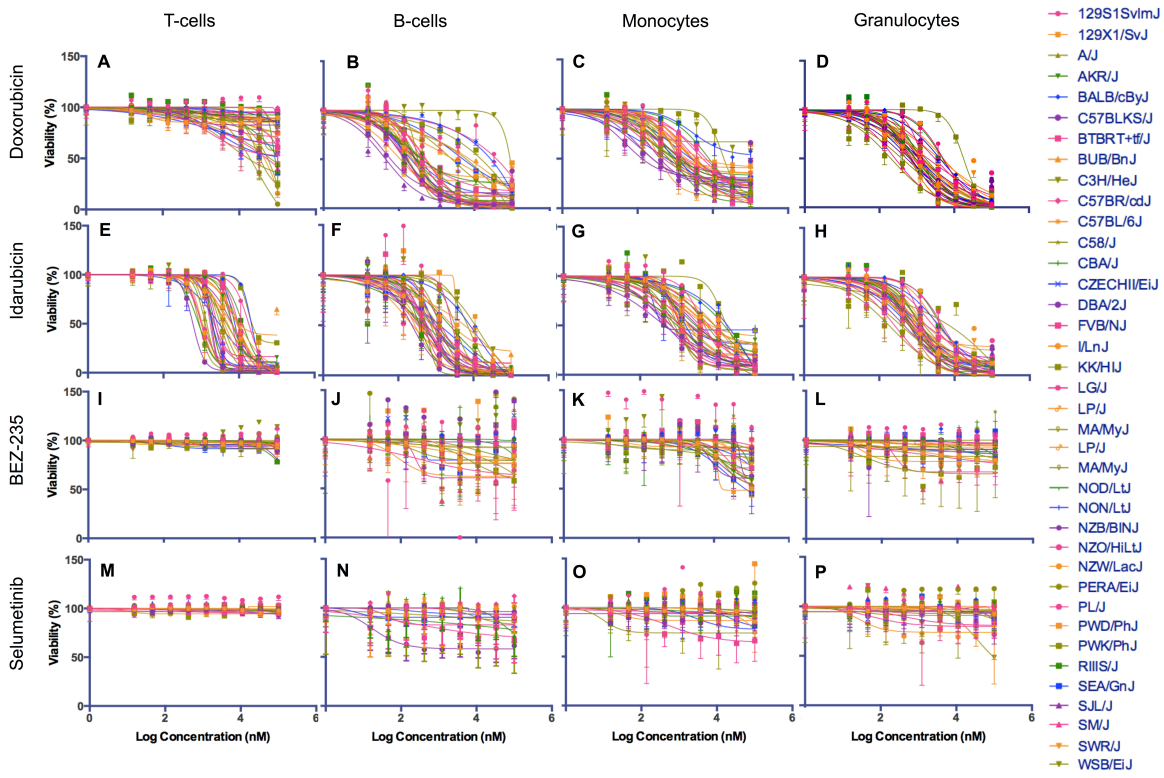

Supplementary Figure 2.3. Interstrain phenotype comparisons for area under the curve.

Notes: Area under the curve values across strains, heritability, and correlation to $\log_{10}(IC_{50}(nM))$ values, when relevant, are displayed for T-cells exposed to selumetinib (**A**), T-cells exposed to BEZ-235 (**B**), T-cells exposed to doxorubicin (**C**), T-cells exposed to idarubicin (**D**), B-cells exposed to selumetinib (**E**), B-cells exposed to BEZ-235 (**F**), B-cells exposed to doxorubicin (**G**), B-cells exposed to idarubicin (**H**), monocytes exposed to selumetinib (**I**), monocytes exposed to BEZ-235 (**J**), monocytes exposed to doxorubicin (**K**), and monocytes exposed to idarubicin (**L**). Strains are arranged from largest to smallest area under the curve (±SEM) along the x-axis.

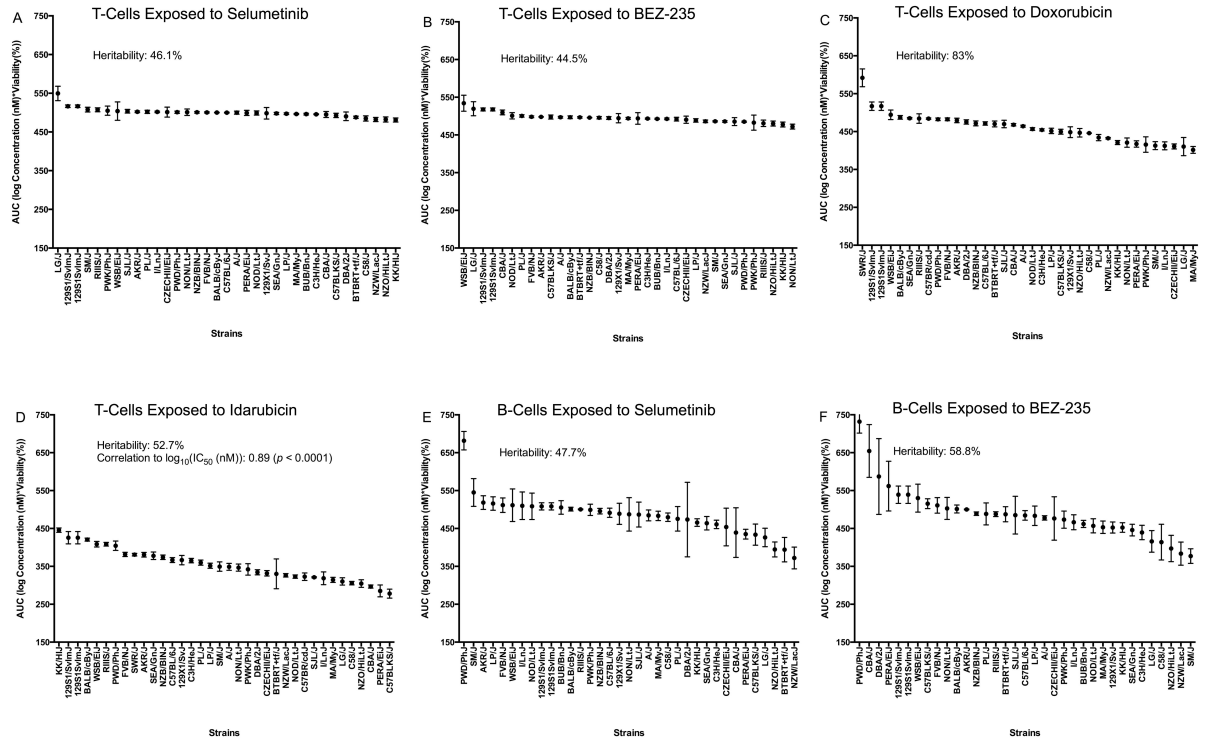

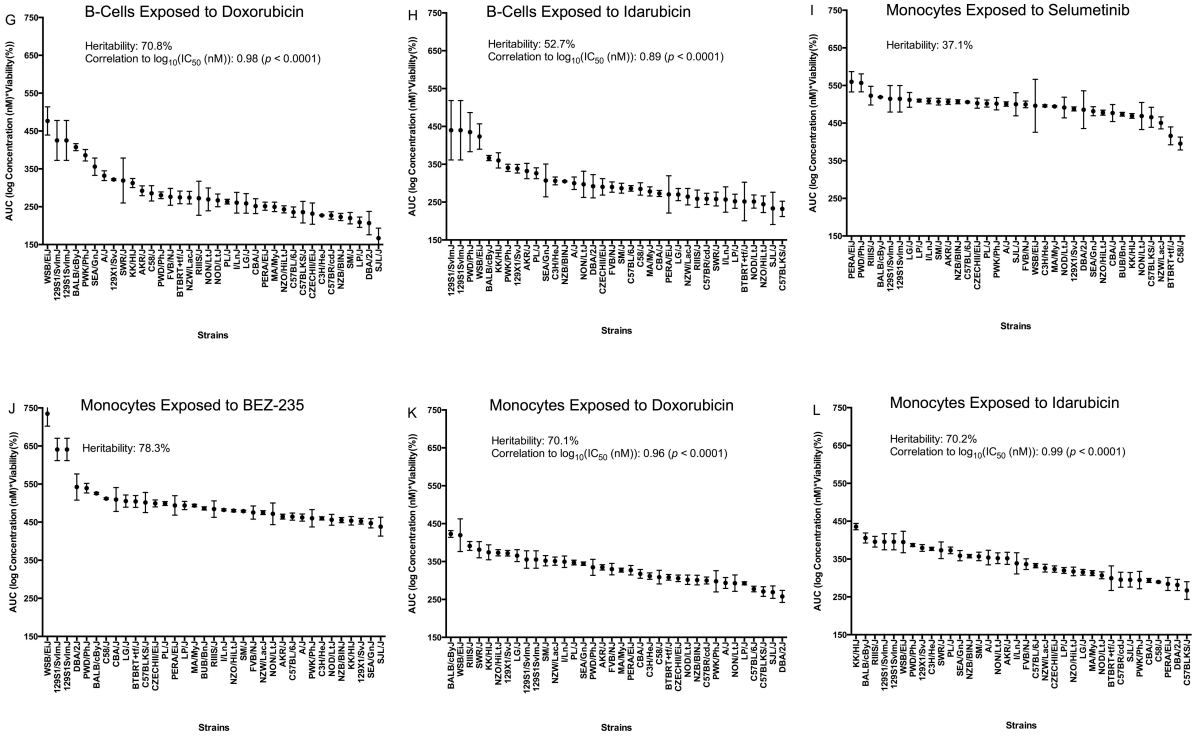
G
B-Cells Exposed to Doxorubicin
Heritability: 70.8%
Correlation to log10(IC50 (nM)): 0.98 (p < 0.0001)
H
B-Cells Exposed to Idarubicin
Heritability: 52.7%
Correlation to log10(IC50 (nM)): 0.89 (p < 0.0001)
I
Monocytes Exposed to Selumetinib
Heritability: 37.1%
J
Monocytes Exposed to BEZ-235
Heritability: 78.3%
K
Monocytes Exposed to Doxorubicin
Heritability: 70.1%
Correlation to log10(IC50 (nM)): 0.96 (p < 0.0001)
L
Monocytes Exposed to Idarubicin
Heritability: 70.2%
Correlation to log10(IC50 (nM)): 0.99 (p < 0.0001)
AUC (log Concentration (nM)*Viability(%))
Strains

Supplementary Figure 2.4. Interstrain phenotype comparisons for slope coefficients.

Notes: Slope coefficients across strains and correlation to $\log_{10}(IC_{50}(nM))$ values are displayed for T-cells exposed to idarubicin (**A**), B-cells exposed to doxorubicin (**B**), B-cells exposed to idarubicin (**C**), monocytes exposed to doxorubicin (**D**), and monocytes exposed to idarubicin (**E**). Strains are arranged from largest to smallest slope coefficient (±SEM) along the x-axis.

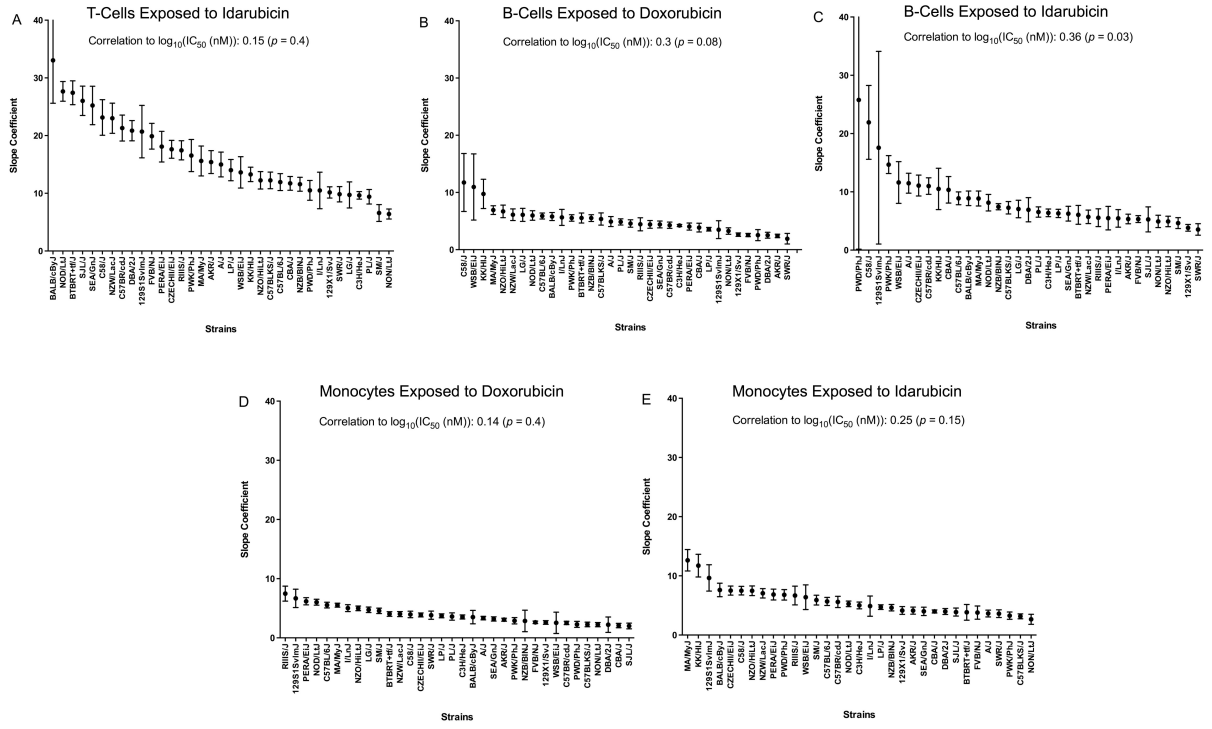

REFERENCES

1. Zitvogel L, Kepp O, Senovilla L, Menger L, Chaput N, Kroemer G. Immunogenic tumor cell death for optimal anticancer therapy: the calreticulin exposure pathway. *Clin Cancer Res*. 2010;16(12):3100–3104. doi:10.1158/1078-0432.CCR-09-2891.

2. Zitvogel L, Apetoh L, Ghiringhelli F, Kroemer G. Immunological aspects of cancer chemotherapy. *Nat Rev Immunol*. 2008;8(1):59–73. doi:10.1038/nri2216.

3. Laoui D, Van Overmeire E, Van Ginderachter JA. Unsuspected allies: Chemotherapy teams up with immunity to fight cancer. *Eur J Immunol*. 2013;43(10):2538–2542. doi:10.1002/eji.201344042.

4. Obeid M, Tesniere A, Ghiringhelli F, et al. Calreticulin exposure dictates the immunogenicity of cancer cell death. *Nat Med*. 2006;13(1):54–61. doi:10.1038/nm1523.

5. Ghiringhelli F, Apetoh L. Chemotherapy and immunomodulation: from immunogenic chemotherapies to novel therapeutic strategies. *Future Oncol*. 2013;9(4):469–472. doi:10.2217/fon.12.207.

6. Hodge JW, Garnett CT, Farsaci B, et al. Chemotherapy-induced immunogenic modulation of tumor cells enhances killing by cytotoxic T lymphocytes and is distinct from immunogenic cell death. *Int J Cancer*. 2013;133(3):624–636. doi:10.1002/ijc.28070.

7. Garnett CT, Schlom J, Hodge JW. Combination of docetaxel and recombinant vaccine enhances T-cell responses and antitumor activity: effects of docetaxel on immune enhancement. *Clin Cancer Res*. 2008;14(11):3536–3544. doi:10.1158/1078-0432.CCR-07-4025.

8. Zitvogel L, Galluzzi L, Smyth MJ, Kroemer G. Mechanism of action of conventional and targeted anticancer therapies: reinstating immunosurveillance. *Immunity*. 2013;39(1):74–88. doi:10.1016/j.immuni.2013.06.014.

9. Galon J, Angell HK, Bedognetti D, Marincola FM. The continuum of cancer immunosurveillance: prognostic, predictive, and mechanistic signatures. *Immunity*. 2013;39(1):11–26. doi:10.1016/j.immuni.2013.07.008.

10. Chen DS, Mellman I. Oncology meets immunology: the cancer-immunity cycle. *Immunity*. 2013;39(1):1–10. doi:10.1016/j.immuni.2013.07.012.

11. Andre F, Dieci MV, Dubsky P, et al. Molecular pathways: involvement of immune pathways in the therapeutic response and outcome in breast cancer. *Clin Cancer Res*. 2013;19(1):28–33. doi:10.1158/1078-0432.CCR-11-2701.

12. Ghiringhelli F, Apetoh L, Tesniere A, et al. Activation of the NLRP3 inflammasome in dendritic cells induces IL-1β–dependent adaptive immunity against tumors. *Nat Med*. 2009;15(10):1170–1178. doi:10.1038/nm.2028.

13. Kreisel D, Gelman AE, Higashikubo R, et al. Strain-specific variation in murine natural killer gene complex contributes to differences in immunosurveillance for urethane-induced lung cancer. *Cancer Res*. 2012;72(17):4311–4317. doi:10.1158/0008-5472.CAN-12-0908.

14. Liu S, Kurzrock R. Toxicity of targeted therapy: implications for response and impact of genetic polymorphisms. *Cancer Treat Rev*. 2014;40(7):883–891. doi:10.1016/j.ctrv.2014.05.003.

15. Ross C, Visscher H, Rassekh SR, et al. Pharmacogenomics of serious adverse drug reactions in pediatric oncology. *J Popul Ther Clin Pharmacol*. 2011;18(1):e134–e151.

16. van Kuilenburg A, Haasjes J, Richel DJ, et al. Clinical implications of dihydropyrimidine dehydrogenase (DPD) deficiency in patients with severe 5-fluorouracil-associated toxicity: identification of new mutations in the *DPD* gene. *Clin Cancer Res*. 2000;6:4705–4712.

17. Stocco G, Cheok MH, Crews KR, et al. Genetic polymorphism of inosine triphosphate pyrophosphatase is a determinant of mercaptopurine metabolism and toxicity during treatment for acute lymphoblastic leukemia. *Clin Pharmacol Ther*. 2008;85(2):164–172. doi:10.1038/clpt.2008.154.

18. Fisher EMC, Beck JA, Lloyd S, et al. Genealogies of mouse inbred strains. *Nat Genet*. 2000;24(1):23–25. doi:10.1038/71641.

19. Pletcher MT, McClurg P, Batalov S, et al. Use of a dense single nucleotide polymorphism map for in silico mapping in the mouse. *Plos Biol*. 2004;2(12):e393. doi:10.1371/journal.pbio.0020393.

20. National Institutes of Health. *ClinicalTrials.gov*. 2014. Available at: https://clinicaltrialsgov. Accessed September 30, 2014.

21. Roberts PJ, Usary JE, Darr DB, et al. Combined PI3K/mTOR and MEK inhibition provides broad antitumor activity in faithful murine cancer models. *Clin Cancer Res*. 2012;18(19):5290–5303. doi:10.1158/1078-0432.CCR-12-0563.

22. Bekaii-Saab T, Phelps MA, Li X, et al. Multi-institutional phase II study of selumetinib in patients with metastatic biliary cancers. *J Clin Oncol*. 2011;29(17):2357–2363. doi:10.1200/JCO.2010.33.9473.

23. World Health Organization. *International Clinical Trials Registry Platform*. 2014. Available at: http://apps.who.int/trialsearch/. Accessed October 1, 2014.

24. Burris H, Rodon J, Sharma S, et al. First-in-human phase I study of the oral PI3K inhibitor BEZ235 in patients (pts) with advanced solid tumors. *J Clin Oncol (Meeting Abstracts)*. 2010;28(15_suppl3005).

25. Banerji U, Camidge DR, Verheul HMW, et al. The first-in-human study of the hydrogen sulfate (Hyd-sulfate) capsule of the MEK1/2 inhibitor AZD6244 (ARRY-142886): a phase I open-label multicenter trial in patients with advanced cancer. *Clin Cancer Res*. 2010;16(5):1613–1623. doi:10.1158/1078-0432.CCR-09-2483.

26. Bogue MA, Grubb SC. The Mouse Phenome Project. *Genetica*. 2004;122:71–74.

27. Johnson I, Spence MT, eds. *The Molecular Probes® Handbook—A Guide to Fluorescent Probes and Labeling Technologies*. 2010. Available at: http://www.lifetechnologies.com/us/en/home/brands/molecular-probes.html. Accessed July 17, 2014.

28. Buchser W, Collins M, Garyantes T, Guha R, Haney S. Assay development guidelines for image-based high content screening, high content analysis and high content imaging. In: Lemmon V, Li Z, Trask OJ, eds. *Assay Guidance Manual*; 2014:1–71.

29. Beam A, Motsinger-Reif AA. Beyond IC_{50}s: towards robust statistical methods for in vitro association studies. *J Pharmacogenomics Pharmacoproteomics*. 2014;5(1). doi:10.4172/2153-0645.1000120.

30. Reed DR, Bachmanov AA, Tordoff MG. Forty mouse strain survey of body composition. *Physiol Behav*. 200;91(5):593-600.

31. Moeller M, Hirose M, Mueller S, et al. Inbred mouse strains reveal biomarkers that are pro-longevity, antilongevity or role switching. *Aging Cell*. 2014;13(4):729–738. doi:10.1111/acel.12226.

32. Brown C, Havener TM, Everitt L, McLeod H, Motsinger-Reif AA. A comparison of association methods for cytotoxicity mapping in pharmacogenomics. *Front Genet*. 2011;2(86):1–14. doi:10.3389/fgene.2011.00086/abstract.

33. Nichols JL, Gladwell W, Verhein KC, et al. Genome-wide association mapping of acute lung injury in neonatal inbred mice. *FASEB J*. 2014;28(6):2538–2550. doi:10.1096/fj.13-247221.

34. The Jackson Laboratory. Flow-cytometric analysis of 11 inbred strains of mice. MPD:Jaxpheno6. *Mouse Phenome Database web site*. 2014. Available at: http://phenome.jax.org. Accessed July 17, 2014.

35. Wiltshire T. Toxicity of anti-cancer agents in immune cells from 36 inbred mouse strains. MPD:Wiltshire4. *Mouse Phenome Database web site*. 2014. Available at: http://phenome.jax.org. Accessed August 26, 2014.

36. Lu SX, Na I-K, McIntyre CA, Sasaki D, Balderas R, van den Brink MRM. Construction of multicolor antibody panels for the flow cytometric analysis of murine thymic stromal cells. *BD Biosciences Application Note*. 2009. Available at: https://www.bdbiosciences.com/documents/lsr_appnote02.pdf. Accessed August 7, 2014.

37. An introduction to compensation for multicolor assays on digital flow cytometers. *BD Biosciences Technical Bulletin.* 2009. Available at: http://www.bdbiosciences.com/documents/Compensation_Multicolor_TechBulletin.pdf. Accessed August 7, 2014.

38. GraphPad Software Inc. GraphPad Prism Learning Guide. 2007. Available at: http://www.graphpad.com/help/Prism5/Prism5Help.html?using_regression_guide_2.htm. Accessed September 30, 2014.

39. Heuvers ME, Aerts JG, Cornelissen R, Groen H, Hoogsteden HC, Hegmans JP. Patient-tailored modulation of the immune system may revolutionize future lung cancer treatment. *BMC Cancer*. 2012;12(1):580–591. doi:10.1186/1471-2407-12-580.

40. Hanahan D, Weinberg RA. Hallmarks of cancer: the next generation. *Cell*. 2011;144(5):646–674. doi:10.1016/j.cell.2011.02.013.

41. Taube JM, Klein AP, Brahmer JR, et al. Association of PD-1, PD-1 ligands, and other features of the tumor immune microenvironment with response to anti-PD-1 therapy. *Clin Cancer Res*. 2014. doi:10.1158/1078-0432.CCR-13-3271.

42. Obeid M, Tesniere A, Ghiringhelli F, et al. Calreticulin exposure dictates the immunogenicity of cancer cell death. *Nat Med*. 2006;13(1):54–61. doi:10.1038/nm1523.

43. Barpe DR, Rosa DD, Froehlich PE. Pharmacokinetic evaluation of doxorubicin plasma levels in normal and overweight patients with breast cancer and simulation of dose adjustment by different indexes of body mass. *Eur J Pharm Sci*. 2010;41(3-4):458–463. doi:10.1016/j.ejps.2010.07.015.

44. Bengala C, Danesi R, Guarneri V, et al. High-dose consolidation chemotherapy with idarubicin and alkylating agents following induction with gemcitabine–epirubicin–paclitaxel in metastatic breast cancer: a dose finding study. *Bone Marrow Transplant*. 2003;31(4):275–280. doi:10.1038/sj.bmt.1703827.

45. Maira SM, Stauffer F, Brueggen J, et al. Identification and characterization of NVP-BEZ235, a new orally available dual phosphatidylinositol 3-kinase/mammalian target of rapamycin inhibitor with potent. in vivo antitumor activity. *Mol Cancer Ther*. 2008;7(7)1851-1863. doi:10.1158/1535-7163.MCT-08-0017.

46. Bracci L, Schiavoni G, Sistigu A, Belardelli F. Immune-based mechanisms of cytotoxic chemotherapy: implications for the design of novel and rationale-based combined treatments against cancer. *Cell Death Differ*. 2013;21(1):15–25. doi:10.1038/cdd.2013.67.

47. Bronte V, Pittet MJ. The spleen in local and systemic regulation of immunity. *Immunity*. 2013;39(5):806–818. doi:10.1016/j.immuni.2013.10.010.

48. Frick A, Suzuki O, Butz N, Chan E, Wiltshire T. In vitro and in vivo mouse models for pharmacogenetic studies. In: Innocenti F, Schaik RHN, eds. *Pharmacogenomics*. Vol 1015. Methods in Molecular Biology. Totowa, NJ: Humana Press; 2013:263–278. doi:10.1007/978-1-62703-435-7_17.

49. Harrill AH, Watkins PB, Su S, et al. Mouse population-guided resequencing reveals that variants in CD44 contribute to acetaminophen-induced liver injury in humans. *Genome Res*. 2009;19(9):1507–1515. doi:10.1101/gr.090241.108.

50. Fallahi-Sichani M, Honarnejad S, Heiser LM, Gray JW, Sorger PK. Metrics other than potency reveal systematic variation in responses to cancer drugs. *Nat Chem Biol*. 2013;9(11):708–714. doi:10.1038/nchembio.1337.

51. Haibe-Kains B, El-Hachem N, Birkbak NJ, et al. Inconsistency in large pharmacogenomic studies. *Nature*. 2014;504(7480):389–393. doi:10.1038/nature12831.

52. Paolini GV, Lyons RA, Laflin P. How desirable are your IC50s? A way to enhance screening-based decision making. *J Biomol Screen*. 2010;15(10):1183–1193. doi:10.1177/1087057110384402.

CHAPTER 3[3]: IDENTIFYING GENETIC MARKERS FOR CYTOTOXIC RESPONSE TO ANTHRACYCLINES IN IMMUNE CELLS

3.1. Overview

Background: While the role of the immune system in cancer development is known, its role in response to chemotherapeutic agents remains elusive. Interpatient variability in immune and chemotherapeutic cytotoxic responses is likely due to complex genetic differences. Through the use of a panel of genetically diverse mouse inbred strains, we developed a drug screening platform aimed at examining genes underlying these chemotherapeutic cytotoxic responses on immune cells.

Methods: Methods for our phenotypic screen are well described elsewhere. Briefly, splenocytes were isolated from 36 isogenic strains of mice using standard procedures. Cells were incubated with doxorubicin, idarubicin, BEZ235, or selumetinib on a 9-point logarithmic dosing scale ranging from 15 nM to 100 μM. At 4 hours post-treatment, cells were labeled with antibodies and physiological indicator dyes and were fixed prior to analysis by flow cytometry. Cellular phenotypes were collected using multiplexed flow cytometry assays and analyzed for variable phenotypic response. Dose response curves with response normalized to the zero dose as a function of log concentration were subsequently generated. Furthermore, two genome-wide association (GWA) algorithms were used to perform GWA mapping, providing precision in localizing quantitative trait loci (1 to 2 Mb). Potential candidate genes for validation studies were prioritized based on several criteria, including association scores (-log(*p*) scores), spleen

[3] This chapter has been prepared for journal publication.

expression data, and biological relevance. This approach led to the selection of *App* for downstream validation studies. The role of *App* in immune-mediated cytotoxicity was investigated by comparing splenic T-cell response to idarubicin between *App* knockout and C57BL/6J mice.

Results: Using GWA studies, we identified loci that contributed to the sensitivity of doxorubicin and idarubicin in immune cells. We identified four genome-wide significant quantitative trait loci (QTL) from three phenotypes. Of particular interest, a locus on chromosome 16 was significantly associated with cell viability following idarubicin administration ($p = 5.01 \times 10^{-8}$). from viability of T-cells exposed to idarubicin. Within this QTL lies *App*, which encodes amyloid beta precursor protein. Comparison of dose response curves verified that T-cells in App knockout mice were more sensitive to idarubicin than those of C57BL/6J control mice ($p < 0.05$).

Conclusions: Using a cellular screening approach, we identified and subsequently validated a gene involved in mediating T-cell response to idarubicin. Previous studies have suggested a role for *App* in in vitro and in vivo cytotoxicity to anticancer agents; the overexpression of *App* enhances resistance, while the knockdown of this gene is deleterious to cell viability. In the future, we aim to perform mechanistic studies and to ultimately translate our findings to in vivo and human studies.

3.2. Introduction

The role of the immune system in cancer development is well established with the evasion of immune elimination described as one of Hanahan and Weinberg's hallmarks of cancer.[1] Developing tumors commonly avoid immune surveillance by inducing an immunosuppressive tumor microenvironment with regulatory T-cells, myeloid-derived

suppressor cells, alternatively activated macrophages, and tolerant dendritic cells.[2] Thus, the induction, potency, and persistence of the patient's functional immune system is critical to combating tumor advancement.[3]

The generation of an efficacious clinical antitumor response depends upon the successful initiation of several immune processes. In this regard, the adaptive immune system has been described as an ideal anticancer agent with features including diversity, specificity, and memory. Recent advances in immune-based therapeutic approaches have focused on boosting the adaptive antitumor immune response using various approaches, including vaccination, adoptive T-cell therapy, anti-tumor antibodies, and the advent of immune checkpoint blockade agents.[4-8] Clinically, monitoring T- and B-cell response may prove useful in correlating specific immune responses to patient outcomes.[3] For instance, patients with denser T-cell infiltrates in a variety of cancer tumors have better clinical responses to traditional, cytotoxic chemotherapy compared to patients with smaller infiltrates.[9] Some cytotoxic chemotherapeutics, such as anthracyclines, promote immunogenic cell death by releasing molecules such as calreticulin, which subsequently primes T-cells for modulation to an antitumor Th1 phenotype.[10,11] Therefore, assessing the functionality of an immune system is crucial for evaluating clinical responses to cytotoxic chemotherapy.[12]

Previous studies have noted intersubject variability in chemotherapy-induced cytotoxic responses within the immune system.[13-15] Although several genes have been linked to the toxicity of anticancer chemotherapy on the innate immune system (ie, neutropenia), the role of pharmacogenomics in the cytotoxicity of the adaptive immune system requires further investigation. A model organism approach was used to evaluate pharmacotherapeutic response, as the effects of chemotherapy on the normal immune system are difficult to ascertain in humans.

We previously developed a cell-based screen using immune cells from 36 inbred mouse strains to measure phenotypic differences in immune cell sensitivity to anticancer therapeutics.[16] We were able to robustly identify interstrain variation in T- and B-cell viability to cytotoxic anthracycline agents, doxorubicin and idarubicin. In this study, we examined the underlying genetic components that may be responsible for these differences. Following genome-wide association studies (GWAS), we identified a candidate gene, *App* (encoding amyloid beta precursor protein) that was further shown to be involved in mediating T-cell response to idarubicin.

3.3. Materials and Methods

3.3.1. Phenotype Determination

The methods and results of our drug-screening platform in normal, noncancerous, murine immune cells have been previously described.[16] Briefly, splenocytes were collected from a panel of 36 inbred mouse strains (n = 4 per strain, 129S1/SvImJ, 129X1/SvJ, A/J, AKR/J, BALB/cByJ, BTBR T^{+} *Itpr3*^{tf}*/J*, BUB/BnJ, C3H/HeJ, C57BLKS/J, C57BL/6J, C57BR/cdJ, C58/J, CBA/J, CZECHII/EiJ, DBA/2J, FVB/NJ, I/LnJ, KK/HiJ, LG/J, LP/J, MA/MyJ, NOD/LtJ, NON/LtJ, NZB/BINJ, NZO/HiLtJ, NZW/LacJ, PERA/EiJ, PL/J, PWD/PhJ, PWK/PhJ, RIIIS/J, SEA/GnJ, SJL/J, SM/J, SWR/J, and WSB/EiJ), aged 10-12 weeks, obtained from The Jackson Laboratory Mouse Diversity Panel (Bar Harbor, ME). Splenocytes were isolated using standard procedures and exposed to nine logarithmic concentrations of doxorubicin, idarubicin, BEZ-235, and selumetinib ranging from 15 nM to 100 μM. At 4 h post-treatment, cells were sequentially incubated (37°C, 5% CO_2) with physiological indicator dyes (eg, 7-AAD, CellEvent™ Caspase-3/7 Green Detection Reagent, and Mitotracker® Deep Red) and cell surface marker antibodies and then fixed with 4% paraformaldehyde. Samples were analyzed by flow cytometry using a

BD FACSCanto™ II flow cytometer and Flow Jo version X. Dose response curves with response normalized to the zero dose as a function of log concentration were generated. Viability measurements of B-cells and T-cells exposed to the anthracyclines provided the most heritable phenotypes in our screen and were reserved for QTL mapping.[16]

3.3.2. Quantitative Trait Loci (QTL) Mapping

GWAS were performed for IC_{50} values, AUC values, and individual drug concentrations that corresponded to cell viability for splenic B-cells and T-cells exposed to doxorubicin and idarubicin. SNPster and efficient mixed-model association (EMMA) algorithms, which are well described elsewhere, were used for QTL mapping.[17,18] Briefly, SNPster performs QTL mapping analysis from an inferred haplotype structure determined by overlapping 3-SNP windows for each strain. Using one-way ANOVA, an *F*-statistic was calculated following association analyses of phenotypic values with haplotypes. *p* values are then estimated by bootstrapping phenotypic values $1x10^6$ times, providing a maximum –log(*p*) score of 6.0.[17] EMMA uses *F*-tests for single marker association mapping while accounting for population structure and genetic relatedness.[18] SNP genotypes used for GWA were obtained from the Mouse Diversity Array set at the CGDSNPdb website (http://cgd.jax.org/cgsnpdb/).[19] The SNP panel was trimmed for redundancy (SNPs showing identical haplotype pattern at a locus), missingness (genotyping call rates <95%), and non-informative nature (SNPs without variation amongst the 36 strains), leaving a panel of 356,596 SNPs. Manhattan plots were visualized using R version 3.1.0 and the UCSC Mouse Genome Browser on the Mouse July 2007 (NCBI37/mm9) Assembly (https://genome.ucsc.edu).[20] The threshold of significance for QTL mapping was adjusted using the conservative Bonferroni correction. QTL were considered significant when -log(*p*) score was ≥ 6.853.

3.3.3. Candidate Gene Selection

QTL regions that overlapped using both association mapping algorithms, although both were not required to be genome-wide significant ($-\log(p) \geq 6.853$), were further selected for candidate gene selection. Candidate genes were prioritized based on the following: literature evidence for biological involvement with the immune system or anthracycline response, differential gene expression in spleens and immune cells, the correlation between phenotypic values and gene expression levels in spleens and immune cells, similarity in the haplotype structure between the QTL and the candidate gene, the presence of potentially deleterious non-synonymous coding SNPs, and apoptotic or immune cell pathway involvement (Figure 3.1).[21] Candidate genes were only included if they were expressed in the spleen, the tissue originally assayed to produce our phenotypes of interest. Expression levels were measured in spleens and immune cells from inbred strains of mice using the Affymetrix Mouse Genome 2.0 Array (Santa Clara, CA). Genes were considered expressed if their expression level was greater than 50 for at least one of the strains following data processing with the gcRMA algorithm. Non-synonymous coding SNPs were obtained from dbSNP (http://www.ncbi.nlm.nih.gov/projects/SNP/). The likely effect of amino acid substitutions in protein sequences was determined using PROVEAN (Protein Variation Effect Analyzer) version 1.1.3[22] and PANTHER (Protein Analysis Through Evolutionary Relationships) version 9.0 software. [23,24] Using PROVEAN, a score of -2.5 indicates a functional effect on the protein. For the PANTHER algorithm, a subSPEC (substitution position-specific evolutionary conservation) score of -3 corresponds to a 50% probability that a score is deleterious ($P_{deleterious} = 0.5$). Chilibot[25] (http://www.chilibot.net) was used to search the PubMed literature database for biological relevance of gene involvement

Figure 3.1. Candidate gene prioritization.

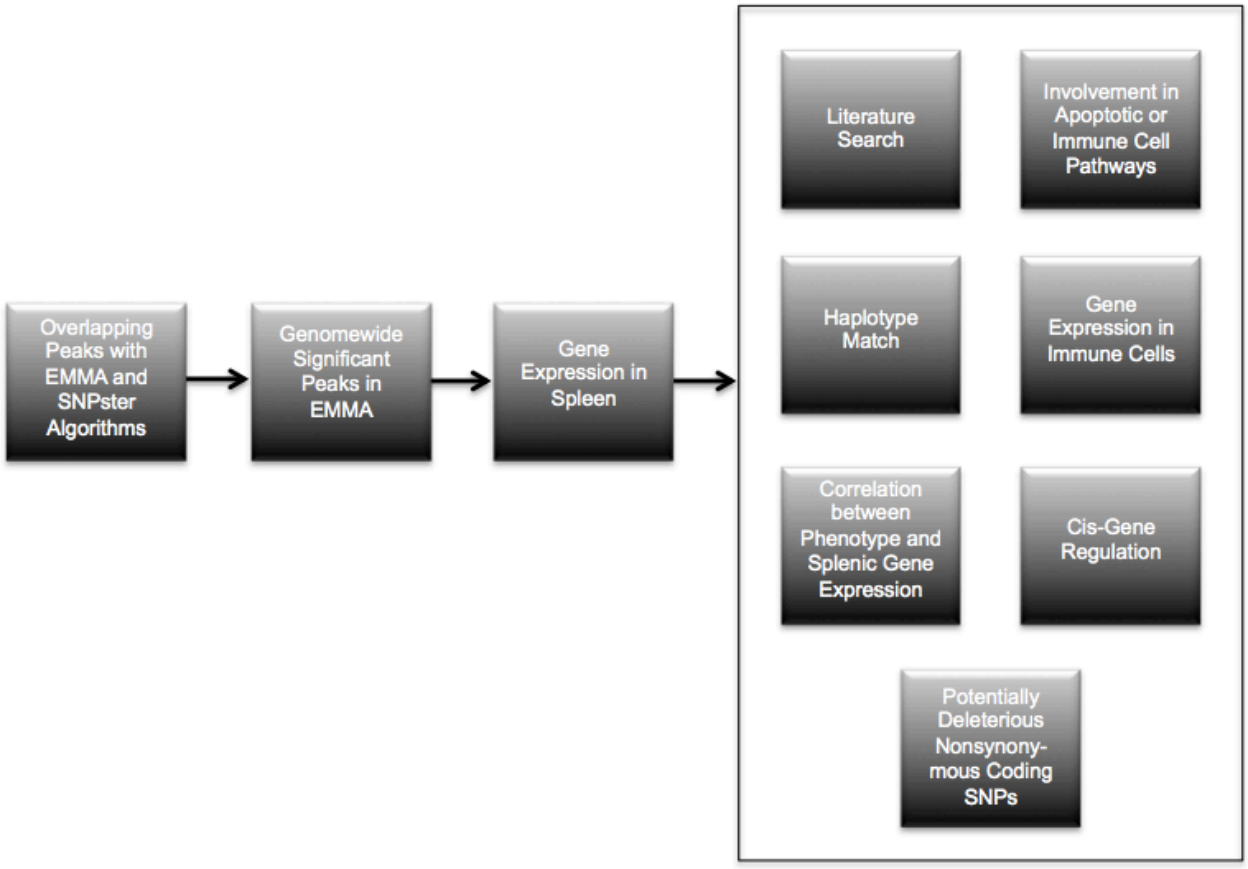

in immune cells or anthracycline response. Ingenuity® Pathway Analysis was used to gauge the involvement of genes in apoptotic or various immune function pathways (http://www.ingenuity.com/). Haplotype structure for the interval and for specific genes was reviewed with the Mouse Phylogeny Viewer (https://msub.csbio.unc.edu/).[26]

3.3.4. App *Gene Validation*

Based on the criteria for candidate gene validation as described above, *App* was chosen for downstream validation studies. An in vitro knockout approach was used for validation of *App*. *App* knockout (B6.129S7-*App*^{tm1Dbo}/J, stock number: 004133) and C57BL/6J control (stock number: 000664) male mice aged 10-12 weeks were obtained from the Jackson Laboratory (Bar

Harbor, ME). Mice homozygous for the targeted allele are viable without blatant physical and behavioral abnormalities at birth other than a reduced body weight of 15-20% less than wildtype age-matched controls. At 14 weeks of age, an age beyond the range we included in our assay, the mice exhibit evidence of reactive gliosis with significantly reduced forearm grip strength and reduced locomotion.[27] Mice were housed three per cage in polycarbonate cages on a 12 h light/dark cycle (lights on at 0700 hours) with access to food and water ad libitum. Following one week of habituation, splenic phenotypes from these knockout and control mice were generated as described above.[16] All procedures were approved by the UNC Institutional Animal Care and Use Committee and followed the guidelines set forth by the National Institutes of Health Guide for the Care and Use of Laboratory Animals.

3.3.5. Statistical Analyses

After detecting immune cell populations of interest (ie, CD19+ B-cells, CD3e+ T-cells, and CD11b+ monocytes), cells positive for physiological indicator dyes in each subpopulation were gated. Dose response curves with response normalized to the zero dose as a function of log concentration were generated using GraphPad Prism 6 (La Jolla, CA) and the Hill equation: $f(x)=Max-((Max-Min)/(1+(x/IC_{50})^{\gamma}))$, where Max is the maximum asymptote, Min is the minimum asymptote, γ is the Hill slope, and x is the drug concentration.[28] Additional statistical analyses, including Pearson correlations, *t*-tests, and partial *F*-tests, were performed with SAS version 5.2 (Cary, NC) and GraphPad Prism 6 with $p < 0.05$ considered to be statistically significant. Pearson correlations were performed to determine the relatedness between metrics.[29] Dose response curves from knockout and control populations were compared using *t*-tests for IC_{50} and viability measurements. Finally, a partial *F*-test was used to determine if the data fitting would be best using one or two dose response curves.

Figure 3.2. Phenotypes for GWAS.

Notes: Dose response curves reflecting interstrain variation in viability are shown for T-cells exposed to idarubicin (**A**), B-cells exposed to doxorubicin (**B**), and B-cells exposed to doxorubicin (**C**). Thirty-six strains are represented: 129S1/SvImJ, 129X1/SvJ, A/J, AKR/J, BALB/cByJ, BTBR T^{+} *Itpr3*^{tf}*/J*, BUB/BnJ, C3H/HeJ, C57BLKS/J, C57BL/6J, C57BR/cdJ, C58/J, CBA/J, CZECHII/EiJ, DBA/2J, FVB/NJ, I/LnJ, KK/HiJ, LG/J, LP/J, MA/MyJ, NOD/LtJ, NON/LtJ, NZB/BINJ, NZO/HiLtJ, NZW/LacJ, PERA/EiJ, PL/J, PWD/PhJ, PWK/PhJ, RIIIS/J, SEA/GnJ, SJL/J, SM/J, SWR/J, and WSB/EiJ. Concentrations used to generate genomewide significant QTL (respectively 1, 0.3, and 3 μM) are enclosed with a black box.

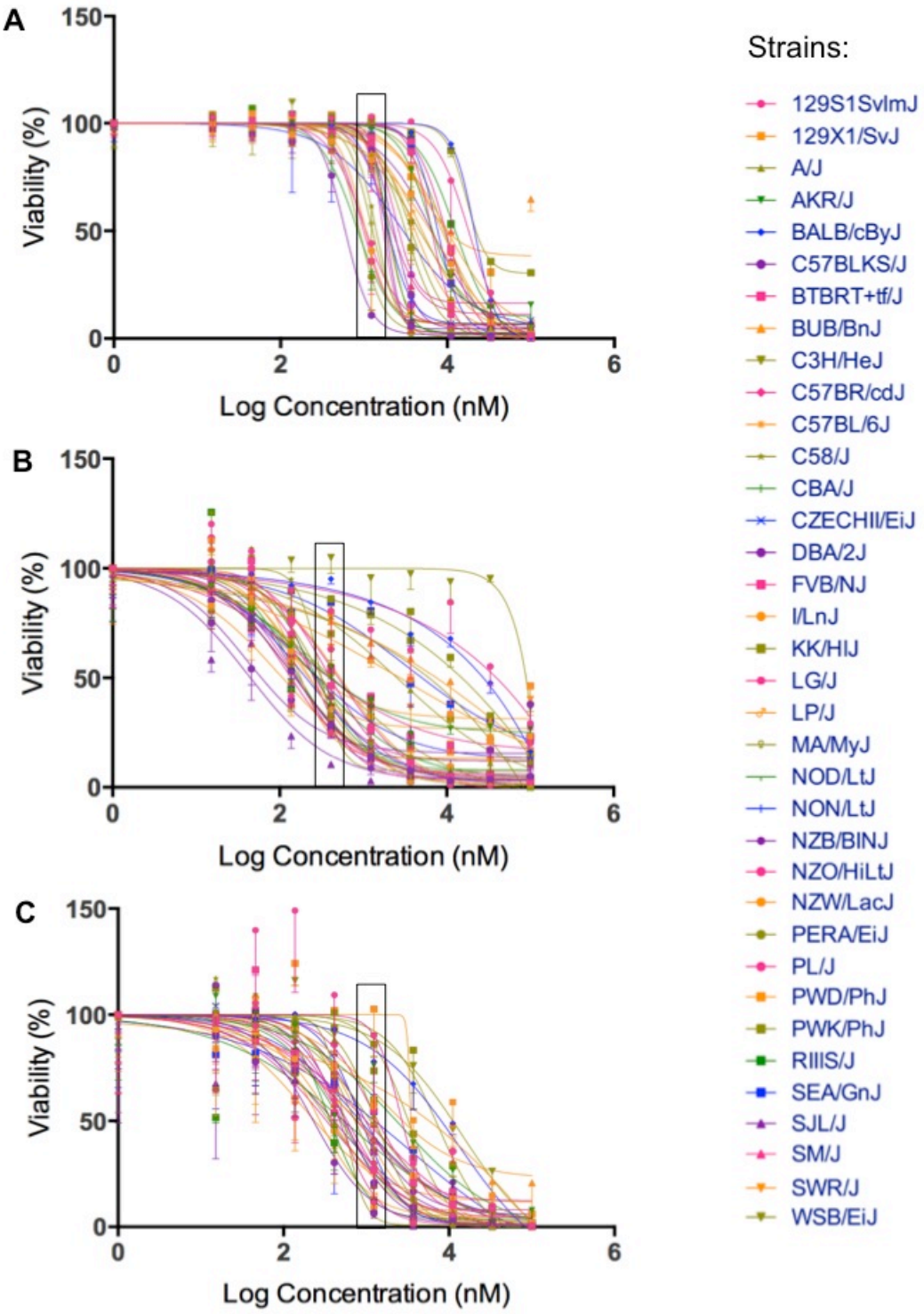
A
B
C
Viability (%)
Log Concentration (nM)
150
100
50
0
0
2
4
6
Strains:
129S1SvImJ
129X1/SvJ
A/J
AKR/J
BALB/cByJ
C57BLKS/J
BTBRT+tf/J
BUB/BnJ
C3H/HeJ
C57BR/cdJ
C57BL/6J
C58/J
CBA/J
CZECHII/EiJ
DBA/2J
FVB/NJ
I/LnJ
KK/HIJ
LG/J
LP/J
MA/MyJ
NOD/LtJ
NON/LtJ
NZB/BINJ
NZO/HiLtJ
NZW/LacJ
PERA/EiJ
PL/J
PWD/PhJ
PWK/PhJ
RIIIS/J
SEA/GnJ
SJL/J
SM/J
SWR/J
WSB/EiJ

3.4. Results

Results from our initial phenotypic screen for downstream GWA analyses have been previously discussed.[16] Although we measured multiple cell health parameters, the cell viability phenotype was most robust for GWAS. Figure 3.2 displays the interstrain phenotypic variation for the most heritable viability phenotypes: T-cells exposed to idarubicin (Figure 3.2A), B-cells exposed to doxorubicin (Figure 3.2B), and B-cells exposed to idarubicin (Figure 3.2C). Several strains repeatedly appear to be more sensitive (eg, C57BLKS/J and DBA/2J) or less sensitive (eg, BALB/cByJ, KK/HiJ, and WSB/EiJ) to the cytotoxic effects of the different anthracycline agents across cell type. The concentrations (respectively 1, 0.3, and 3 μM) contained in black boxes corresponded to the phenotypic values that generated genomewide significant QTL with respective heritability measurements of 87.5, 70.6, and 85%. The viability measurements at these concentrations significantly correlated with IC_{50} values obtained from our assay with respective Pearson correlations of 0.82489 ($p < 0.0001$), 0.85942 ($p < 0.0001$), and 0.92028 ($p < 0.0001$).

Using a GWA approach, we identified four genomewide significant QTLs that overlapped using both SNPster and EMMA algorithms: chr16 84.7 Mb to 85.6 Mb for T-cells exposed to idarubicin (Figure 3.3A), chr6 146.5 Mb to 147.5 Mb for B-cells exposed to doxorubicin (Figure 3.3B), and chr7 151.4 Mb to 152.0 Mb and chr5 74.5 Mb to 74.9 Mb for B-cells exposed to idarubicin (Figure 3.3C). Within these four QTL peaks, there were 25 genes that were further prioritized using the criteria described previously (Figure 3.1). Only 16 out of 25 genes affiliated with genomewide significant peaks were expressed in the spleen (expression level > 50) and included for prioritization (Table 3.1).

The viability of splenic T-cells following idarubicin exposure is a robust phenotype exhibiting strong interstrain variability. This phenotype was strongly linked to a 0.9 Mb region

(84.7 Mb to 85.6 Mb) on chromosome 16 containing eight genes, six of which met criteria for candidate gene prioritization (Figure 3.4). Table 1 lists characteristics for all candidate genes across various dose-response phenotypes. Briefly, of the six genes, *App* was one of four (ie, *Atp5j*, *Gabpa*, and *Mir155*) that is involved in apoptosis and immune cell pathways via Ingenuity®. Per Chilibot, *App* is the only gene with a known relation to anthracyclines and one of two genes (ie, *Mir155*) that is related in the literature to the immune system. The haplotype structure of *App*, *Gabpa*, and *Mrpl39* contained groupings of strains corresponding to sensitive and resistant phenotypes. *App* and *Mrpl39* have potentially deleterious SNPs. *App* is also the only gene under this peak that is differentially expressed (≥2 fold difference in expression levels) across our selected inbred mouse strains in the spleen, CD4+ cells, CD4+ Th1 cells, and macrophages. For these reasons, *App*, encoding amyloid beta precursor protein, was chosen for validation.

Figure 3.3. Manhattan plots for immune cell cytotoxicity to anthracycline agents.

Notes: Manhattan plots were obtained from GWAS using EMMA and SNPster algorithms for T-cells exposed to idarubicin (**A**), B-cells exposed to doxorubicin (**B**), and B-cells exposed to doxorubicin (**C**). Manhattan plots derived from EMMA are displayed above Manhattan plots from SNPster. The threshold of genomewide significance ($-\log(p) \geq 6.853$ following Bonferroni correction) is represented by the horizontal red line. The black boxes contain matching QTL peaks obtained with both EMMA and SNPster algorithms respectively on chromosomes 16 (**A**), 6 (**B**) 5, and 7 (**C**).

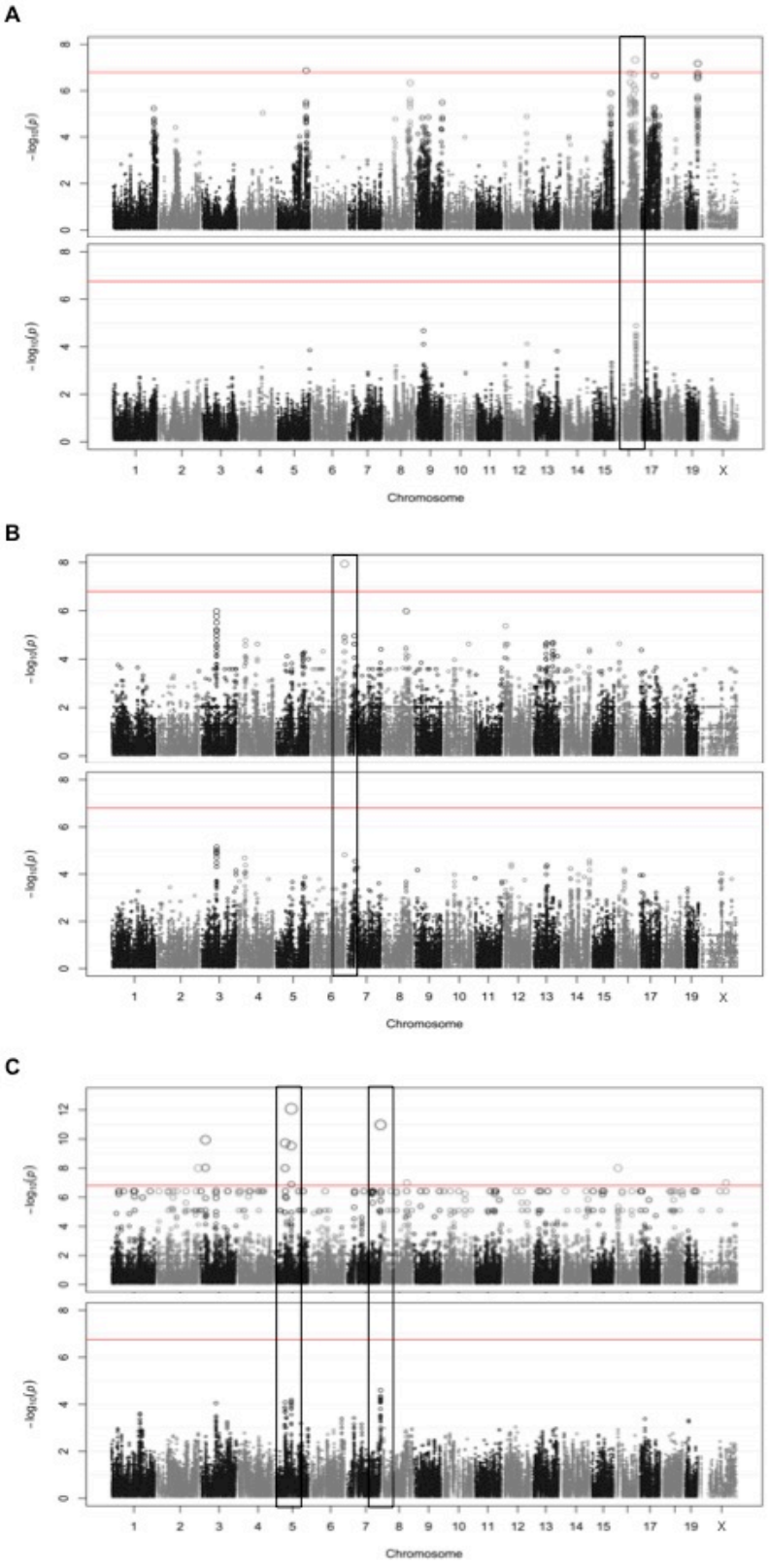
A
B
C
Chromosome
1 2 3 4 5 6 7 8 9 10 11 12 13 14 15 17 19 X

Figure 3.4. Genomic region associated with T-cell toxicity following idarubicin exposure.

Notes: Potential candidate genes from the Reference Sequence database on chromosome 16 are displayed using Manhattan plots that were generated from both EMMA and SNPster algorithms. The candidate QTL within a 0.9 Mb region is visualized with the UCSC Genome Browser (http://genome.ucsc.edu) with the QTL region derived from EMMA displayed above the QTL region from SNPster.

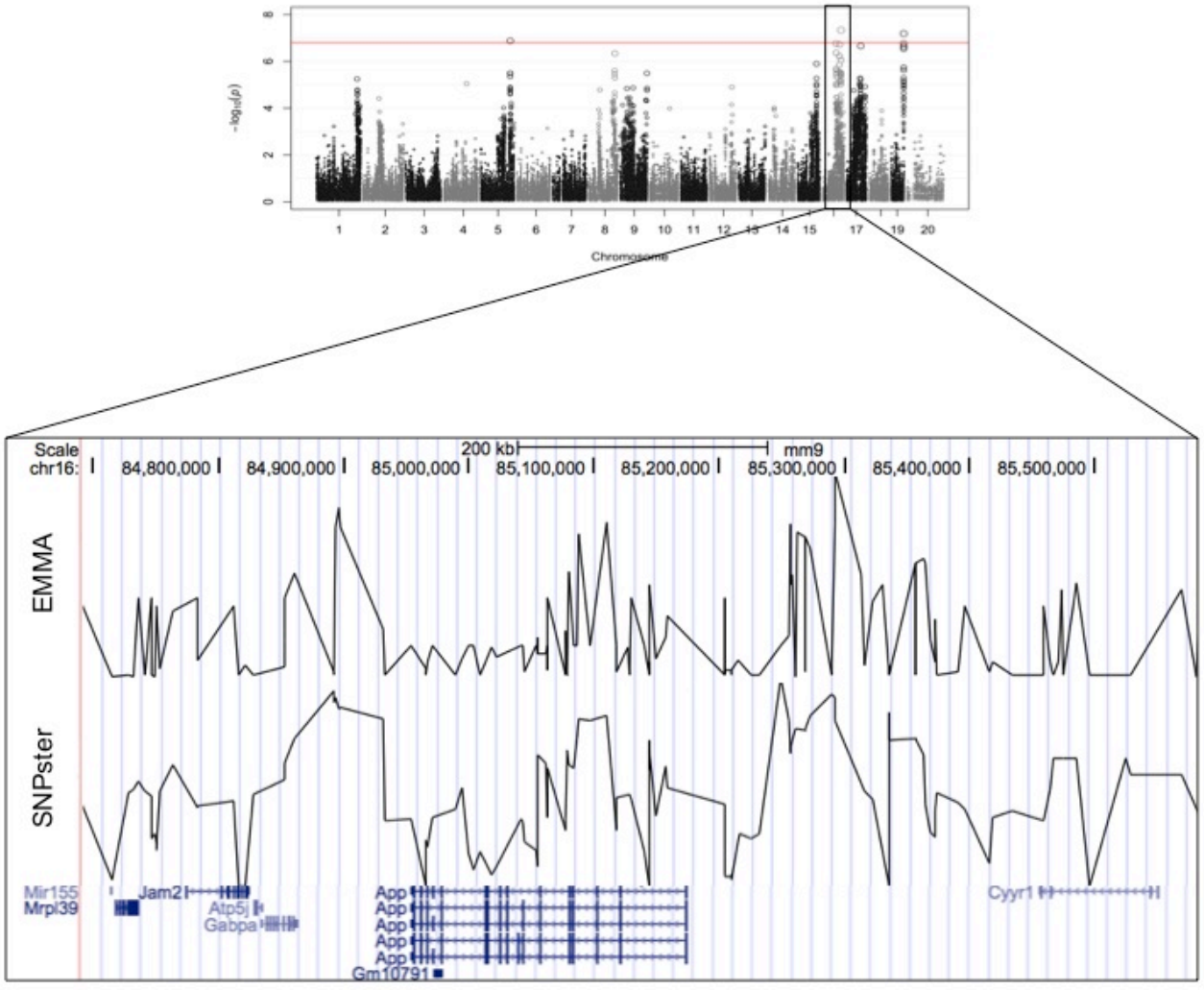

Figure 3.5. Haplotype structure of *App*.

Notes: The haplotype structure of the inbred mouse strains within *App* is shown. Strains are arranged in descending order of phenotype from most to least sensitive. The haplotype structure was visualized with the Mouse Phylogeny Viewer (https://msub.csbio.unc.edu/). Within *App*, non-synonymous coding SNPs are indicated by arrows.

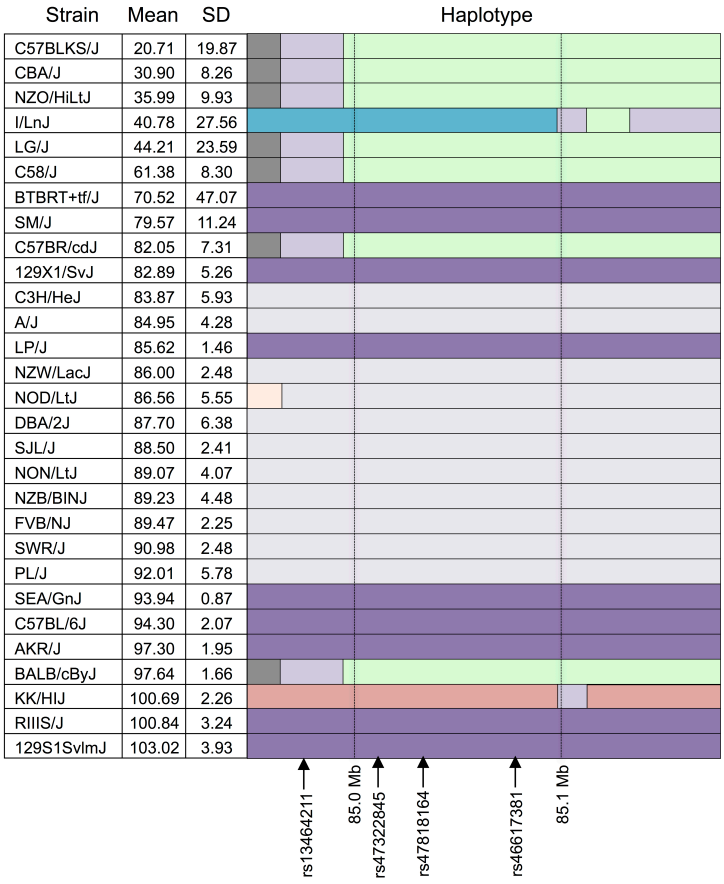

As shown in Figure 3.5, the haplotype structure of *App* illustrates the grouping of strains with a particular haplotype, which corresponds to sensitive and resistant phenotypes. Additionally, the gene does contain non-synonymous coding SNPs, which introduce the following amino acid sequence changes in the protein: D516E, A480V, D309E, and G221S. Using PROVEAN and PANTHER algorithms, A480V and D309E were classified as likely deleterious to App (Figure 3.6). Finally, based on literature review, although associated

mutations and differences in expression in *App* are typically linked to Alzheimer's disease, there is a role for *App* in cytotoxicity involving chemotherapeutics.[30,31]

Figure 3.6. *App* non-synonymous coding SNPs and associated protein structure.

Notes: Non-synonymous coding SNPs within *App* from the Center for Genome Dynamics (http://cgd.jax.org/cgdsnpdb) and the likelihood of SNPs causing deleterious effects within the associated protein's structure using PROVEAN and the PANTHER Classification System are displayed. Using PROVEAN, a score of -2.5 indicates a functional effect on the protein. For the PANTHER algorithm, a subSPEC (substitution position-specific evolutionary conservation) score of -3 corresponds to a 50% probability that a score is deleterious ($P_{deleterious} = 0.5$). The structure of App is provided below with key domains and the sites of amino acid substitutions.

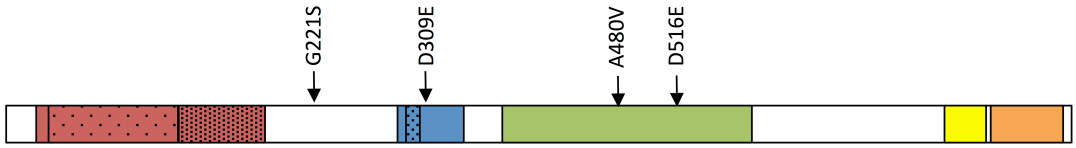

Residues	Domain
24-188	A4
30-131	N-terminal heparin binding
132-188	Copper-binding
295-342	KU
299-305	Trypsin-interaction site
365-549	E2 domain
682-713	Beta-App
715-766	Amyloid C-terminus

Gene	Position m38	Position 37	SNP ID	Protein Change	PROVEAN Score	Prediction	subPSEC	P deleterious	MSA position	Pwt	P substituted	NIC
App	Chr16:84978200	Chr16:84978445	rs13464211	D516E	-1.388	Neutral	-2.55755	0.39116	593	0.68652	0.05813	1.461
App	Chr16:85013650	Chr16:85013895	rs47322845	A480V	-3.156	Deleterious	-4.47146	0.81328	558	0.8039	0.01569	2.794
App	Chr16:85030304	Chr16:85030549	rs47818164	D309E	-1.501	Neutral	-3.67619	0.66289	387	0.82081	0.03466	2.49
App	Chr16:85079841	Chr16:85080086	rs46617381	G221S	1.273	Neutral	-1.74936	0.22259	240	0.09802	0.49028	1.39

A gene validation study was performed using splenocytes from *App* knockout (B6.129S7-*App*^{tm1Dbo}/J) and C57BL/6J control mice, subjected to the same conditions within our cellular screen. Without drug exposure, the relative splenic T-cell composition and viability of *App* knockout versus control mice were not statistically different using a *t*-test ($p > 0.05$, respectively

$p = 0.344$ and $p = 0.386$). However, T-cells from *App* knockout mice were less viable than that of the control mice following exposure to idarubicin (Figure 3.7). Given that the IC_{50} value for the control mice (3.48, 95% CI: 3.401-3.56) is significantly higher than the IC_{50} value for the *App* knockout mice (3.28, 95% CI: 3.18-3.38), this result suggests that susceptibility to idarubicin-induced cytotoxicity on T-cells is greater with the absence of *App* ($p < 0.05$). Additionally, the knockout of *App* was significantly associated with increased cell toxicity as observed by the shift to the left in the dose response curve from the control mice (partial *F*-test, $p = 0.0056$, Figure 3.7).

Figure 3.7. In vitro validation of *App* in T-cell toxicity following idarubicin exposure.

Notes: Dose response curves were generated following exposure of splenic T-cells from C57BL/6J control mice (N = 3) and *App* knockout mice (N = 3) to idarubicin. A significant shift to the left was observed in *App* knockout cells as calculated using a partial *F* test ($p = 0.0056$).

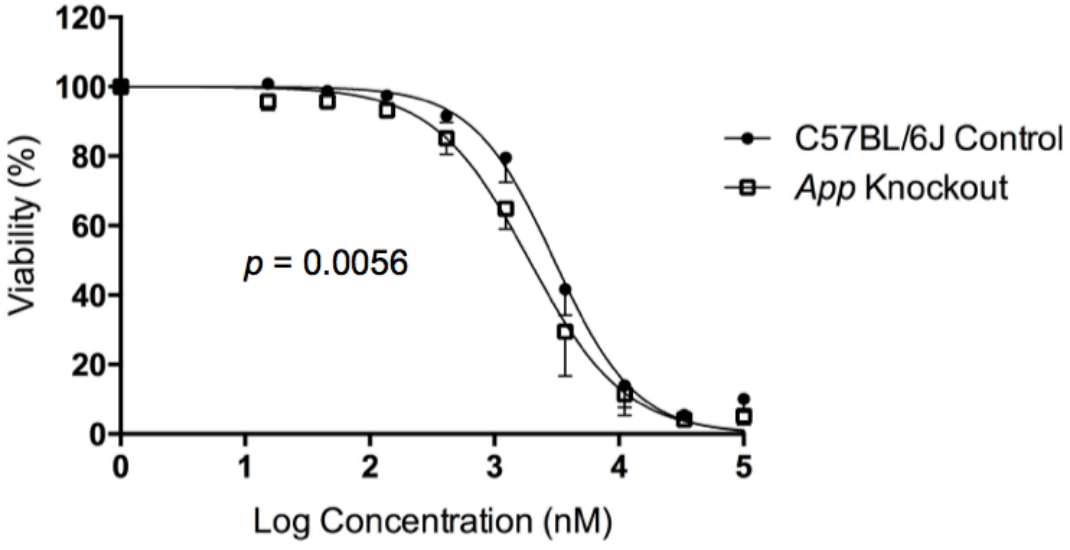

Table 3.1. Candidate genes from the phenotypic screen.

Cell Type	Drug and Dose	Gene Symbol	Gene Name	Genomewide Significance	Expressed in Spleen	Differentially Expressed in Spleen	Correlated in Spleen	Cis-Regulated	Expressed in CD4	Differentially Expressed in CD4	Correlated in CD4	Expressed in CD4 Th1	Differentially Expressed in CD4 Th1	Correlated in CD4 Th1	Expressed in Macrophages	Differentially Expressed in Macrophages	Correlated in Macrophages	Haplotype Match	Nonsynonymous SNPs	Deleterious SNPs	Immune System or Cancer Related	Anthracycline Related	Ingenuity Pathway
B-cells	Idarubicin 3μM	Ano1	anoctamin 1, calcium activated chloride channel	10.98	Yes	Yes	-	-	-	-	-	-	-	-	-	-	-	Trend	R731H F643L H270Q	R731H F643L	Yes	-	Immune Cell
T-cells	Idarubicin 1μM	App	amyloid beta (A4) precursor protein	7.34	Yes	Yes	-	-	Yes	Yes	-	Yes	Yes	-	Yes	Yes	-	Yes	D516E A480V D309E G221S	D516E A480V D309E	Yes	Yes	Apoptosis and Immune Cell
T-cells	Idarubicin 1μM	Atp5j	ATP synthase, H+ transporting, mitochondrial F0 complex, subunit F	7.34	Yes	Yes	-	-	Yes	-	-	Yes	-	Yes	Yes	-	Yes	-	-	-	-	-	Apoptosis and Immune Cell
B-cells	Doxorubicin 0.3μM	Ccdc91	coiled-coil domain containing 91	7.94	Yes	Yes	-	-	Yes	Yes	-	Yes	Yes	-	Yes	Yes	-	Yes	S70T G324E A346E V439L I441V	-	-	-	-
B-cells	Idarubicin 3μM	Cttn	cortactin	10.98	Yes	Yes	-	Yes	-	-	-	Yes	Yes	-	Yes	Yes	Yes	Trend	Y475Ter I449L H111Q	Y475Ter H111Q	Yes	Yes	Apoptosis and Immune Cell
T-cells	Idarubicin 1μM	Cyyr1	cysteine and tyrosine-rich protein 1	7.34	Yes	Yes	-	-	-	-	-	-	-	-	-	-	-	-	H36R	-	-	-	-
B-cells	Idarubicin 3μM	Fadd	Fas-associated via death domain	10.98	Yes	Yes	-	-	Yes	-	Yes	Yes	-	-	Yes	Yes	Yes	Trend	-	-	Yes	Yes	Apoptosis and Immune Cell
T-cells	Idarubicin 1μM	Gabpa	GA repeat binding protein, alpha	7.34	Yes	Yes	-	-	Yes	Yes	Yes	Yes	-	-	Yes	-	-	Yes	I434M	-	-	-	Apoptosis and Immune Cell

Cell Type	Drug and Dose	Gene Symbol	Gene Name	Genomewide Significance	Expressed in Spleen	Differentially Expressed in Spleen	Correlated in Spleen	Cis-Regulated	Expressed in CD4	Differentially Expressed in CD4	Correlated in CD4	Expressed in CD4 Th1	Differentially Expressed in CD4 Th1	Correlated in CD4 Th1	Expressed in Macrophages	Differentially Expressed in Macrophages	Correlated in Macrophages	Haplotype Match	Nonsynonymous SNPs	Deleterious SNPs	Immune System or Cancer Related	Anthracycline Related	Ingenuity Pathway
B-cells	Doxorubicin 0.3μM	Klhdc5	kelch-like 42	7.94	Yes	Yes	-	Yes	Yes	Yes	-	Yes	Yes	-	Yes	Yes	-	Yes	-	-	-	-	-
T-cells	Idarubicin 1μM	Mir155	microRNA 155	7.34	Yes	Yes	-	Yes	-	-	-	Yes	Yes	-	-	-	-	-	-	-	Yes	-	Apoptosis and Immune Cell
T-cells	Idarubicin 1μM	Mrpl39	mitochondrial ribosomal protein L39	7.34	Yes	Yes	-	Yes	Yes	Yes	-	Yes	Yes	-	Yes	Yes	-	Yes	E315A V280A D235E V164L K133T	E315A	-	-	-
B-cells	Doxorubicin 0.3μM	Mrps35	mitochondrial ribosomal protein S35	7.94	Yes	Yes	Yes	-	Yes	Yes	-	Yes	Yes	-	Yes	-	Yes	Yes	T11S C216Y I293V A320V	C216Y	-	-	-
B-cells	Idarubicin 3μM	Ppfia1	protein tyrosine phosphatase, receptor type, f polypeptide (PTPRF), interacting protein (liprin), alpha 1	10.98	Yes	Yes	-	-	Yes	Yes	Yes	Yes	Yes	Yes	Yes	Yes	-	Trend	L1061M H964Q E678D S554R	L1061M H964Q E678D S554R	Yes	-	Apoptosis
B-cells	Doxorubicin 0.3μM	Ppfibp1	PTPRF interacting protein, binding protein 1 (liprin beta 1)	7.94	Yes	Yes	Yes	-	Yes	Yes	-	Yes	Yes	-	Yes	Yes	-	Yes	D195H V186C E166K H50C D400E	D195H V186C E166K H50C	Yes	-	Apoptosis
B-cells	Idarubicin 3μM	Rasl11b	RAS-like, family 11, member B	12.08	Yes	Yes	Yes	-	Yes	Yes	Yes	Yes	Yes	Yes	-	-	-	-	-	-	Yes	Yes	-
B-cells	Doxorubicin 0.3μM	Stk38l	serine/threonine kinase 38 like	7.94	Yes	Yes	-	-	Yes	Yes	-	Yes	Yes	-	Yes	Yes	-	Yes	-	-	Yes	-	Immune Cell

3.5. Discussion

This investigation aimed to uncover genetic components of the normal immune system's response to chemotherapeutic agents. The importance of this comes from studies that implicate the uncompromised immune system in the efficacy of chemotherapeutic treatments.[1] Therefore we need to assess the resilience of immune function cells to potentially toxic drugs, including anticancer agents. As this investigation is difficult to conduct in human patients, we proposed a model system to examine cytotoxic responses in immune cells from inbred strains of mice with the objective of identifying genetic biomarkers of immune cytotoxic response.[16]

Recently, standardization of pharmacogenomic screening has come under intense scrutiny, necessitating improvements in the design, application, and implementation of robust assays for phenotypic measurement.[32,33] For our GWAS, we examined IC_{50} values, AUC values, and individual viability concentrations (only GWAS for viability concentrations are shown). All three measurements used for GWAS present their own challenges and benefits. IC_{50} could not be estimated in some cases as necessary concentrations for 50% viability were outside of our selected, generic concentration range from 15 nM to 100 μM and far beyond physiological boundaries. While IC_{50} is a biologically relevant measurement if slopes are comparable, it can be regarded as a moving target and differs based on software and equations used to fit the dose response curve. AUC measures can always be estimated from the dose response curve and all points are used in data analysis. However, the appropriateness of this model in regards to its biology has been questioned. [29,34] The viability concentrations chosen were located on either side of the mean logarithmic IC_{50} for all strains and provided precise, replicable, and robust measurements and the necessary interstrain variation for GWAS. Therefore, the cell viability data from these viability concentrations provided genomewide significant QTL.

In this study, we uncovered four genome-wide significant QTL that were identified using the same phenotype and genotype data but using two different GWA algorithms (EMMA and SNPster). Because the two mapping approaches determine QTL using different methodologies, the use of both algorithms minimizes identification of false positive QTLs. Results from both analyses identified four loci containing twenty-five potential candidate genes. These candidate genes subsequently underwent careful inspection to examine as much available data that can be garnered to rank these genes and select the "most likely" candidate for validation.

Here, we selected one gene for a validation study; *App* was initially validated in vitro using knockout and control mice. *App* knockout mice are commercially available and viable, and only with a concurrent knockout of *Aplp2* (amyloid precursor-like protein 2) is this loss of function perinatally lethal. The downstream processing of App is fairly complex, and the role of domains in addition to the plaque forming β-APP, typically associated with Alzheimer's disease, is under investigation. *App* consists of multiple domains (ie, A4, N-terminal heparin-binding, copper-binding, KU, E2, β-App, and amyloid C-terminal domains as shown in Figure 3.6) with numerous cleavage sites.[35] Alzheimer's disease has been suggested to result from an imbalance in the production and clearance of β-APP. However, additional theories have been proposed, suggesting β-APP is a marker of oxidation rather than a symptom of neurodegeneration.

APP has been studied primarily in terms of Alzheimer's disease, but knowledge of its biological function remains elusive. This gene is ubiquitously expressed, suggesting roles outside of various neuronal functions and diseases subsequent to aberrant processes that are typically associated with *APP*. The extracellular portion of the protein has been implicated in cell adhesion, signaling, and growth, and the intracellular portion has been associated with cell signaling and apoptosis.[36,37] Overexpression of *APP*, particularly the soluble N-terminal

ectodomain (sAPP), has been linked to carcinogenesis, including cancers originating from the nasopharynx, oral cavity, lung, breast, thyroid, parathyroid, colon, testicles, and pancreas.[38,39] Ryan et al. exposed rat hippocampus slice cultures to sAPP, which elicited an inflammatory and immune gene response that was suggested to cause a neuroprotective environment. Apoptotic pathways were downregulated, while cell proliferation and survival pathways were upregulated.[40] In addition, *APP* expression is indirectly linked to Ras/MAPK and PI3K/Akt pathways, which are often upregulated in various cancers.[41] These findings suggest a potential role of *App* in cellular processes involved in cancer or in chemotherapy response.

Epidemiologically, an inverse comorbidity with cancer was found in two studies of 500 patients with Alzheimer's disease.[42] This inverse correlation was hypothesized to be driven by molecular processes common to CNS disorders and cancer. Ibáñez et al. found a significant overlap between genes (eg, *PIN1*, *Wnt* pathway, p53 pathway, and pathways related to protein folding and folding degradation) upregulated in CNS disorders (ie, Alzheimer's disease, Parkinson's disease, and schizophrenia) and genes downregulated in cancer (ie, lung, prostate, and colorectal cancers) and vice versa. *APP* also appears to have a role in cytotoxic response to anticancer chemotherapeutics. A recent clinical observational study indicated that the risk of Alzheimer's disease was reduced following the administration of anticancer chemotherapy,[43] suggesting upregulation of MDR transporters may enhance β-APP clearance. Additionally, in CHO cells, carmustine administration reduced β-APP and was suggested to cause altered intracellular trafficking and processing of APP with an increase in immature APP at the cell surface and sAPP levels.[44] *APP* overexpressing cell lines have also been found to have a higher resistance to cytotoxicity; overexpression of wild-type *APP* in HEK cells resulted in a conformational change in p53 and a subsequent reduced sensitivity to doxorubicin.[31] The link

between APP and p53 has been previously suggested, and APP has been proposed to activate gene transcription in a similar way as Notch, a protein with roles in cell differentiation, cell proliferation, neuronal function, and T-cell lineage commitment.[37]

We have not investigated a mechanistic solution as to why a lack of *App* leads to enhanced toxicity to idarubicin. As discussed above, we can hypothesize that an increase in wild type APP and subsequent sAPP leads to a decrease in functional proteins within the p53 pathway, which causes a downregulation in apoptotic processes, upregulation in cell survival, and subsequent resistance to toxic insults such as anticancer chemotherapy. This situation could present a clinical conundrum in how to treat patients with cancers overexpressing *APP*.[45] Also, genomic differences in molecular machinery processing APP could add an additional layer of complexity. In this study, the expression of *App* in the spleen and other immune cells did not correlate with the strain order for sensitivity of T-cells to idarubicin. Thus, the effect of *App* on anticancer response is not likely driven by *App* expression in this study. An additional proof for the validation of *App* may include creating specific polymorphisms introducing the potentially deleterious nonsynonymous coding changes mentioned previously to see how the viability of T-cells exposed to idarubicin is affected. Furthermore, we have additional candidate genes from our screen for future validation. Of particular interest, *Ppfia1* and *Ppfibp1* were found using the viability of B-cells exposed to doxorubicin and idarubicin, respectively. These genes encode liprin-alpha-1 and liprin-beta-1, members of the LAR protein tyrosine phosphatase-interacting protein family, which orchestrate cell-matrix interactions (http://omim.org/).[46]

3.6. Conclusions

We have shown that we can identify genes implicated in the immune cell response to chemotherapeutic agents. Using a cellular screening approach, we identified and subsequently validated a gene involved in cytotoxic T-cell response to idarubicin. In the future, we aim to perform mechanistic studies, investigate additional candidate genes of interest, and to ultimately translate our findings to in vivo and human studies.

REFERENCES

1. Hanahan D, Weinberg RA. Hallmarks of cancer: the next generation. *Cell*. 2011;144(5):646–674. doi:10.1016/j.cell.2011.02.013.

2. Alizadeh D, Larmonier N. Chemotherapeutic targeting of cancer-induced immunosuppressive cells. *Cancer Res*. 2014;74(10):2663–2668. doi:10.1158/0008-5472.CAN-14-0301.

3. Raval RR, Sharabi, AB, Walker AJ, CG D, Padmanee S. Tumor immunology and cancer immunotherapy: summary of the 2013 SITC primer. *J Immunother Cancer*. 2014;2:2014.

4. Kalos M, June CH. Adoptive T cell transfer for cancer immunotherapy in the era of synthetic biology. *Immunity*. 2013;39(1):49–60. doi:10.1016/j.immuni.2013.07.002.

5. Kantoff PW, Higano CS, Shore ND, et al. Sipuleucel-T immunotherapy for castration-resistant prostate cancer. *N Engl J Med*. 2012;363(5):411–422. doi:10.1056/NEJMoa1001294).

6. Hodi FS, O'Day SJ, McDermott DF, et al. Improved survival with ipilimumab in patients with metastatic melanoma. *N Engl J Med*. 2010;363(8):711–723. doi:10.1056/NEJMoa1003466.

7. Topalian SL, Hodi FS, Brahmer JR, et al. Safety, activity, and immune correlates of anti–PD-1 antibody in cancer. *N Engl J Med*. 2012;366(26):2443–2454. doi:10.1056/NEJMoa1200690.

8. Brahmer JR, Tykodi SS, Chow LQM, et al. Safety and activity of anti–PD-L1 antibody in patients with advanced cancer. *N Engl J Med*. 2012;366(26):2455–2465. doi:10.1056/NEJMoa1200694.

9. Galluzzi L, Senovilla L, Zitvogel L, Kroemer G. The secret ally: immunostimulation by anticancer drugs. 2012:1–19. doi:10.1038/nrd3626.

10. Ma Y, Aymeric L, Locher C, et al. Contribution of IL-17-producing gamma delta T cells to the efficacy of anticancer chemotherapy. *J Exp Med*. 2011;208(3):491–503. doi:10.1084/jem.20100269.

11. Mattarollo SR, Loi S, Duret H, Ma Y, Zitvogel L, Smyth MJ. Pivotal role of innate and adaptive immunity in anthracycline chemotherapy of established tumors. *Cancer Res*. 2011;71(14):4809–4820. doi:10.1158/0008-5472.CAN-11-0753.

12. Vanneman M, Dranoff G. Combining immunotherapy and targeted therapies in cancer treatment. *Nat Rev Cancer*. 2012;12(4):237–251. doi:10.1038/nrc3237.

13. Ross C, Visscher H, Rassekh SR, et al. Pharmacogenomics of serious adverse drug reactions in pediatric oncology. *J Popul Ther Clin Pharmacol*. 2011;18(1):e134–e151.

14. van Kuilenburg A, Haasjes J, Richel DJ, et al. Clinical implications of dihydropyrimidine dehydrogenase (DPD) deficiency in patients with severe 5-fluorouracil-associated toxicity: identification of new mutations in the *DPD* gene. *Clin Cancer Res*. 2000;6:4705–4712.

15. Stocco G, Cheok MH, Crews KR, et al. Genetic polymorphism of inosine triphosphate pyrophosphatase is a determinant of mercaptopurine metabolism and toxicity during treatment for acute lymphoblastic leukemia. *Clin Pharmacol Ther*. 2008;85(2):164–172. doi:10.1038/clpt.2008.154.

16. Frick A, Fedoriw Y, Richards K, et al. Immune cell-based screening assay for response to anti-cancer agents: applications in pharmacogenomics. *Pharmgenomics Pers Med*. 2014.

17. McClurg P, Janes J, Wu C, et al. Genomewide association analysis in diverse inbred mice: power and population structure. *Genetics*. 2007;176(1):675–683. doi:10.1534/genetics.106.066241.

18. Kang HM, Zaitlen NA, Wade CM, et al. Efficient control of population structure in model organism association mapping. *Genetics*. 2008;178(3):1709–1723. doi:10.1534/genetics.107.080101.

19. Yang H, Wang JR, Didion JP, et al. Subspecific origin and haplotype diversity in the laboratory mouse. *Nat Genet*. 2011;43(7):648–655. doi:10.1038/ng.847.

20. Mouse Genome Sequencing Consortium. Initial sequencing and comparative analysis of the mouse genome. *Nature*. 2002;420(6915):520-562. doi:10.1038/nature01262.

21. Moreau Y, Tranchevent L-C. Computational tools for prioritizing candidate genes: boosting disease gene discovery. *Nat Rev Genet*. 2012;13(8):523–536. doi:10.1038/nrg3253.

22. Choi Y, Sims GE, Murphy S, Miller JR, Chan AP. Predicting the functional effect of amino acid substitutions and indels. de Brevern AG, ed. *PLoS ONE*. 2012;7(10):e46688. doi:10.1371/journal.pone.0046688.

23. Thomas PD, Campbell MJ, Kejariwal A, et al. PANTHER: a library of protein families and subfamilies indexed by function. *Genome Res*. 2003;13(9):2129–2141. doi:10.1101/gr.772403.

24. Mi H, Lazareva-Ulitsky B, Loo R, et al. The PANTHER database of protein families, subfamilies, functions and pathways. *Nucleic Acids Res*. 2005;33(Database issue):D284–8. doi:10.1093/nar/gki078.

25. Chen H, Sharp BM. Content-rich biological network constructed by mining PubMed abstracts. *BMC Bioinformatics*. 2004;5(1):147. doi:10.1186/1471-2105-5-147.

26. Wang JR, de Villena FP-M, McMillan L. Comparative analysis and visualization of multiple collinear genomes. *BMC Bioinformatics*. 2012;13(Suppl 3):S13. doi:10.1186/1471-2105-13-S3-S13.

27. Zheng H, JIang M, Trumbauer ME, et al. beta-amyloid precursor protein-deficient mice show reactive gliosis and decreased locomotor activity. *Cell.* 2003;81(4):525-531.

28. Beam A, Motsinger-Reif AA. Beyond IC_{50}s: towards robust statistical methods for in vitro association studies. *Pharmgenomics Pers Med*. 2014;5(1). doi:10.4172/2153-0645.1000120.

29. Brown C, Havener TM, Everitt L, McLeod H, Motsinger-Reif AA. A comparison of association methods for cytotoxicity mapping in pharmacogenomics. *Front Genet*. 2011;2(86):1–14. doi:10.3389/fgene.2011.00086/abstract.

30. Woods NK, Padmanabhan J. Inhibition of amyloid precursor protein processing enhances gemcitabine-mediated cytotoxicity in pancreatic cancer cells. *J Biol Chem*. 2013;288(42):30114–30124. doi:10.1074/jbc.M113.459255.

31. Uberti D, Cenini G, Olivari L, et al. Over-expression of amyloid precursor protein in HEK cells alters p53 conformational state and protects against doxorubicin. *J Neurochem*. 2007;0(0):070702072507003. doi:10.1111/j.1471-4159.2007.04757.x.

32. Hatzis C, Bedard PL, Birkbak NJ, et al. Enhancing reproducibility in cancer drug screening: how do we move forward? *Cancer Res*. 2014;74(15):4016–4023. doi:10.1158/0008-5472.CAN-14-0725.

33. Haibe-Kains B, El-Hachem N, Birkbak NJ, et al. Inconsistency in large pharmacogenomic studies. *Nature*. 2014;504(7480):389–393. doi:10.1038/nature12831.

34. Fallahi-Sichani M, Honarnejad S, Heiser LM, Gray JW, Sorger PK. Metrics other than potency reveal systematic variation in responses to cancer drugs. *Nat Chem Biol*. 2013;9(11):708–714. doi:10.1038/nchembio.1337.

35. Sherry ST, Ward MH, Kholodov M, et al. dbSNP: the NCBI database of genetic variation. *Nucleic Acids Res*. 2000;29(1):308-311.

36. Dawkins E, Small DH. Insights into the physiological function of the β-amyloid precursor protein: beyond Alzheimer's disease. *J Neurochem*. 2014;129(5):756–769. doi:10.1111/jnc.12675.

37. Thinakaran G, Koo EH. Amyloid precursor protein trafficking, processing, and function. *J Biol Chem*. 2008;283(44):29615–29619. doi:10.1074/jbc.R800019200.

38. Yamada Y, Fujimura T, Takahashi S, et al. Clinical significance of amyloid precursor protein in patients with testicular germ cell tumor. *Adv Urol*. 2013;2013(2):1–6. doi:10.1155/2013/348438.

39. Takagi K, Ito S, Miyazaki T, et al. Amyloid precursor protein in human breast cancer: an androgen-induced gene associated with cell proliferation. *Cancer Sci*. 2013;104(11):1532–1538. doi:10.1111/cas.12239.

40. Ryan MM, Morris GP, Mockett BG, et al. Time-dependent changes in gene expression induced by secreted amyloid precursor protein-alpha in the rat hippocampus. *BMC Genomics*. 2013;14(1):1–1. doi:10.1186/1471-2164-14-376.

41. Ruiz-León Y, Pascual A. Regulation of β-amyloid precursor protein expression by brain-derived neurotrophic factor involves activation of both the Ras and phosphatidylinositide 3-kinase signalling pathways. *J Neurochem*. 2004;88(4):1010–1018. doi:10.1046/j.1471-4159.2003.02226.x.

42. Tabarés-Seisdedos R, Rubenstein JL. Inverse cancer comorbidity: a serendipitous opportunity to gain insight into CNS disorders. 2013:1–12. doi:10.1038/nrn3464.

43. Ibáñez K, Boullosa C, Tabarés-Seisdedos R, Baudot A, Valencia A. Molecular evidence for the inverse comorbidity between central nervous system disorders and cancers detected by transcriptomic meta-analyses. *PLoS Genet*. 2014;10(2):e1004173. doi:10.1371/journal.pgen.1004173.

44. Hayes CD, Dey D, Palavicini JP, et al. Striking reduction of amyloid plaque burden in an Alzheimer's mouse model after chronic administration of carmustine. *BMC Medicine*. 2013;11(1):81. doi:10.1186/1741-7015-11-81.

45. Lanni C, Racchi M, Memo M, Govoni S, Uberti D. p53 at the crossroads between cancer and neurodegeneration. *Free Radic Biol and Med*. 2012;52(9):1727–1733. doi:10.1016/j.freeradbiomed.2012.02.034.

46. Online Mendelian Inheritance in Man, OMIM®. McKusick-Nathans Institute of Genetic Medicine, Johns Hopkins University (Baltimore, MD) Accessed October 2014. Available at: http://omim.org/.

CHAPTER 4: IMMUNOPHENOTYPIC SCREEN FOR ANTICANCER DRUGS AND ASSOCIATED GENOMEWIDE ASSOCIATION STUDIES: THE SKY'S THE LIMIT

4.1. Introduction

Complex interactions exist between the immune system and cancerous cells, and these interactions and the immunomodulation of tumors can be heavily influenced by the administration of anticancer chemotherapy.[1] While potentially detrimental to the viability of normal cells, anticancer agents can induce an immune response that contributes to their efficacy.[2] We successfully developed a multiplexed assay for measuring toxicity responses to anticancer agents in murine immune cells.[3] This assay generated thousands of data points, which were used to identify quantitative trait loci (QTL) and promising candidate genes using genomewide association studies (GWAS). Furthermore, we completed the initial validation of a candidate gene (*App*) encoding for amyloid beta precursor protein in murine T-cells exposed to idarubicin. In this chapter, we examine additional phenotypes, GWAS, and candidate genes generated from this endeavor. Following the ramifications of our immunophenotypic assay and associated GWAS, we examine current limitations, areas for improvement, and potential future developments.

4.2. Materials and Methods

4.2.1. Phenotypes

The methods and results of our drug-screening platform in normal, noncancerous, murine immune cells have been previously described.[3] Briefly, splenocytes were collected from a panel of 36 inbred mouse strains (n = 4 per strain, 129S1/SvImJ, 129X1/SvJ, A/J, AKR/J, BALB/cByJ,

BTBR T+ Itpr3tf/J, BUB/BnJ, C3H/HeJ, C57BLKS/J, C57BL/6J, C57BR/cdJ, C58/J, CBA/J, CZECHII/EiJ, DBA/2J, FVB/NJ, I/LnJ, KK/HiJ, LG/J, LP/J, MA/MyJ, NOD/LtJ, NON/LtJ, NZB/BINJ, NZO/HiLtJ, NZW/LacJ, PERA/EiJ, PL/J, PWD/PhJ, PWK/PhJ, RIIIS/J, SEA/GnJ, SJL/J, SM/J, SWR/J, and WSB/EiJ), aged 10-12 weeks from The Jackson Laboratory Mouse Diversity Panel. Splenocytes were isolated using standard procedures and exposed to nine logarithmic concentrations of doxorubicin, idarubicin, BEZ-235, and selumetinib ranging from 15 nM to 100 μM. At 4 h post-treatment, cells were sequentially incubated (37°C, 5% CO2) with physiological indicator dyes (eg, 7-AAD, CellEvent™ Caspase-3/7 Green Detection Reagent, and Mitotracker® Deep Red) and cell surface marker antibodies and then fixed with 4% paraformaldehyde. Samples were analyzed by flow cytometry using a BD FACSCanto II flow cytometer and Flow Jo version X. Dose-response curves with response normalized to the zero dose as a function of log concentration were generated. Viability measurements of B-cells, T-cells, and monocytes exposed to the anthracyclines provided the most heritable phenotypes in our screen and were reserved for QTL mapping.

4.2.2. Quantitative Trait Loci (QTL) Mapping

Genome-wide association (GWA) studies were performed using IC_{50} values, AUC values, and individual drug concentrations that corresponded to cell viability for splenic B-cells and T-cells exposed to doxorubicin and idarubicin. SNPster and efficient mixed-model association (EMMA) algorithms, which are well described elsewhere, were used for QTL mapping. [4,5] Briefly, SNPster uses an inferred haplotype structure from overlapping 3-SNP windows for each strain. An *F*-statistic is calculated by comparing associated phenotype values to haplotypes using one-way ANOVA. *p* values are estimated by bootstrapping phenotypic values $1x10^6$ times, providing a maximum -log(*p*) score of 6.0.[4] EMMA uses F-tests for single

marker association mapping while accounting for population structure and genetic relatedness.[5] SNP genotypes used for GWA were obtained from the Mouse Diversity Array set at the CGDSNPdb website (http://cgd.jax.org/cgsnpdb/).[6] The SNP panel was trimmed for redundancy (SNPs showing identical haplotype pattern at a locus), missingness (SNPs with few calls for all strains), and non-informative nature (SNPs without variation amongst the 36 strains), leaving a panel of 356,596 SNPs. Manhattan plots were visualized using R version 3.1.0 and the UCSC Mouse Genome Browser on the Mouse July 2007 (NCBI37/mm9) Assembly (https://genome.ucsc.edu). The threshold of significance for QTL mapping was adjusted using the conservative Bonferroni correction. QTL were considered significant when $-\log(p) \geq 6.853$.

4.2.3. Candidate Gene Selection

QTL regions that overlapped using both association mapping algorithms, although both were not required to be genome-wide significant ($-\log(p) \geq 6.853$), were further narrowed down for candidate gene selection. Candidate genes were prioritized based on the following: literature evidence for biological involvement with the immune system or anthracycline response, differential gene expression in spleens and immune cells, the correlation between phenotypic values and gene expression levels in spleens and immune cells, the presence of potentially deleterious non-synonymous coding SNPs, and apoptotic or immune cell pathway involvement.[7] Candidate genes were only included if they were expressed in the spleen, the tissue originally assayed to produce our phenotypes of interest. Expression levels were measured in spleens and immune cells from inbred strains of mice using the Affymetrix Mouse Genome 2.0 Array (Santa Clara, CA). Genes were considered expressed if their expression level was greater than 50 for at least one of the strains following data processing with the gcRMA algorithm. Nonsynonymous coding SNPs were obtained from dbSNP (http://www.ncbi.nlm.nih.gov/projects/SNP/). The

likely effect of amino acid substitutions in protein sequences was determined using PROVEAN (Protein Variation Effect Analyzer) version 1.1.322[8] and PANTHER (Protein Analysis Through Evolutionary Relationships) version 9.0 software. [9,10] Using PROVEAN, a score of -2.5 indicates a functional effect on the protein. For the PANTHER algorithm, a subSPEC (substitution position-specific evolutionary conservation) score of -3 corresponds to a 50% probability that a score is deleterious ($P_{deleterious} = 0.5$). Haplotype structure for the interval, and for specific genes was reviewed with the Mouse Phylogeny Viewer (https://msub.csbio.unc.edu/).[11]

4.3. Results

Optimization of a number of parameters was performed prior to initiation of our phenotypic screen. These included cell and drug selection, cell culture conditions (eg, cell density, growth medium, drug concentration range, controls), flow cytometry conditions (eg, optimal cell number measurement, detection of markers and cellular health parameters of interest, overlap and subsequent compensation of fluorochromes, and gating strategy), modeling and normalization of dose response curves, and statistics for drug sensitivity (data not shown for parameter optimization experiments). We examined cell viability (Figure 4.1), anthracycline uptake (Figure 4.2), caspase activity (Figure 4.3), and mitochondrial health (Figure 4.4) of immune cells following treatment with anthracyclines. Viability measurements had heritable, interstrain variability at physiological concentrations and IC_{50} values within our range of logarithmic concentrations. As expected, our more targeted agents, BEZ-235 and selumetinib, did not produce a detrimental effect on the viability of cells. Anthracycline uptake did not correlate directly with cell viability. In comparison to cell viability, the data for anthracycline uptake was more variable, limiting its use for GWAS (Figure 4.2). Caspase and mitochondrial health measurements did not act as expected, with a decrease in caspase activity, especially with

doxorubicin administration (Figure 4.3), and little to no reduction in mitochondrial health with increasing drug concentration (Figure 4.4). Thus, viability measurements of T-cells, B-cells, and monocytes following administration of doxorubicin and idarubicin were used as our phenotypes for GWAS.

Figure 4.1. Interstrain variation of viability across immune cell types and anti-cancer drugs.

Notes: Dose response curves depict cell populations (columns, ie, T-cells, B-cells, monocytes, and granulocytes) exposed to anti-cancer drugs (rows, ie, doxorubicin, idarubicin, BEZ-235, and selumetinib). Thirty-six strains are included.

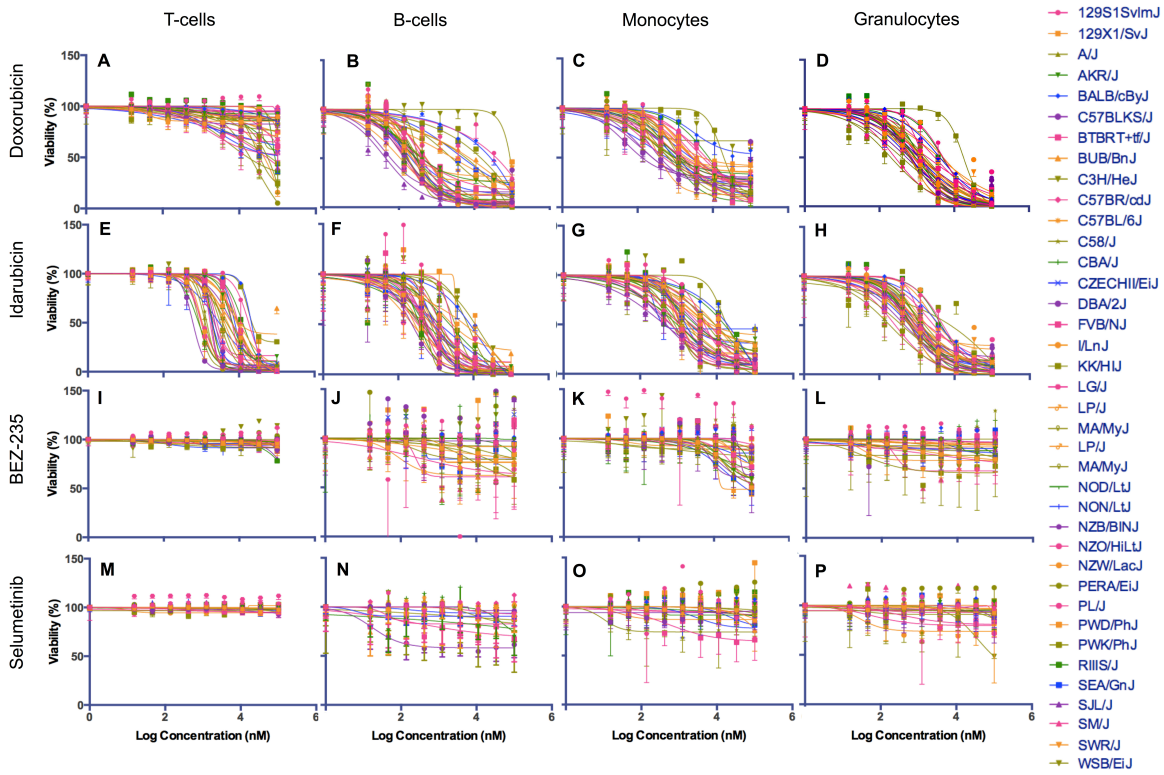

Figure 4.2. Interstrain variation of anthracycline uptake across immune cell types and anti-cancer drugs.

Notes: Dose response curves depict cell populations (columns, ie, T-cells, B-cells, monocytes, and granulocytes) exposed to anti-cancer drugs (rows, ie, doxorubicin and idarubicin). The dose response curves depict cells negative for anthracycline uptake as concentrations increase. Thirty-six strains are included.

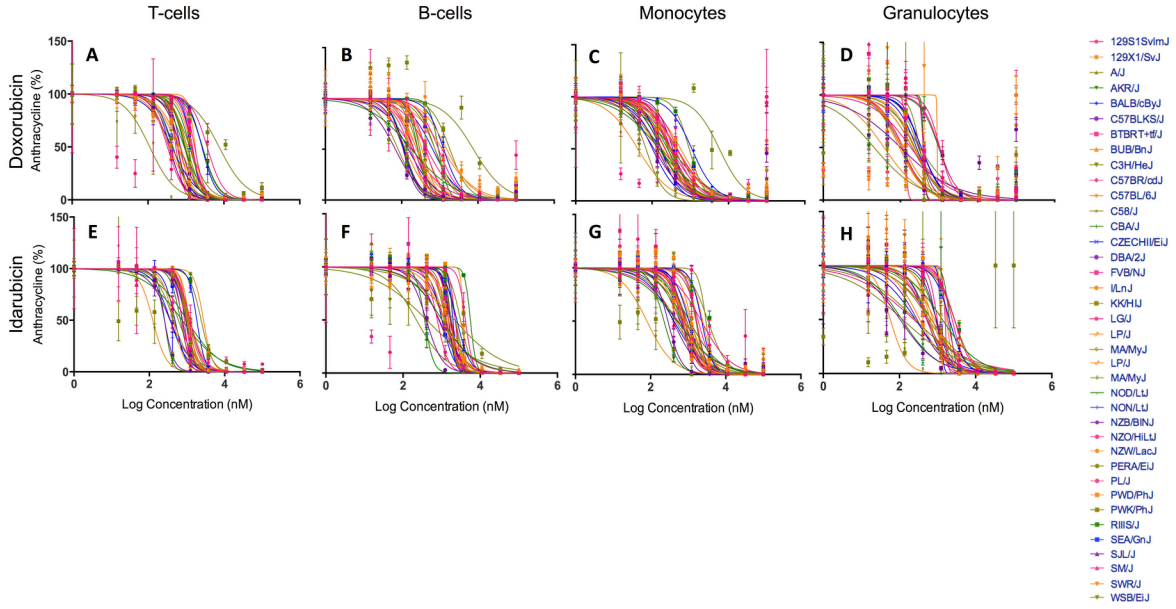

Figure 4.3. Interstrain variation of active caspase-3/7 across immune cell types and anti-cancer drugs.

Notes: Dose response curves depict cell populations (columns, ie, T-cells, B-cells, monocytes, and granulocytes) exposed to anti-cancer drugs (rows, ie, doxorubicin. idarubicin). Thirty-six strains are included.

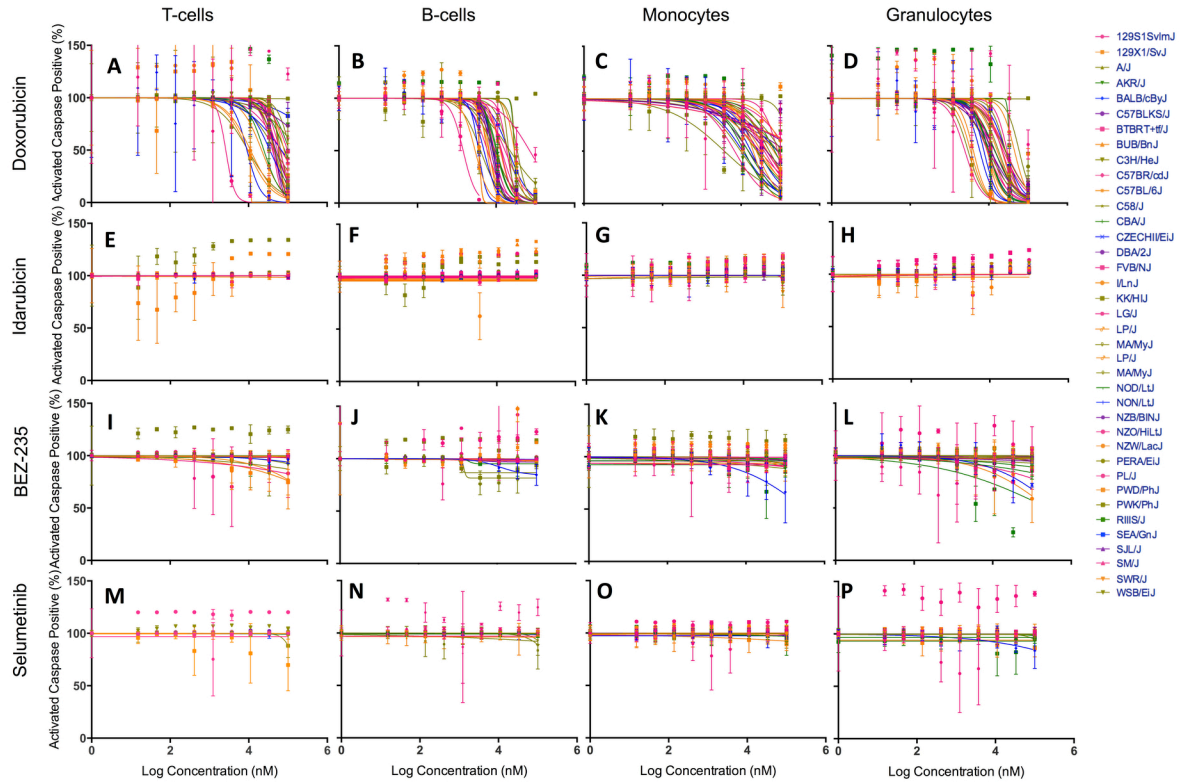

Figure 4.4. Interstrain variation of mitochondrial health across immune cell types and anti-cancer drugs.

Notes: Dose response curves depict cell populations (columns, ie, T-cells, B-cells, monocytes, and granulocytes) exposed to anti-cancer drugs (rows, ie, doxorubicin. idarubicin). Thirty-six strains are included.

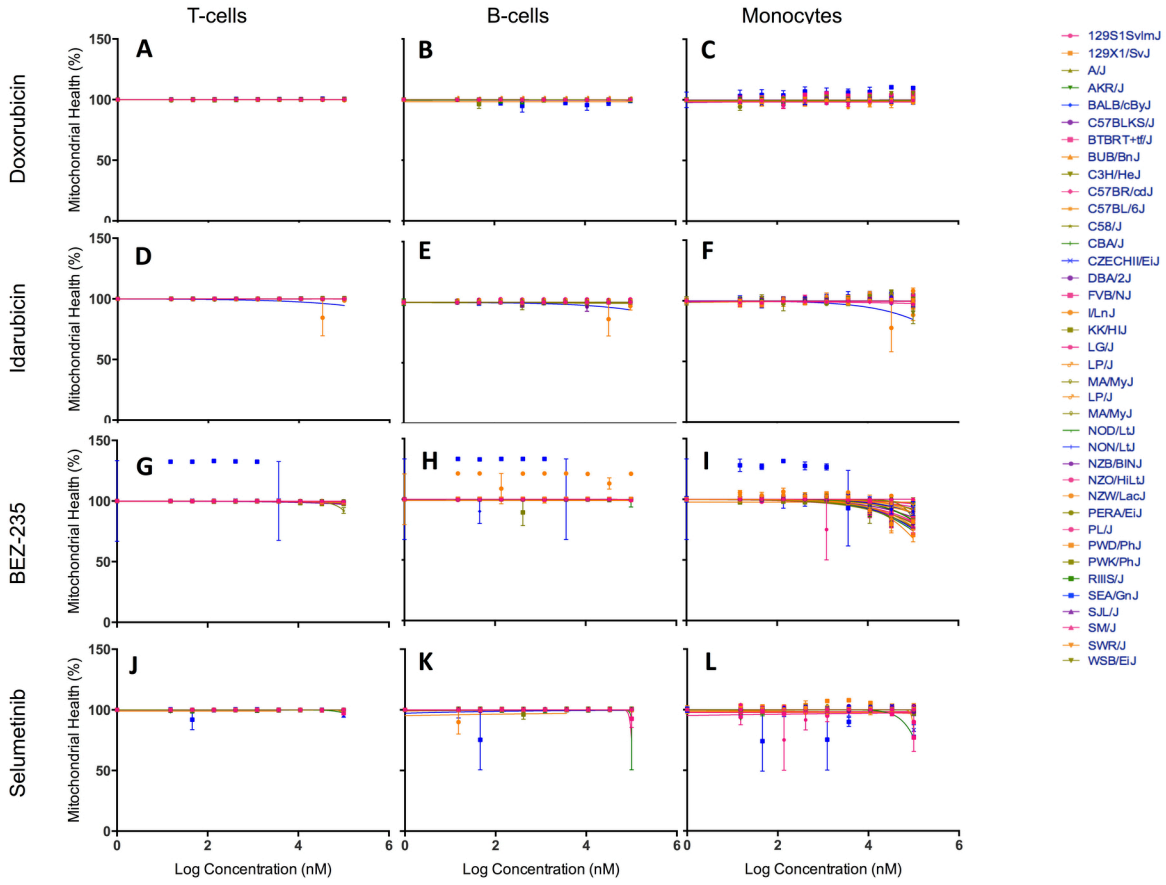

After performing GWAS with IC_{50} values, AUC values, and individual drug concentrations (Figures 4.5-4.10), we obtained eight genomewide significant QTL on the following chromosomes: chr6 for B-cells exposed to 0.3 μM doxorubicin (Figure 4.5B), chr5 for B-cells exposed to 1 μM doxorubicin (Figure 4.5C), chr14 for AUC values for B-cells exposed to idarubicin (Figure 4.6B), chr5 and chr 7 for B-cells exposed to 3 μM idarubicin (Figure 4.6D), chr 12 and chr 15 for T-cells exposed to 100 μM doxorubicin (Figure 4.9D), and chr 16 for T-cells exposed to idarubicin (Figure 4.10C). The structure and size of each QTL derived from various drug concentrations and associated genes under each genomewide significant peak are in Figures 4.11-4.16. The haplotype structure of the following genes displayed grouping according to sensitive or resistant phenotypes: *Arntl2*, *Ccdc91*, *Cdh11*, *Gm5887*, *Klhdc5*, *Mrps35*, *Ppfibp1*, *Rep15*, and *Stk38l* for B-cells exposed to 0.3 μM doxorubicin (Figure 4.12); *Arntl2*, *Ccdc91*, *Cdh11*, *Gm5887, Klhdc5*, *Mrps35*, *Ppfibp1*, *Rasl11b*, *Rep15*, and *Stkl38* for B-cells exposed to 1 μM doxorubicin (Figure 4.13); *Cttn*, *Fadd*, and *Ppfia1* for B-cells exposed to 3 μM idarubicin (Figure 4.14); *Fam84b* and *Mycn* for T-cells exposed to 100 μM doxorubicin (Figure 4.15); and *App*, *Gabpa*, and *Jam2* for T-cells exposed to 1 μM idarubicin (Figure 4.16).

Expression data for genes within putative peaks are presented in Tables 4.1-4.5. Only 25 genes were expressed in the spleen (*Ano1*, *App*, *Atp5j*, *Ccdc91*, *Ccdc99*, *Cdh11*, *Cttn*, *Cyyr1*, *Ddx1*, *Dhcr7*, *Dock2*, *Fadd*, *Fam84b*, *Gabpa*, *Klhdc5*, *Mir155*, *Mrpl39*, *Mrps35*, *Mycn*, *Nadsyn1*, *Nbas*, *Ppfia1*, *Ppfibp1*, *Rasl11b*, *Slit3*, and *Stk38l*). The likelihood of nonsynonymous coding SNPs causing changes in the associated protein for the candidate gene is located in Table 4.6. *A1bg*, *Ano1*, *Arntl2*, *Ccdc99, Cdh11*, *Cttn*, *Dock2*, *Jam2*, *Mycn*, *Nadsyn1*, *Ppfia1*, *Ppfibp1*, and *Rep15* have potential deleterious proteins when various nonsynonymous coding SNPs are introduced.

Figure 4.5. Manhattan plots generated for B-cells exposed to doxorubicin.

Notes: Plots for IC50 values (**A**), AUC values (**B**), and viability at various doxorubicin concentrations (0.3, 1, and 3 μM, respectively **C**, **D**, and **E**) are shown. Plots generated from EMMA are above those plots generated from SNPster. Matching peaks are in black boxes with significant matching peaks bolded.

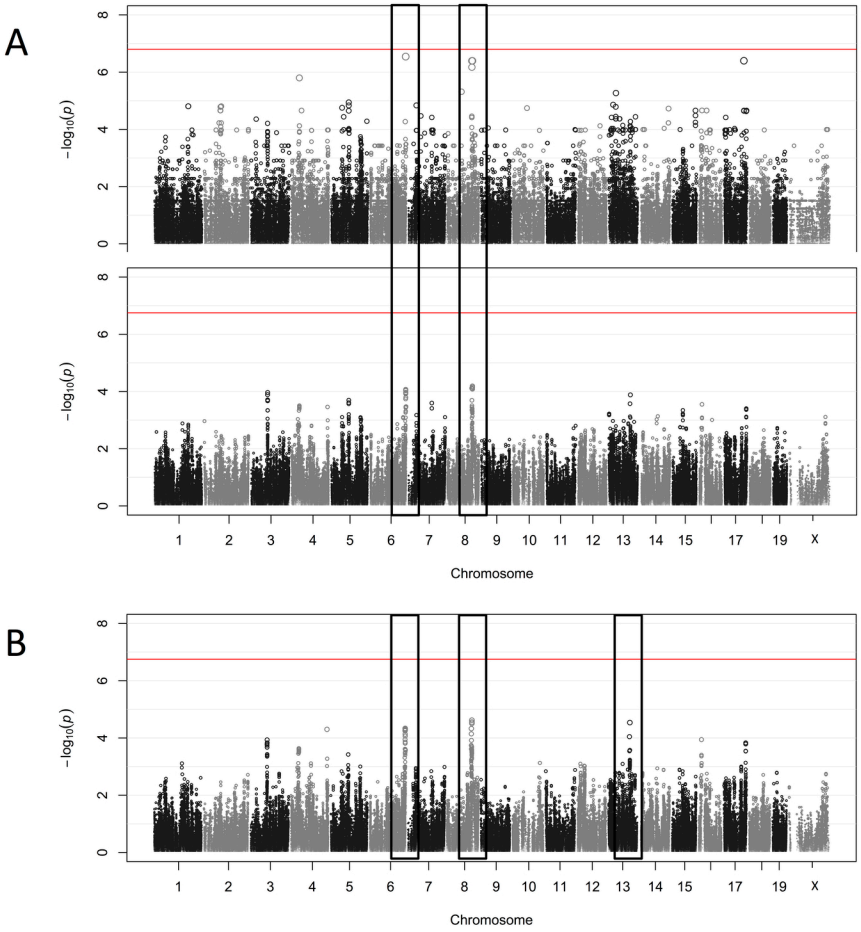

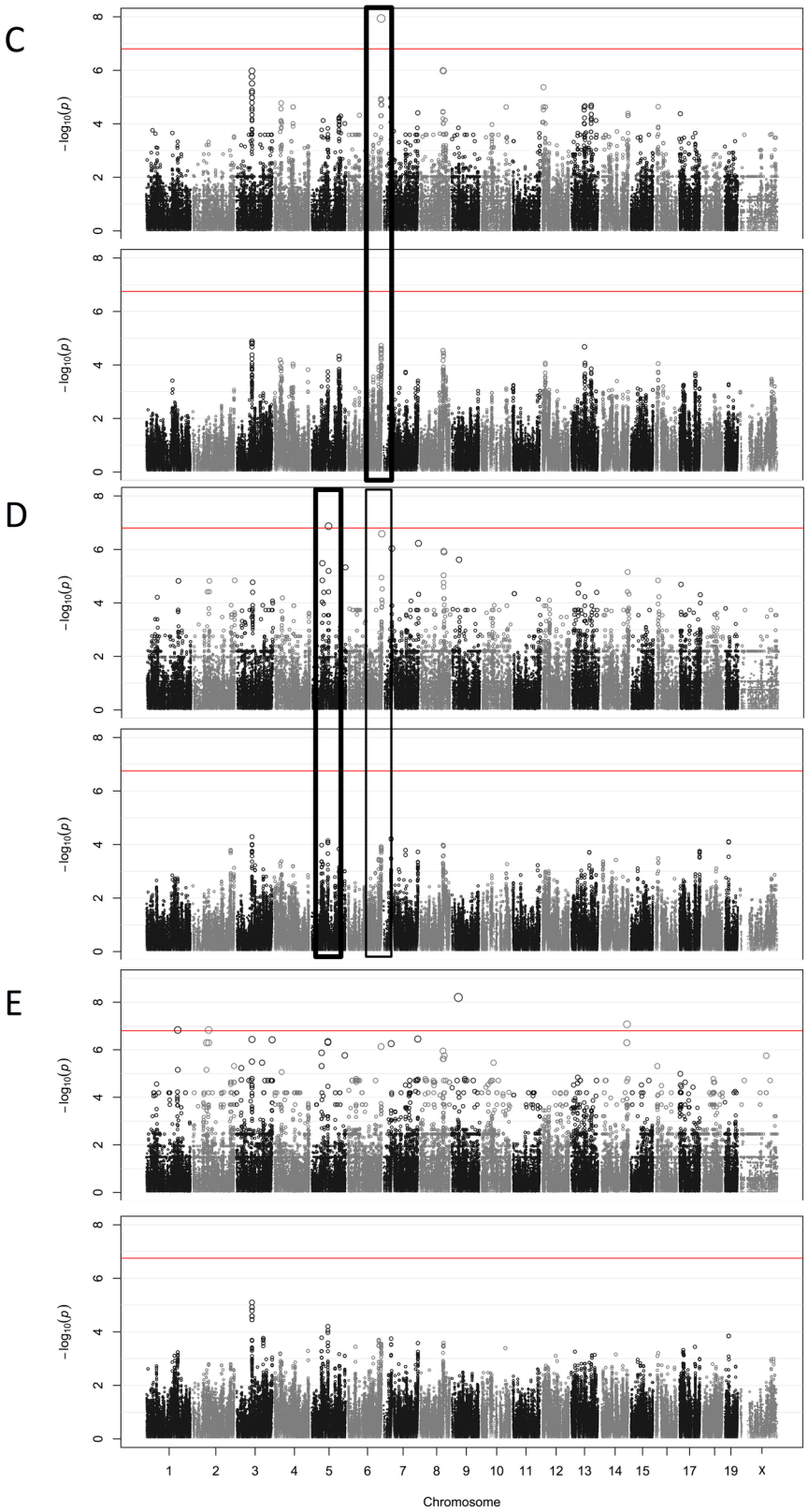
C
D
E
−log10(p)
0
2
4
6
8
1
2
3
4
5
6
7
8
9
10
11
12
13
14
15
17
19
X
Chromosome

Figure 4.6. Manhattan plots generated for B-cells exposed to idarubicin.

Notes: Plots for IC50 values (**A**), AUC values (**B**), and viability at various idarubicin concentrations (1 and 3 μM, respectively **C** and **D**) are shown. Plots generated from EMMA are above those plots generated from SNPster. Matching peaks are in black boxes with significant matching peaks bolded.

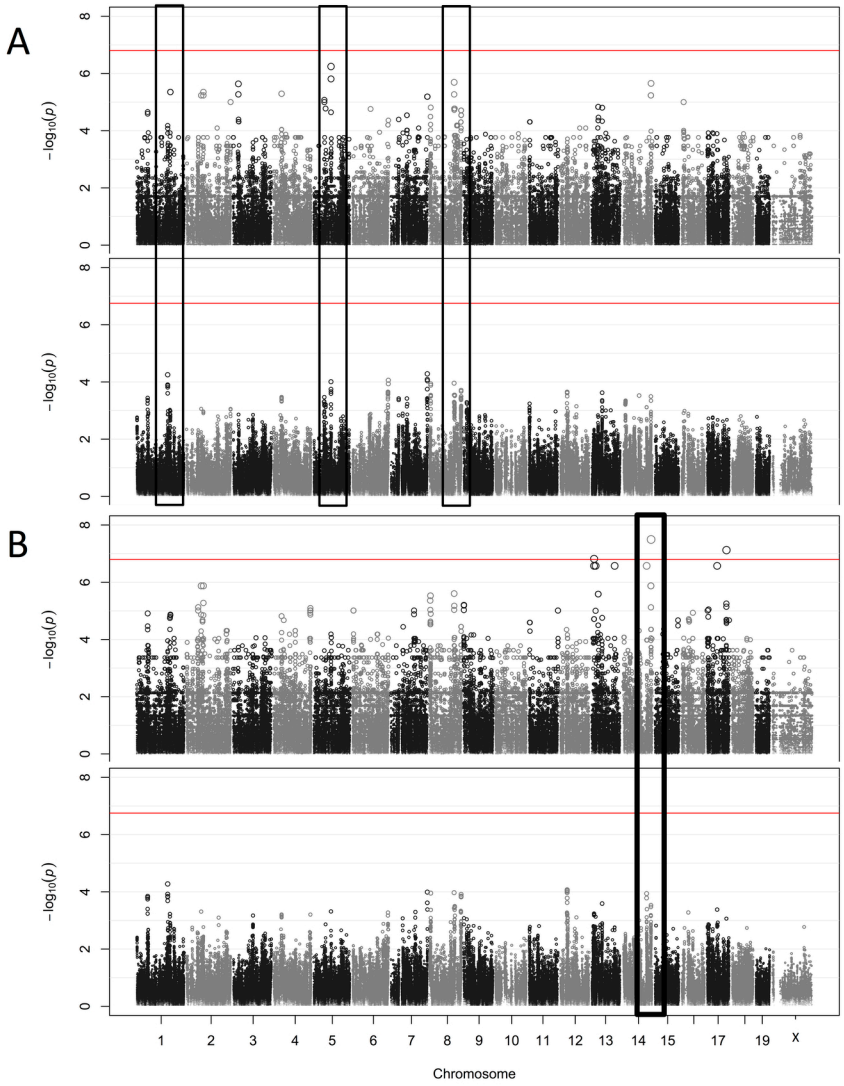

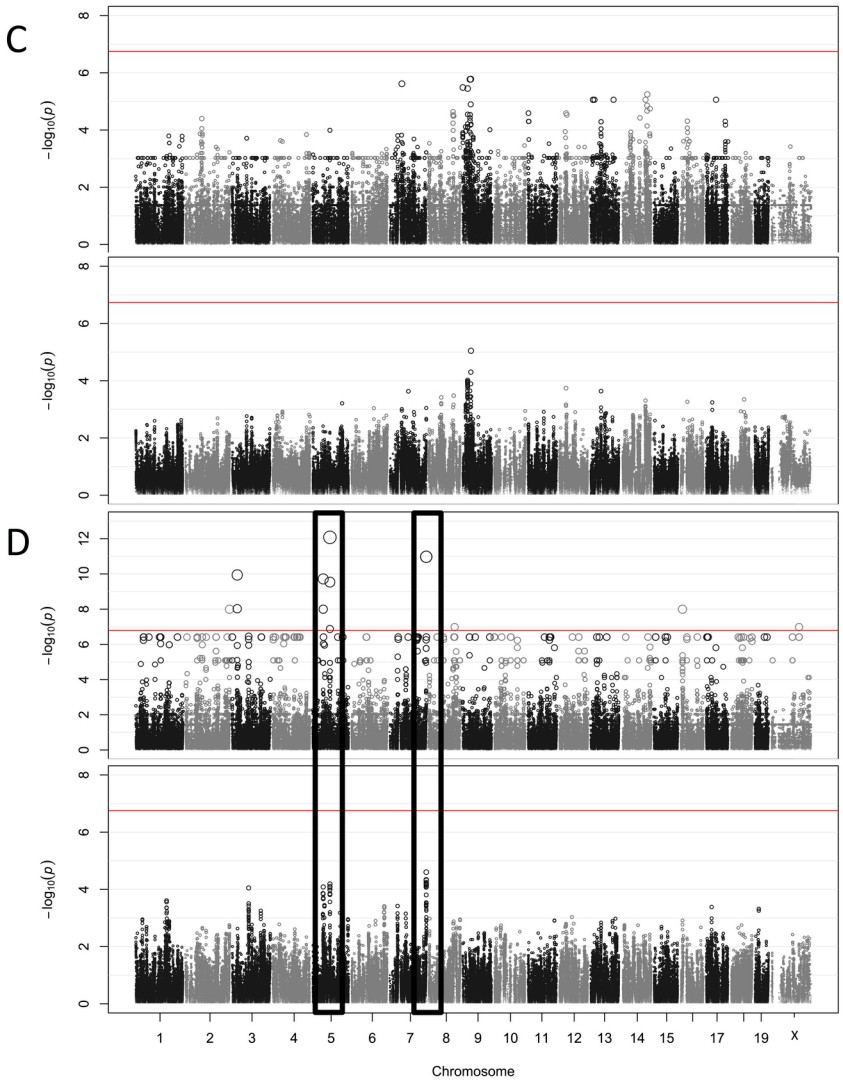
C
D
$-\log_{10}(p)$
Chromosome
1
2
3
4
5
6
7
8
9
10
11
12
13
14
15
17
19
X

Figure 4.7. Manhattan plots generated for monocytes exposed to doxorubicin.

Notes: Plots for IC50 values (**A**), AUC values (**B**), and viability at various doxorubicin concentrations (1, 3, and 10 μM, respectively **C**, **D**, and **E**) are shown. Plots generated from EMMA are above those plots generated from SNPster. Matching peaks are in black boxes with significant matching peaks bolded.

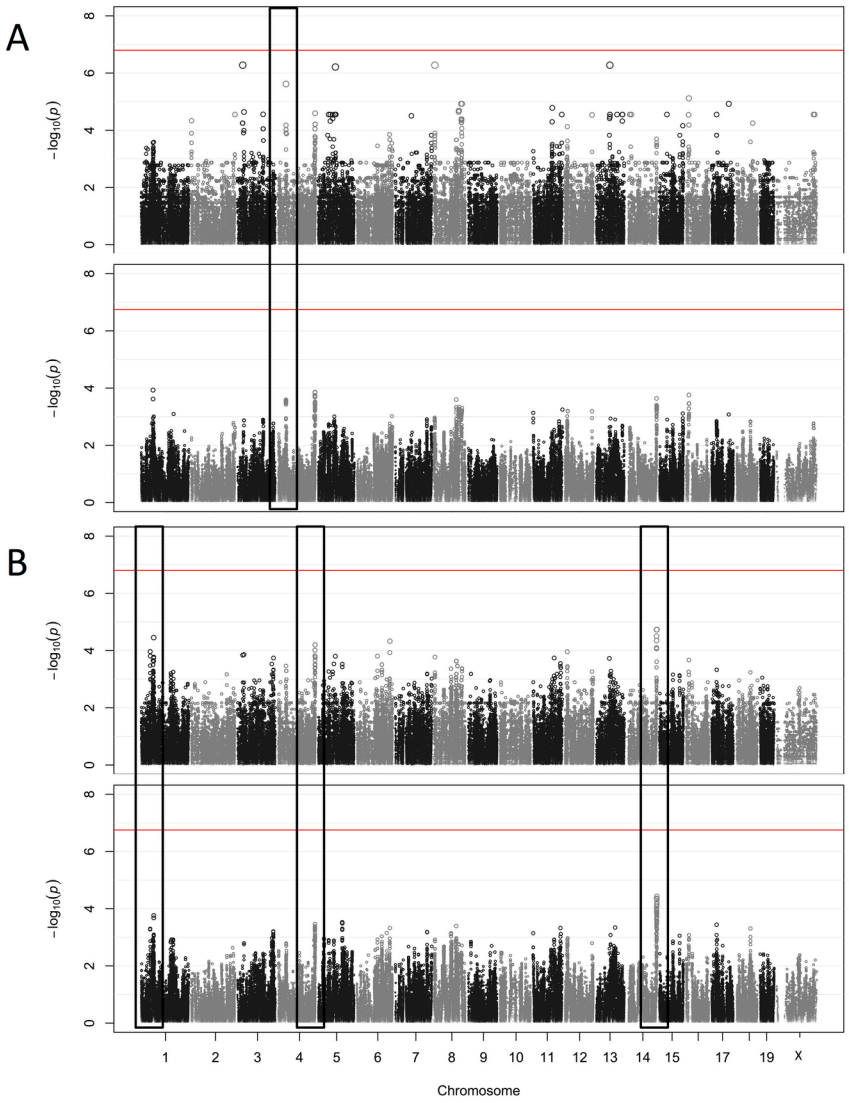

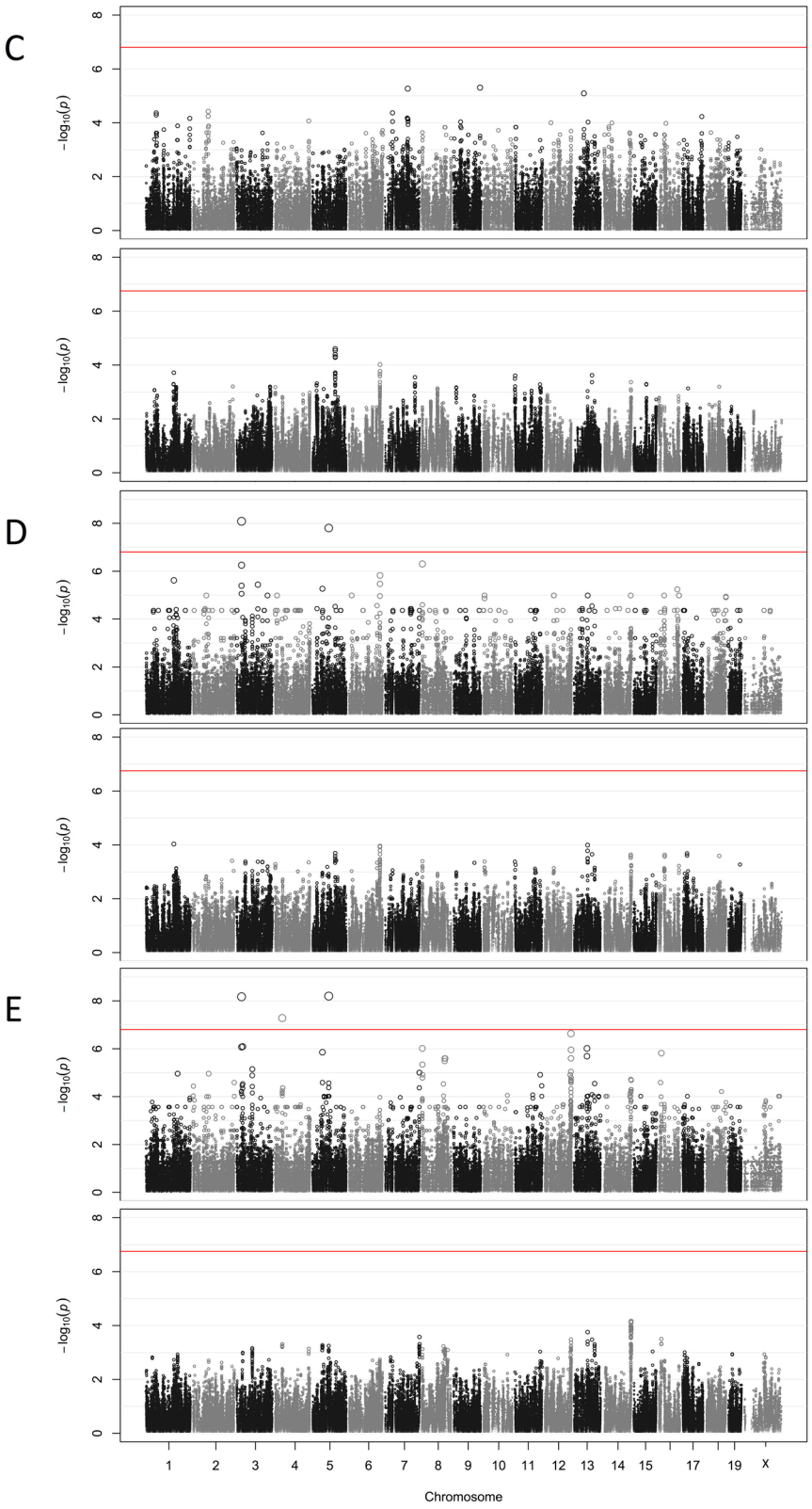
C
D
E
−log10(p)
0
2
4
6
8
1
2
3
4
5
6
7
8
9
10
11
12
13
14
15
17
19
X
Chromosome

Figure 4.8. Manhattan plots generated for monocytes exposed to idarubicin.

Notes: Plots for IC50 values (**A**), AUC values (**B**), and viability at various idarubicin concentrations (1 and 3 μM, respectively **C** and **D**) are shown. Plots generated from EMMA are above those plots generated from SNPster. Matching peaks are in black boxes with significant matching peaks bolded.

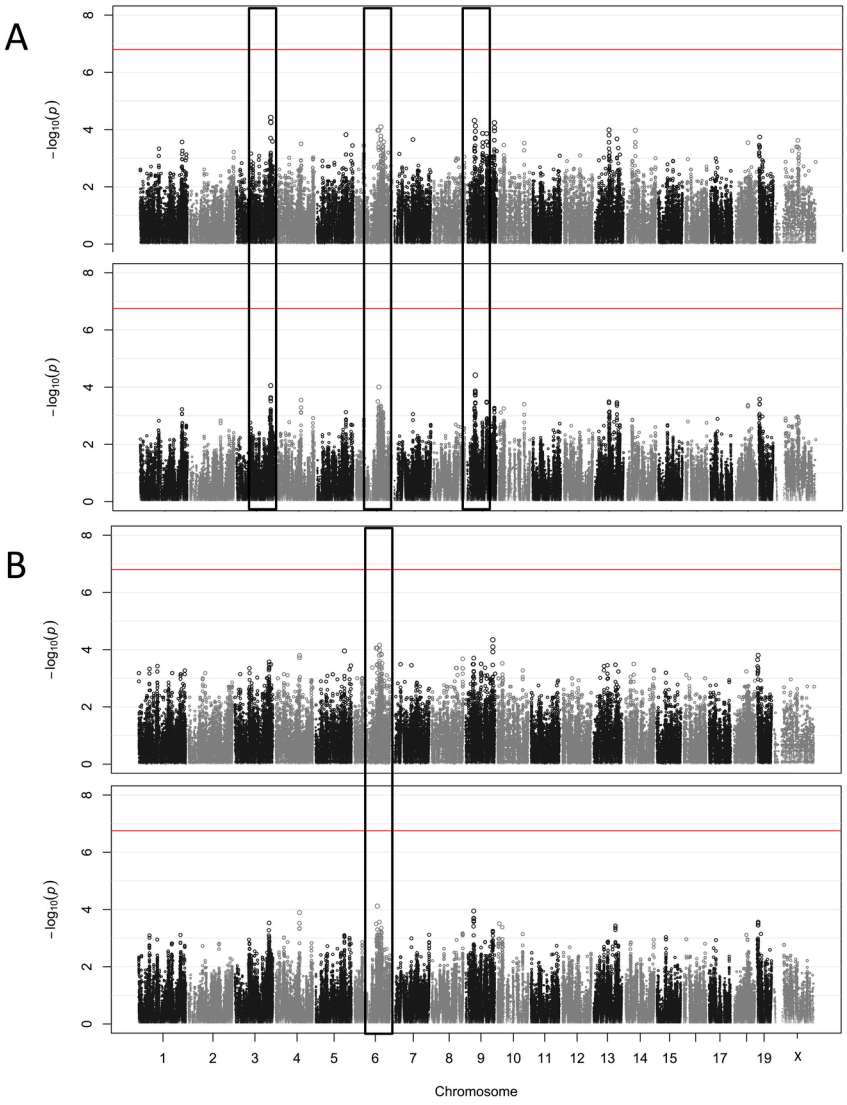

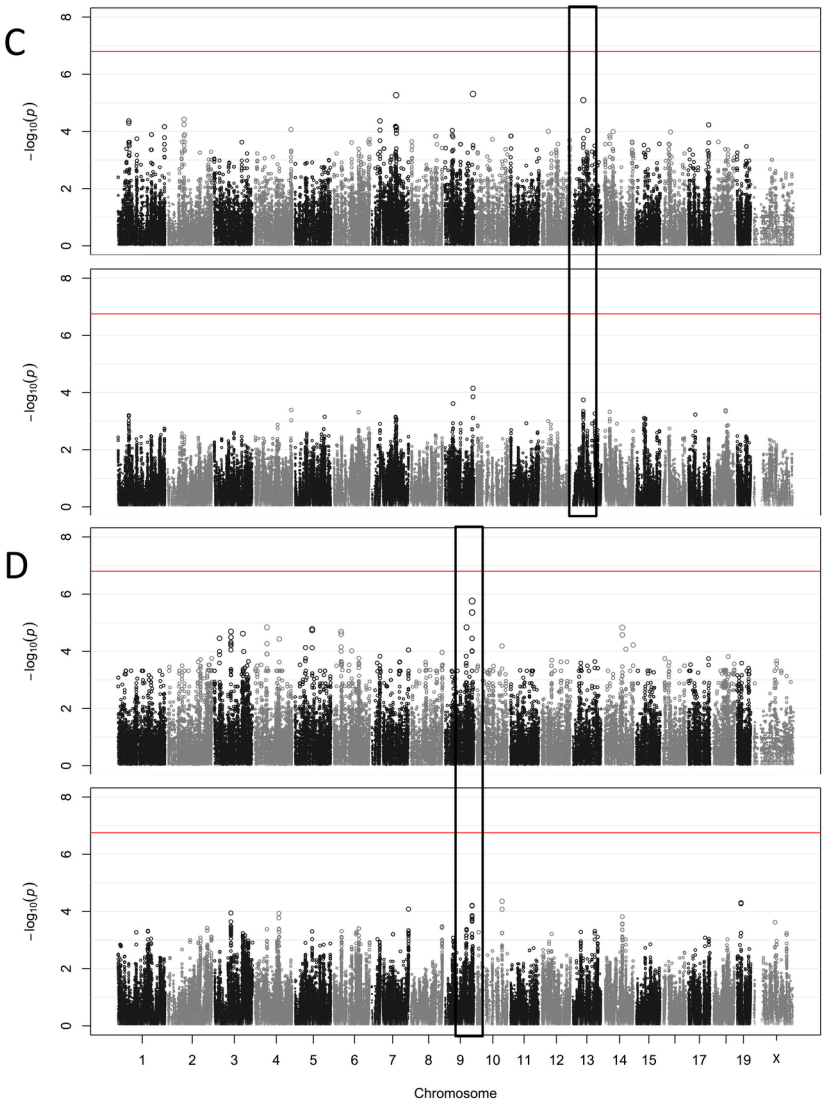
C
D
$-\log_{10}(p)$
0
2
4
6
8
1
2
3
4
5
6
7
8
9
10
11
12
13
14
15
17
19
X
Chromosome

Figure 4.9. Manhattan plots generated for T-cells exposed to doxorubicin.

Notes: Plots for IC50 values (**A**), AUC values (**B**), and viability at various doxorubicin concentrations (33 and 100 μM, respectively **C** and **D**) are shown. Plots generated from EMMA are above those plots generated from SNPster. Matching peaks are in black boxes with significant matching peaks bolded.

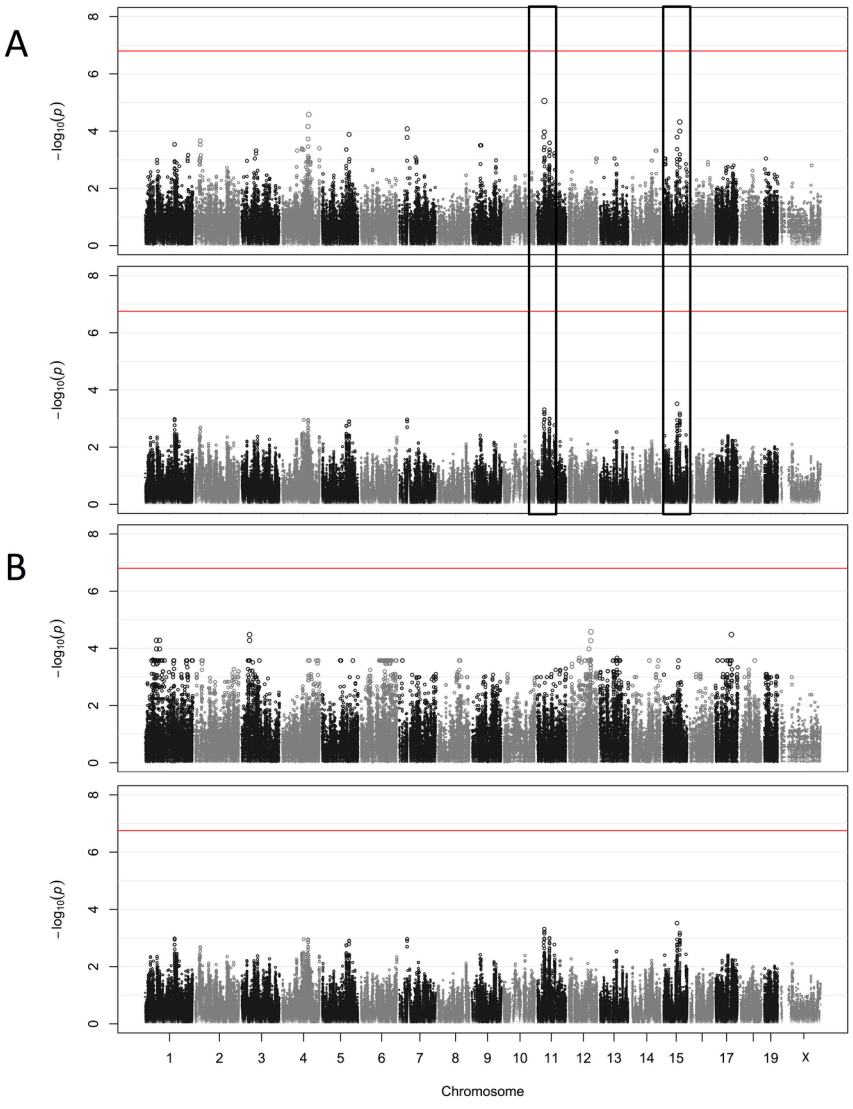

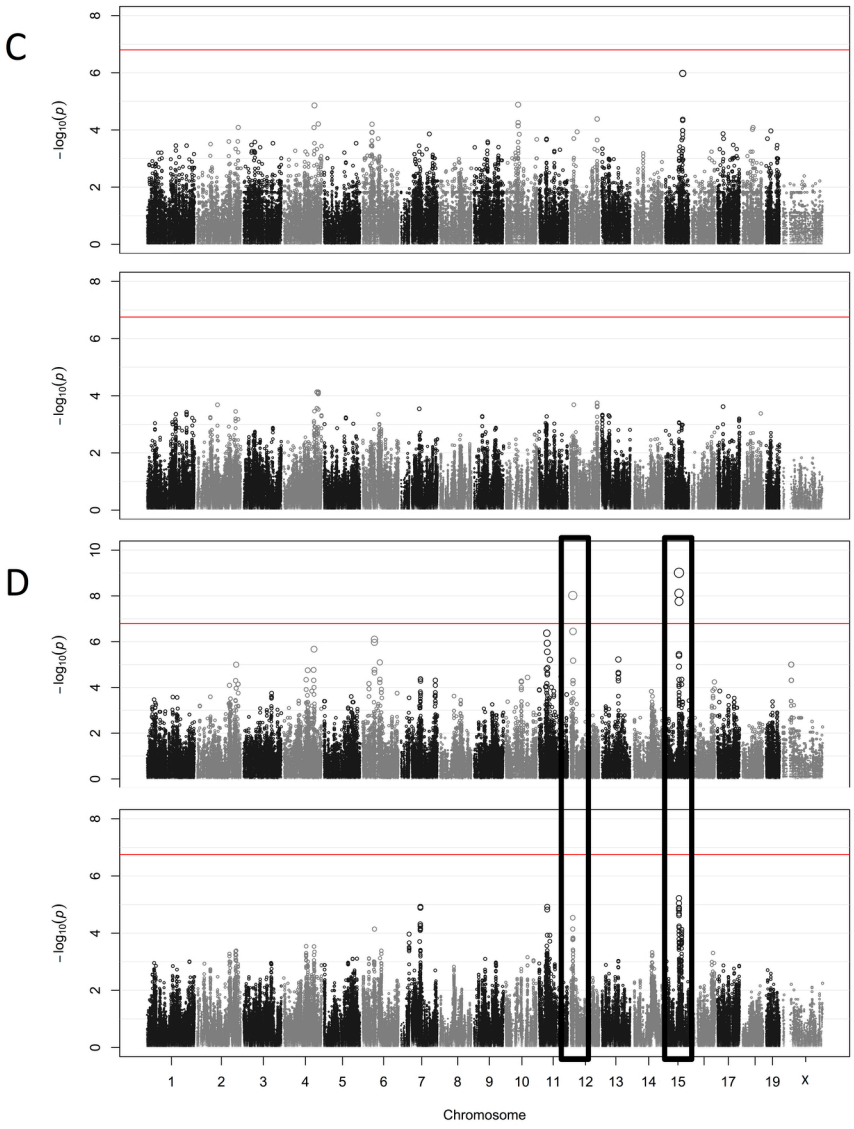
C
D
$-\log_{10}(p)$
Chromosome
1
2
3
4
5
6
7
8
9
10
11
12
13
14
15
17
19
X

Figure 4.10. Manhattan plots generated for T-cells exposed to idarubicin.

Notes: Plots for IC50 values (**A**), AUC values (**B**), and viability at various doxorubicin concentrations (1 and 3 μM, respectively **C** and **D**) are shown. Plots generated from EMMA are above those plots generated from SNPster. Matching peaks are in black boxes with significant matching peaks bolded.

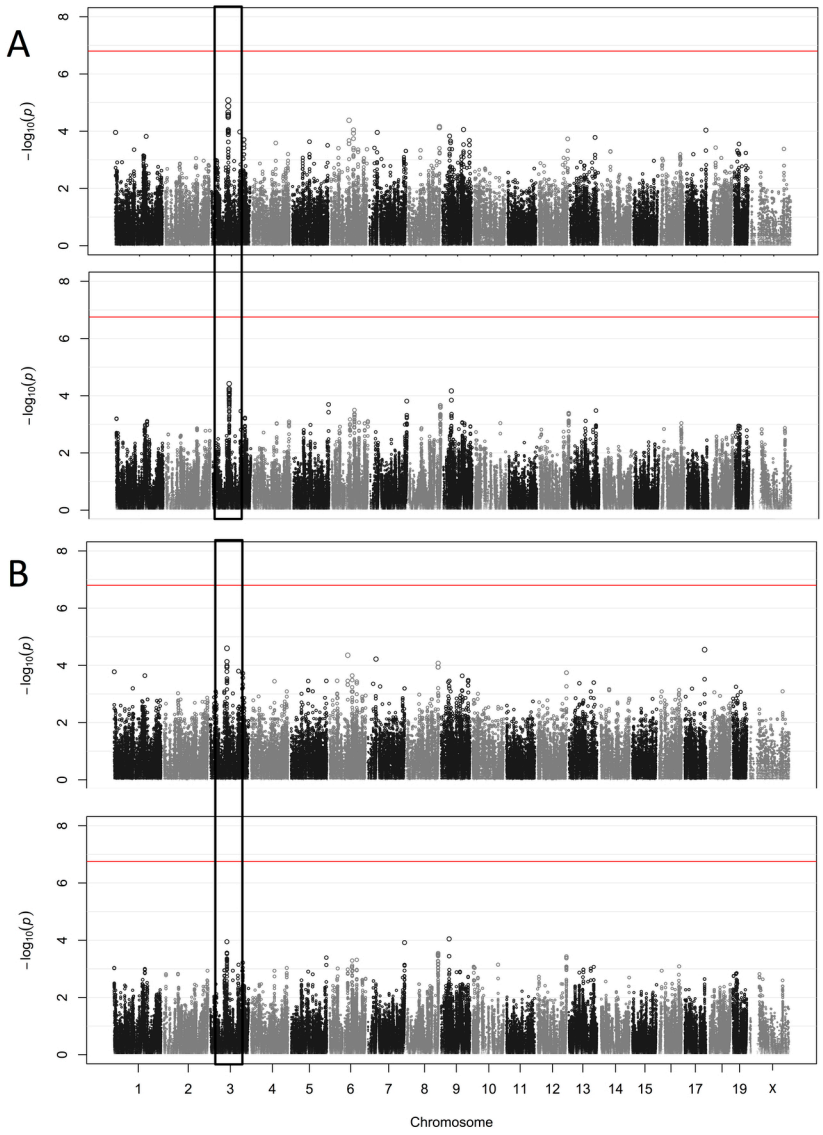

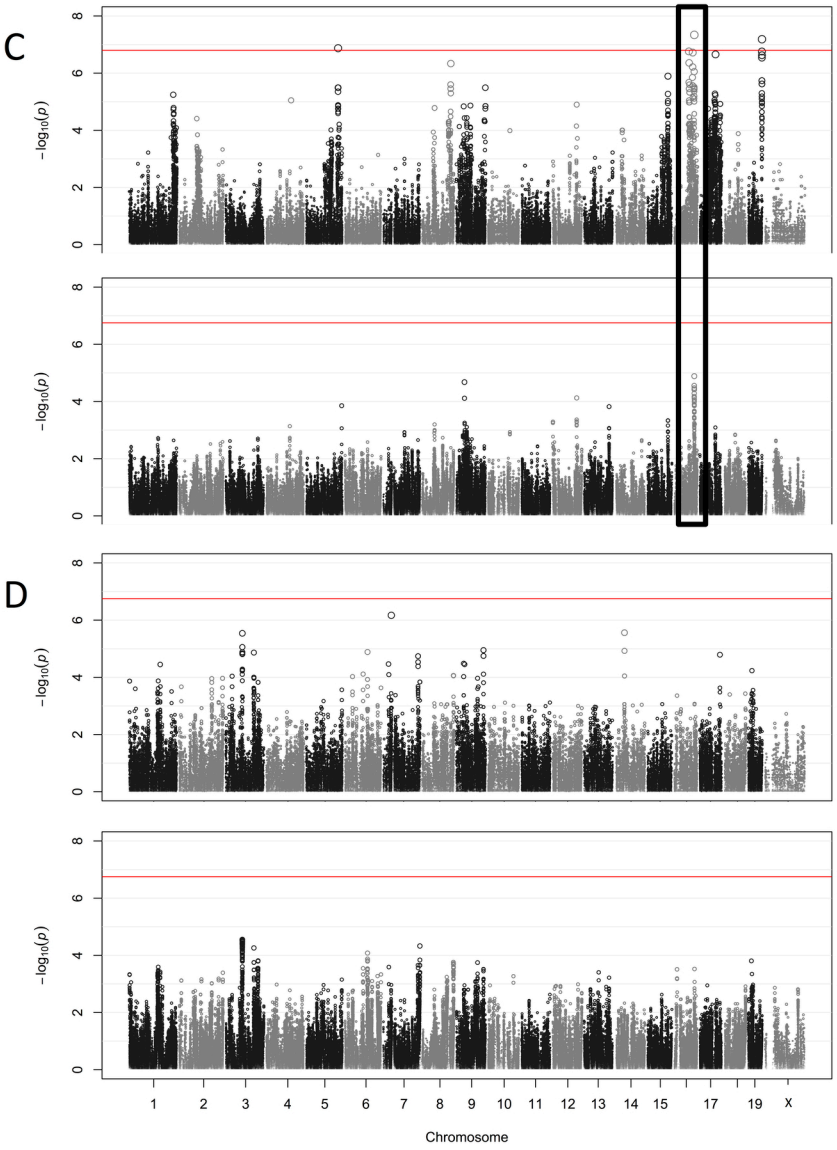
C
D
$-\log_{10}(p)$
0
2
4
6
8
1
2
3
4
5
6
7
8
9
10
11
12
13
14
15
17
19
X
Chromosome

Figure 4.11. Genomewide significant peaks and associated genes.

Notes: Peaks of genomewide significance with underlying genes from GWAS using various phenotypes: B-cells exposed to doxorubicin (0.3 μM and 1 μM, respectively **A** and **B**), B-cells exposed to idarubicin (3 μM, **C**), T-cells exposed to doxorubicin (100 μM, **D**), and T-cells exposed to idarubicin (1 μM, **E**).

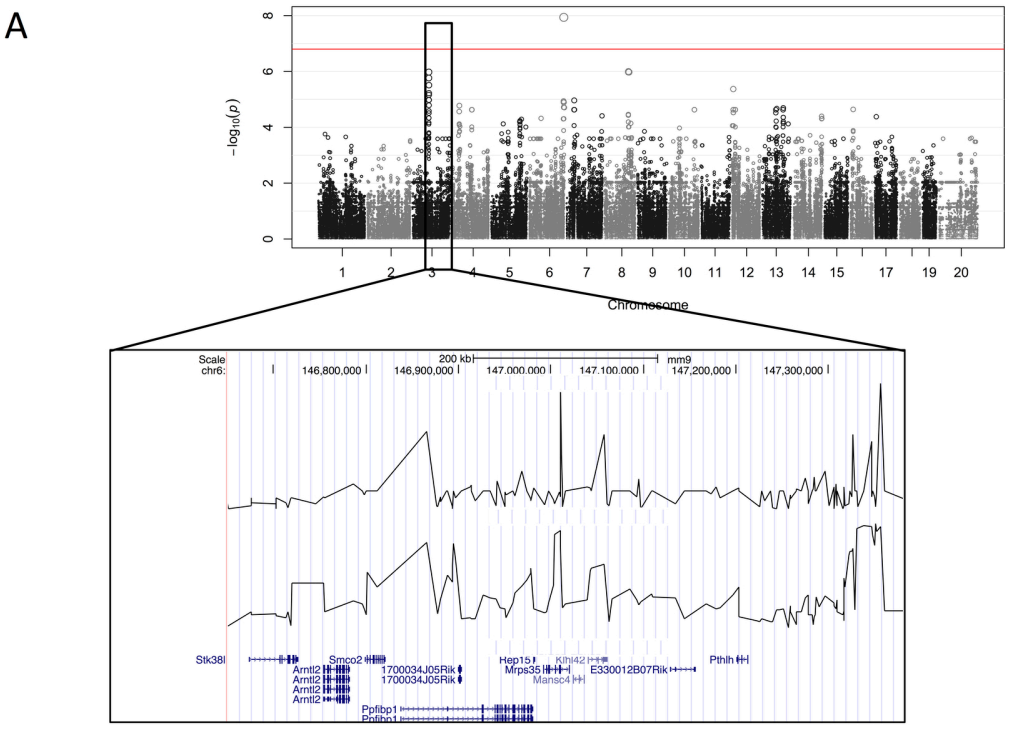

B

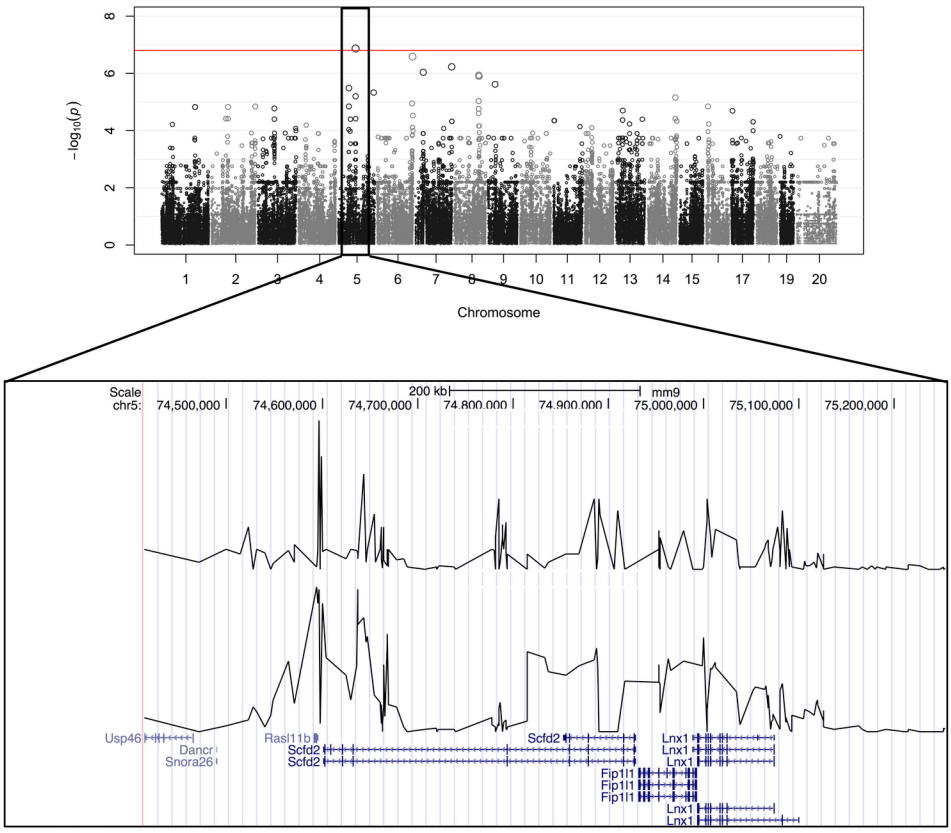
−log10(p)
0
2
4
6
8
1
2
3
4
5
6
7
8
9
10
11
12
13
14
15
17
19
20
Chromosome
Scale
chr5:
200 kb
mm9
74,500,000
74,600,000
74,700,000
74,800,000
74,900,000
75,000,000
75,100,000
75,200,000
Usp46
Dancr
Snora26
Rasl11b
Scfd2
Scfd2
Scfd2
Lnx1
Lnx1
Lnx1
Fip1l1
Fip1l1
Fip1l1
Lnx1
Lnx1

C

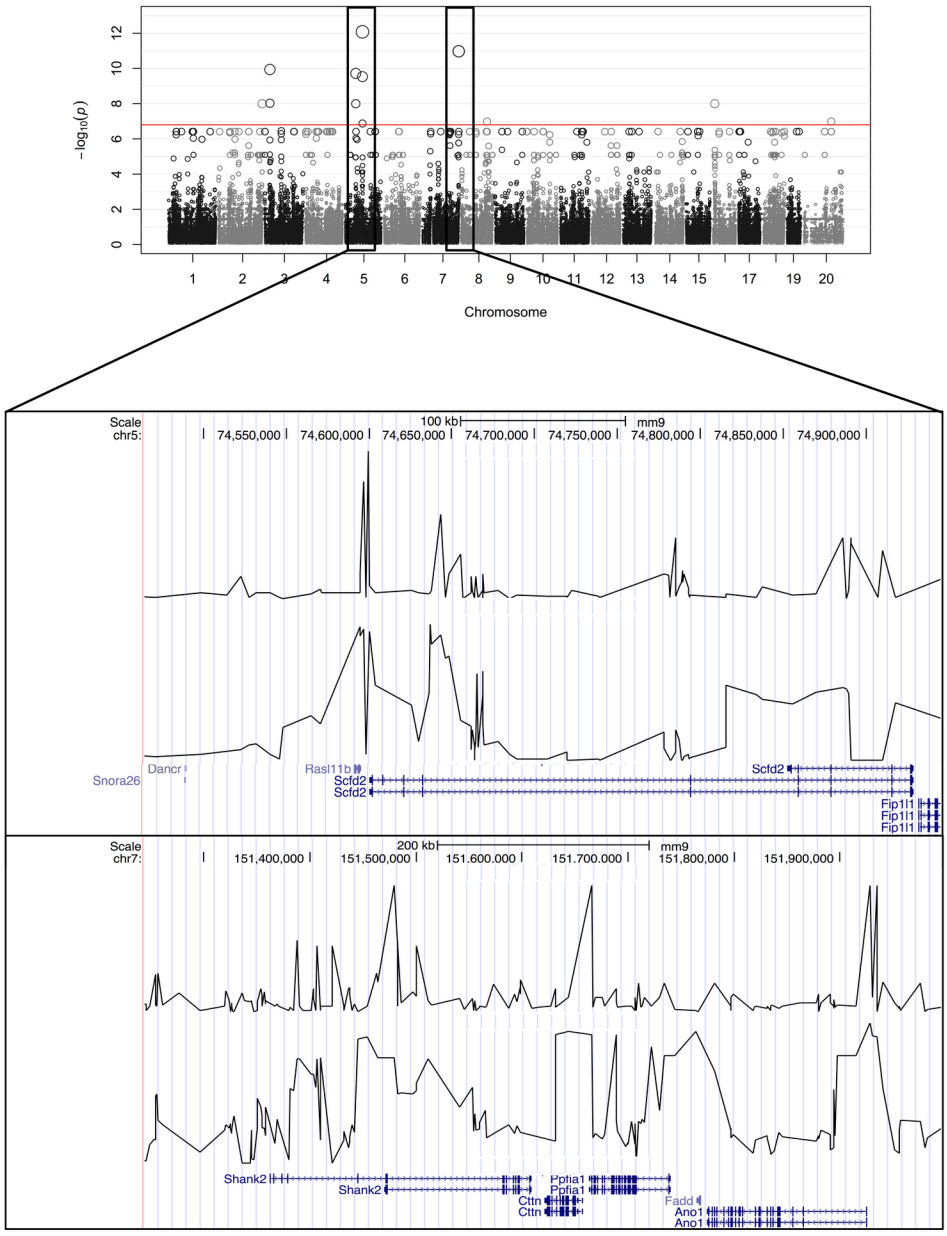
$-\log_{10}(p)$
0
2
4
6
8
10
12
1
2
3
4
5
6
7
8
9
10
11
12
13
14
15
17
19
20
Chromosome
Scale
chr5:
100 kb
mm9
74,550,000
74,600,000
74,650,000
74,700,000
74,750,000
74,800,000
74,850,000
74,900,000
Snora26
Dancr
Rasl11b
Scfd2
Scfd2
Scfd2
Fip1l1
Fip1l1
Fip1l1
Scale
chr7:
200 kb
mm9
151,400,000
151,500,000
151,600,000
151,700,000
151,800,000
151,900,000
Shank2
Shank2
Ppfia1
Ppfia1
Cttn
Cttn
Fadd
Ano1
Ano1

D

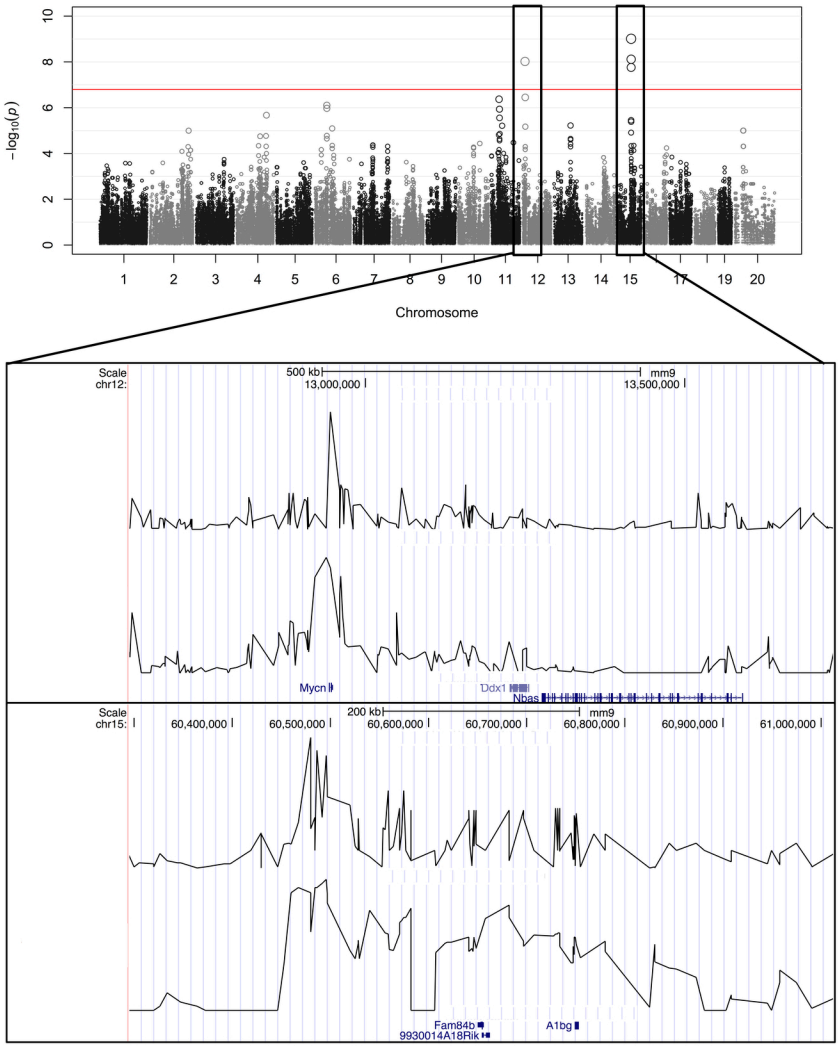
$-\log_{10}(p)$
0
2
4
6
8
10
1
2
3
4
5
6
7
8
9
10
11
12
13
14
15
17
19
20
Chromosome
Scale
chr12:
500 kb
13,000,000
mm9
13,500,000
Mycn
Ddx1
Nbas
Scale
chr15:
200 kb
60,400,000
60,500,000
60,600,000
60,700,000
60,800,000
60,900,000
61,000,000
mm9
Fam84b
9930014A18Rik
A1bg

E

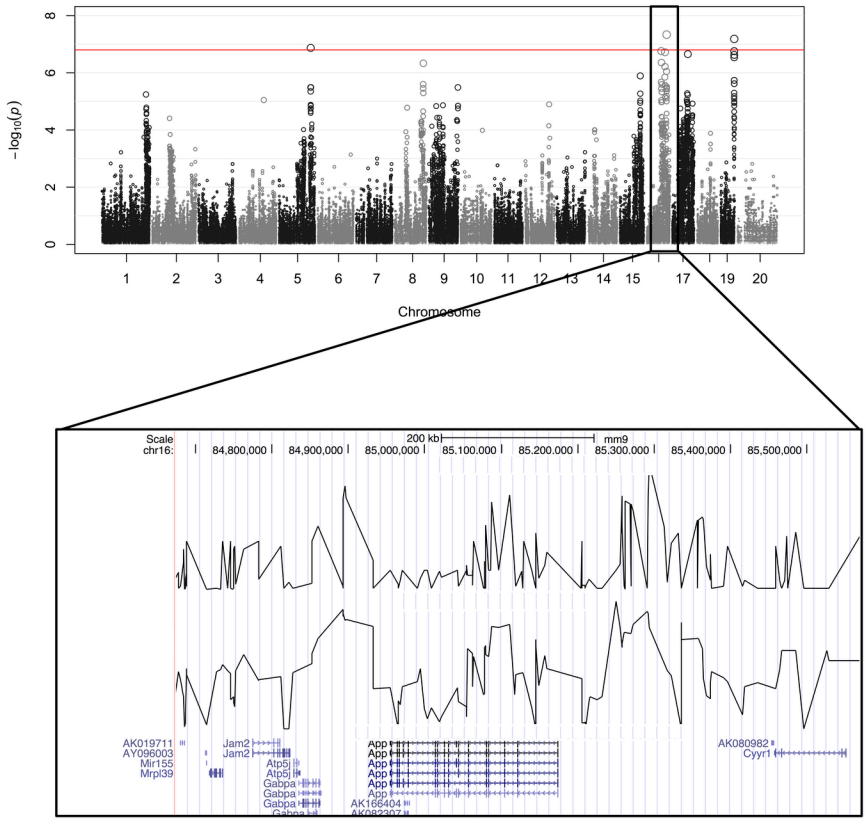
−log10(p)
0
2
4
6
8
1
2
3
4
5
6
7
8
9
10
11
12
13
14
15
17
19
20
Chromosome
Scale
chr16:
200 kb
mm9
84,800,000
84,900,000
85,000,000
85,100,000
85,200,000
85,300,000
85,400,000
85,500,000
AK019711
AY096003
Mir155
Mrpl39
Jam2
Jam2
Atp5j
Atp5j
Gabpa
Gabpa
Gabpa
Gabpa
App
App
App
App
App
App
AK166404
AK080982
Cyyr1

Figure 4.12. Haplotype structure for genes found from B-cells exposed to doxorubicin (0.3 μM).

Notes: Strains are arranged in descending order of phenotype from most to least sensitive. The haplotype structure was visualized with the Mouse Phylogeny Viewer (https://msub.csbio.unc.edu/).

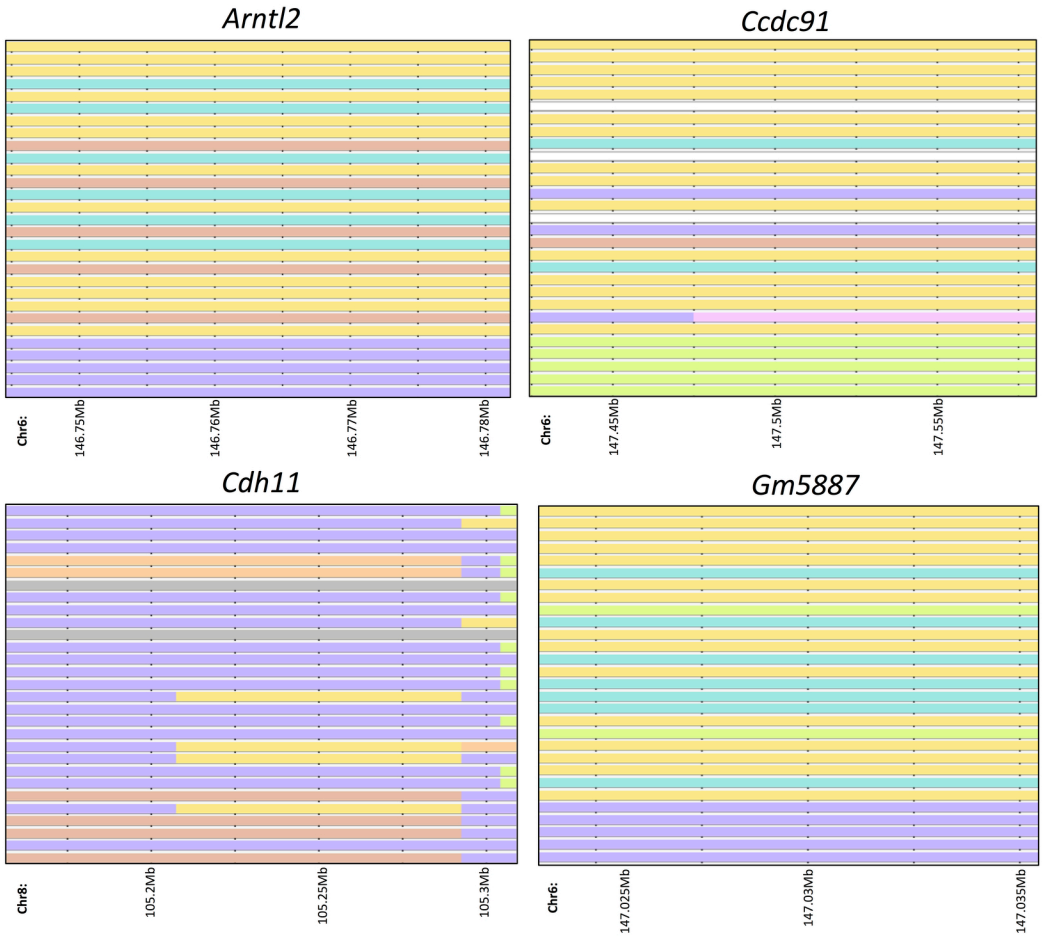

Strain	Mean	SD
SJL/J	10.42	1.28
C57BR/cdJ	25.30	2.50
I/LnJ	25.38	3.05
DBA/2J	26.38	6.35
NZB/BINJ	26.68	7.95
C57BLKS/J	28.87	0.89
SM/J	30.61	16.36
C58/J	30.78	9.30
NZO/HiLtJ	30.81	14.46
NOD/LtJ	31.46	7.96
CBA/J	32.09	9.12
C3H/HeJ	32.54	4.03
PL/J	33.07	0.28
LP/J	35.56	12.73
C57BL/6J	36.28	9.59
RIIIS/J	36.95	4.57
MA/MyJ	39.61	20.99
PWD/PhJ	41.53	11.86
CZECHII/EiJ	42.49	3.96
BTBRT+tf/J	46.46	18.40
PERA/EiJ	51.97	12.32
NON/LtJ	53.05	15.23
FVB/NJ	54.04	15.34
AKR/J	55.06	11.08
NZW/LacJ	55.43	6.70
LG/J	63.06	14.87
SWR/J	64.12	51.34
KK/HIJ	70.14	24.31
BUB/BnJ	75.85	8.19
A/J	77.92	2.77
129X1/SvJ	79.40	5.63
129S1SvImJ	80.68	33.93
SEA/GnJ	84.64	10.43
PWK/PhJ	86.09	6.54
BALB/cByJ	95.17	4.54
WSB/EiJ	105.00	12.74

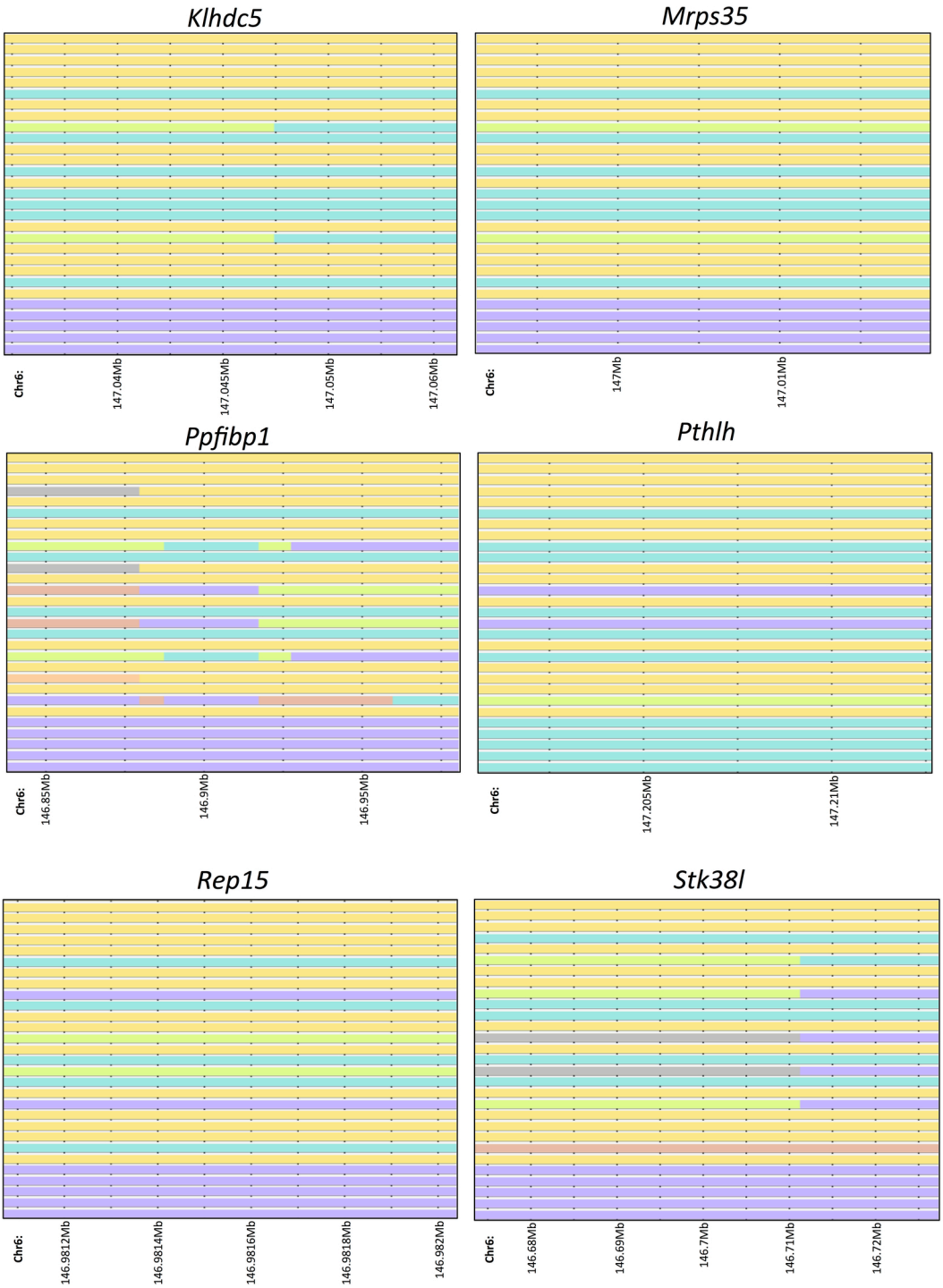
Klhdc5
Chr6:
147.04Mb
147.045Mb
147.05Mb
147.06Mb
Mrps35
Chr6:
147Mb
147.01Mb
Ppfibp1
Chr6:
146.85Mb
146.9Mb
146.95Mb
Pthlh
Chr6:
147.205Mb
147.21Mb
Rep15
Chr6:
146.9812Mb
146.9814Mb
146.9816Mb
146.9818Mb
146.982Mb
Stk38l
Chr6:
146.68Mb
146.69Mb
146.7Mb
146.71Mb
146.72Mb

Figure 4.13. Haplotype structure for genes found from B-cells exposed to doxorubicin (1 μM).

Notes: Strains are arranged in descending order of phenotype from most to least sensitive. The haplotype structure was visualized with the Mouse Phylogeny Viewer (https://msub.csbio.unc.edu/).

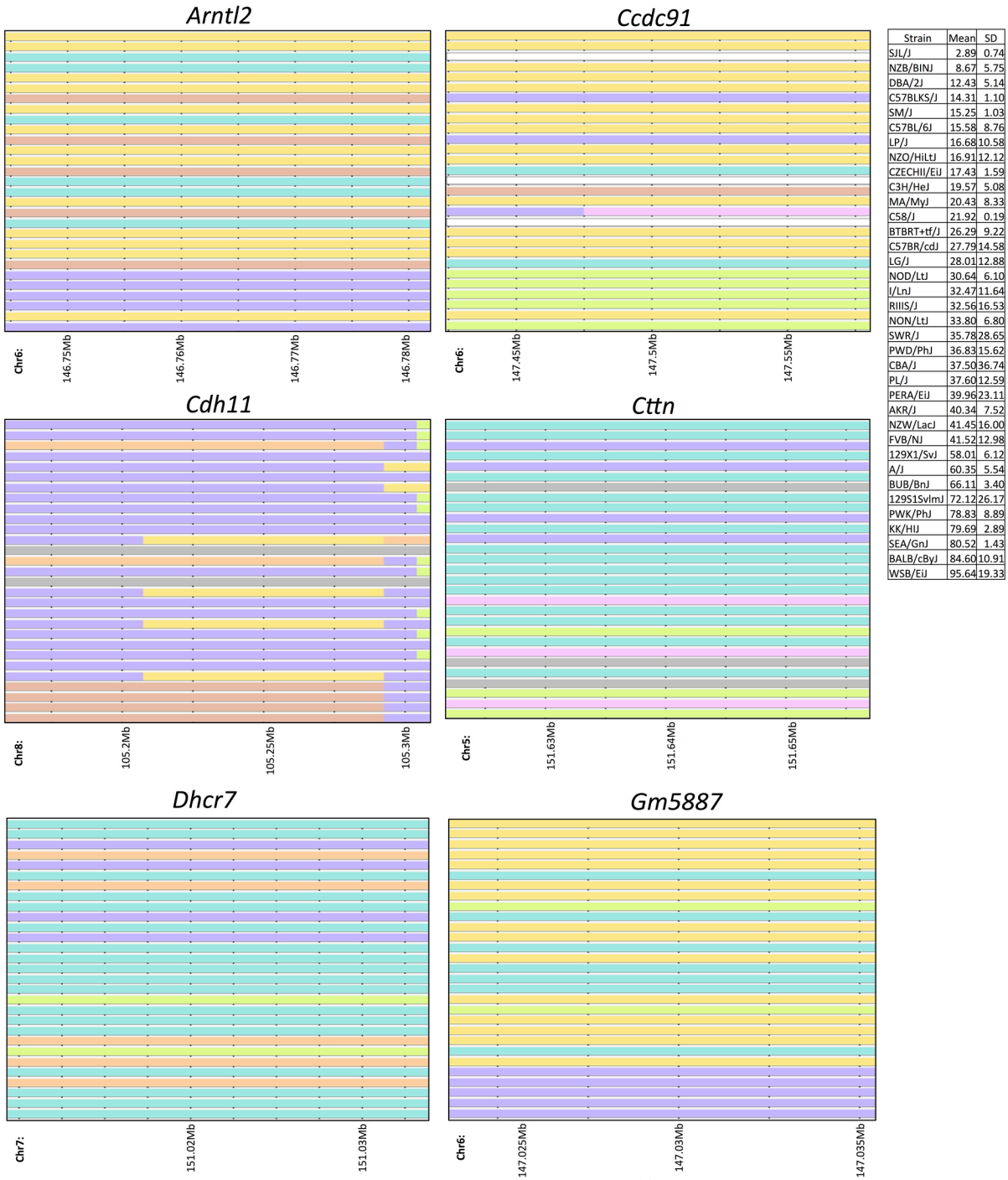

Strain	Mean	SD
SJL/J	2.89	0.74
NZB/BINJ	8.67	5.75
DBA/2J	12.43	5.14
C57BLKS/J	14.31	1.10
SM/J	15.25	1.03
C57BL/6J	15.58	8.76
LP/J	16.68	10.58
NZO/HiLtJ	16.91	12.12
CZECHII/EiJ	17.43	1.59
C3H/HeJ	19.57	5.08
MA/MyJ	20.43	8.33
C58/J	21.92	0.19
BTBRT+tf/J	26.29	9.22
C57BR/cdJ	27.79	14.58
LG/J	28.01	12.88
NOD/LtJ	30.64	6.10
I/LnJ	32.47	11.64
RIIIS/J	32.56	16.53
NON/LtJ	33.80	6.80
SWR/J	35.78	28.65
PWD/PhJ	36.83	15.62
CBA/J	37.50	36.74
PL/J	37.60	12.59
PERA/EiJ	39.96	23.11
AKR/J	40.34	7.52
NZW/LacJ	41.45	16.00
FVB/NJ	41.52	12.98
129X1/SvJ	58.01	6.12
A/J	60.35	5.54
BUB/BnJ	66.11	3.40
129S1SvImJ	72.12	26.17
PWK/PhJ	78.83	8.89
KK/HlJ	79.69	2.89
SEA/GnJ	80.52	1.43
BALB/cByJ	84.60	10.91
WSB/EiJ	95.64	19.33

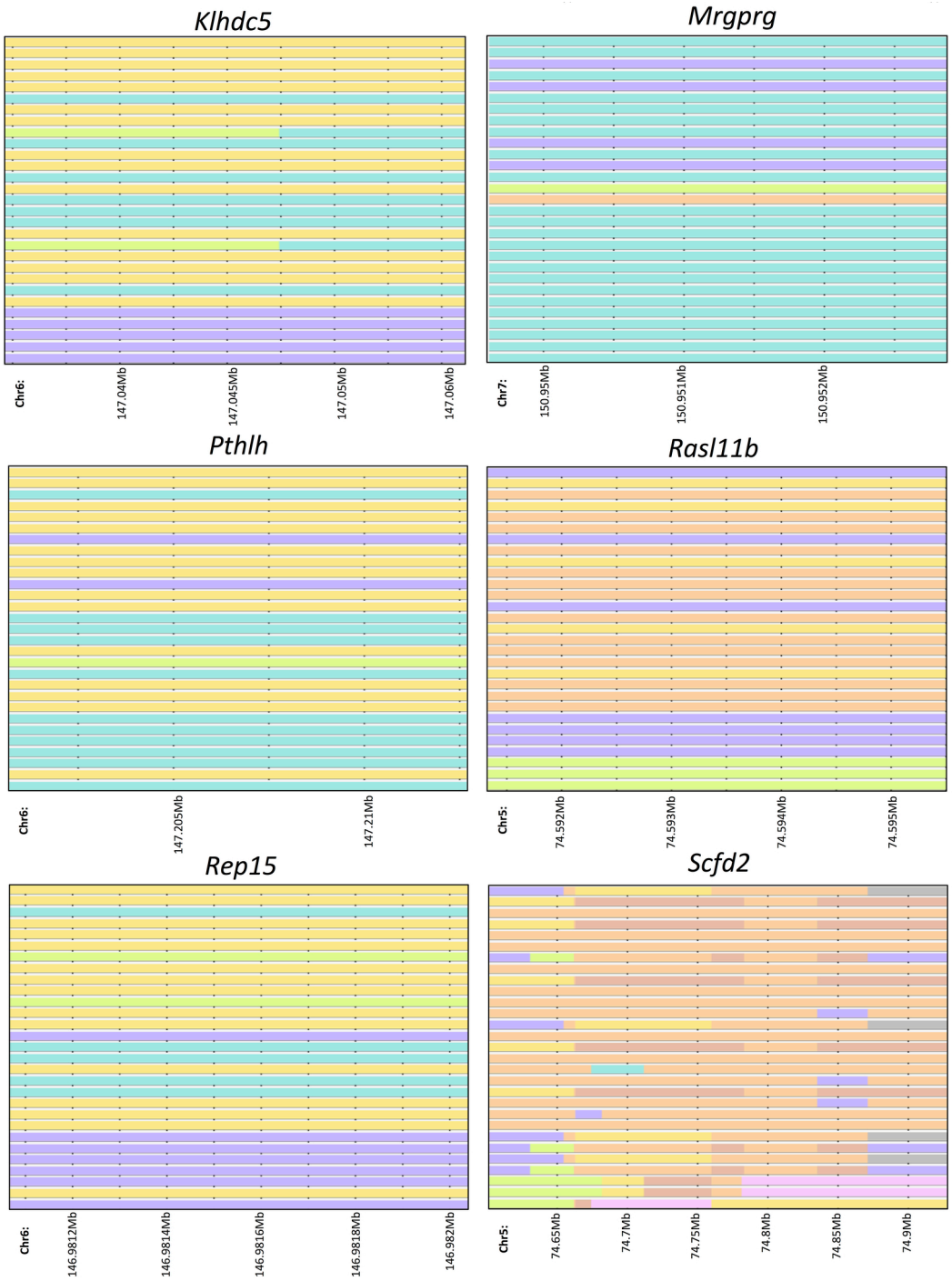
Klhdc5
Chr6:
147.04Mb
147.045Mb
147.05Mb
147.06Mb
Mrgprg
Chr7:
150.95Mb
150.951Mb
150.952Mb
Pthlh
Chr6:
147.205Mb
147.21Mb
Rasl11b
Chr5:
74.592Mb
74.593Mb
74.594Mb
74.595Mb
Rep15
Chr6:
146.9812Mb
146.9814Mb
146.9816Mb
146.9818Mb
146.982Mb
Scfd2
Chr5:
74.65Mb
74.7Mb
74.75Mb
74.8Mb
74.85Mb
74.9Mb


Shank2
Stk38l
Chr7:
151.25Mb
151.3Mb
151.35Mb
151.4Mb
151.45Mb
151.5Mb
151.55Mb
151.6Mb
Chr6:
146.68Mb
146.69Mb
146.7Mb
146.71Mb
146.72Mb

Figure 4.14. Haplotype structure for genes found from B-cells exposed to idarubicin (3 μM).

Notes: Strains are arranged in descending order of phenotype from most to least sensitive. The haplotype structure was visualized with the Mouse Phylogeny Viewer (https://msub.csbio.unc.edu/).

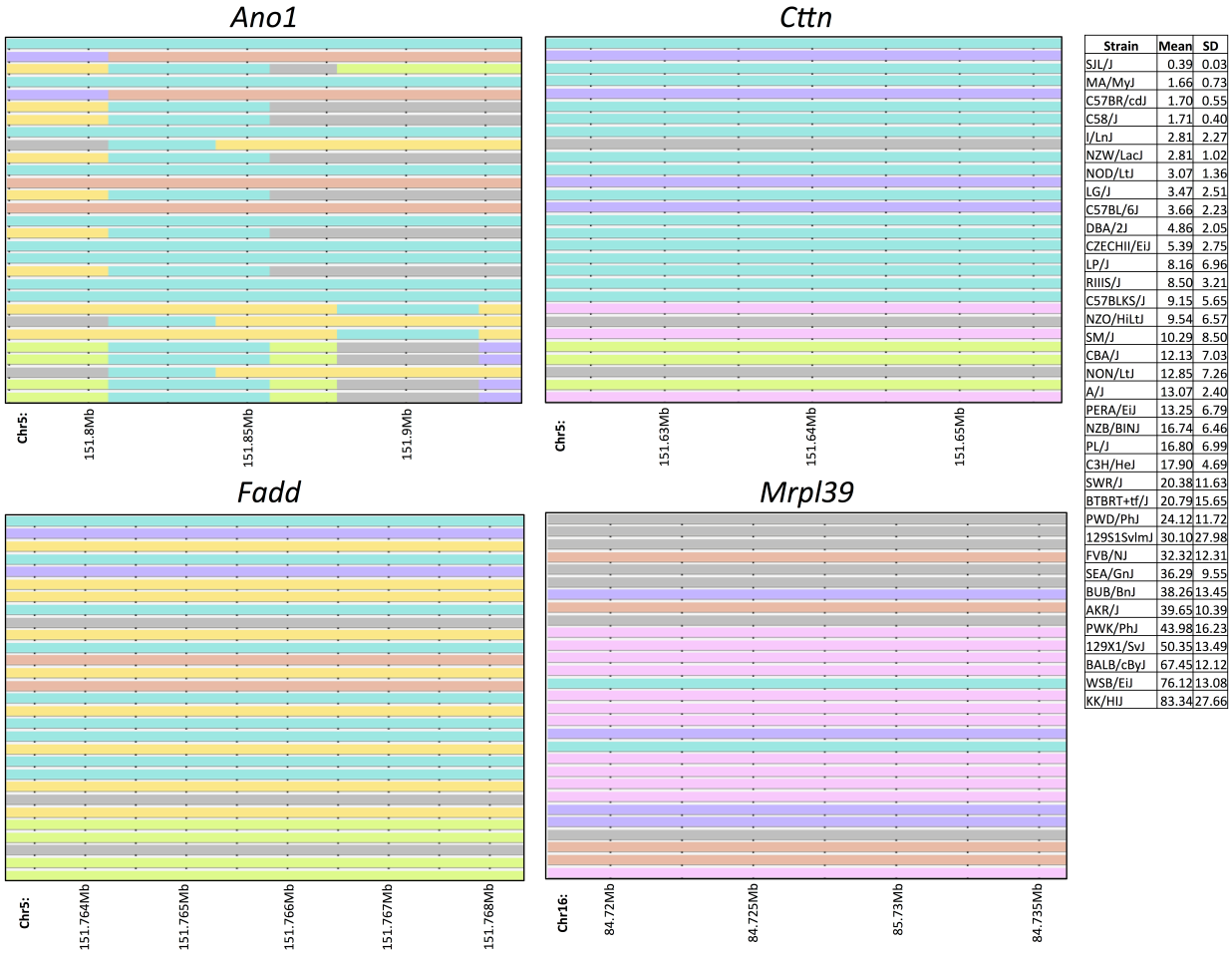

Strain	Mean	SD
SJL/J	0.39	0.03
MA/MyJ	1.66	0.73
C57BR/cdJ	1.70	0.55
C58/J	1.71	0.40
I/LnJ	2.81	2.27
NZW/LacJ	2.81	1.02
NOD/LtJ	3.07	1.36
LG/J	3.47	2.51
C57BL/6J	3.66	2.23
DBA/2J	4.86	2.05
CZECHII/EiJ	5.39	2.75
LP/J	8.16	6.96
RIIIS/J	8.50	3.21
C57BLKS/J	9.15	5.65
NZO/HiLtJ	9.54	6.57
SM/J	10.29	8.50
CBA/J	12.13	7.03
NON/LtJ	12.85	7.26
A/J	13.07	2.40
PERA/EiJ	13.25	6.79
NZB/BINJ	16.74	6.46
PL/J	16.80	6.99
C3H/HeJ	17.90	4.69
SWR/J	20.38	11.63
BTBRT+tf/J	20.79	15.65
PWD/PhJ	24.12	11.72
129S1SvImJ	30.10	27.98
FVB/NJ	32.32	12.31
SEA/GnJ	36.29	9.55
BUB/BnJ	38.26	13.45
AKR/J	39.65	10.39
PWK/PhJ	43.98	16.23
129X1/SvJ	50.35	13.49
BALB/cByJ	67.45	12.12
WSB/EiJ	76.12	13.08
KK/HIJ	83.34	27.66

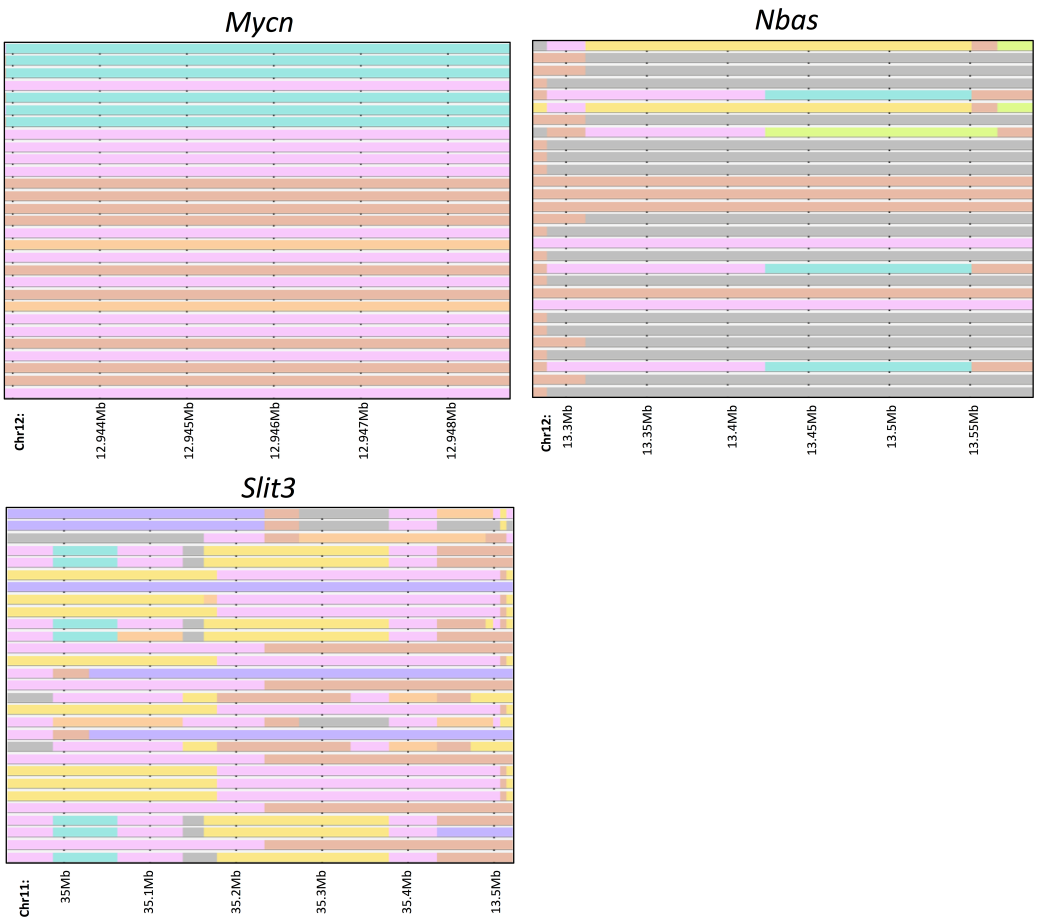
Mycn
Chr12:
12.944Mb
12.945Mb
12.946Mb
12.947Mb
12.948Mb
Nbas
Chr12:
13.3Mb
13.35Mb
13.4Mb
13.45Mb
13.5Mb
13.55Mb
Slit3
Chr11:
35Mb
35.1Mb
35.2Mb
35.3Mb
35.4Mb
13.5Mb

Figure 4.15. Haplotype structure for genes found from T-cells exposed to doxorubicin (100 µM).

Notes: Strains are arranged in descending order of phenotype from most to least sensitive. The haplotype structure was visualized with the Mouse Phylogeny Viewer (https://msub.csbio.unc.edu/).

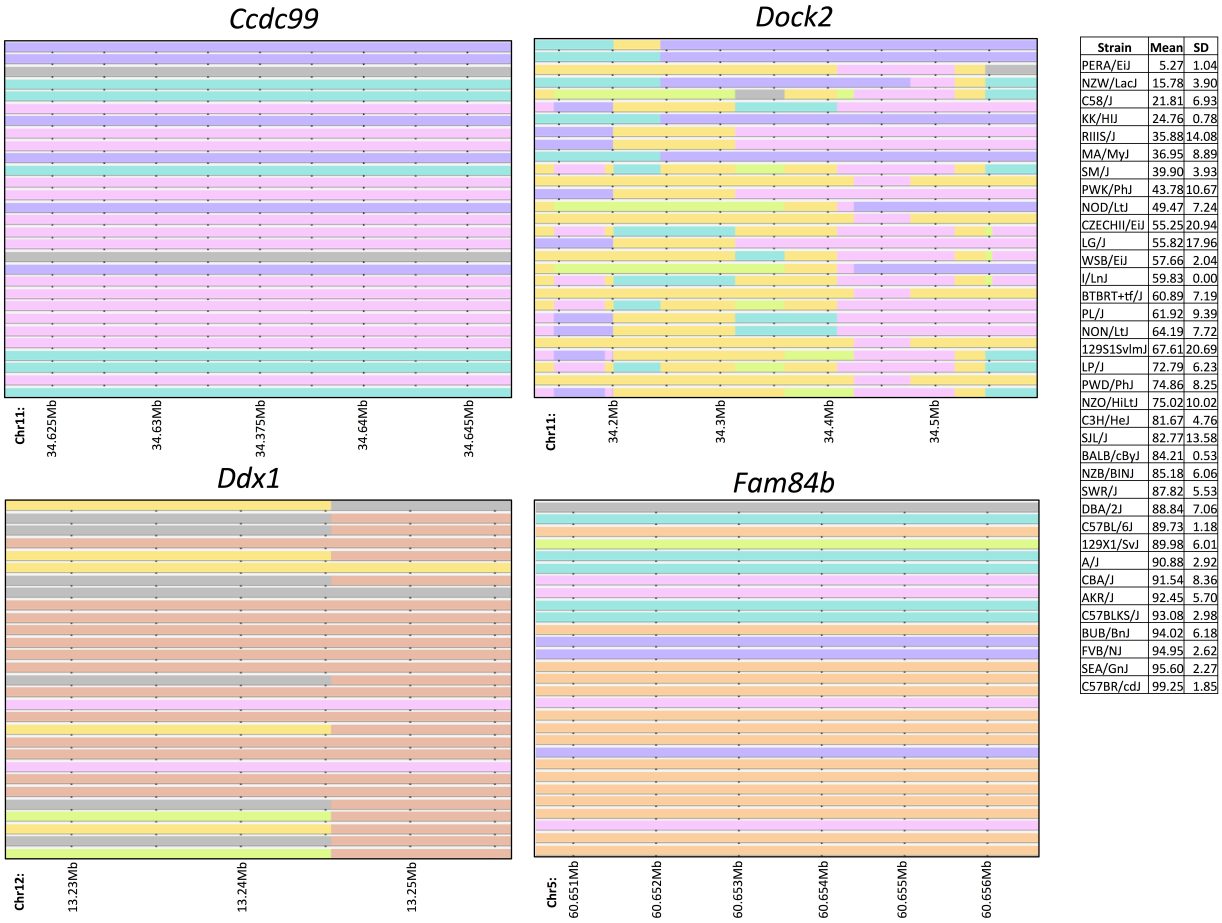

Strain	Mean	SD
PERA/EiJ	5.27	1.04
NZW/LacJ	15.78	3.90
C58/J	21.81	6.93
KK/HlJ	24.76	0.78
RIIIS/J	35.88	14.08
MA/MyJ	36.95	8.89
SM/J	39.90	3.93
PWK/PhJ	43.78	10.67
NOD/LtJ	49.47	7.24
CZECHII/EiJ	55.25	20.94
LG/J	55.82	17.96
WSB/EiJ	57.66	2.04
I/LnJ	59.83	0.00
BTBRT+tf/J	60.89	7.19
PL/J	61.92	9.39
NON/LtJ	64.19	7.72
129S1SvImJ	67.61	20.69
LP/J	72.79	6.23
PWD/PhJ	74.86	8.25
NZO/HlLtJ	75.02	10.02
C3H/HeJ	81.67	4.76
SJL/J	82.77	13.58
BALB/cByJ	84.21	0.53
NZB/BINJ	85.18	6.06
SWR/J	87.82	5.53
DBA/2J	88.84	7.06
C57BL/6J	89.73	1.18
129X1/SvJ	89.98	6.01
A/J	90.88	2.92
CBA/J	91.54	8.36
AKR/J	92.45	5.70
C57BLKS/J	93.08	2.98
BUB/BnJ	94.02	6.18
FVB/NJ	94.95	2.62
SEA/GnJ	95.60	2.27
C57BR/cdJ	99.25	1.85

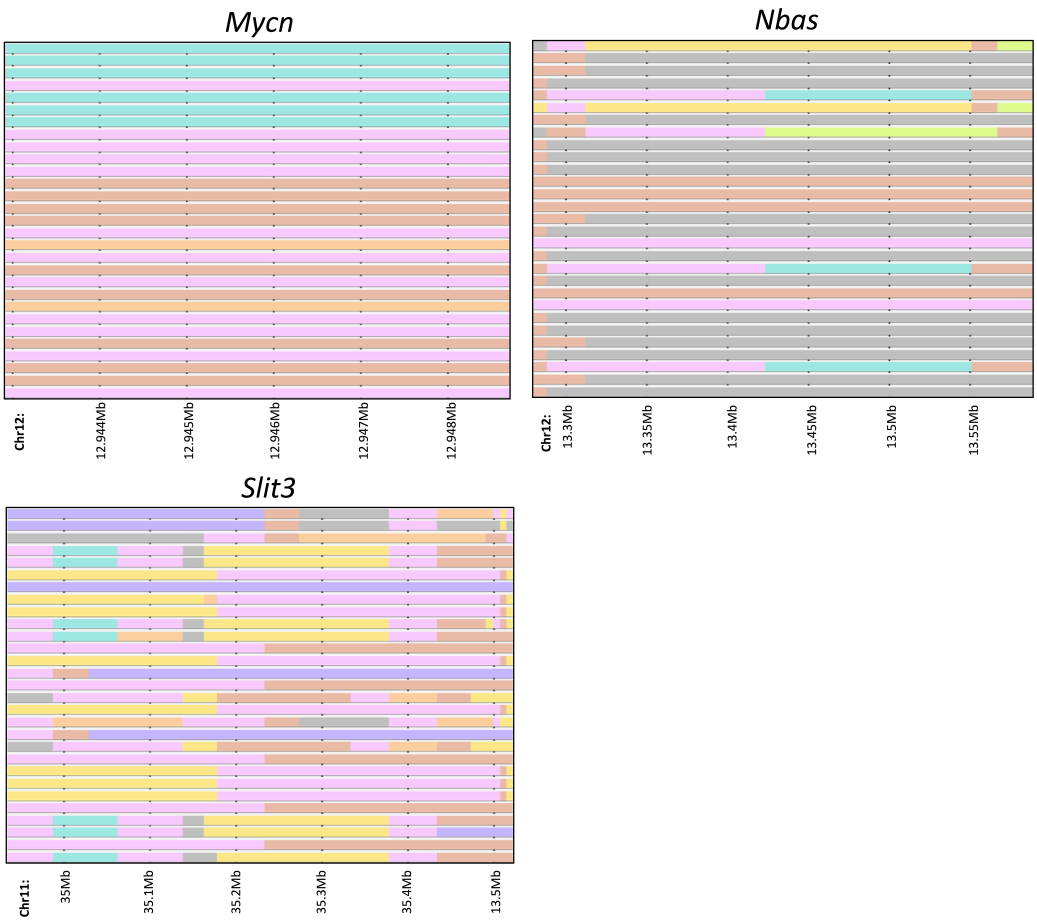
Mycn
Chr12:
12.944Mb
12.945Mb
12.946Mb
12.947Mb
12.948Mb
Nbas
Chr12:
13.3Mb
13.35Mb
13.4Mb
13.45Mb
13.5Mb
13.55Mb
Slit3
Chr11:
35Mb
35.1Mb
35.2Mb
35.3Mb
35.4Mb
13.5Mb

Figure 4.16. Haplotype structure for genes found from T-cells exposed to idarubicin (1 μM).

Notes: Strains are arranged in descending order of phenotype from most to least sensitive. The haplotype structure was visualized with the Mouse Phylogeny Viewer (https://msub.csbio.unc.edu/).

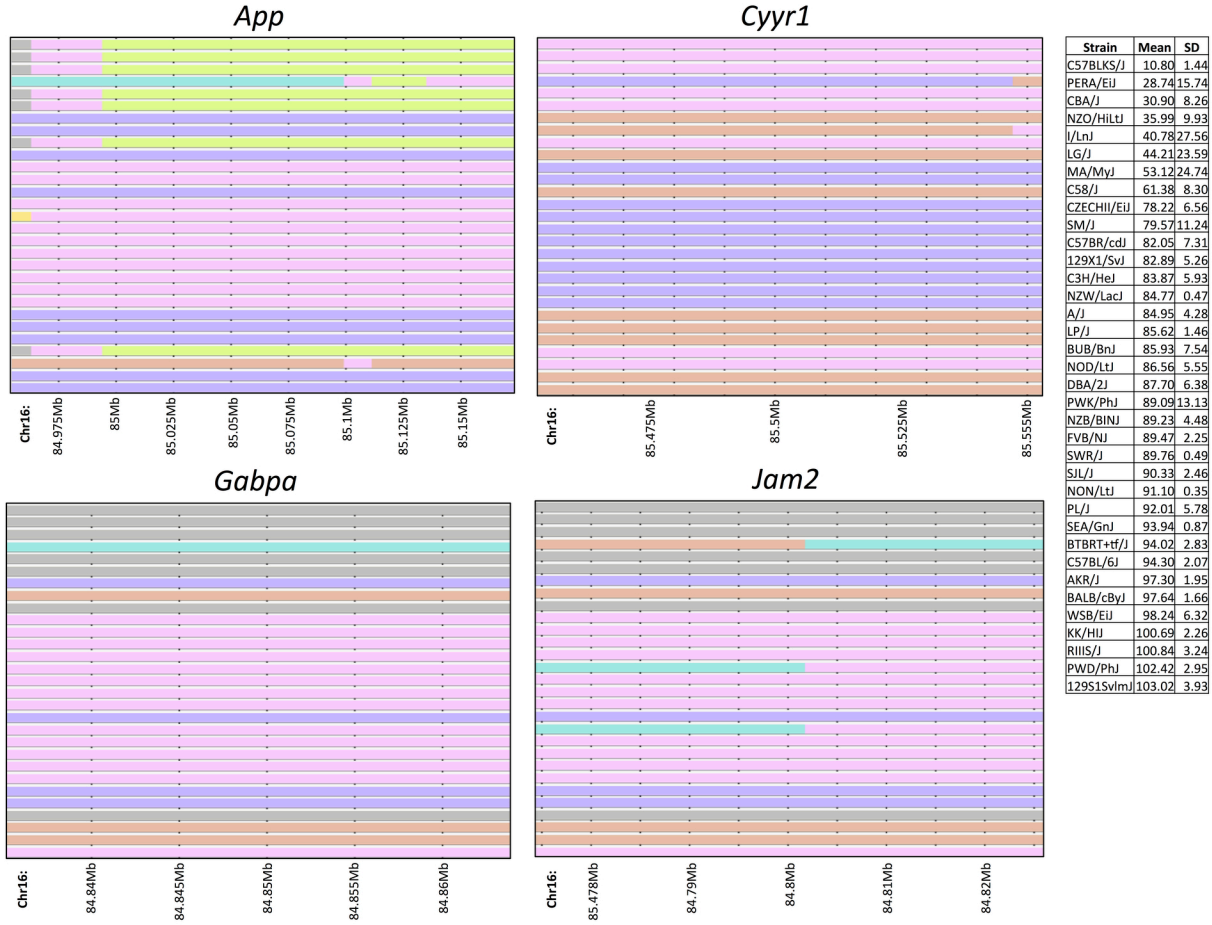

Strain	Mean	SD
C57BLKS/J	10.80	1.44
PERA/EiJ	28.74	15.74
CBA/J	30.90	8.26
NZO/HiLtJ	35.99	9.93
I/LnJ	40.78	27.56
LG/J	44.21	23.59
MA/MyJ	53.12	24.74
C58/J	61.38	8.30
CZECHII/EiJ	78.22	6.56
SM/J	79.57	11.24
C57BR/cdJ	82.05	7.31
129X1/SvJ	82.89	5.26
C3H/HeJ	83.87	5.93
NZW/LacJ	84.77	0.47
A/J	84.95	4.28
LP/J	85.62	1.46
BUB/BnJ	85.93	7.54
NOD/LtJ	86.56	5.55
DBA/2J	87.70	6.38
PWK/PhJ	89.09	13.13
NZB/BINJ	89.23	4.48
FVB/NJ	89.47	2.25
SWR/J	89.76	0.49
SJL/J	90.33	2.46
NON/LtJ	91.10	0.35
PL/J	92.01	5.78
SEA/GnJ	93.94	0.87
BTBRT+tf/J	94.02	2.83
C57BL/6J	94.30	2.07
AKR/J	97.30	1.95
BALB/cByJ	97.64	1.66
WSB/EiJ	98.24	6.32
KK/HlJ	100.69	2.26
RIIIS/J	100.84	3.24
PWD/PhJ	102.42	2.95
129S1SvImJ	103.02	3.93

Table 4.1. Expression data for genes found from B-cells exposed to doxorubicin (0.3 μM).

Notes: QTL, -log(*p*) of the peak, gene symbol, expression probesets and fold difference in expression, expression range (minimum and maximum), and Pearson and Spearman correlations with *p* values respectively in the spleen, CD4+ T-cells, CD4+ Th1 cells, and macrophages are shown. Measurements in red and yellow are supportive for identification of candidate genes.

Expression data was marked in red if relative expression was > 100, if the fold expression difference in tissue was > 2, and if the *p* value for correlation was < 0.05 and in yellow if relative expression was > 50 and if the *p* value for correlation was ≤ 0.1. *A1bg* and *Gm5887* did not have expression information available.

QTL	Log P of Peak	Gene	Unique Expression Probesets	Spleen Expression	Fold Difference in Spleen	Expression Range in Spleen		Pearson Correlation		Spearman Correlation		CD4 Expression	Fold Difference in CD4	Expression Range in CD4 Cells		Pearson Correlation		Spearman Correlation	
chr6 147.0Mb	7.94	Arntl2	1425931_a_at	No	1.51	3.93	5.94	-0.29	0.16	-0.54	0.01	No	1.28	4.09	5.25	0.06	0.78	0.13	0.54
chr6 147.0Mb	7.94	Arntl2	1429688_at	No	3.70	6.75	24.97	-0.15	0.49	-0.21	0.33	>100	23.73	6.65	157.85	0.57	0.00	0.21	0.35
chr6 147.0Mb	7.94	Klhdc5	1426988_at	>100	12.86	55.98	720.10	-0.01	0.97	0.23	0.29	>100	11.07	84.57	936.17	-0.13	0.54	-0.10	0.65
chr6 147.0Mb	7.94	Mrps35	1452111_at	>100	2.25	99.03	222.72	-0.38	0.07	-0.37	0.08	>100	1.91	412.33	789.14	0.30	0.16	0.22	0.31
chr6 147.0Mb	7.94	Ppfibp1	1445577_at	No	1.11	3.31	3.66	-0.19	0.36	-0.11	0.61	No	1.03	3.23	3.32	0.02	0.95	-0.17	0.43
chr6 147.0Mb	7.94	Ppfibp1	1443029_at	No	2.40	4.28	10.25	-0.14	0.53	0.02	0.92	No	1.40	4.48	6.28	-0.01	0.96	0.08	0.73
chr6 147.0Mb	7.94	Ppfibp1	1452759_s_at	>100	2.53	102.51	259.38	0.31	0.14	0.37	0.07	>50	2.54	21.52	54.66	0.07	0.76	0.18	0.41
chr6 147.0Mb	7.94	Pthlh	1427527_a_at	No	2.11	7.47	15.80	-0.08	0.71	-0.30	0.15	No	1.14	6.55	7.44	-0.22	0.32	-0.18	0.42
chr6 147.0Mb	7.94	Pthlh	1422324_a_at	No	2.24	6.83	15.33	-0.15	0.50	-0.03	0.88	No	1.07	5.92	6.35	-0.16	0.46	-0.24	0.26
chr6 147.0Mb	7.94	Rep15	1420328_at	No	1.40	7.21	10.08	-0.08	0.70	-0.09	0.67	No	1.38	9.33	12.91	-0.11	0.61	-0.19	0.37
chr6 147.0Mb	7.94	Stk38l	1435877_at	No	4.04	5.21	21.08	0.51	0.01	0.40	0.06	No	3.42	4.97	16.98	-0.21	0.34	-0.06	0.78
chr6 147.0Mb	7.94	Stk38l	1435878_at	>50	3.60	20.12	72.51	0.09	0.66	0.24	0.27	>50	4.63	12.82	59.34	0.11	0.62	0.17	0.43
chr6 147.0Mb	7.94	Stk38l	1455183_at	>50	5.86	14.33	84.03	0.07	0.76	0.15	0.48	>50	5.93	15.13	89.66	0.26	0.22	0.22	0.32
chr6 147.3Mb	7.94	Ccdc91	1430670_at	No	1.66	4.85	8.06	-0.25	0.24	-0.53	0.01	No	1.15	4.82	5.52	-0.03	0.90	-0.02	0.94
chr6 147.3Mb	7.94	Ccdc91	1453605_s_at	No	2.58	9.36	24.17	0.36	0.09	0.18	0.41	No	1.25	37.42	46.87	0.11	0.62	0.15	0.50
chr6 147.3Mb	7.94	Ccdc91	1418459_at	>50	6.70	10.52	70.56	0.34	0.10	0.20	0.36	>50	3.58	20.23	72.42	-0.19	0.38	-0.10	0.63
chr6 147.3Mb	7.94	Ccdc91	1449083_at	>100	2.33	49.72	115.75	0.27	0.20	0.23	0.27	>100	2.36	94.48	222.80	-0.05	0.80	-0.09	0.70
chr8 105.1Mb	5.98	Cdh11	1450757_at	>100	2.35	162.63	382.28	0.03	0.89	-0.06	0.77	No	1.08	4.79	5.17	0.03	0.89	-0.07	0.76

QTL	Log P of Peak	Gene	Unique Expression Probesets	Th1 Expression	Fold Difference in Th1	Expression Range in Th1 Cells		Pearson Correlation		Spearman Correlation		Macrophage Expression	Fold Difference in Macrophages	Expression Range in Macrophages		Pearson Correlation		Spearman Correlation	
chr6 147.0Mb	7.94	Arntl2	1425931_a_at	No	1.29	4.08	5.27	0.40	0.06	0.36	0.09	No	1.22	4.44	5.44	-0.19	0.37	0.07	0.74
chr6 147.0Mb	7.94	Arntl2	1429688_at	>50	9.01	6.63	59.70	0.55	0.01	0.35	0.10	>50	9.18	7.52	69.05	-0.29	0.17	0.04	0.86
chr6 147.0Mb	7.94	Klhdc5	1426988_at	>100	6.51	52.35	340.98	-0.18	0.41	-0.17	0.43	>100	9.21	71.69	660.39	-0.05	0.80	0.00	0.98
chr6 147.0Mb	7.94	Mrps35	1452111_at	>100	2.12	466.24	990.68	-0.26	0.24	-0.19	0.39	>100	1.89	215.87	408.67	-0.43	0.03	-0.39	0.06
chr6 147.0Mb	7.94	Ppfibp1	1445577_at	No	1.02	3.23	3.30	0.02	0.94	0.15	0.49	No	1.03	3.07	3.16	0.05	0.82	0.04	0.87
chr6 147.0Mb	7.94	Ppfibp1	1443029_at	No	6.05	5.06	30.58	-0.22	0.30	-0.19	0.39	>50	15.34	5.12	78.54	0.13	0.56	0.17	0.44
chr6 147.0Mb	7.94	Ppfibp1	1452759_s_at	>100	8.99	71.40	641.70	-0.20	0.36	-0.16	0.47	>100	19.78	217.04	4,293.44	0.28	0.19	0.27	0.21
chr6 147.0Mb	7.94	Pthlh	1427527_a_at	No	1.12	6.49	7.30	-0.12	0.60	-0.04	0.85	No	1.13	6.58	7.44	-0.17	0.43	-0.12	0.58
chr6 147.0Mb	7.94	Pthlh	1422324_a_at	No	1.05	5.92	6.23	0.05	0.84	0.08	0.70	No	1.11	5.82	6.46	-0.05	0.81	-0.09	0.68
chr6 147.0Mb	7.94	Rep15	1420328_at	No	2.45	9.32	22.88	-0.19	0.38	-0.22	0.32	No	2.95	6.74	19.89	0.21	0.33	0.28	0.19
chr6 147.0Mb	7.94	Stk38l	1435877_at	>100	12.49	11.38	142.14	0.14	0.51	0.21	0.34	No	4.87	9.35	45.52	0.20	0.35	0.26	0.21
chr6 147.0Mb	7.94	Stk38l	1435878_at	>100	4.69	69.67	327.09	-0.08	0.73	-0.11	0.61	>50	3.21	16.68	53.52	-0.18	0.39	-0.11	0.61
chr6 147.0Mb	7.94	Stk38l	1455183_at	>100	4.33	136.36	590.13	0.15	0.49	0.21	0.33	>50	4.78	15.07	72.06	0.25	0.23	0.25	0.24
chr6 147.3Mb	7.94	Ccdc91	1430670_at	No	1.47	4.82	7.08	-0.38	0.08	-0.29	0.18	No	1.91	4.56	8.71	0.42	0.04	0.12	0.59
chr6 147.3Mb	7.94	Ccdc91	1453605_s_at	No	1.32	36.06	47.44	0.22	0.30	0.21	0.33	>100	2.23	50.05	111.41	0.16	0.45	0.14	0.51
chr6 147.3Mb	7.94	Ccdc91	1418459_at	>50	5.08	17.07	86.72	0.08	0.72	0.14	0.52	>50	3.65	22.34	81.44	0.26	0.22	0.17	0.41
chr6 147.3Mb	7.94	Ccdc91	1449083_at	>100	3.66	46.97	171.93	-0.29	0.18	-0.07	0.76	>100	2.45	137.14	335.89	0.22	0.31	0.13	0.56
chr8 105.1Mb	5.98	Cdh11	1450757_at	No	1.04	4.81	5.00	-0.07	0.74	0.08	0.72	No	1.19	4.61	5.50	-0.10	0.65	-0.19	0.38

Table 4.2. Expression data for genes found from B-cells exposed to doxorubicin (1 μM).

Notes: QTL, -log(*p*) of the peak, gene symbol, expression probesets and fold difference in expression, expression range (minimum and maximum), and Pearson and Spearman correlations with *p* values respectively in the spleen, CD4+ T-cells, CD4+ Th1 cells, and macrophages are shown. Measurements in red and yellow are supportive for identification of candidate genes.

Expression data was marked in red if relative expression was > 100, if the fold expression difference in tissue was > 2, and if the *p* value for correlation was < 0.05 and in yellow if relative expression was > 50 and if the *p* value for correlation was ≤ 0.1. *A1bg* and *Gm5887* did not have expression information available.

QTL	Log P of Peak	Gene	Unique Expression Probesets	Spleen Expression	Fold Difference in Spleen	Expression Range in Spleen		Pearson Correlation		Spearman Correlation		CD4 Expression	Fold Difference in CD4	Expression Range in CD4 Cells		Pearson Correlation		Spearman Correlation	
chr5 74.6Mb	6.87	Rasl11b	1423854_a_at	>100	11.10	11.82	131.09	0.58	0.00	0.48	0.02	>100	51.99	8.06	419.22	0.49	0.02	0.29	0.17
chr5 74.6Mb	6.87	Scfd2	1433608_at	No	2.45	16.91	41.49	-0.20	0.36	-0.06	0.80	>50	7.67	9.53	73.14	-0.12	0.58	-0.12	0.57
chr5 74.6Mb	6.87	Scfd2	1447367_at	No	1.42	5.81	8.25	-0.19	0.36	-0.15	0.48	No	1.44	5.16	7.41	-0.26	0.24	-0.04	0.86
chr6 147.0Mb	6.59	Arntl2	1425931_a_at	No	1.51	3.93	5.94	-0.29	0.17	-0.44	0.03	No	1.28	4.09	5.25	0.19	0.39	0.14	0.51
chr6 147.0Mb	6.59	Arntl2	1429688_at	No	3.70	6.75	24.97	-0.12	0.57	0.00	0.99	>100	23.73	6.65	157.85	0.52	0.01	0.28	0.20
chr6 147.0Mb	6.59	Klhdc5	1426988_at	>100	12.86	55.98	720.10	-0.16	0.47	0.14	0.52	>100	11.07	84.57	936.17	-0.25	0.25	-0.20	0.37
chr6 147.0Mb	6.59	Mrps35	1452111_at	>100	2.25	99.03	222.72	-0.35	0.10	-0.36	0.08	>100	1.91	412.33	789.14	0.26	0.22	0.21	0.33
chr6 147.0Mb	6.59	Ppfibp1	1445577_at	No	1.11	3.31	3.66	-0.12	0.58	-0.05	0.83	No	1.03	3.23	3.32	0.03	0.88	-0.19	0.39
chr6 147.0Mb	6.59	Ppfibp1	1443029_at	No	2.40	4.28	10.25	-0.19	0.38	0.04	0.87	No	1.40	4.48	6.28	-0.11	0.61	0.01	0.96
chr6 147.0Mb	6.59	Ppfibp1	1452759_s_at	>100	2.53	102.51	259.38	0.22	0.30	0.21	0.32	>50	2.54	21.52	54.66	0.04	0.86	0.14	0.52
chr6 147.0Mb	6.59	Pthlh	1427527_a_at	No	2.11	7.47	15.80	-0.01	0.96	-0.32	0.13	No	1.14	6.55	7.44	-0.08	0.72	-0.05	0.84
chr6 147.0Mb	6.59	Pthlh	1422324_a_at	No	2.24	6.83	15.33	-0.19	0.38	0.00	1.00	No	1.07	5.92	6.35	-0.07	0.75	-0.14	0.52
chr6 147.0Mb	6.59	Rep15	1420328_at	No	1.40	7.21	10.08	0.06	0.79	0.19	0.36	No	1.38	9.33	12.91	0.02	0.95	-0.06	0.78
chr6 147.0Mb	6.59	Stk38l	1435877_at	No	4.04	5.21	21.08	0.39	0.06	0.23	0.28	No	3.42	4.97	16.98	-0.26	0.23	-0.26	0.24
chr6 147.0Mb	6.59	Stk38l	1435878_at	>50	3.63	20.12	72.51	-0.03	0.90	0.09	0.66	>50	4.63	12.82	59.34	0.24	0.26	0.34	0.12
chr6 147.0Mb	6.59	Stk38l	1455183_at	>50	5.86	14.33	84.03	-0.01	0.96	0.04	0.86	>50	5.93	15.13	89.66	0.30	0.16	0.36	0.10
chr6 147.3Mb	6.59	Ccdc91	1430670_at	No	1.66	4.85	8.06	-0.15	0.49	-0.34	0.10	No	1.15	4.82	5.52	-0.06	0.78	-0.06	0.80
chr6 147.3Mb	6.59	Ccdc91	1453605_s_at	No	2.58	9.36	24.17	0.32	0.13	0.17	0.43	No	1.25	37.42	46.87	0.01	0.96	-0.03	0.88
chr6 147.3Mb	6.59	Ccdc91	1418459_at	>50	6.70	10.52	70.56	0.34	0.10	0.21	0.33	>50	3.58	20.23	72.42	-0.06	0.79	-0.05	0.84
chr6 147.3Mb	6.59	Ccdc91	1449083_at	>100	2.33	49.72	115.75	0.29	0.16	0.22	0.30	>100	2.36	94.48	222.80	0.07	0.74	0.04	0.86
chr7 151.1Mb	6.23	Cttn	1421314_at	No	2.25	7.61	17.12	-0.29	0.17	-0.33	0.11	No	2.18	10.90	23.79	0.08	0.71	-0.10	0.66
chr7 151.1Mb	6.23	Cttn	1421313_s_at	>100	3.95	27.68	110.07	-0.33	0.12	-0.31	0.14	No	1.29	13.46	17.36	-0.09	0.67	-0.09	0.70
chr7 151.1Mb	6.23	Cttn	1421315_s_at	>100	3.02	69.33	209.29	-0.09	0.67	0.01	0.96	No	1.11	9.55	10.63	0.05	0.84	-0.08	0.71
chr7 151.1Mb	6.23	Cttn	1423917_a_at	>100	10.20	18.75	191.28	0.11	0.62	0.00	0.98	No	3.74	3.74	13.97	0.46	0.03	0.22	0.30
chr7 151.1Mb	6.23	Cttn	1433908_a_at	>100	3.44	226.16	778.13	-0.11	0.59	-0.05	0.82	No	7.77	4.60	35.77	0.38	0.07	0.20	0.36
chr7 151.1Mb	6.23	Dhcr7	1448619_at	>100	2.08	114.22	228.79	-0.15	0.48	-0.06	0.77	>100	2.07	176.33	364.21	0.48	0.02	0.44	0.04
chr7 151.1Mb	6.23	Mrgprq	1445458_at	No	1.12	5.86	6.54	-0.24	0.27	-0.29	0.17	No	1.35	6.46	8.71	-0.14	0.53	-0.09	0.68
chr7 151.1Mb	6.23	Nadsyn1	1430359_a_at	>100	2.74	47.56	130.48	0.13	0.53	0.15	0.48	>100	1.59	79.05	125.46	-0.08	0.72	-0.13	0.54
chr7 151.1Mb	6.23	Ppfia1	1435861_at	>50	4.82	17.91	86.39	-0.14	0.50	-0.17	0.42	>100	2.04	61.88	126.25	0.02	0.93	0.14	0.54
chr7 151.1Mb	6.23	Ppfia1	1455478_at	>100	2.62	72.81	190.58	0.10	0.65	-0.01	0.96	>100	1.59	259.40	412.40	0.30	0.16	0.44	0.04
chr7 151.1Mb	6.23	Shank2	1442823_at	No	1.09	5.80	6.31	-0.02	0.91	-0.13	0.53	No	1.03	3.72	3.85	0.04	0.86	-0.15	0.49
chr8 105.1Mb	5.90	Cdh11	1450757_at	>100	2.35	162.63	382.28	0.16	0.47	0.08	0.71	No	1.08	4.79	5.17	0.07	0.76	0.05	0.84

QTL	Log P of Peak	Gene	Unique Expression Probesets	Th1 Expression	Fold Difference in Th1	Expression Range in Th1 Cells		Pearson Correlation		Spearman Correlation		Macrophage Expression	Fold Difference in Macrophages	Expression Range in Macrophages		Pearson Correlation		Spearman Correlation	
chr5 74.6Mb	6.87	Rasl11b	1423854_a_at	>100	23.85	9.94	236.99	0.56	0.01	0.38	0.07	No	1.04	4.57	4.78	0.00	0.99	0.06	0.79
chr5 74.6Mb	6.87	Scfd2	1433608_at	>100	3.20	52.71	168.77	-0.06	0.79	0.07	0.74	>50	4.42	20.65	91.33	-0.22	0.31	0.00	0.99
chr5 74.6Mb	6.87	Scfd2	1447367_at	No	1.53	5.33	8.13	-0.27	0.22	-0.04	0.87	No	1.15	5.79	6.66	0.11	0.61	0.21	0.32
chr6 147.0Mb	6.59	Arntl2	1425931_a_at	No	1.29	4.08	5.27	0.34	0.11	0.34	0.11	No	1.22	4.44	5.44	-0.18	0.41	0.15	0.48
chr6 147.0Mb	6.59	Arntl2	1429688_at	>50	9.01	6.63	59.70	0.50	0.01	0.27	0.20	>50	9.18	7.52	69.05	-0.39	0.06	-0.14	0.52
chr6 147.0Mb	6.59	Klhdc5	1426988_at	>100	6.51	52.35	340.98	-0.31	0.15	-0.34	0.11	>100	9.21	71.69	660.39	-0.18	0.39	-0.18	0.41
chr6 147.0Mb	6.59	Mrps35	1452111_at	>100	2.12	466.24	990.68	-0.19	0.39	-0.03	0.89	>100	1.89	215.87	408.67	-0.43	0.04	-0.33	0.12
chr6 147.0Mb	6.59	Ppfibp1	1445577_at	No	1.02	3.23	3.30	0.03	0.91	0.11	0.63	No	1.03	3.07	3.16	0.06	0.78	0.08	0.70
chr6 147.0Mb	6.59	Ppfibp1	1443029_at	No	6.05	5.06	30.58	-0.09	0.69	-0.12	0.60	>50	15.34	5.12	78.54	0.03	0.88	0.16	0.45
chr6 147.0Mb	6.59	Ppfibp1	1452759_s_at	>100	8.95	71.40	641.70	-0.14	0.52	-0.11	0.63	>100	19.78	217.04	4,293.44	0.26	0.22	0.34	0.11
chr6 147.0Mb	6.59	Pthlh	1427527_a_at	No	1.12	6.49	7.30	-0.23	0.28	-0.23	0.29	No	1.13	6.58	7.44	-0.09	0.68	0.02	0.93
chr6 147.0Mb	6.59	Pthlh	1422324_a_at	No	1.05	5.92	6.23	0.04	0.85	0.05	0.82	No	1.11	5.82	6.46	-0.03	0.90	0.01	0.96
chr6 147.0Mb	6.59	Rep15	1420328_at	No	2.45	9.32	22.88	-0.23	0.30	-0.25	0.25	No	2.95	6.74	19.89	0.15	0.48	0.29	0.16
chr6 147.0Mb	6.59	Stk38l	1435877_at	>100	12.49	11.38	142.14	0.14	0.54	0.19	0.38	No	4.87	9.35	45.52	0.24	0.25	0.37	0.08
chr6 147.0Mb	6.59	Stk38l	1435878_at	>100	4.63	69.67	327.09	-0.03	0.89	-0.06	0.80	>50	3.21	16.68	53.52	-0.21	0.32	-0.14	0.51
chr6 147.0Mb	6.59	Stk38l	1455183_at	>100	4.33	136.36	590.13	0.12	0.57	0.18	0.41	>50	4.78	15.07	72.06	0.10	0.63	0.16	0.47
chr6 147.3Mb	6.59	Ccdc91	1430670_at	No	1.47	4.82	7.08	-0.25	0.24	-0.30	0.17	No	1.91	4.56	8.71	0.41	0.04	0.22	0.30
chr6 147.3Mb	6.59	Ccdc91	1453605_s_at	No	1.32	36.06	47.44	0.24	0.28	0.30	0.16	>100	2.23	50.05	111.41	0.27	0.21	0.29	0.17
chr6 147.3Mb	6.59	Ccdc91	1418459_at	>50	5.08	17.07	86.72	0.09	0.69	0.29	0.18	>50	3.65	22.34	81.44	0.20	0.35	0.15	0.47
chr6 147.3Mb	6.59	Ccdc91	1449083_at	>100	3.68	46.97	171.93	-0.25	0.26	-0.06	0.77	>100	2.45	137.14	335.89	0.14	0.52	0.13	0.54
chr7 151.1Mb	6.23	Cttn	1421314_at	No	1.90	9.75	18.57	-0.40	0.06	-0.51	0.01	No	1.41	10.98	15.51	0.13	0.55	0.20	0.35
chr7 151.1Mb	6.23	Cttn	1421313_s_at	>50	3.43	14.79	50.79	-0.07	0.75	0.07	0.76	>50	6.85	12.10	82.87	0.31	0.14	0.40	0.05
chr7 151.1Mb	6.23	Cttn	1421315_s_at	>50	7.14	10.24	73.13	-0.03	0.91	0.15	0.49	>100	14.07	7.38	103.86	0.72	<.0001	0.67	0.00
chr7 151.1Mb	6.23	Cttn	1423917_a_at	>100	54.25	3.85	209.04	-0.10	0.65	-0.10	0.66	>100	32.47	5.19	168.46	0.71	0.00	0.63	0.00
chr7 151.1Mb	6.23	Cttn	1433908_a_at	>100	41.24	17.87	736.78	-0.15	0.50	-0.11	0.62	>100	79.52	4.81	382.16	0.68	0.00	0.62	0.00
chr7 151.1Mb	6.23	Dhcr7	1448619_at	>100	4.48	164.90	737.97	-0.25	0.25	-0.19	0.39	>100	4.01	95.94	384.52	-0.09	0.67	-0.06	0.78
chr7 151.1Mb	6.23	Mrgprq	1445458_at	>100	2.71	1,169.90	3,170.56	0.19	0.40	0.12	0.57	No	1.26	6.88	8.67	0.04	0.86	0.10	0.63
chr7 151.1Mb	6.23	Nadsyn1	1430359_a_at	>100	3.70	49.53	183.30	-0.37	0.08	-0.37	0.08	>100	1.97	51.74	101.81	-0.51	0.01	-0.44	0.03
chr7 151.1Mb	6.23	Ppfia1	1435861_at	>100	3.06	51.18	156.40	0.26	0.23	0.28	0.20	>100	2.30	46.07	106.09	0.21	0.33	0.21	0.32
chr7 151.1Mb	6.23	Ppfia1	1455478_at	>100	1.52	294.37	446.45	-0.31	0.15	-0.30	0.16	>100	1.78	224.15	398.00	-0.15	0.48	-0.14	0.51
chr7 151.1Mb	6.23	Shank2	1442823_at	No	1.08	3.74	4.03	-0.16	0.46	-0.14	0.53	No	1.06	5.85	6.21	0.03	0.91	0.07	0.76
chr8 105.1Mb	5.90	Cdh11	1450757_at	No	1.04	4.81	5.00	-0.08	0.71	0.00	0.99	No	1.19	4.61	5.50	0.01	0.96	0.00	0.99

Table 4.3. Expression data for genes found from B-cells exposed to idarubicin (3 μM).

Notes: QTL, -log(*p*) of the peak, gene symbol, expression probesets and fold difference in expression, expression range (minimum and maximum), and Pearson and Spearman correlations with *p* values respectively in the spleen, CD4+ T-cells, CD4+ Th1 cells, and macrophages are shown. Measurements in red and yellow are supportive for identification of candidate genes. Expression data was marked in red if relative expression was > 100, if the fold expression difference in tissue was > 2, and if the *p* value for correlation was < 0.05 and in yellow if relative expression was > 50 and if the *p* value for correlation was ≤ 0.1. *A1bg* and *Gm5887* did not have expression information available.

QTL	Log P of Peak	Gene	Unique Expression Probesets	Spleen Expression	Fold Difference in Spleen	Expression Range in Spleen		Pearson Correlation		Spearman Correlation		CD4 Expression	Fold Difference in CD4	Expression Range in CD4 Cells		Pearson Correlation		Spearman Correlation	
chr5 74.6Mb	**12.08**	Rasl11b	1423854_a_at	>100	11.10	11.82	131.09	0.60	0.00	0.43	0.04	>100	51.99	8.06	419.22	0.61	0.00	0.22	0.32
chr5 74.6Mb	**12.08**	Scfd2	1433608_at	No	2.45	16.91	41.49	-0.14	0.52	-0.09	0.68	>50	7.67	9.53	73.14	-0.29	0.18	-0.11	0.61
chr5 74.6Mb	**12.08**	Scfd2	1447367_at	No	1.42	5.81	8.25	-0.12	0.56	-0.25	0.25	No	1.44	5.16	7.41	-0.15	0.49	-0.05	0.82
chr7 151.4Mb	**10.98**	Ano1	1426571_at	No	1.66	6.15	10.23	-0.04	0.84	0.23	0.26	No	1.18	5.72	6.75	-0.07	0.77	-0.18	0.41
chr7 151.4Mb	**10.98**	Ano1	1459713_s_at	>50	2.41	21.91	52.86	0.14	0.48	0.23	0.24	No	1.03	4.18	4.32	0.15	0.49	-0.09	0.68
chr7 151.4Mb	**10.98**	Cttn	1421314_at	No	2.25	7.61	17.12	-0.05	0.81	-0.19	0.38	No	2.18	10.90	23.79	0.08	0.72	0.00	0.98
chr7 151.4Mb	**10.98**	Cttn	1421313_s_at	>100	3.98	27.68	110.07	-0.26	0.23	-0.04	0.84	No	1.29	13.46	17.36	-0.07	0.75	-0.11	0.61
chr7 151.4Mb	**10.98**	Cttn	1421315_s_at	>100	3.02	69.33	209.29	-0.02	0.91	-0.01	0.97	No	1.11	9.55	10.63	0.08	0.73	-0.27	0.21
chr7 151.4Mb	**10.98**	Cttn	1423917_a_at	>100	10.20	18.75	191.28	0.19	0.37	0.23	0.28	No	3.74	3.74	13.97	0.36	0.10	0.08	0.72
chr7 151.4Mb	**10.98**	Cttn	1433908_a_at	>100	3.44	226.16	778.13	0.07	0.76	-0.02	0.92	No	7.77	4.60	35.77	0.41	0.05	0.25	0.24
chr7 151.4Mb	**10.98**	Fadd	1446499_at	No	1.30	7.20	9.35	-0.24	0.26	-0.37	0.08	No	3.11	8.26	25.70	-0.08	0.73	-0.12	0.57
chr7 151.4Mb	**10.98**	Fadd	1416888_at	>100	2.11	78.49	165.92	-0.16	0.44	-0.02	0.93	>100	1.91	122.96	235.24	-0.22	0.32	-0.43	0.04
chr7 151.4Mb	**10.98**	Ppfia1	1435861_at	>50	4.82	17.91	86.39	-0.07	0.73	-0.18	0.39	>100	2.04	61.88	126.25	0.15	0.51	0.42	0.05
chr7 151.4Mb	**10.98**	Ppfia1	1455478_at	>100	2.62	72.81	190.58	0.17	0.44	0.11	0.60	>100	1.59	259.40	412.40	0.11	0.63	0.18	0.41
chr7 151.4Mb	**10.98**	Shank2	1442823_at	No	1.09	5.80	6.31	-0.01	0.97	-0.24	0.26	No	1.03	3.72	3.85	0.14	0.53	-0.21	0.34

QTL	Log P of Peak	Gene	Unique Expression Probesets	Th1 Expression	Fold Difference in Th1	Expression Range in Th1 Cells		Pearson Correlation		Spearman Correlation		Macrophage Expression	Fold Difference in Macrophages	Expression Range in Macrophages		Pearson Correlation		Spearman Correlation	
chr5 74.6Mb	**12.08**	Rasl11b	1423854_a_at	>100	23.85	9.94	236.99	0.59	0.00	0.17	0.43	No	1.04	4.57	4.78	-0.12	0.57	-0.10	0.64
chr5 74.6Mb	**12.08**	Scfd2	1433608_at	>100	3.20	52.71	168.77	-0.10	0.66	0.07	0.74	>50	4.42	20.65	91.33	-0.23	0.29	-0.07	0.73
chr5 74.6Mb	**12.08**	Scfd2	1447367_at	No	1.53	5.33	8.13	-0.15	0.48	-0.09	0.69	No	1.15	5.79	6.66	0.02	0.92	-0.01	0.98
chr7 151.4Mb	**10.98**	Ano1	1426571_at	No	1.06	5.65	5.98	-0.07	0.76	-0.21	0.35	No	1.06	5.58	5.93	-0.09	0.68	-0.14	0.52
chr7 151.4Mb	**10.98**	Ano1	1459713_s_at	No	1.06	4.19	4.43	-0.12	0.57	-0.17	0.44	No	1.20	4.03	4.84	-0.17	0.43	-0.03	0.89
chr7 151.4Mb	**10.98**	Cttn	1421314_at	No	1.90	9.75	18.57	-0.28	0.19	-0.41	0.05	No	1.41	10.98	15.51	0.06	0.77	0.02	0.92
chr7 151.4Mb	**10.98**	Cttn	1421313_s_at	>50	3.43	14.79	50.79	0.00	1.00	0.23	0.28	>50	6.85	12.10	82.87	0.22	0.30	0.30	0.15
chr7 151.4Mb	**10.98**	Cttn	1421315_s_at	>50	7.14	10.24	73.13	-0.15	0.50	-0.13	0.55	>100	14.07	7.38	103.86	0.49	0.02	0.39	0.06
chr7 151.4Mb	**10.98**	Cttn	1423917_a_at	>100	54.25	3.85	209.04	-0.17	0.45	-0.02	0.94	>100	32.47	5.19	168.46	0.62	0.00	0.47	0.02
chr7 151.4Mb	**10.98**	Cttn	1433908_a_at	>100	41.24	17.87	736.78	-0.21	0.33	-0.08	0.73	>100	79.52	4.81	382.16	0.48	0.02	0.37	0.07
chr7 151.4Mb	**10.98**	Fadd	1446499_at	No	3.30	6.81	22.45	0.03	0.90	0.12	0.58	No	2.49	11.57	28.82	-0.35	0.10	-0.45	0.03
chr7 151.4Mb	**10.98**	Fadd	1416888_at	>100	1.63	198.63	324.75	-0.11	0.63	0.10	0.64	>100	2.97	109.73	326.41	-0.32	0.12	-0.16	0.46
chr7 151.4Mb	**10.98**	Ppfia1	1435861_at	>100	3.06	51.18	156.40	0.31	0.16	0.36	0.09	>100	2.30	46.07	106.09	0.14	0.50	0.13	0.53
chr7 151.4Mb	**10.98**	Ppfia1	1455478_at	>100	1.52	294.37	446.45	-0.19	0.38	-0.36	0.09	>100	1.78	224.15	398.00	-0.12	0.57	-0.06	0.80
chr7 151.4Mb	**10.98**	Shank2	1442823_at	No	1.08	3.74	4.03	-0.16	0.47	-0.10	0.64	No	1.06	5.85	6.21	-0.07	0.76	-0.08	0.71

Table 4.4. Expression data for genes found from T-cells exposed to doxorubicin (100 μM).

Notes: QTL, -log(*p*) of the peak, gene symbol, expression probesets and fold difference in expression, expression range (minimum and maximum), and Pearson and Spearman correlations with *p* values respectively in the spleen, CD4+ T-cells, CD4+ Th1 cells, and macrophages are shown. Measurements in red and yellow are supportive for identification of candidate genes. Expression data was marked in red if relative expression was > 100, if the fold expression difference in tissue was > 2, and if the *p* value for correlation was < 0.05 and in yellow if relative expression was > 50 and if the *p* value for correlation was ≤ 0.1. *A1bg* and *Gm5887* did not have expression information available.

QTL	Log P of Peak	Gene	Unique Expression Probesets	Spleen Expression	Fold Difference in Spleen	Expression Range in Spleen		Pearson Correlation		Spearman Correlation		CD4 Expression	Fold Difference in CD4	Expression Range in CD4 Cells		Pearson Correlation		Spearman Correlation	
chr11 34.8Mb	6.37	Ccdc99	1424971_at	>100	6.13	43.13	264.29	-0.10	0.65	-0.18	0.39	>100	4.48	164.90	737.97	-0.11	0.62	0.12	0.60
chr11 34.8Mb	6.37	Dock2	1438334_at	>100	4.11	54.00	222.14	0.49	0.01	0.55	0.01	>100	3.70	49.53	183.30	-0.04	0.86	0.01	0.98
chr11 34.8Mb	6.37	Dock2	1422808_s_at	>100	2.37	835.39	1,981.01	0.04	0.85	0.09	0.66	>100	2.71	1,169.90	3,170.56	0.04	0.85	0.02	0.94
chr11 34.8Mb	**7.37**	Slit3	1452296_at	No	3.78	6.09	23.04	0.04	0.87	0.02	0.91	No	1.10	4.50	4.95	-0.38	0.07	-0.29	0.18
chr11 34.8Mb	6.37	Slit3	1427086_at	>50	6.28	11.98	75.29	-0.37	0.07	-0.38	0.07	No	1.35	6.55	8.86	-0.25	0.25	-0.23	0.29
chr12 13.8Mb	6.45	Ddx1	1415915_at	>100	1.83	268.21	489.98	0.10	0.66	0.08	0.70	>100	1.92	1,484.56	2,849.52	-0.29	0.17	-0.28	0.20
chr12 13.8Mb	6.45	Ddx1	1440816_x_at	>100	1.79	316.11	565.06	-0.09	0.68	-0.13	0.53	>100	1.64	1,922.55	3,158.18	-0.20	0.36	-0.26	0.24
chr12 13.8Mb	6.45	Mycn	1425922_a_at	No	1.33	11.36	15.07	-0.07	0.74	0.02	0.91	No	1.32	9.80	12.91	-0.13	0.56	-0.24	0.28
chr12 13.8Mb	6.45	Mycn	1425923_at	No	3.03	8.10	24.54	0.26	0.22	0.32	0.13	No	1.15	10.81	12.39	-0.45	0.03	-0.43	0.04
chr12 13.8Mb	6.45	Mycn	1417155_at	>50	2.98	22.28	66.31	-0.03	0.89	0.07	0.76	No	1.07	6.13	6.54	-0.31	0.15	-0.32	0.14
chr12 13.8Mb	6.45	Nbas	1430587_at	No	1.37	4.02	5.51	-0.03	0.91	0.13	0.56	No	1.03	3.96	4.07	-0.27	0.21	-0.25	0.25
chr12 13.8Mb	6.45	Nbas	1436143_at	>100	1.90	59.48	113.08	-0.19	0.37	-0.24	0.26	>100	1.81	115.89	209.66	-0.10	0.65	-0.17	0.44
chr15 60.4Mb	**7.76**	Fam84b	1434301_at	>100	3.58	34.09	122.06	0.50	0.01	0.53	0.01	>100	4.85	86.14	417.85	0.34	0.11	0.24	0.28

QTL	Log P of Peak	Gene	Unique Expression Probesets	Th1 Expression	Fold Difference in Th1	Expression Range in Th1 Cells		Pearson Correlation		Spearman Correlation		Macrophage Expression	Fold Difference in Macrophages	Expression Range in Macrophages		Pearson Correlation		Spearman Correlation	
chr11 34.8Mb	6.37	Ccdc99	1424971_at	>100	2.07	176.33	364.21	0.28	0.19	0.23	0.28	>50	10.64	5.86	62.33	0.04	0.87	-0.02	0.91
chr11 34.8Mb	6.37	Dock2	1438334_at	>100	1.64	1,922.55	3,158.18	-0.20	0.36	-0.21	0.33	>100	34.72	17.62	611.69	0.35	0.09	0.33	0.11
chr11 34.8Mb	6.37	Dock2	1422808_s_at	>100	1.92	1,484.56	2,849.52	-0.09	0.68	-0.12	0.58	>100	1.61	4,081.35	6,580.42	-0.12	0.59	-0.10	0.63
chr11 34.8Mb	**7.37**	Slit3	1452296_at	No	1.10	4.50	4.95	-0.15	0.48	-0.20	0.35	No	1.05	4.40	4.61	-0.05	0.81	0.05	0.81
chr11 34.8Mb	6.37	Slit3	1427086_at	No	1.35	6.55	8.86	-0.24	0.27	-0.12	0.58	No	1.09	5.40	5.88	-0.08	0.70	-0.05	0.83
chr12 13.8Mb	6.45	Ddx1	1415915_at	No	1.35	6.46	8.71	0.08	0.73	0.06	0.80	>100	1.70	558.32	950.81	-0.40	0.05	-0.38	0.07
chr12 13.8Mb	6.45	Ddx1	1440816_x_at	>100	1.59	79.05	125.46	0.09	0.70	0.19	0.40	>100	1.86	709.10	1,320.84	-0.30	0.15	-0.26	0.22
chr12 13.8Mb	6.45	Mycn	1425922_a_at	No	1.38	9.40	12.95	0.01	0.98	-0.36	0.09	No	1.46	9.61	14.04	-0.18	0.39	-0.11	0.62
chr12 13.8Mb	6.45	Mycn	1425923_at	No	1.61	11.37	18.27	-0.05	0.81	-0.02	0.92	No	1.42	8.10	11.51	-0.04	0.85	-0.04	0.84
chr12 13.8Mb	6.45	Mycn	1417155_at	No	1.42	6.12	8.68	-0.29	0.18	-0.43	0.04	No	1.15	6.13	7.04	-0.02	0.93	-0.06	0.80
chr12 13.8Mb	6.45	Nbas	1430587_at	No	1.03	3.96	4.07	-0.31	0.15	-0.26	0.24	No	1.05	3.81	4.02	0.06	0.77	0.07	0.74
chr12 13.8Mb	6.45	Nbas	1436143_at	>100	1.81	115.89	209.66	-0.10	0.65	-0.06	0.78	>100	2.53	100.03	252.87	-0.53	0.01	-0.32	0.13
chr15 60.4Mb	**7.76**	Fam84b	1434301_at	>50	3.88	23.51	91.29	0.02	0.91	0.03	0.88	>100	3.53	146.79	518.68	0.12	0.58	0.06	0.79

Table 4.5. Expression data for genes found from T-cells exposed to idarubicin (1 μM).

Notes: QTL, -log(*p*) of the peak, gene symbol, expression probesets and fold difference in expression, expression range (minimum and maximum), and Pearson and Spearman correlations with *p* values respectively in the spleen, CD4+ T-cells, CD4+ Th1 cells, and macrophages are shown. Measurements in red and yellow are supportive for identification of candidate genes. Expression data was marked in red if relative expression was > 100, if the fold expression difference in tissue was > 2, and if the *p* value for correlation was < 0.05 and in yellow if relative expression was > 50 and if the *p* value for correlation was ≤ 0.1. *A1bg* and *Gm5887* did not have expression information available.

QTL	Log P of Peak	Gene	Unique Expression Probesets	Spleen Expression	Fold Difference in Spleen	Expression Range in Spleen		Pearson Correlation		Spearman Correlation		CD4 Expression	Fold Difference in CD4	Expression Range in CD4 Cells		Pearson Correlation		Spearman Correlation	
chr16 85.3Mb	7.34	App	1438373_at	No	1.11	3.39	3.76	-0.16	0.44	-0.06	0.79	No	1.03	3.31	3.43	-0.07	0.74	-0.11	0.63
chr16 85.3Mb	7.34	App	1438374_x_at	No	1.11	4.02	4.46	0.09	0.68	-0.02	0.94	No	1.04	3.95	4.09	-0.12	0.59	-0.10	0.65
chr16 85.3Mb	7.34	App	1420621_a_at	>100	2.41	693.46	1,671.70	0.08	0.70	-0.11	0.61	>100	6.90	114.11	787.54	0.18	0.42	0.10	0.63
chr16 85.3Mb	7.34	App	1427442_a_at	>100	1.66	1,593.67	2,637.82	0.11	0.62	-0.02	0.91	>100	5.46	303.12	1,654.48	-0.05	0.83	-0.05	0.83
chr16 85.3Mb	7.34	Atp5j	1416143_at	>100	2.01	1,936.63	3,897.72	0.06	0.77	-0.02	0.92	>100	1.28	5,504.34	7,054.28	0.36	0.10	0.32	0.13
chr16 85.3Mb	7.34	Atp5j	1435395_s_at	>100	1.91	2,177.06	4,147.87	0.07	0.74	-0.07	0.76	>100	1.28	8,187.35	10,446.92	0.17	0.44	0.14	0.51
chr16 85.3Mb	7.34	Cyyr1	1435701_at	>50	3.42	15.32	52.39	0.22	0.43	0.26	0.34	No	1.10	4.28	4.70	0.09	0.67	-0.04	0.86
chr16 85.3Mb	7.34	Cyyr1	1452019_at	No	2.87	5.76	16.51	-0.03	0.90	-0.05	0.81	No	1.56	5.98	9.34	-0.01	0.97	-0.18	0.42
chr16 85.3Mb	7.34	Gabpa	1450665_at	>100	2.57	60.36	155.07	-0.01	0.98	-0.01	0.98	>100	2.59	119.19	309.05	0.38	0.07	0.35	0.10
chr16 85.3Mb	7.34	Gabpa	1450664_at	>100	1.73	404.74	701.53	0.03	0.88	0.08	0.70	>100	1.62	1,079.10	1,750.64	-0.12	0.57	0.17	0.45
chr16 85.3Mb	7.34	Jam2	1431416_a_at	No	1.32	3.47	4.59	0.29	0.18	0.22	0.30	No	1.03	4.05	4.18	-0.13	0.55	-0.16	0.45
chr16 85.3Mb	7.34	Jam2	1419288_at	No	1.80	3.66	6.58	-0.41	0.05	-0.07	0.76	No	1.03	3.83	3.97	-0.09	0.68	0.00	0.98
chr16 85.3Mb	7.34	Jam2	1431417_at	No	3.40	6.11	20.77	0.14	0.52	0.36	0.08	No	1.05	5.24	5.50	-0.17	0.44	-0.14	0.53
chr16 85.3Mb	7.34	Jam2	1436568_at	No	4.45	7.46	33.18	0.04	0.86	0.11	0.60	No	1.04	4.03	4.18	-0.13	0.55	-0.15	0.48
chr16 85.3Mb	7.34	Jam2	1449408_at	No	4.53	9.08	41.12	0.14	0.51	-0.01	0.95	No	1.04	4.51	4.69	-0.15	0.50	-0.15	0.50
chr16 85.3Mb	7.34	Mir155	1428027_at	>50	8.48	6.86	58.15	-0.10	0.65	0.07	0.76	No	3.18	6.96	22.13	0.27	0.22	0.39	0.07
chr16 85.3Mb	7.34	Mrpl39	1417966_at	>100	3.07	144.54	443.61	-0.09	0.67	-0.03	0.89	>100	2.31	325.74	751.76	0.31	0.15	0.35	0.10
chr16 85.3Mb	7.34	Mrpl39	1448909_a_at	>100	2.12	676.77	1,435.15	0.01	0.95	0.01	0.95	>100	2.33	1,331.83	3,103.30	0.11	0.61	0.15	0.49

QTL	Log P of Peak	Gene	Unique Expression Probesets	Th1 Expression	Fold Difference in Th1	Expression Range in Th1 Cells		Pearson Correlation		Spearman Correlation		Macrophage Expression	Fold Difference in Macrophages	Expression Range in Macrophages		Pearson Correlation		Spearman Correlation	
chr16 85.3Mb	7.34	App	1438373_at	No	1.03	3.32	3.40	0.14	0.52	0.13	0.56	No	1.04	3.15	3.26	-0.21	0.31	-0.21	0.33
chr16 85.3Mb	7.34	App	1438374_x_at	No	1.03	3.96	4.06	0.12	0.60	0.20	0.36	No	1.04	3.83	3.97	-0.27	0.21	-0.25	0.23
chr16 85.3Mb	7.34	App	1420621_a_at	>50	5.31	17.50	92.89	0.09	0.67	0.23	0.30	>100	3.26	7,738.86	25,191.28	0.33	0.11	0.15	0.48
chr16 85.3Mb	7.34	App	1427442_a_at	>100	7.39	18.29	135.10	-0.17	0.45	0.12	0.57	>100	1.99	11,389.87	22,685.06	0.21	0.32	-0.05	0.83
chr16 85.3Mb	7.34	Atp5j	1416143_at	>100	1.43	9,217.63	13,214.29	0.51	0.01	0.48	0.02	>100	1.89	4,156.00	7,852.71	0.08	0.72	-0.02	0.92
chr16 85.3Mb	7.34	Atp5j	1435395_s_at	>100	1.21	10,954.57	13,299.38	0.44	0.04	0.52	0.01	>100	1.26	6,313.77	7,967.44	-0.19	0.36	-0.21	0.33
chr16 85.3Mb	7.34	Cyyr1	1435701_at	No	1.03	4.30	4.43	0.19	0.39	0.16	0.46	No	1.05	4.21	4.41	-0.33	0.11	-0.32	0.12
chr16 85.3Mb	7.34	Cyyr1	1452019_at	No	1.19	6.04	7.17	0.16	0.47	0.00	0.99	No	1.70	5.28	8.97	0.06	0.79	0.00	0.98
chr16 85.3Mb	7.34	Gabpa	1450665_at	>100	1.78	309.99	551.84	-0.02	0.93	-0.17	0.45	>100	1.68	353.60	595.07	0.09	0.69	-0.06	0.78
chr16 85.3Mb	7.34	Gabpa	1450664_at	>100	1.52	951.22	1,449.81	-0.27	0.21	-0.11	0.62	>100	1.34	1,401.14	1,877.67	0.17	0.42	0.19	0.38
chr16 85.3Mb	7.34	Jam2	1431416_a_at	No	1.03	4.06	4.19	0.19	0.39	0.27	0.21	>100	49.31	3.23	159.27	-0.24	0.26	-0.33	0.12
chr16 85.3Mb	7.34	Jam2	1419288_at	No	2.03	3.84	7.82	0.00	0.98	0.10	0.64	>100	80.74	3.18	257.09	-0.01	0.95	-0.06	0.77
chr16 85.3Mb	7.34	Jam2	1431417_at	No	1.19	5.26	6.25	0.09	0.69	0.03	0.89	No	5.11	5.55	28.37	-0.21	0.33	-0.06	0.77
chr16 85.3Mb	7.34	Jam2	1436568_at	No	1.03	4.04	4.14	0.14	0.52	0.22	0.32	>100	208.80	4.71	982.84	-0.09	0.66	-0.17	0.43
chr16 85.3Mb	7.34	Jam2	1449408_at	No	1.15	4.51	5.18	0.02	0.92	0.06	0.78	>100	121.81	4.84	589.55	-0.33	0.12	-0.14	0.52
chr16 85.3Mb	7.34	Mir155	1428027_at	>100	14.82	94.89	1,406.00	0.00	0.99	0.14	0.54	No	3.24	5.34	17.29	-0.21	0.32	-0.14	0.52
chr16 85.3Mb	7.34	Mrpl39	1417966_at	>100	2.97	628.51	1,867.28	-0.04	0.85	-0.11	0.61	>100	2.19	373.49	819.53	0.01	0.98	0.07	0.74
chr16 85.3Mb	7.34	Mrpl39	1448909_a_at	>100	2.67	2,245.99	5,993.99	-0.09	0.69	-0.21	0.34	>100	2.10	1,083.66	2,280.63	0.15	0.49	0.25	0.24

Table 4.6. Non-synonymous coding SNPs and deleterious protein effects.

Notes: Non-synonymous coding SNPs within candidate genes from dbSNP (http://cgd.jax.org/cgdsnpdb) and the likelihood of SNPs causing deleterious effects within the associated protein's structure using PROVEAN and the PANTHER Classification System are displayed. Using PROVEAN, a score of -2.5 indicates a functional effect on the protein. For the PANTHER algorithm, a subSPEC (substitution position-specific evolutionary conservation) score of -3 corresponds to a 50% probability that a score is deleterious ($P_{deleterious} = 0.5$). MSA indicates the number of multiple sequence alignments. NIC (number of independent counts) is an estimate of observations used to calculate the amino acid probabilities. P_{wt} and $P_{substituted}$ refer to the respective probabilities of the wild type and substituted amino acids. Protein data was highlighted in red if the protein was likely deleterious using PROVEAN or had a PANTHER score $\leq$ -3. Protein data was highlighted in yellow if the PANTHER score was $\leq$ -2 but > -3. *Ddx1*, *Klhcdc5*, *Stk38l*, and *Fadd* did not have any nonsynonymous SNPs according to dbSNP.

Gene	Position m38	Position 37	SNP ID	Protein Change	PROVEAN Score	Prediction	subPSEC	P deleterious	MSA position	Pwt	P substituted	NIC
A1bg	Chr15:60917966	N/A	rs48693526	V478I	-0.35	Neutral	-1.43788	0.17334	235	0.52709	0.12063	1.135
A1bg	Chr15:60918013	N/A	rs49948401	A462E	0.182	Neutral	-0.19944	0.05729	215	0.04237	0.04011	1.135
A1bg	Chr15:60918103	N/A	rs51355219	H432R	0.602	Neutral	-1.69215	0.21285	185	0.25985	0.04505	1.135
A1bg	Chr15:60918898	N/A	rs48955674	V410M	0.172	Neutral	-2.20149	0.31035	163	0.35986	0.03507	1.135
A1bg	Chr15:60919074	N/A	rs47093613	R351L	-4.447	Deleterious	-1.36828	0.16359	102	0.15438	0.03873	1.135
A1bg	Chr15:60920306	N/A	rs47959112	R158W	-3.491	Deleterious	N/A	Not Likely	N/A	N/A	N/A	N/A
Ano1	Chr7:144608007	Chr7:151793912	rs36458754	R731H	0.177	Neutral	-2.04242	0.27736	419	0.06153	0.05095	7.131
Ano1	Chr7:144611382	Chr7:151797287	rs36562043	F643L	-4.534	Deleterious	-4.20396	0.76923	329	0.75598	0.06723	8.83
Ano1	Chr7:144655655	Chr7:151841560	rs252052521	H270Q	-1.729	Neutral	N/A	Not Likely	N/A	N/A	N/A	N/A
App	Chr16:84978200	Chr16:84978445	rs13464211	D516E	-1.388	Neutral	-2.55755	0.39116	593	0.68652	0.05813	1.461
App	Chr16:85013650	Chr16:85013895	rs47322845	A480V	-3.156	Deleterious	-4.47146	0.81328	558	0.8039	0.01569	2.794
App	Chr16:85030304	Chr16:85030549	rs47818164	D309E	-1.501	Neutral	-3.67619	0.66289	387	0.82081	0.03466	2.49
App	Chr16:85079841	Chr16:85080086	rs46617381	G221S	1.273	Neutral	-1.74936	0.22259	240	0.09802	0.49028	1.39
Arntl2	Chr6:146805555	Chr6:146754077	rs30804877	G9D	-1.796	Neutral	N/A	Not Likely	N/A	N/A	N/A	N/A
Arntl2	Chr6:146809710	Chr6:146758232	rs36388854	L71M	-1.818	Neutral	-6.76861	0.97744	17	0.95987	0.00582	10.666
Arntl2	Chr6:146818831	Chr6:146767353	rs48247052	I164M	-0.415	Neutral	-0.8187	0.10144	110	0.17516	0.09798	1.353
Arntl2	Chr6:146820551	Chr6:146769073	rs29924777	Y207H	1.823	Neutral	-1.37197	0.1641	157	0.06836	0.23377	1.323
Arntl2	Chr6:146820569	Chr6:146769091	rs30073811	M213V	0.02	Neutral	-1.77854	0.22768	163	0.06965	0.37816	1.323
Arntl2	Chr6:146825200	Chr6:146773722	rs48852525	H423Q	1.018	Neutral	-0.95932	0.115	371	0.04276	0.09101	1.323
Arntl2	Chr6:146825207	Chr6:146773729	rs49229642	G426S	-0.328	Neutral	-1.09659	0.12972	374	0.16176	0.40854	1.323
Arntl2	Chr6:146828173	Chr6:146776695	rs49176210	N494S	0.056	Neutral	-0.97854	0.11697	440	0.33174	0.15034	1.323
Arntl2	Chr6:146829709	Chr6:146778231	rs49078756	P504L	0.858	Neutral	-1.74257	0.22142	449	0.04365	0.22631	1.323
Arntl2	Chr6:146829729	Chr6:146778251	rs50619963	E511K	-1.126	Neutral	-2.76274	0.44096	456	0.61106	0.03705	1.323
Arntl2	Chr6:146829801	Chr6:146778323	rs50518043	G535S	0.325	Neutral	-1.09659	0.12972	480	0.16176	0.40854	1.323
Arntl2	Chr6:146832558	Chr6:146781080	rs30954526	I551T	2.219	Neutral	-1.33176	0.15866	496	0.1074	0.35267	1.323
Ccdc91	Chr6:147534127	Chr6:147482649	rs30017715	S70T	-0.702	Neutral	N/A	No Hit	N/A	N/A	N/A	N/A
Ccdc91	Chr6:147592082	Chr6:147540604	rs29923070	G324E	2.726	Neutral	N/A	No Hit	N/A	N/A	N/A	N/A
Ccdc91	Chr6:147592148	Chr6:147540670	rs32279191	A346E	1.649	Neutral	N/A	No Hit	N/A	N/A	N/A	N/A
Ccdc91	Chr6:147631671	Chr6:147580193	rs32283052	V439L	-0.24	Neutral	N/A	No Hit	N/A	N/A	N/A	N/A
Ccdc91	Chr6:147631677	Chr6:147580199	rs30120374	I441V	0.036	Neutral	N/A	No Hit	N/A	N/A	N/A	N/A
Ccdc99	Chr11:34820955	Chr11:34634457	rs50113265	I323V	-0.703	Neutral	N/A	No Hit	N/A	N/A	N/A	N/A
Ccdc99	Chr11:34823362	Chr11:34636864	rs49954904	E167Q	1.55	Neutral	N/A	No Hit	N/A	N/A	N/A	N/A
Ccdc99	Chr11:34823364	Chr11:34636866	rs47468580	L166H	-4.05	Deleterious	N/A	No Hit	N/A	N/A	N/A	N/A
Ccdc99	Chr11:34823386	Chr11:34636888	rs49718855	M159V	-2.038	Neutral	N/A	No Hit	N/A	N/A	N/A	N/A
Ccdc99	Chr11:34825433	Chr11:34638935	rs45977048	A88V	0.619	Neutral	N/A	No Hit	N/A	N/A	N/A	N/A
Cdh11	Chr8:102634454	Chr8:105158354	rs30742273	V751M	-1.693	Neutral	-2.92587	0.48148	715	0.52586	0.02249	1.129
Cdh11	Chr8:102650627	Chr8:105174527	rs33464298	E462D	-2.768	Deleterious	-3.3989	0.59842	445	0.76818	0.03966	2.241
Cdh11	Chr8:102679663	Chr8:105203563	rs33142871	Q59H	-4.349	Deleterious	-5.5081	0.92471	57	0.82985	0.00538	2.967
Cttn	Chr7:144438773	Chr7:151624678	rs36360222	Y475Ter	-228.748	Deleterious	N/A	N/A	N/A	N/A	N/A	N/A
Cttn	Chr7:144438853	Chr7:151624758	rs38335552	I449L	0.069	Neutral	-0.43903	0.07169	363	0.08596	0.10378	1.303
Cttn	Chr7:144457738	Chr7:151643643	rs37969206	H111Q	-5.184	Deleterious	-4.9827	0.87897	92	0.83538	0.00797	2.445
Cyyr1	Chr16:85544890	Chr16:85545135	rs244292017	H36R	2.188	Neutral	-1.63027	0.20266	60	0.15576	0.04452	1.697
Dhcr7	Chr7:143837878	Chr7:151023783	rs248337659	A68V	0.938	Neutral	-1.09814	0.1299	62	0.08831	0.28754	1.038
Dock2	Chr11:34402837	Chr11:34302837	rs26825963	I293L	-1.522	Neutral	-1.57243	0.19348	298	0.39477	0.12868	1.825
Dock2	Chr11:34403093	Chr11:34303093	rs26825961	G378H	-6.445	Deleterious	-2.85231	0.46315	382	0.23786	0.01807	1.784
Fam84b	Chr15:60822984	Chr15:60654539	rs51533371	N304K	-0.142	Neutral	N/A	Excluded	N/A	N/A	N/A	N/A
Gabpa	Chr16:84860540	Chr16:84860785	rs50356497	I434M	-0.382	Neutral	0.17154	0.04025	229	0.21354	0.03954	0.166
Gm5887	Chr6:147075128	N/A	rs38169684	R330H	-1.025	Neutral	N/A	No Hit	N/A	N/A	N/A	N/A
Gm5887	Chr6:147075159	N/A	rs30810127	M320V	0.038	Neutral	N/A	No Hit	N/A	N/A	N/A	N/A
Gm5887	Chr6:147075176	N/A	rs216702758	R314Q	-0.038	Neutral	N/A	No Hit	N/A	N/A	N/A	N/A
Gm5887	Chr6:147075228	N/A	rs30902417	I297V	-0.278	Neutral	N/A	No Hit	N/A	N/A	N/A	N/A
Gm5887	Chr6:147075291	N/A	rs30360873	W276R	0.496	Neutral	N/A	No Hit	N/A	N/A	N/A	N/A
Gm5887	Chr6:147075340	N/A	rs218917975	K259N	-1.99	Neutral	N/A	No Hit	N/A	N/A	N/A	N/A
Gm5887	Chr6:147075477	N/A	rs37135391	M214V	-0.01	Neutral	N/A	No Hit	N/A	N/A	N/A	N/A
Gm5887	Chr6:147075503	N/A	rs51447380	N205T	-1.292	Neutral	N/A	No Hit	N/A	N/A	N/A	N/A
Gm5887	Chr6:147075522	N/A	rs38169236	L199I	-0.14	Neutral	N/A	No Hit	N/A	N/A	N/A	N/A
Gm5887	Chr6:147075590	N/A	rs231086955	T176I	-1.463	Neutral	N/A	No Hit	N/A	N/A	N/A	N/A
Gm5887	Chr6:147075597	N/A	rs243121057	A174P	0.41	Neutral	N/A	No Hit	N/A	N/A	N/A	N/A
Gm5887	Chr6:147075612	N/A	rs256627108	P169S	-2.146	Neutral	N/A	No Hit	N/A	N/A	N/A	N/A
Gm5887	Chr6:147075620	N/A	rs108092497	R166H	1.225	Neutral	N/A	No Hit	N/A	N/A	N/A	N/A
Gm5887	Chr6:147075623	N/A	rs48099460	N165S	-0.475	Neutral	N/A	No Hit	N/A	N/A	N/A	N/A
Gm5887	Chr6:147075659	N/A	rs224117204	S153T	-0.455	Neutral	N/A	No Hit	N/A	N/A	N/A	N/A
Gm5887	Chr6:147075710	N/A	rs248552030	S136T	0.815	Neutral	N/A	No Hit	N/A	N/A	N/A	N/A

Gene	Position m38	Position 37	SNP ID	Protein Change	PROVEAN Score	Prediction	subPSEC	P deleterious	MSA position	Pwt	P substituted	NIC
Jam2	Chr16:84809476	Chr16:84809721	rs48761727	K126T	1.144	Neutral	-0.47282	0.07397	158	0.24269	0.17527	1.197
Jam2	Chr16:84813036	Chr16:84813281	rs48897005	N179D	-0.443	Neutral	-2.22155	0.31465	211	0.53496	0.04985	1.116
Jam2	Chr16:84816434	Chr16:84816679	rs50527301	G257S	-4.376	Deleterious	-5.1311	0.89389	295	0.9231	0.00967	3.131
Mrgprg	Chr7:143764545	Chr7:150950450	rs236108013	S277A	0.016	Neutral	-1.68909	0.21233	183	0.51317	0.08102	1.043
Mrpl39	Chr16:84720286	Chr16:84720531	rs47474189	E315A	-3.243	Deleterious	-1.60427	0.19849	246	0.27542	0.05017	1.084
Mrpl39	Chr16:84723911	Chr16:84724156	rs241825540	V280A	-2.38	Neutral	-1.82906	0.23669	211	0.29292	0.05546	1.429
Mrpl39	Chr16:84725178	Chr16:84725423	rs46790239	D235E	-0.202	Neutral	-0.80866	0.10053	166	0.21452	0.1538	1.6987
Mrpl39	Chr16:84730849	Chr16:84731094	rs52007053	V164L	-0.745	Neutral	-0.84692	0.10404	91	0.2165	0.14868	1.697
Mrpl39	Chr16:84732355	Chr16:84732600	rs6405201	K133T	-1.468	Neutral	-1.63027	0.20266	60	0.15576	0.04452	1.697
Mrps35	Chr6:147042826	Chr6:146991348	rs30016550	T11S	0.199	Neutral	N/A	Not Likely	N/A	N/A	N/A	N/A
Mrps35	Chr6:147061446	Chr6:147009968	rs36949762	C216Y	5.521	Neutral	-2.06881	0.28268	177	0.04767	0.28851	1.621
Mrps35	Chr6:147070737	Chr6:147019259	rs30419863	I293V	0.587	Neutral	-0.98054	0.11718	297	0.13913	0.29457	1.377
Mrps35	Chr6:147070819	Chr6:147019341	rs36442894	A320V	-0.931	Neutral	-1.59875	0.19762	324	0.23669	0.03865	0.97
Mycn	Chr12:12937225	Chr12:12944031	rs13481306	Q390H	-4.474	Deleterious	-5.84147	0.94488	439	0.86076	0.00441	3.383
Nadsyn1	Chr7:143795999	Chr7:150981904	rs6305405	F710I	0.53	Neutral	N/A	Not Likely	N/A	N/A	N/A	N/A
Nadsyn1	Chr7:143797867	Chr7:150983772	rs36747124	Y676Ter	-50.858	Deleterious	N/A	N/A	N/A	N/A	N/A	N/A
Nadsyn1	Chr7:143804088	Chr7:150989993	rs36612792	M461L	-0.077	Neutral	-2.21796	0.31388	457	0.03237	0.09167	3.852
Nadsyn1	Chr7:143806046	Chr7:150991951	rs225270992	D396E	-0.2	Neutral	-1.35852	0.16226	392	0.09915	0.11433	3.623
Nadsyn1	Chr7:143808020	Chr7:150993925	rs247321994	M321I	1.303	Neutral	-2.44974	0.3658	317	0.03019	0.11009	3.887
Nadsyn1	Chr7:143811259	Chr7:150997164	rs251167215	D236E	-3.823	Deleterious	-1.45462	0.17575	232	0.32747	0.27136	3.887
Nadsyn1	Chr7:143811262	Chr7:150997167	rs223404618	C235Ter	-1515.265	Deleterious	N/A	N/A	N/A	N/A	N/A	N/A
Nadsyn1	Chr7:143811294	Chr7:150997199	rs247805404	G225R	-7.747	Deleterious	-3.03034	0.50758	221	0.20188	0.02864	3.887
Nadsyn1	Chr7:143812600	Chr7:150998505	rs218798877	I186L	-1.856	Neutral	-2.34559	0.342	182	0.20358	0.06232	3.887
Nbas	Chr12:13271165	Chr12:13277971	rs29179920	L39P	1.705	Neutral	N/A	No Hit	N/A	N/A	N/A	N/A
Nbas	Chr12:13306959	Chr12:13313765	rs29204999	L313Q	2.081	Neutral	N/A	No Hit	N/A	N/A	N/A	N/A
Nbas	Chr12:13310194	Chr12:13317000	rs29147607	G324S	2.923	Neutral	N/A	No Hit	N/A	N/A	N/A	N/A
Nbas	Chr12:13379732	Chr12:13386538	rs46554776	S1073G	-2.13	Neutral	N/A	No Hit	N/A	N/A	N/A	N/A
Nbas	Chr12:13393456	Chr12:13400262	rs47580923	D1171N	-2.076	Neutral	N/A	No Hit	N/A	N/A	N/A	N/A
Nbas	Chr12:13413606	Chr12:13420412	rs49428474	V1298G	-1.811	Neutral	N/A	No Hit	N/A	N/A	N/A	N/A
Nbas	Chr12:13414916	Chr12:13421722	rs48052881	E1354A	0.185	Neutral	N/A	No Hit	N/A	N/A	N/A	N/A
Nbas	Chr12:13432993	Chr12:13439799	rs48010999	A1424T	-2.153	Neutral	N/A	No Hit	N/A	N/A	N/A	N/A
Nbas	Chr12:13469874	Chr12:13476680	rs49148361	G1596S	1.25	Neutral	N/A	No Hit	N/A	N/A	N/A	N/A
Nbas	Chr12:13558646	Chr12:13565452	rs48784396	R2141Q	-2.355	Neutral	N/A	No Hit	N/A	N/A	N/A	N/A
Nbas	Chr12:13583399	Chr12:13590205	rs49695448	D2268E	-0.922	Neutral	N/A	No Hit	N/A	N/A	N/A	N/A
Ppfia1	Chr7:144485085	Chr7:151670990	rs13460346	L1061M	-1.792	Neutral	-3.70304	0.66886	1113	0.76163	0.0281	2.253
Ppfia1	Chr7:144491527	Chr7:151677432	rs13460345	H964Q	-7.458	Deleterious	-4.76699	0.85408	1031	0.81482	0.00909	2.253
Ppfia1	Chr7:144505104	Chr7:151691009	rs36657434	E678D	-2.574	Deleterious	-3.32141	0.57967	713	0.75816	0.0411	2.161
Ppfia1	Chr7:144508246	Chr7:151694151	rs36910001	S554R	-3.295	Deleterious	-2.81287	0.45335	567	0.5137	0.02299	1.045
Ppfibp1	Chr6:146952958	Chr6:146901480	rs30354215	D195H	-3.147	Deleterious	-2.64633	0.41249	204	0.17391	0.01871	1.985
Ppfibp1	Chr6:146952987	Chr6:146901509	rs36699780	V186C	-2.316	Neutral	-3.59349	0.64417	195	0.26403	0.01088	2.202
Ppfibp1	Chr6:146953047	Chr6:146901569	rs30425488	E166K	-3.472	Deleterious	-5.45037	0.92059	175	0.89398	0.00847	3.998
Ppfibp1	Chr6:146953394	Chr6:146901916	rs30219632	H50C	-5.251	Deleterious	-4.24942	0.7772	54	0.23371	0.00415	1.992
Ppfibp1	Chr6:147010034	Chr6:146958556	rs29834347	D400E	0.47	Neutral	-1.0569	0.12531	403	0.0727	0.138	1.643
Pthlh	Chr6:147256965	Chr6:147205487	rs47671093	P166T	0.66	Neutral	-1.6337	0.20322	185	0.05093	0.35229	0.901
Rep15	Chr6:147032971	Chr6:146981493	rs30267061	Q103E	-0.891	Neutral	N/A	No Hit	N/A	N/A	N/A	N/A
Rep15	Chr6:147033094	Chr6:146981616	rs37277633	E144K	-3.818	Deleterious	N/A	No Hit	N/A	N/A	N/A	N/A
Rep15	Chr6:147033271	Chr6:146981793	rs30302844	I203V	-0.176	Neutral	N/A	No Hit	N/A	N/A	N/A	N/A
Rep15	Chr6:147033311	Chr6:146981833	rs37092403	R216K	1.624	Neutral	N/A	No Hit	N/A	N/A	N/A	N/A
Shank2	Chr7:144410768	Chr7:151596673	rs36708307	D914E	Unknown	Neutral	N/A	Not Likely	N/A	N/A	N/A	N/A
Slit3	Chr11:35700413	Chr11:35513915	rs26912296	V1351I	-0.448	Neutral	N/A	Not Likely	N/A	N/A	N/A	N/A

4.4 Discussion

Enhancing reproducibility is crucial to realizing the full potential of high content drug screening. A comparison between two large-scale pharmacogenomics high throughput studies (ie, the Cancer Genome Project and The Cancer Cell Line Encyclopedia) revealed high, moderate, and low concordance respectively between gene-expression, mutation, and drug sensitivity data. Although 15 drugs and 471 cancer cell lines were screened, the experimental procedures differed largely between the studies, particularly in the variability to drug response. This comparison illustrates the case for standardization in large pharmacogenomics studies and

the need to generate a robust phenotype.[12,13] In our study, we examined the effects of anticancer drugs on the normal immune system with the goal to elucidate genetic reasons for differences in toxicity. We used a panel of inbred mouse strains that were well defined in terms of genotype within controlled experimental conditions. Additionally, we could generate a robust drug response phenotype in this panel, especially in terms of the viability of immune cells to anthracyclines, facilitating downstream GWAS.[3]

In this screen, some of our cellular health markers did not act as expected (Supplementary Figure 4.1). For instance, we expected an increase in caspase with increasing drug concentrations. However, caspase 3/7 activity decreased with increasing drug concentrations. Interestingly, caspases have roles outside of apoptotic activity. Recent research indicates that they have dynamic roles in compensatory proliferation of neighboring cells, determination of cell fate and differentiation, and actin cytoskeleton reorganization. For example, cell cycle regulators are substrates for caspase 3, which cleaves p27 to promote lymphoid cell proliferation.[14] Examining additional caspases, such as caspase 2, 8, or 9 may provide additional information regarding caspase activity, facilitating better approximation of the method of cell death, as the decrease in caspase activity in our unstimulated splenocytes may be a nonapoptotic response to cytotoxic insult in lymphocytes or simply the result of a leaky cellular membrane due to necrotic cell death.

Anthracyclines have also been reported to have differential cell death modalities on cultured cells depending on cell type, cell differentiation status, and experimental settings. In leukemia cell lines, but not healthy leukocytes, Ristic et al. found that doxorubicin and idarubicin induce mTOR dependent autophagy and apoptosis associated with oxidative stress, mitochondrial depolarization, and caspase activation.[15] Timing and concentration are also critical

in anthracycline-induced apoptosis. In HL60 and Jurkat leukemia cell lines, doxorubicin caused an immediate loss of membrane integrity indicating necrosis, while other markers of apoptotic cell death (eg, DNA fragmentation, externalization of phosphatidylserine, caspase activation) occurred following a prolonged exposure (24h) to a low dose (up to 500 nM) of doxorubicin.[16] Cell death through necrosis following substantial concentrations of anthracyclines in our assay would explain a lack of caspase activation and change in mitochondrial health. Also, our assay was limited by the shortened time of exposure to drugs to preserve the integrity of unstimulated splenocytes, which may have affected our detection of certain cell health parameters, such as the stable mitochondrial health observed with increasing drug concentration.

We can examine a vast number of markers in the cell. For instance, Life Technologies' *The Molecular Probes® Handbook* alone contains over 3,000 reagents and kits dedicated to examining nucleic acids, proteins, cell components, cell structure, and cell function.[17] This flexibility and ever-evolving high-content screening platforms, such as the BD LSRII flow cytometer capable of simultaneously detecting 14 fluorochromes, makes the possibilities for custom cell-based screening assays tailored to drug, cell type, and parameters of interest nearly endless.[18] In our screen, we examined generic markers of cell health. However, we can examine more specific markers, such as reactive oxygen species production for anthracyclines and mTOR/PI3K and MEK phosphorylation respectively for targeted agents BEZ-235 and selumetinib. We also examined broad classes of cell types (eg, CD3e+ T-cells, CD19+ B-cells, CD11b+ monocytes, and Ly-6G+ granulocytes). From the phenotypic measures in our screen, it appears that T- and B-cells provide us with the most robust phenotype. Thus, we can explore subpopulations of lymphocytes (eg, CD4+ and CD8+ T-cells) in additional assays to best understand the immune cell response following anticancer drug exposure.

Using viability phenotypes derived from our assay (ie, T-cells, B-cells, and monocytes exposed to doxorubicin and idarubicin), we conducted GWAS and found seven genomewide significant peaks for viability at various drug concentrations and one genomewide significant peak for viability using AUC values (Figure 4.7). These peaks included numerous genes (ie, 35 genes for viability at various drug concentrations) for potential validation. Sixteen of these genes were of particular interest as candidate genes: *Ano1*, *App*, *Atp5j*, *Ccdc91*, *Cttn*, *Cyyr1*, *Fadd*, *Gabpa*, *Klhdc5*, *Mir155*, *Mrpl39*, *Mrps35*, *Ppfia1*, *Ppfibp1*, *Rasl11b*, and *Stk38l*. *App*, encoding amyloid precursor protein, was validated in an in vitro cellular assay for T-cells exposed to idarubicin. However, mechanistic studies and translational human studies have yet to be initiated.

Of the remaining candidate genes, *Ppfia1* and *Ppfibp1* would be most likely pursued initially for additional validation studies. *Ppfia1* and *Ppfibp1* are related liprin proteins found on different chromosomes (5 and 6 respectively) and were significantly linked to differential viability phenotypes of B-cells exposed to both doxorubicin and idarubicin. Using the IC_{50} and AUC measurements from B-cells exposed to doxorubicin and idarubicin, these genes also appear to be involved, although they do not achieve genomewide significance. The proteins encoded by these genes interact with one another to regulate leukocyte common antigen-related proteins and have been shown to have a role in *Drosophilia* axon guidance and mouse mammary gland development and function. *PPFIA1* encodes liprin α, which is involved in cell adhesion, integrin expression, and cell-matrix interactions. In human malignancies, including breast, esophageal squamous cell carcinoma, and head and neck cancers, a region of chromosome 11 containing *FADD*, *TMEM16A*, and *PPFIA1* is upregulated, leading to tumor growth and enhanced cancer cell invasiveness.[19] *PPFIBP1*'s role has been less investigated in comparison to *PPFIA1*.

PPFIBP1 encodes liprin-β, a protein that is predominantly localized to the plasma membrane in mammalian cells and has been identified as a potential regulator of lymphatic vessel integrity.[20,21]

4.5 Conclusions

In this chapter, we have analyzed the results of our immunophenotypic screen, associated GWAS, and candidate gene selection. Lessons and limitations from this process will translate into future improvements and developments. This project is also in an ideal position to be extended given the amount of potential candidate genes that were identified. Ultimately, this project may be translated to in vivo and human studies, leading to improvements in patient care.

Supplementary Figure 4.1. Anticipated versus actual screen results.

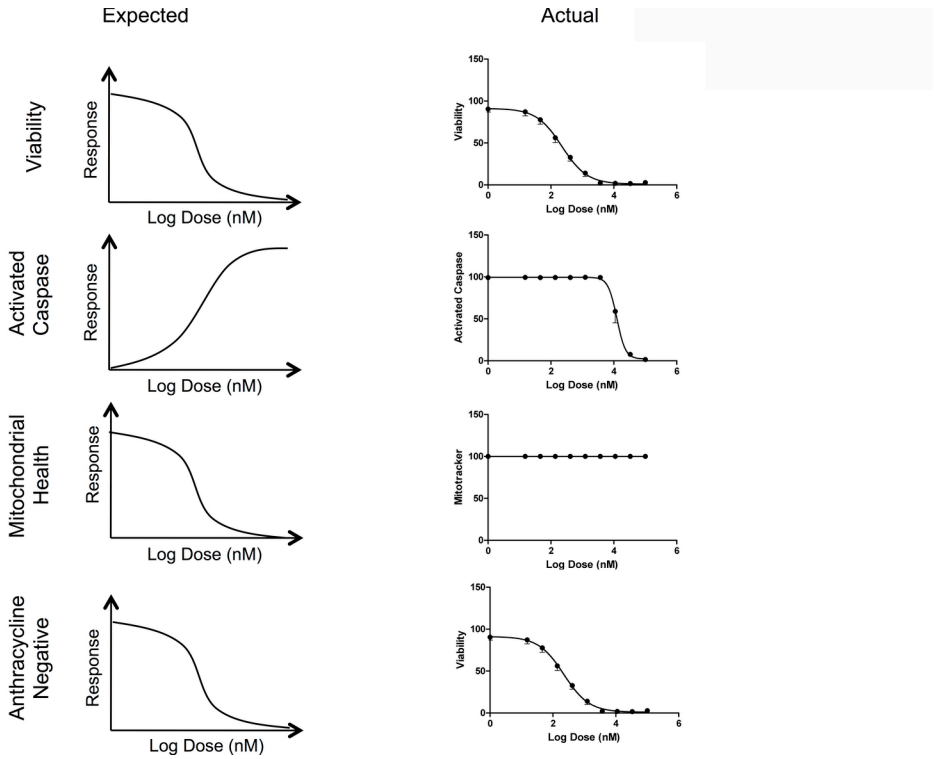

REFERENCES

1. Hanahan D, Weinberg RA. Hallmarks of cancer: the next generation. *Cell*. 2011;144(5):646–674. doi:10.1016/j.cell.2011.02.013.

2. Galluzzi L, Senovilla L, Zitvogel L, Kroemer G. The secret ally: immunostimulation by anticancer drugs. 2012:1–19. doi:10.1038/nrd3626.

3. Frick A, Fedoriw Y, Richards K, et al. Immune cell-based screening assay for response to anti-cancer agents: applications in pharmacogenomics. *Pharmgenomics Pers Med*. 2014.

4. McClurg P, Janes J, Wu C, et al. Genomewide association analysis in diverse inbred mice: power and population structure. *Genetics*. 2007;176(1):675–683. doi:10.1534/genetics.106.066241.

5. Kang HM, Zaitlen NA, Wade CM, et al. Efficient control of population structure in model organism association mapping. *Genetics*. 2008;178(3):1709–1723. doi:10.1534/genetics.107.080101.

6. Yang H, Wang JR, Didion JP, et al. Subspecific origin and haplotype diversity in the laboratory mouse. *Nat Genet*. 2011;43(7):648–655. doi:10.1038/ng.847.

7. Moreau Y, Tranchevent L-C. Computational tools for prioritizing candidate genes: boosting disease gene discovery. *Nat Rev Genet*. 2012;13(8):523–536. doi:10.1038/nrg3253.

8. Choi Y, Sims GE, Murphy S, Miller JR, Chan AP. Predicting the functional effect of amino acid substitutions and indels. *PLoS ONE*. 2012;7(10):e46688. doi:10.1371/journal.pone.0046688.

9. Thomas PD, Campbell MJ, Kejariwal A, et al. PANTHER: a library of protein families and subfamilies indexed by function. *Genome Research*. 2003;13(9):2129–2141. doi:10.1101/gr.772403.

10. Mi H, Lazareva-Ulitsky B, Loo R, et al. The PANTHER database of protein families, subfamilies, functions and pathways. *Nucleic Acids Research*. 2005;33(Database issue):D284–8. doi:10.1093/nar/gki078.

11. Wang JR, de Villena FP-M, McMillan L. Comparative analysis and visualization of multiple collinear genomes. *BMC Bioinformatics*. 2012;13(Suppl 3):S13. doi:10.1186/1471-2105-13-S3-S13.

12. Haibe-Kains B, El-Hachem N, Birkbak NJ, et al. Inconsistency in large pharmacogenomic studies. *Nature*. 2014;504(7480):389–393. doi:10.1038/nature12831.

13. Hatzis C, Bedard PL, Birkbak NJ, et al. Enhancing reproducibility in cancer drug screening: how do we move forward? *Cancer Res*. 2014;74(15):4016–4023. doi:10.1158/0008-5472.CAN-14-0725.

14. Kuranaga E. Caspase signaling in animal development. *Dev, Growth Differ*. 2011;53(2):137–148. doi:10.1111/j.1440-169X.2010.01237.x.

15. Ristic B, Bosnjak M, Arsikin K, et al. Idarubicin induces mTOR-dependent cytotoxic autophagy in leukemic cells. *Exp Cell Res*. 2014;326(1):90–102. doi:10.1016/j.yexcr.2014.05.021.

16. Dartsch D, Schaefer A, Boldt S, Kolch W, Marquardt H. Comparison of anthracycline-induced death of human leukemia cells: programmed cell death versus necrosis. *Apoptosis*. 2002:1–12.

17. Johnson I, Spence MT, eds. *The Molecular Probes® Handbook—A Guide to Fluorescent Probes and Labeling Technologies*. 2010. Available at: http://www.lifetechnologies.com/us/en/home/brands/molecular-probes.html. Accessed July 17, 2014.

18. Lu SX, Na I-K, McIntyre CA, Sasaki D, Balderas R, van den Brink M. *Construction of Multicolor Antibody Panels for the Flow Cytometric Analysis of Murine Thymic Stromal Cells*. Jose, CA, USA; 2009:1–16.

19. Choi EJ, Yun JA, Jabeen S, et al. Prognostic significance of TMEM16A, PPFIA1, and FADD expression in invasive ductal carcinoma of the breast. 2014;12(1):1–7. doi:10.1186/1477-7819-12-137.

20. Kriajevska M, Fischer-Larsen M, Moertz E, et al. Liprin beta 1, a member of the family of LAR transmembrane tyrosine phosphatase-interacting proteins, is a new target for the metastasis-associated protein S100A4 (Mts1). *J Biol Chem*. 2002;277(7):5229–5235. doi:10.1074/jbc.M110976200.

21. Norrmen C, Vandevelde W, Ny A, et al. Liprin 1 is highly expressed in lymphatic vasculature and is important for lymphatic vessel integrity. *Blood*. 2010;115(4):906–909. doi:10.1182/blood-2009-03-212274.

CHAPTER 5: FUTURE DIRECTIONS: POWERFUL TOOLS FOR GENOMIC ENGINEERING

5.1. Summary

There is a synergistic interaction between the immune system and anticancer agents, and this interaction plays a critical role in modulating tumor progression and response to therapy. Therefore, an in vitro toxicogenomic screen was developed to identify genetic biomarkers underlying this process. In this study, we used a novel screen derived from genetically divergent murine immune cells to identify genes responsible for immune cell toxicity following anthracycline administration. Our results showed that cytotoxic responses of immune cells against multiple genetic backgrounds could be successfully measured (Chapter 2). Furthermore, we were able to conduct genome-wide association (GWA) analyses from the multiple drug response phenotypes that we collected (Chapters 3 and 4). Altogether, a putative gene was identified and validated through our screen. Additionally, we were able to delineate immune cell response against selective and nonselective anticancer agents as well as identify immune cells that were sensitive and resistant to anticancer-induced cytotoxic effects. Taken together, our screen provides an effective means by which we can screen for novel agents that would affect specific immune cell types (ie, T-cells vs. B-cells) as well as identify putative genetic biomarkers mediating cytotoxic response.

5.2. Assay Expansion

Through the use of a panel of genetically diverse mouse inbred strains, we developed a drug screening platform aimed at examining genes underlying these chemotherapeutic cytotoxic responses on immune cells. The possibilities for assay improvement have been previously described in Chapter 2. With a vast availability of markers and kits to interrogate cell health, components, structure, and function in high-content screening platforms, nearly limitless options exist for the modification of out immunophenotypic screen. Below is a sample of directions that could be taken.

Due to time and financial constraints, we focused on more general phenotypes such as cell viability. However, in the future, a more direct focus on assessing specific parameters of cell health or drug response is needed. Ideally, this screening process would include biomarkers specific for drugs (eg, protein targets or gene expression changes) or cell-specific response (eg, additional markers of apoptosis), which would allow us to identify change in response in a more concise approach.

In this assay, we are able to differentiate variable cytotoxic response of different immune cells to anticancer agents using a wide range of concentrations (15 nM to 100 μM). The generic concentration selected did not produce IC_{50} values for all strains; therefore, an expansion of this concentration range or the use of a known cytotoxic concentration range would be useful in future experiments.

There were three known markers of drug response that were calculated from dose-response curves, namely AUC, $IC_{50,}$ and slope coefficients. These phenotypes were moderately correlated with each other. All three measurements used for GWA analysis present their own

challenges and benefits as discussed in Chapter 3 and were not the most suitable parameters for GWAS. Therefore, an addition of other more specific, biologically relevant drug response phenotypes (ie, PK/PD drug-receptor/transporter responses) is warranted in future studies.

To improve the assay, we can also examine more specific markers for anthracycline and targeted agent exposure, such as reactive oxygen species production for anthracyclines and mTOR/PI3K and MEK phosphorylation respectively for targeted agents BEZ-235 and selumetinib. We also examined broad classes of cell types (eg, CD3e+ T-cells, CD19+ B-cells, CD11b+ monocytes, and Ly-6G+ granulocytes). Because T- and B-cells provide us with the most robust phenotype, we can explore subpopulations of lymphocytes (eg, CD4+ and CD8+ T-cells) in additional assays to best understand the immune cell response following anticancer drug exposure.[1]

Lastly, it is important to note that chemotherapy agents could both stimulate immune response while at the same time kill highly proliferating immune cells, leading to activation of the adaptive and humoral system for improved anticancer response and drug-induced toxicities (ie, neutropenia), respectively. Thus, an in vitro toxicogenomic screen able to delineate immune-anticancer interaction that is specific to destruction of cancer cells, but not normal immune cells, is an important future direction for this project.

5.3. GWAS and Candidate Gene Selection

Using viability phenotypes derived from our assay (ie, T-cells, B-cells, and monocytes exposed to doxorubicin and idarubicin), we conducted GWAS and found seven genomewide significant peaks for viability at various drug concentrations and one genomewide significant peak for viability using AUC values. These peaks included numerous genes (ie, 35 genes for viability at various drug concentrations) for potential validation. Sixteen of these genes were of

particular interest as candidate genes: *Ano1*, *App*, *Atp5j*, *Ccdc91*, *Cttn*, *Cyyr1*, *Fadd*, *Gabpa*, *Klhdc5*, *Mir155*, *Mrpl39*, *Mrps35*, *Ppfia1*, *Ppfibp1*, *Rasl11b*, and *Stk38l*. Additional studies validating the role of these genes in mediating cytotoxic responses in immune cells are warranted.

App, encoding amyloid precursor protein, was validated in an in vitro cellular assay for T-cells exposed to idarubicin. However, mechanistic studies and translational human studies have yet to be initiated. As discussed above, we can hypothesize that an increase in wild type APP and subsequent sAPP leads to a decrease in functional proteins within the p53 pathway (in addition to the *Wnt* pathway and *PIN1*), which causes a downregulation in apoptotic processes, upregulation in cell survival, and subsequent resistance to toxic insults such as anticancer chemotherapy.[2] We could assess the effects on p53 and additional related pathways while simultaneously adjusting App levels. However, it is challenging to ascertain how to treat patients with overexpressed *APP*.[3] Also, genomic differences in molecular machinery processing APP could add an additional layer of complexity. In this study, the expression of *App* in the spleen and other immune cells did not correlate with the strain order for sensitivity of T-cells to idarubicin. Thus, the polymorphic differences in the gene likely contribute to differences seen in toxicity. An additional proof for the validation of *App* may include creating specific polymorphisms introducing the potentially deleterious nonsynonymous coding changes mentioned previously to see how the viability of T-cells exposed to idarubicin is affected. Additional candidate genes (eg, *Ppfia1* and *Ppfibp1*) also exist for future validation.

Furthermore, more sensitive genetic mouse models, such as the Collaborative Cross, will be readily available for GWAS in the near future. This resource better models the genetic heterogeneity observed in humans and will be useful in future toxicogenomic screens.[4]

5.4. Genomic Engineering

One of the major limitations of gene validation is a paucity of mouse models for knockdown and expression of candidate genes. The International Knockout Mouse Consortium's (IKMC) goal is to mutate all protein coding genes in the mouse using a combination of gene trapping and gene targeting in C57BL/6 mouse embryonic stem cells and subsequently generate phenotypes.[5] However, this process has several challenges; the method is labor-intensive, time-consuming, can affect development, and produces phenotypic effects that are not relevant or similar to the effects of the human ortholog genes.[6,7] With the exception of mouse embronic stem cells, homologous recombination rates are too low in mammalian cells to be a practical approach.[8] Our lab has altered the expression of genes in MEFs using electroporation with the introduction of siRNA or overexpression vectors. However, this approach introduces high cell death and requires substantial optimization.[9]

Available tools for genomic engineering have been crude. However, the newest genome editing strategy, the CRISPR-Cas9 (clustered regularly interspaced short palindromic repeats-Cas9 nuclease) system in a recombinant adeno-associated viral vector, is unprecedented in its power and precision in altering the genome. CRISPR-Cas9 is a system used by bacteria as a form of adaptive immunity. When bacteria are infected with a virus, they retain a signature in their chromosomal DNA, which is transcribed and processed into short RNAs called crRNA. With a second transcript, tacrRNA, the crRNA guides the Cas9 to its target. Thus, Cas9 acts as a programmable enzyme, which can act as a repressor or activator of specific genes via modifications. This system has several benefits, including relative simplicity, multiplexing capability, cost reduction, and efficiency. In addition to enhancing food production, advancing drug discovery, modifying energy sources, and elucidating the multiple genetic alterations

underlying human disease, this system is providing an unparalleled opportunity to essentially modify the genetic code of virtually any organism. Developing a new mouse model for a disease involves multiple generations and can take well over a year, but with the CRISPR technique, a new mouse model could be ready for testing in a matter of weeks by manipulating the embryo and reimplanting it.[8,10]

Using this system, we can create a variety of knockout models and even overexpression models quickly, which will make testing of candidate genes found via GWAS possible in vivo. For this project, available tools largely limited validation of candidate genes. *App* has been largely studied in the realm of Alzheimer's disease, making a knockout mouse model readily available for testing. However, knockout models for additional candidate genes, such as *Ppfia1* and *Ppfibp1*, are not available, necessitating more labor-intensive validation measures, such as optimization of an electroporation protocol, which would be difficult to achieve in sensitive immune system cells. Therefore, the CRISPR technique would allow us the extraordinary and immeasurable opportunity to explore pharmacogenomics findings derived from GWAS, and would hopefully expand our findings to human studies more efficiently.

5.5. Conclusions

Studies aimed at identifying biomarkers that are involved in immune cytotoxicity are needed to advance the development and most appropriate use of drugs, particularly anticancer agents. Through the use of the in vitro toxicogenomic screen developed in this study, we were able to identify genetic biomarkers that are involved in immune cytotoxicity in response to anticancer immunomodulatory drugs. Expansion of this cell-based drug screen through the use of additional phenotypic measures, including gene expression, PK/PD drug-receptor or drug-transporter response, and specific protein markers of cell signaling or cytotoxicity, would

enhance the capability of this screen to identify genetic biomarkers that are critical for a particular drug response or specific aspect of immune cytotoxicity. Additionally, the availability of more sensitive genetic mouse models (ie, the Collaborative Cross) and more advanced genomic engineering techniques make downstream validation studies for our putative genes more feasible in future studies.

REFERENCES

1. Frick A, Fedoriw Y, Richards K, et al. Immune cell-based screening assay for response to anti-cancer agents: applications in pharmacogenomics. *Pharmgenomics Pers Med*. 2014.

2. Ibáñez K, Boullosa C, Tabarés-Seisdedos R, Baudot A, Valencia A. Molecular evidence for the inverse comorbidity between central nervous system disorders and cancers detected by transcriptomic meta-analyses. *PLoS Genet*. 2014;10(2):e1004173. doi:10.1371/journal.pgen.1004173.

3. Lanni C, Racchi M, Memo M, Govoni S, Uberti D. p53 at the crossroads between cancer and neurodegeneration. *Free Radic Biol Med*. 2012;52(9):1727–1733. doi:10.1016/j.freeradbiomed.2012.02.034.

4. Complex Trait Consortium. The Collaborative Cross, a community resource for the genetic analysis of complex traits. *Nat Genet*. 2004;36(11):1133–1137.

5. Skarnes WC, Rosen B, West AP, et al. A conditional knockout resource for the genome-wide study of mouse gene function. *Nature*. 2011;474(7351):337–342. doi:10.1038/nature10163.

6. Liggett SB. Genetically modified mouse models for pharmacogenomic research. *Nat Rev Genet*. 2004;5(9):658–663.

7. Eisener-Dorman AF, Lawrence DA, Bolivar VJ. Cautionary insights on knockout mouse studies: the gene or not the gene? *Brain Behav Immun*. 2009;23(3):318–324. doi:10.1016/j.bbi.2008.09.001.

8. Perkel JM. The power and possibilities of genome engineering. *Science*. 2014;341(6148):822–824.

9. Suzuki O, Frick A, Parks BB, et al. A cellular genetics approach identifies gene-drug interactions and pinpoints drug toxicity pathway nodes. *Front Genet*. 2014;5:1–13. doi:10.3389/fgene.2014.00272.

10. Pennisi E. The CRISPR craze. *Science*. 2014;341(6148):833–836.